Physics of Atomic Nuclei, Vol. 66, No. 11, 2003, pp. 1953–1963. From Yadernaya Fizika, Vol. 66, No. 11, 2003, pp. 2003–2013.

NUCLEI
Theory

Exotic Molecular States in a Strong Magnetic Field: $H_3^{(2+)}$ Ion*

A. V. Turbiner[1)]

Instituto de Ciencias Nucleares, UNAM, México

Received March 23, 2003

Abstract—The existence of the molecular ion $H_3^{(2+)}$ in a magnetic field in a triangular and a linear configuration is discussed. A variational method (with an optimization of the form of the vector potential) is used. It is shown that, in the range of magnetic fields $10^8 < B < 10^{11}$ G, the system $(pppe)$, with the protons forming an equilateral triangle perpendicular to the magnetic line, has a well-pronounced minimum in the total energy. Also, for $B \gtrsim 10^{10}$ G, if the protons are situated along a magnetic line (linear configuration), a well-pronounced minimum in the total energy appears. Both configurations are unstable under the decays $H(\text{atom}) + p + p$ and $H_2^{(+)} + p$. A possible connection between the $H_3^{(2+)}$ molecular ion and a recently discovered absorption feature in a neutron-star atmosphere is discussed.

1. INTRODUCTION

Recently, Sanwal *et al.* [1] announced a discovery of two absorption features around 0.7 and 1.4 keV in the isolated neutron star 1E1207.4-5209. Their analysis was based on Chandra data from January 2000 and January 2002 runs and it was later confirmed by an independent analysis by Mori and Hailey [2]. Although so far there is no agreement among experts about the origin of the absorption, one particular point is not in doubt—this observation is an indication of the atomic–molecular nature of the neutron star atmosphere, which occurs in spite of a surface temperature of $(1.4–1.9) \times 10^6$ K [3]. These results do not sound very surprising, since as far back as the 1970s Kadomtsev–Kudryavtsev [4] and Ruderman [5] presented independent arguments for the existence of new chemical compounds in a strong magnetic field, different from the ones we deal with in everyday life. In the present paper, I want to describe the simplest exotic molecular system that does not exist in the absence of a magnetic field—the molecular ion $H_3^{(2+)}$. It sounds natural to study the two most symmetric configurations: (i) where the protons form an equilateral triangle with a magnetic field directed perpendicular to it and (ii) where the protons are situated along a magnetic line forming a linear polymer. Certain immediate physical arguments in favor of the existence of $H_3^{(2+)}$ in the linear and triangular configurations also can be presented. In a strong magnetic field, the electron cloud takes a cucumber-like form elongated along the magnetic line. Thus, for the triangular configuration, the protons themselves are kept stable if the system rotates, developing a Lorentz force, which compensates for the electrostatic repulsion. It is easy to see that the protons forming an equilateral triangle are stabilized by the cucumber-like electron cloud of total charge one perpendicular to the triangle and situated at its center. In the case of the linear configuration, the argument is different—we arrive at electrostatics in a quasi-one-dimensional domain which assures the existence of a stable configuration. Of course, as a natural approximation, the protons are assumed to be infinitely heavy, so that the Born–Oppenheimer approximation can be used.

Some time ago, there was presented theoretical evidence based on the solution of the Schrödinger equation that the molecular ion $H_3^{(2+)}$ in a linear configuration can exist in a strong magnetic field $B \gtrsim 10^{10}$ G [6]. Later, it was demonstrated that it even becomes the most stable one-electron system at $B \gtrsim 10^{13}$ G [7]. Recently, it was shown that the $H_3^{(2+)}$ molecular ion can also exist in a triangular configuration—the protons form an equilateral triangle, where a magnetic field is directed perpendicular to it—for a range of magnetic fields $10^8 \lesssim B \lesssim 10^{10}$ G [8]. Both studies have used quite sophisticated variational techniques. Our present goal is to present an overview of the present situation of the molecular

*This article was submitted by the author in English.

[1)]On leave of absence from the Institute for Theoretical and Experimental Physics, Bol'shaya Cheremushkinskaya ul. 25, Moscow, 117259 Russia; e-mail: turbiner@nuclecu.unam.mx, turbiner@heron.itep.ru

1063-7788/03/6611-1953$24.00

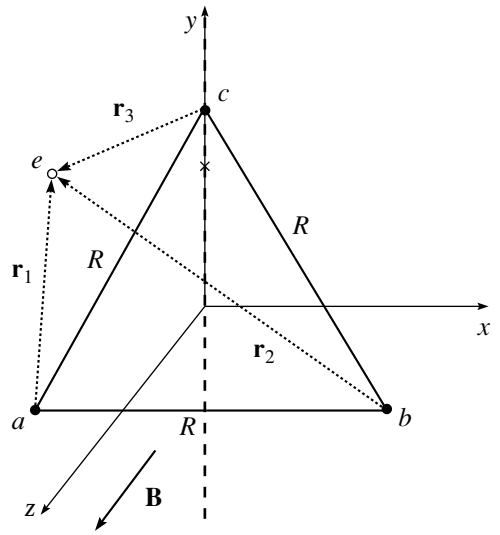

Fig. 1. Geometrical setting for the (*pppe*) ion in a magnetic field directed along the z axis. For the triangular configuration (see text), the protons are situated in the x–y plane and marked by bullets. It is assumed that the gauge center is situated along the bold dashed line which connects the center of the triangle and the position of the proton c (see text).

ion $H_3^{(2+)}$ and to discuss briefly the possibility of detecting such a system.

The Hamiltonian that describes three infinitely heavy protons and one electron placed in a uniform constant magnetic field directed along the z axis, $\mathbf{B} = (0, 0, B)$, is given by

$$\mathcal{H} = \hat{p}^2 + \frac{2}{R_{ab}} + \frac{2}{R_{ac}} + \frac{2}{R_{bc}} - \frac{2}{r_1} - \frac{2}{r_2} - \frac{2}{r_3} + 2(\hat{p}\mathcal{A}) + \mathcal{A}^2 \qquad (1)$$

(see Fig. 1 for notation), where $\hat{p} = -i\nabla$ is the momentum and $\mathcal{A}$ is the vector potential which corresponds to the magnetic field $\mathbf{B}$. As mentioned above, a natural triangular configuration appears if we assume that the protons a, b, c form an equilateral triangle, $R_{ab} = R_{bc} = R_{ac} = R$, and the magnetic field $\mathbf{B}$ is perpendicular to it. This configuration of the protons is stable from the classical-mechanical point of view, since electrostatic repulsion of the protons is compensated for by the Lorentz force. This justifies the use of the Born–Oppenheimer approximation and also adds extra stability to the whole system (*pppe*). It seems natural that a small perturbation of the position of a proton outside the plane perpendicular to the magnetic line can distort the above triangular configuration. However, our calculations show that the presence of the electron can stabilize the configuration, at least, for small perturbations. Thus, the stability of this configuration is of a different nature than the linear one (see details below). There, it appears to be a consequence of the quasi-one-dimensionality of the problem and compensation for the proton repulsion by the interaction with the almost one-dimensional electronic cloud [6, 7].

Atomic units are used throughout ($\hbar = m_e = e = 1$), albeit energies are expressed in Rydbergs (Ry). Sometimes, the magnetic field B is given in atomic units with $B_0 = 2.3505 \times 10^9$ G.

2. OPTIMIZATION OF VECTOR POTENTIAL

It is well known that the vector potential for a given magnetic field, even in the Coulomb gauge ($\nabla \cdot \mathcal{A}) = 0$, is ambiguous, up to the gradient of an arbitrary function. This is related to a feature of gauge invariance: the Hermitian Hamiltonian is gauge-independent as well as the eigenvalues and other observables. However, since we are going to use an approximate method for solving the Schrödinger equation with the Hamiltonian (1), our energies can be gauge-dependent (only the exact ones should be gauge-independent). Hence, one can choose the form of the vector potential in a certain optimal way, looking for a gauge that leads to minimal energy for a given (fixed) class of trial functions. In particular, if the variational method is used, an optimal gauge can be considered as a variational function and then is chosen by a procedure of minimization.

Let us consider a certain one-parameter family of vector potentials in the Coulomb gauge corresponding to a constant magnetic field B (see, for example, [9])

$$\mathcal{A} = B(-\xi(y - y_0), (1 - \xi)(x - x_0), 0), \qquad (2)$$

where ξ, x_0, y_0 are parameters. The position of the *gauge center*, for which $\mathcal{A}(x, y) = 0$, is defined by $x = x_0$, $y = y_0$. If the gauge center is at the origin, $x_0 = y_0 = 0$ and $\xi = 1/2$, we get the well-known and widely used gauge that is called the symmetric or circular gauge (see, for example, [10]). Otherwise, if $\xi = 1$, this corresponds to the asymmetric or Landau gauge (see [10]). By substituting (2) into (1), we arrive at the Hamiltonian in the form

$$\mathcal{H} = -\nabla^2 + \frac{6}{R} - \frac{2}{r_1} - \frac{2}{r_2} - \frac{2}{r_3} + 2iB[-\xi(y - y_0)\partial_x + (1 - \xi)(x - x_0)\partial_y] + B^2[(1 - \xi)^2(x - x_0)^2 + \xi^2(y - y_0)^2], \qquad (3)$$

where R is the length of one side of a triangle.

The idea of choosing an optimal (convenient) gauge has widely been exploited in quantum field-theory calculations. It has also been discussed in quantum mechanics, in particular, in connection with the present problem (see, for example, [11] and

references therein). Perhaps, the first constructive (and remarkable) attempt to apply this idea is due to Larsen [9]. In his variational study of the ground state of the $H_2^{(+)}$ molecular ion, it was explicitly shown that gauge dependence of the energy can be quite significant and even an oversimplified optimization procedure improves the numerical results.

Our present aim is to study the ground state of (1) and (3). It can be easily demonstrated that, for a one-electron problem, there always exists a certain gauge for which the ground-state eigenfunction is a real function. Let us fix the vector potential in (1). Assume that we have solved the spectral problem exactly and have found the exact ground-state eigenfunction. In general, it is a certain complex function with a nontrivial, coordinate-dependent phase. Considering the phase as a gauge phase and then gauging it away finally results in a new vector potential. This vector potential has the property we want—the ground-state eigenfunction of the Hamiltonian (1) is real. It is obvious that similar considerations can be performed for any excited state. In general, for a given eigenstate, there exists a certain gauge in which the eigenfunction is real. These gauges can be different for different eigenstates. A similar situation occurs for any one-electron problem.

Dealing with real trial functions has an obvious advantage: the expectation value of the term $\sim\mathcal{A}$ in (1) or $\sim B$ in (3) vanishes when it is taken over any real, normalizable function. Thus, without loss of generality, the term $\sim B$ in (3) can be omitted. Furthermore, it can be easily shown that, if the original problem possesses axial symmetry with the axis coinciding with the direction of the magnetic field, the real ground-state eigenfunction always corresponds to the symmetric gauge.

3. CHOOSING TRIAL FUNCTIONS

The choice of trial functions contains two important ingredients: (i) a search for the gauge that leads to the real ground-state eigenfunction and (ii) performance of a variational calculation based on *real* trial functions. The main assumption is that a gauge corresponding to a real ground-state eigenfunction is of the type (2) (or somehow is close to it).[2)] In other words, one can say that we are looking for a gauge of the type (2) which admits the best possible approximation of the ground-state eigenfunction by real functions. Finally, in regard to our problem, the following recipe for a variational consideration is used: First of all we construct an adequate variational real trial function Ψ_{var} [12], $\Delta\Psi_{\text{var}}/\Psi_{\text{var}} = V_{\text{var}}$, which allows us to reproduce the original potential near Coulomb singularities and at large distances, where ξ, x_0, y_0 would appear as parameters. Then, we perform a minimization of the energy functional by treating the free parameters of the trial function and ξ, x_0, y_0 on the same footing.

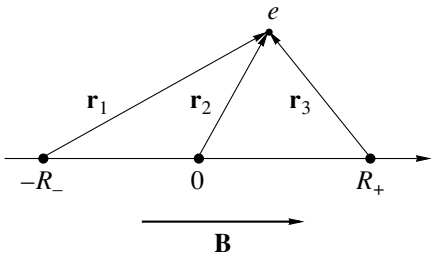

Fig. 2. Geometrical setting for the linear configuration of $H_3^{(2+)}$. The positions of the charged centers are marked by bullets.

In particular, such an approach enables us to eventually find the *optimal* form of the Hamiltonian as a function of ξ, x_0, y_0. It is evident that, for small interproton distances R, the electron prefers to be near the center of the triangle (coherent interaction with all three protons); hence, x_0, y_0 should correspond to the center of the triangle. In the opposite limit (large R), the electron is situated near one of the protons (a situation of incoherence—the electron selects and then interacts essentially with one proton); therefore, x_0, y_0 should correspond to the position of a proton. We make the natural assumption that the gauge center is situated on a line connecting the center of the triangle and one of the protons; hence,

$$x_0 = 0, \quad y_0 = \frac{R}{\sqrt{3}}d$$

(see Fig. 1). Thus the position of the gauge center is measured by the parameter d—the relative distance between the center of the triangle and the gauge center. If the gauge center coincides with the center of the triangle, then $d = 0$. On the other hand, if the gauge center coincides with the position of proton, $d = 1$.

In the case of the linear configuration, where the protons are situated along the magnetic field direction (along the z axis) (see Fig. 2), the parameters x_0, y_0 do not make much sense. Without loss of generality, we set $x_0 = y_0 = 0$ in (2). Moreover, as a consequence of the axial symmetry of the original physical problem, the vector field should be axially symmetric and, hence, the parameter ξ should be $1/2$. This makes the gauge fixing (2) unambiguous and we

[2)] This can be formulated as a problem—for a fixed value of B and fixed triangle size, find a gauge for which the ground state eigenfunction is real.

have arrived at the vector potential in the celebrated symmetric gauge.

The above recipe was successfully applied in a study of the $H_2^{(+)}$ ion in a magnetic field, leading to a unified description with very high accuracy for all magnetic fields, where nonrelativistic considerations hold [8, 13].

One of the simplest trial functions satisfying the above-mentioned criterion is

$$\Psi_1 = e^{-\alpha_1(r_1+r_2+r_3)-B[\beta_{1x}(1-\xi)(x-x_0)^2+\beta_{1y}\xi(y-y_0)^2]} \tag{4}$$

(cf. [13]), where α_1, $\beta_{1x,1y}$, ξ, x_0, y_0 are variational parameters. The requirement of normalizability of (4) implies that α_1, $\beta_{1x,1y}$ must be nonnegative numbers and $\xi \in [0,1]$. Actually, this is a Heitler–London-type function multiplied by the lowest (shifted) Landau orbital associated with the gauge (2). It is natural to assume that the function (4) describes the domain of coherence—small interproton distances and probably distances near the equilibrium.

Another trial function,

$$\Psi_2 = (e^{-\alpha_2 r_1} + e^{-\alpha_2 r_2} + e^{-\alpha_2 r_3})e^{-B[\beta_{2x}(1-\xi)(x-x_0)^2+\beta_{2y}\xi(y-y_0)^2]} \tag{5}$$

(cf. [13]), is of the Hund–Mulliken type multiplied by the lowest (shifted) Landau orbital. Here, α_2, $\beta_{2x,2y}$, ξ, x_0, y_0 are variational parameters. Presumably, this function dominates for sufficiently large interproton distances R, giving an essential contribution there. Hence, it models an interaction of a hydrogen atom and protons (charged centers) and can also describe a possible decay mode into them, $H_3^{(2+)} \to H + p + p$.

In a similar way, one can construct a trial function that would model the interaction $H_2^{(+)} + p$,

$$\Psi_3 = (e^{-\alpha_3(r_1+r_2)} + e^{-\alpha_3(r_1+r_3)} + e^{-\alpha_3(r_2+r_3)})e^{-B[\beta_{3x}(1-\xi)(x-x_0)^2+\beta_{3y}\xi(y-y_0)^2]}. \tag{6}$$

One can say that this is a mixed Hund–Mulliken and Heitler–London-type trial function multiplied by the lowest (shifted) Landau orbital. Here, α_3, $\beta_{3x,3y}$, ξ, x_0, y_0 are variational parameters. It is clear that this function gives a subdominant contribution at large R and a certain sizable contribution in the domain of intermediate distances.

There are two natural ways—linear and nonlinear—to incorporate the behavior of the system both near equilibrium and at large distances in a single trial function. A general nonlinear interpolation involving the above trial functions is of the form

$$\Psi_{4-1} = (e^{-\alpha_4 r_1-\alpha_5 r_2-\alpha_6 r_3} + e^{-\alpha_4 r_1-\alpha_5 r_3-\alpha_6 r_2} + e^{-\alpha_4 r_2-\alpha_5 r_1-\alpha_6 r_3} + e^{-\alpha_4 r_2-\alpha_5 r_3-\alpha_6 r_1} + e^{-\alpha_4 r_3-\alpha_5 r_1-\alpha_6 r_2} + e^{-\alpha_4 r_3-\alpha_5 r_2-\alpha_6 r_1})e^{-B[\beta_{4x}(1-\xi)(x-x_0)^2+\beta_{4y}\xi(y-y_0)^2]} \tag{7}$$

(cf. [13]), where $\alpha_{4,5,6}$, $\beta_{4x,4y}$, ξ, x_0, y_0 are variational parameters. In fact, this is a Guillemin–Zener-type function multiplied by the lowest (shifted) Landau orbital. If $\alpha_4 = \alpha_5 = \alpha_6$, the function (7) reproduces (4). However, if $\alpha_5 = \alpha_6 = 0$, it reproduces (5). If $\alpha_4 = \alpha_5$ and $\alpha_6 = 0$, it reproduces (6). The linear superposition of (4)–(6) leads to

$$\Psi_{4-2} = A_1\Psi_1 + A_2\Psi_2 + A_3\Psi_3, \tag{8}$$

where one of the parameters A_1, A_2, and A_3 is kept fixed, being related to the normalization factor. The final form of the trial function is a linear superposition of functions (7) and (8)

$$\Psi_{\text{trial}} = A_1\Psi_1 + A_2\Psi_2 + A_3\Psi_3 + A_{4-1}\Psi_{4-1}, \tag{9}$$

where three out of the four A parameters are defined variationally. For a given magnetic field, the total number of variational parameters in (9) is equal to 20 for the triangular configuration when ξ and d are included. In the case of the linear configuration, the number of free parameters is reduced, since $x_0 = y_0 = 0$ ($d = 0$) and $\xi = 1/2$; also, $\beta_{1x} = \beta_{1y}$, $\beta_{2x} = \beta_{2y}$, $\beta_{3x} = \beta_{3y}$, and $\beta_{4x} = \beta_{4y}$. Finally, the total number of variational parameters in (9) for the triangular configuration is equal to 14.

It is worth mentioning the strategy of the calculations. The variational energy is defined by a ratio of two three- or two-dimensional integrals, correspondingly, depending on which configuration is considered: triangular or linear. The domain of integration is the whole space, $R^3(R^2)$, respectively. In a numerical analysis, each infinite domain must be limited to a certain finite domain. This finite domain is chosen in such a way that the relative contribution coming from outside does not exceed 10^{-8}. In turn, for each finite domain, a certain dynamical partitioning is introduced following the profile of the integrand to make the calculations reliable. Of course, a variation of parameters in (9) changes the profile and hence leads to a change of partitioning. Depending on the value of the studied magnetic field, the number of subdomains in each integral is varied, reaching about 50 for the highest magnetic fields.

Calculations were performed using the minimization package MINUIT of CERN-LIB. Numerical integrations were carried out with a relative accuracy of $\sim 10^{-7}$ by use of the adaptive NAG-LIB (D01FCF) routine. All calculations were performed on a 450-MHz Pentium-II PC.

Table 1. Total energy, equilibrium distances, and characteristics of the vector potential (2) [8] (comparison is given with $H_3^{(2+)}$ in a linear configuration aligned along the magnetic line [7, 13], hydrogen atom [14] as well as the $H_2^{(+)}$ ion aligned along the magnetic line [7, 13])

B, G		$H_3^{(2+)}$ (triangle)	$H_3^{(2+)}$ (linear)	H atom	$H_2^{(+)}$ (parallel)
10^9	E_T [Ry]	−0.524934	−	−0.920821	−1.150697
	R [au]	3.161			1.9235
	ξ	0.50005			
	d	0.0			
10^{10}	E_T [Ry]	2.724209	1.846367	1.640404	1.090440
	R [au]	1.4012	2.0529		1.2463
	ξ	0.50102			
	d	0.00041			
5×10^{10}	E_T [Ry]	19.331448	16.661543	16.749684	15.522816
	R [au]	0.7766	1.0473		0.7468
	ξ	0.50205			
	d	0.0011			

4. RESULTS (TRIANGULAR CONFIGURATION)

The variational study [8] shows that, in the range of magnetic fields $10^8 < B < 10^{11}$ G, the system ($pppe$), with the protons forming an equilateral triangle perpendicular to the magnetic line, has a well-pronounced minimum in the total energy (see Table 1 and Figs. 3–6). With a magnetic field increase, the total energy becomes larger, the size of the triangle shrinks, but the height of the barrier increases (for example, it grows from ∼0.028 Ry at 10^9 G to ∼0.037 Ry at 10^{10} G). It was checked that the equilibrium configuration remains stable under small deviations of the proton positions but is unstable globally, decaying to $H + p + p$ and $H_2^{(+)} + p$. This implies the existence of the molecular ion $H_3^{(2+)}$ in a triangular configuration for the range of magnetic fields $10^8 < B < 10^{11}$ G.

The calculations show that the equilibrium position always corresponds to the situation where the gauge center coincides with the center of the triangle, $d = 0$. Therefore, the optimal vector potential appears in the symmetric gauge, $\xi = 0.5$ (see Table 1 and the discussion above). In Figs. 3 and 6, two typical situations of the absence of a bound state are presented. At $B = 10^8$ G, a certain irregularity appears on the potential curve, but neither $d = 1$ and $d = 0$, nor $d_{\min}$ curves develop a minimum. A similar situation holds for smaller magnetic fields $B < 10^8$ G. At $B = 10^{11}$ G, the situation is more complicated. If the gauge center is kept fixed and coincides with the center of the triangle, the potential curve displays a very explicit minimum, which disappears after varying the gauge center position (!). Something analogous to what is displayed in Fig. 5 appears for larger mag-

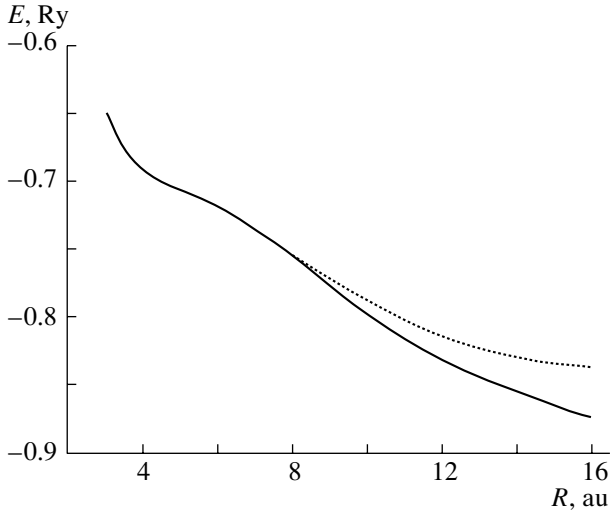

Fig. 3. Total variational energy of the system ($pppe$) at the magnetic field 10^8 G as a function of the size of the triangle (solid curve). The dotted curve is a variational energy if the parameter d is kept fixed, $d = 0$ (the gauge center coincides with the center of the triangle). If $d = 1$, the curve of the variational energy at $R > 6$ au coincides with the solid curve.

Table 2. The comparison of the total energies and equilibrium distances of $H_3^{(2+)}$ ion in a linear configuration [6] with the hydrogen atom [14], the $H_2^{(+)}$ ion aligned along the magnetic line [7, 13], and the Landau energy (total energies and equilibrium distances are in au)

	$B=0$		$B=10^{11}$ G		$B=10^{12}$ G		$B=10^{13}$ G	
	E_T	L	E_T	L	E_T	L	E_T	L
H	−1.000	–	36.929	–	413.57	–	4231.6	–
$H_2^{(+)}$	−1.205	1.997	35.036	0.593	408.300	0.283	4218.662	0.147
$H_3^{(2+)}$	–	–	36.429	1.606	410.296	0.692	4220.090	0.330
Free e	–	–	42.544	–	425.441	–	4254.41	–

netic fields, $B > 10^{11}$ G. This artifact of the gauge center fixing at $d = 0$ led to an erroneous statement in [15] about the existence of $H_3^{(2+)}$ in a triangular configuration at $B \geq 10^{11}$ G.

Figure 4 displays the plots of different potential curves corresponding to the gauge center fixed at the position of one proton, at the center of the triangle and also varying the gauge center at $B = 10^9$ G. A curve describing the total energy demonstrates a clear, sufficiently deep minimum. As was expected, small distances correspond to a gauge center coinciding with the center of the triangle, while large distances are described by a gauge center situated on a proton. It is important to emphasize that the domain of near-equilibrium distances (and approximately up to the position of the maximum) is described by the gauge-center-at-center-of-triangle curve. The well allows a vibrational state with energy $E_{\text{vib}} = 0.0113$ Ry.

In Fig. 5, there are plots of different potential curves corresponding to the gauge center fixed at the position of one proton, at the center of the triangle and also varying the gauge center at $B = 10^{10}$ G. A curve describing the total energy demonstrates a clear, sufficiently deep minimum. Unlike the situation for $B = 10^9$ G, this well is unable to allow a vibrational state. Similar to what happens for $B = 10^9$ G, small distances correspond to a gauge center coinciding with the center of the triangle, large distances are described by a gauge center situated on a proton, the domain of near-equilibrium distances and up to the position of the maximum is described by the

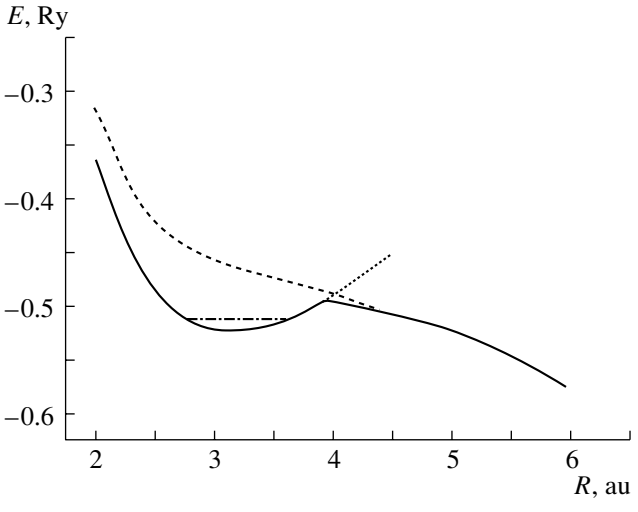

Fig. 4. Total energy of ($pppe$) at 10^9G as a function of the size of the triangle (solid curve). The dotted curve is the result of minimization if $d = 0$ is kept fixed. The dashed curve describes a result of minimization if $d = 1$ (the gauge center and position of a proton coincide—see text). The dash-dotted line displays the position of the first vibrational state.

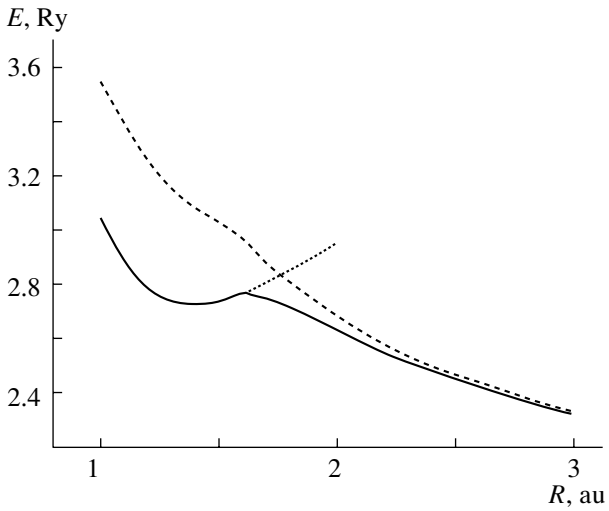

Fig. 5. Total energy of the system ($pppe$) at 10^{10} G as a function of the size of the triangle (solid curve). The dotted curve is the result of minimization if $d = 0$ is kept fixed. The dashed curve describes a result of minimization if $d = 1$ (the gauge center and position of proton coincide—see text).

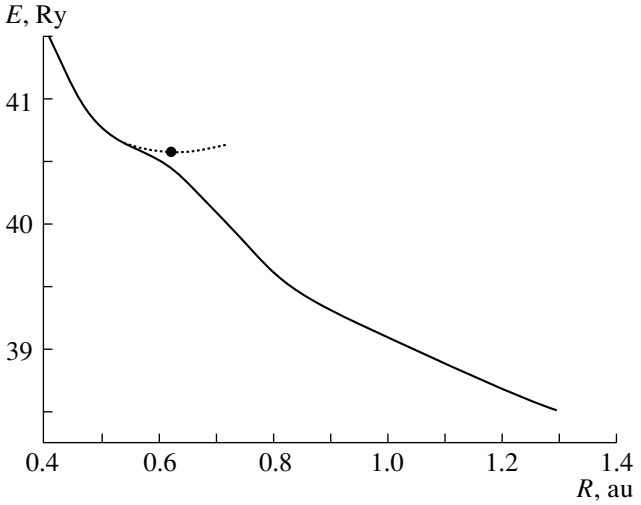

Fig. 6. Total energy of the system (*pppe*) at 10^{11} G as a function of the size of the triangle (solid curve). The bullet denotes the position of a spurious minimum that appears if the gauge center is kept fixed at $x_0 = y_0 = 0$ ($d = 0$, dotted curve) (the gauge center and the center of the triangle coincide).

gauge-center-at-center-of-triangle curve. It is quite interesting to investigate the behavior of the gauge center position d as well as a gauge "asymmetry," ξ vs. R. Both plots are of a phase transition-type, with change of behavior near the maximum of the barrier (see Figs. 7, 8). The width of the transition domain is $\sim$0.02 au (and $\sim$0.1 au for $B = 10^{10}$ G). The evolution of the electronic distributions with respect to the size of the triangle is shown in Figs. 9 and 10 for 10^9 and 10^{10} G, respectively. For small and intermediate R at $B = 10^9$ G, the distribution is characterized by three more or less similar peaks near the proton positions. However, it changes drastically after crossing the point of phase transition at $R \sim 3.93$ au. One peak disappears almost completely, while another one decreases in height. At large distances, two peaks disappear completely, and the distribution is characterized by one single peak, centered approximately at the position of one of the protons. For the case of $B = 10^{10}$ G, the electronic distribution is always characterized by a single peak, which is situated at the center of the triangle at small and intermediate distances. Then, at $R > 1.7$ au, the position of the peak shifts to a position of the proton. For both values of the magnetic field at asymptotically large distances, the center of the peak coincides exactly with the position of the proton. This picture describes a decay $H_3^{(2+)} \to H + p + p$.

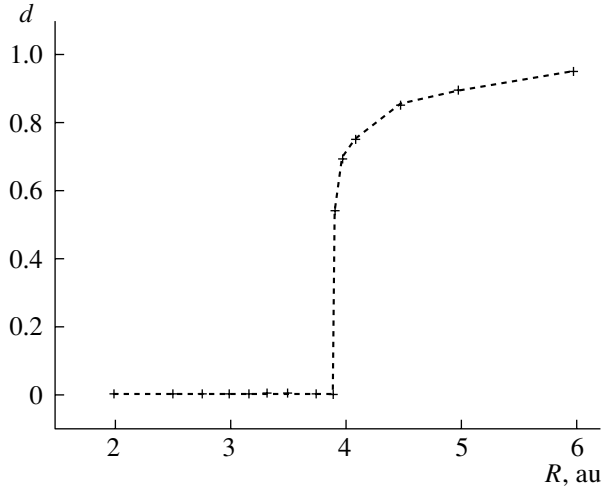

Fig. 7. Dependence of the position of the gauge center d on the size of the triangle for 10^9 G.

5. RESULTS (LINEAR CONFIGURATION)

Theoretical evidence for the existence the exotic system $H_3^{(2+)}$ in a linear configuration (see Fig. 2 for a geometrical setting) for magnetic fields $B \gtrsim 10^{11}$ G was provided in [6]. A great advantage of our approach is that the same trial function (9) can be used. From the computational point of view, a study of the system (*pppe*) in the linear configuration is much simpler than for a triangular one. Due to axial symmetry, the symmetric gauge is the optimal one, since it is a unique gauge, which supports this symmetry. The number of parameters in (9) is effectively reduced to 14 and the three-dimensional integration becomes a two-dimensional one.

For magnetic field $B < 10^{11}$ G, the variational electronic total energy $E(R_+, R_-)$ of the system

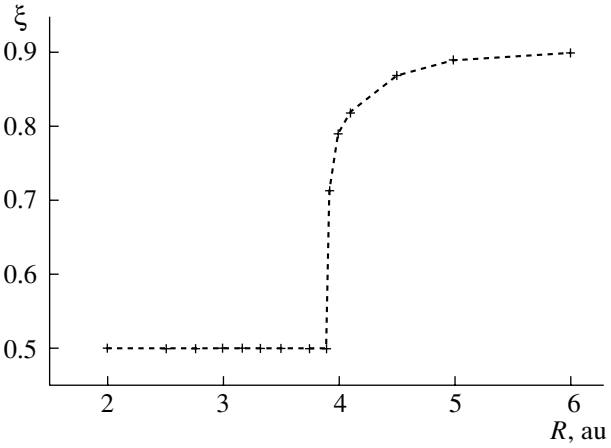

Fig. 8. Dependence of the parameter ξ on the size of the triangle for 10^9 G.

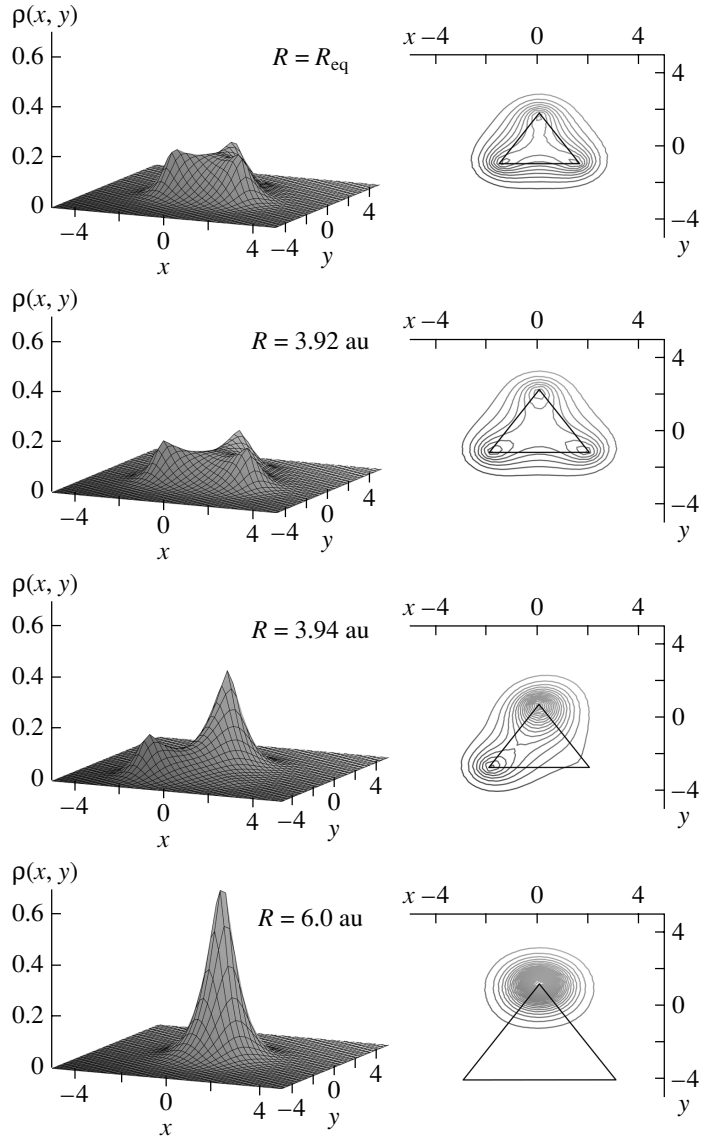

Fig. 9. Evolution with R of the integrated, normalized (to unity), electronic distributions $\rho(x,y) = \int |\Psi|^2(x,y,z)dz$ for $H_3^{(2+)}$ in an equilateral triangular configuration at $B = 10^9$ G. The coordinates x, y are given in au, $\rho(x,y)$ is in $(\text{au})^{-2}$.

($pppe$) does not indicate any minimum for finite values of R_+, R_-. However, starting from $B \sim 10^{11}$ G, the energy surface $E(R_+, R_-)$ starts to develop a well-pronounced minimum for finite values of R_+, R_-. Moreover, this minimum turns out to be stable under small deviations from linearity. It shows the existence of the exotic molecular ion $H_3^{(2+)}$. In Table 2, a comparison of the total energies and equilibrium distances for different one-electron systems is presented. It is quite striking that the total energy of the ion $H_3^{(2+)}$ once it appears becomes immediately smaller than the total energy of the hydrogen atom but remains larger than $H_2^{(+)}$. It implies that a decay $H_3^{(2+)} \to H + p + p$ is prohibited. It is worth noting that the difference between the total energies of $H_2^{(+)}$ and $H_3^{(2+)}$ is very small in comparison to their total

Table 3. Longitudinal localization length $\langle|z|\rangle$ and a natural size L for $H_2^{(+)}$ and $H_3^{(2+)}$ for different magnetic fields (all distances are in au)

B, G	$H_2^{(+)}$		$H_3^{(2+)}$	
	$\langle|z|\rangle$	$L = R$	$\langle|z|\rangle$	$L = R_+ + R_-$
10^{11}	0.624	0.593	0.864	1.606
10^{12}	0.348	0.283	0.438	0.692
10^{13}	0.214	0.147	0.242	0.330

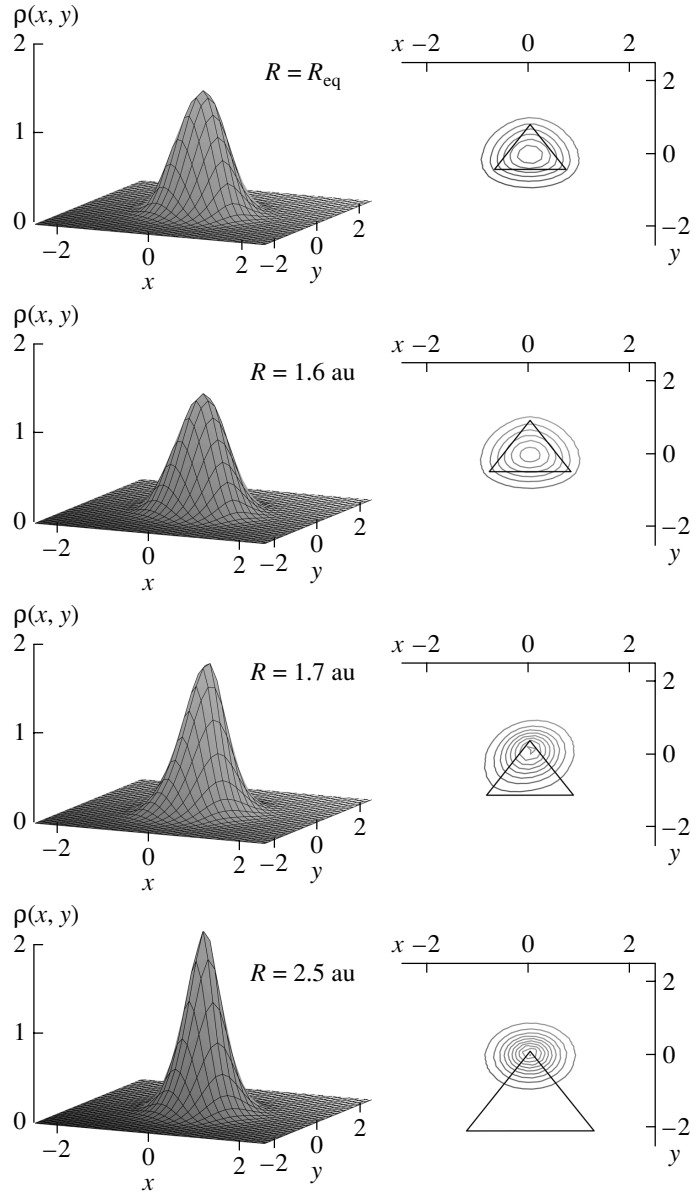

Fig. 10. Evolution with R of the integrated, normalized (to unity), electronic distributions $\rho(x,y) = \int |\Psi|^2(x,y,z)dz$ for $H_3^{(2+)}$ in an equilateral triangular configuration at $B = 10^{10}$ G. The coordinates x, y are given in au, $\rho(x,y)$ is in $(\text{au})^{-2}$.

and even binding energies. For some magnetic field of the order of 10^{13} G, the total energies even become equal and then the total energy of $H_3^{(2+)}$ is smaller than $H_2^{(+)}$ (see below).

As in the case of $H_2^{(+)}$, the binding energy of $H_3^{(2+)}$ increases with magnetic field. The natural size $L = R_+ + R_-$ of the $H_3^{(2+)}$ system defined by classical position of the protons decreases as the magnetic field grows similar to what happens with the natural size $L = R_{\text{eq}}$ of $H_2^{(+)}$. However, the striking difference between these two systems is revealed. In

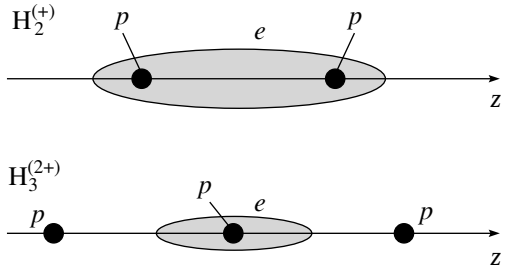

Fig. 11. An illustration of the difference between electronic distributions for $H_2^{(+)}$ and $H_3^{(2+)}$. The positions of the protons are marked by bullets. The electron cloud is in shadow domain.

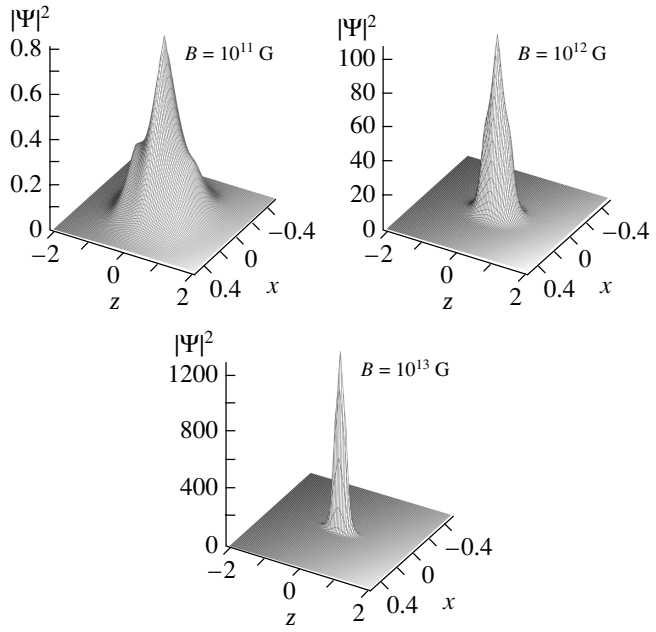

Fig. 12. Electronic distributions (integrated over y and normalized to unity) for $H_3^{(2+)}$ in a linear configuration for different magnetic fields. Dominant coupling of $H_3^{(2+)}$ is determined by a coherent interaction of the electron with all protons. The distances are in au, $\rho(x, y)$ is in $(\text{au})^{-2}$.

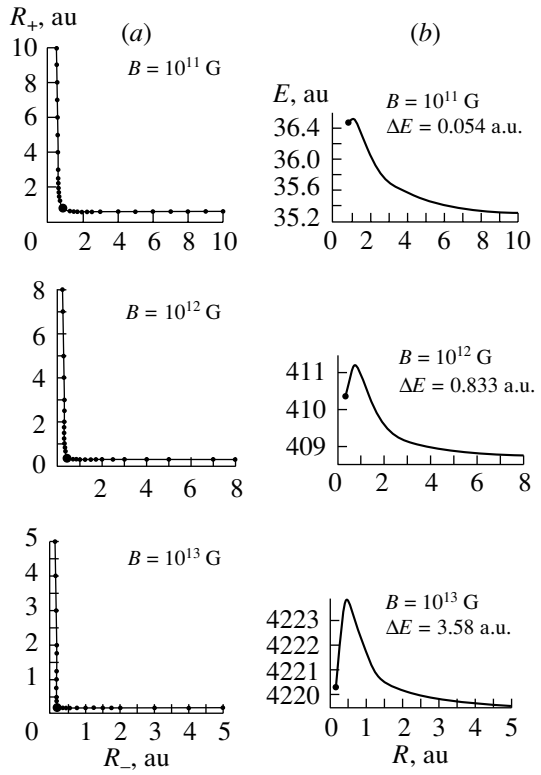

Fig. 13. Valleys in the electronic potential energy surfaces for $H_3^{(2+)}$ in a linear configuration in (R_+, R_-) variables for different magnetic fields (a) and their profiles (b) for various magnetic fields. The minimum is indicated by a bullet. ΔE denotes the height of the barrier.

contrast to the $H_2^{(+)}$ ion, for $H_3^{(2+)}$, the longitudinal localization length of the electron $\langle|z|\rangle$ is smaller (or much smaller) than the natural size L of the system determined by the classical positions of the protons (see Table 3). Therefore, for $H_3^{(2+)}$, the electronic cloud mainly surrounds the central proton unlike $H_2^{(+)}$, where both protons are surrounded by the electron cloud (see Figs. 11 and 12).

In Fig. 13a, behavior of the potential energy surfaces in the (R_+, R_-) variables (see Fig. 2) is illustrated for different magnetic fields. These surfaces develop valleys corresponding to a decay of $H_3^{(2+)} \to H_2^{(+)} + p$ at large interproton distances. For a certain $R_+(R_+ = R_-)$, the potential energy surfaces exhibit a well-pronounced minimum. However, for $B \approx 10^{11}$ G, the minimum is shallow. The energy of the lowest longitudinal vibrational state at $B = 10^{11}$ G in the harmonic approximation is equal to $\delta E = 0.189$ au and lies much above the top of the barrier, whose height is $\Delta E = 0.054$ au. However, with growth of the magnetic field, the situation starts to change. Already for $B = 10^{12}$ G, the potential well becomes sufficiently deep that $\delta E = 1.033$ au is comparable with barrier height $\Delta E = 0.833$ au, while for $B = 10^{13}$ G the lowest vibrational state is kept inside of the well (see Fig. 13b): $\delta E = 2.406$ au and $\Delta E = 3.58$ au.

In the region $B = 10^{11}$–10^{13} G, the system $H_3^{(2+)}$ is unstable towards a decay to $H_2^{(+)} + p$. With the growth of magnetic field, the total energy of $H_3^{(2+)}$ becomes lower than the total energy for $H_2^{(+)}$. This happens at $B \approx 10^{13}$ G. For example, concrete calculations show that, at $B = 4.414 \times 10^{13}$ G, the total electronic energies of $H_3^{(2+)}$ and $H_2^{(+)}$ are 18 723.88 and 18 724.48 au, respectively. Hence, for $B \gtrsim 10^{13}$ G, the exotic molecular ion $H_3^{(2+)}$ becomes the most bound one-electron system.

6. CONCLUSION

We presented theoretical arguments based on a variational study that three protons can be bound by one electron in triangular and linear configurations at magnetic fields $B \approx 10^9$–10^{11} G and $B \gtrsim 10^{11}$ G, respectively. Therefore, the exotic molecular ion $H_3^{(2+)}$ can exist in a strong magnetic field. This ion in a linear configuration becomes the most bound one-electron system at $B > 10^{13}$ G having the lowest total energy in comparison with H, $H_2^{(+)}$, and exotic system $H_4^{(3+)}$ (see [7]). Each of these systems is characterized by a monotonic increase in the binding (ionization) energy with the magnetic field. These energies reach extremely high values. For example, at $B = 4.414 \times 10^{13}$ G, the ionization energies are

$$E_B(\mathrm{H}) = 0.430\ \mathrm{keV}, \quad E_B(\mathrm{H}_2^{(+)}) = 0.741\ \mathrm{keV},$$
$$E_B(\mathrm{H}_3^{(2+)}) = 0.750\ \mathrm{keV}, \quad E_B(\mathrm{H}_4^{(3+)}) = 0.589\ \mathrm{keV}.$$

Therefore, the absorption feature at 0.7 keV can be explained naturally by the ionization of the ions $H_2^{(+)}$ and $H_3^{(2+)}$ if they are in a magnetic field $B \approx 3 \times 10^{13}$ G. This explanation is different than the ones presented in [1, 2], where, in particular, the absorption feature was assigned to a singly ionized helium atom at a magnetic field $B \approx 2 \times 10^{14}$ G.

ACKNOWLEDGMENTS

The present paper is in honor of the 80th birthday of my teacher, Professor Karen A. Ter-Martirosyan, for whom I have maintained the deepest appreciation and respect throughout my life.

I want to express my deep gratitude to J.C. López Vieyra (Nuclear Science Institute, México), with whom I shared the pleasure of working on this exciting subject. I thank B.I. Ivlev (IF-UASLP, México) for useful conversations and M. Ryan (ICN, México) for careful reading of the manuscript. This work was supported in part by grants DGAPA IN120199 and CONACyT 36600-E (México).

REFERENCES

1. D. Sanwal, G. G. Pavlov, V. E. Zavlin, and M. A. Teter, Astrophys. J. Lett. **574**, L61 (2002).
2. K. Mori and C. J. Hailey, astro-ph/0301161.
3. V. E. Zavlin, G. G. Pavlov, and J. Trumper, Astron. Astrophys. **331**, 821 (1998).
4. B. B. Kadomtsev and V. S. Kudryavtsev, Pis'ma Zh. Éksp. Teor. Fiz. **13**, 15 (1971); Pis'ma Zh. Éksp. Teor. Fiz. **13**, 61 (1971); Zh. Éksp. Teor. Fiz. **62**, 144 (1972).
5. M. Ruderman, Phys. Rev. Lett. **27**, 1306 (1971); IAU Symp. Proc. **53**, 117 (1974).
6. A. V. Turbiner, J. C. López, and U. H. Solis, Pis'ma Zh. Éksp. Teor. Fiz. **69**, 800 (1999) [JETP Lett. **69**, 844 (1999)]; astro-ph/9809298.
7. J. C. López Vieyra and A. V. Turbiner, Phys. Rev. A **62**, 022510 (2000).
8. J. C. López Vieyra and A. V. Turbiner, Phys. Rev. A **66**, 023409 (2002).
9. D. Larsen, Phys. Rev. A **25**, 1295 (1982).
10. L. D. Landau and E. M. Lifshitz, *Quantum Mechanics* (Pergamon Press, London, 1977).
11. P. Schmelcher, L. S. Cederbaum, and U. Kappes, *Conceptual Trends in Quantum Chemistry* (Kluwer, Dordrecht, 1994), p. 1.
12. A. V. Turbiner, Zh. Éksp. Teor. Fiz. **79**, 1719 (1980) [Sov. Phys. JETP **52**, 868 (1980)]; Usp. Fiz. Nauk **144**, 35 (1984).
13. J. C. López Vieyra, P. O. Hess, and A. V. Turbiner, Phys. Rev. A **56**, 4496 (1997); astro-ph/9707050.
14. A. Potekhin and A. Turbiner, Phys. Rev. A **63**, 065402 (2001); physics/0101050.
15. J. C. López Vieyra, Rev. Mex. Fis. **46**, 309 (2000).

Physics of Atomic Nuclei, Vol. 66, No. 11, 2003, pp. 1964–1971. Translated from Yadernaya Fizika, Vol. 66, No. 11, 2003, pp. 2014–2021.

NUCLEI
Theory

Zeldovich's Regularization Method in the Theory of Quasistationary States

V. D. Mur, S. G. Pozdnyakov, S. V. Popruzhenko*, and V. S. Popov[1)]

Moscow Engineering Physics Institute (State University), Kashirskoe sh. 31, Moscow, 115409 Russia

Received December 9, 2002

Abstract—The complex quasienergy, including the level width Γ, is calculated for a loosely bound atomic state in an intense monochromatic laser field of circular polarization. The method proposed by Zeldovich for regularizing divergent integrals that involve the Gamow wave function is employed in this calculation. The convergence of the method is demonstrated, and the conditions of its applicability are indicated.

Dedicated to
Karen Avetovich Ter-Martirosyan
on the occasion of his 80th birthday.
We are greatly indebted
to the hero of the celebration
for numerous enlightening discussions
on various physics problems
and heartily wish him
good health, longevity, and
and many years of creative activity

1. INTRODUCTION

In atomic, nuclear, and elementary-particle physics, as well as in some other realms of physics, there often occur quasistationary states. Such states correspond to particles or systems of particles that, albeit undergoing decay within a finite time interval, behave as stable formations in many respects and which manifest themselves as resonances in scattering processes. The widespread examples of this kind include the alpha decay of nuclei and the ionization of atoms and molecules that is induced by external fields—in particular, by an intense laser radiation.

Quasistationary states are described in terms of a Gamow wave function satisfying the Sommerfeld radiation condition, $\chi_k(r) \sim \exp(ikr)$ for $r \to \infty$; here, $k = \sqrt{2E} = k_1 - ik_2$, where k_1, $k_2 > 0$ and $E = E_r - i\Gamma/2$ is the complex-valued energy of a quasistationary state, with E_r and Γ being the resonance position and width, respectively.

In view of an exponential growth of the wave function $\chi_k(r)$ at infinity, there arise serious difficulties in solving specific problems, since even the normalization integral $\int_0^\infty |\chi_k(r)|^2 dr$ diverges. A possible method for overcoming this difficulty was suggested by Zeldovich [1], who proposed treating a divergent integral in a regularized sense. In particular, the normalization integral N for the radial wave function in a spherically symmetric case is defined as the limit

$$N = \int_0^\infty \chi_k^2(r)dr = \lim_{\alpha\to+0} \int_0^\infty \chi_k^2(r)e^{-\alpha r^2}dr. \quad (1)$$

This makes it possible to construct perturbation theory for quasistationary states [1, 2] and to trace an analogy between them and ordinary stationary states.

Here, problems related to the applicability of Zeldovich's method will be discussed without recourse to perturbation theory. This will be done by considering, by way of example, the problem in which an atomic level associated with short-range forces undergoes ionization under the effect of the field of a circularly polarized electromagnetic wave.

[1)]Institute of Theoretical and Experimental Physics, Bol'shaya Cheremushkinskaya ul. 25, Moscow, 117218 Russia.
*e-mail: poprz@theor.mephi.ru

1063-7788/03/6611-1964$24.00

Table 1. Convergence of Zeldovich's method

$\gamma = 10, K_0 = 4.5$		$\gamma = 3, K_0 = 5.55$	
α	$\Gamma \times 10^{13}$	α	$\Gamma \times 10^{9}$
1.6(−5)	1.2249	1.6(−5)	1.02429
4.0(−6)	1.2059	4.0(−6)	1.01786
1.0(−6)	1.2015	1.0(−6)	1.01626
2.5(−7)	1.2006	2.5(−7)	1.01586
$\alpha \to 0$	1.2006	$\alpha \to 0$	1.01573
$\gamma = 3, K_0 = 2$		$\gamma = 1, K_0 = 3$	
α	$\Gamma \times 10^{3}$	α	$\Gamma \times 10^{3}$
2.5(−5)	1.06792	1.0(−4)	1.47816
6.25(−6)	1.06707	2.5(−5)	1.47415
1.56(−6)	1.06686	6.25(−6)	1.47314
3.91(−7)	1.06681	1.56(−6)	1.47289
$\alpha \to 0$	1.06679	$\alpha \to 0$	1.47281

Note: Quoted in this table are values obtained for the level width Γ via regularization according to Zeldovich's method ($\beta = 2$). The relevant calculation was performed for a few values of the parameter α. The limit $\alpha \to +0$ was obtained by means of the extrapolation described in Appendix 1. Here $\kappa_0 = 1$ and the following notation was used: $a(b) \equiv a \times 10^b$.

2. BASIC EQUATIONS

Upon going over to a rotating reference frame [3], the dipole-approximation expression for the Hamiltonian $H(t)$ describing a charged particle subjected to the effect of a central potential and the field of a circularly polarized electromagnetic wave assumes the form

$$H_\omega = -\frac{1}{2}\Delta + U(r) - \omega L_z + \mathcal{E}x, \qquad (2)$$

where ω and $\mathcal{E}$ are, respectively, the frequency and the amplitude of the electric field of the wave and L_z is the projection of the electron orbital angular momentum onto the direction of wave propagation; here, we have used the system of units where $\hbar = m = e = 1$. The spectrum of states of the operator $H(t)$ that are characterized by complex-valued quasienergies [4, 5] coincides with the spectrum of quasistationary levels of the Hamiltonian H_ω. We will restrict our consideration to the case of s-wave states, for which one can use the zero-range approximation for $U(r)$ (three-dimensional delta-function potential). As is well known from [2], this is equivalent to the boundary condition

$$\frac{1}{\chi}\frac{d\chi(r)}{dr}\bigg|_{r=0} = -\kappa_0, \qquad (3)$$

where $\kappa_0 = \sqrt{2I_0}$, I_0 is the ionization potential for the ion being considered, and $E_0 = -I_0 = -\kappa_0^2/2$ is the energy of a level in the absence of a wave.

The complex-valued quasienergy $E = E_r - i\Gamma/2$ of a quasistationary state is determined from the equation that was first derived by Berson [6] and by Manakov and Rapoport [7]. We represent this equation in the form

$$I(\epsilon; \gamma, K_0) = \sqrt{\epsilon} - 1, \qquad (4)$$

where

$$\epsilon = \varepsilon + \gamma^{-2}, \qquad \varepsilon = E/E_0 = 1 + \delta + i\eta,$$

$$E_r = E_0(1+\delta), \qquad \Gamma = \kappa_0^2\eta, \qquad (5)$$
$$\gamma = \omega\kappa_0/\mathcal{E} = 1/(2K_0F),$$

ε is the reduced quasienergy, γ is the Keldysh adiabaticity parameter [8], $F = \mathcal{E}/\kappa_0^3$ is the reduced wave field, and $K_0 = I_0/\omega = \kappa_0^2/2\omega$ is a parameter associated with the multiquantum character of the process. Equation (4) formally holds for arbitrary F and makes it possible to go beyond the region of applicability of the weak-field approximation.

The left-hand side of Eq. (4) is obtained by analytically continuing, to the upper half-plane, the function

specified by the integral

$$I = \frac{1}{(8\pi i K_0)^{1/2}} \int_0^\infty \frac{du}{u^{3/2}} \times \left\{ \exp\left(i \frac{2K_0}{\gamma^2} \frac{\sin^2 u}{u} \right) - 1 \right\} \exp\left(-2iK_0 \epsilon u\right), \quad (6)$$

which is convergent in the lower half-plane $\mathrm{Im}\epsilon < 0$.

In order to construct the required analytic continuation of this integral, we will make use of Zeldovich's method. For solutions to Eq. (4), we will consider functions obtained by going over to the limit $\alpha \to +0$ in solutions to the equation

$$I_\alpha(\epsilon; \gamma, K_0) = \sqrt{\epsilon} - 1, \quad (7)$$

where the function $I_\alpha(\epsilon)$ is obtained from (6) by means of the substitution

$$\exp(-2i\epsilon K_0 u) \to \exp(-2i\epsilon K_0 u) R_\beta, \quad (8)$$
$$R_\beta = \exp(-\alpha\, u^\beta), \qquad \beta > 1.$$

The value of $\beta = 2$ corresponds to the regularization method proposed by Zeldovich.

3. RESULTS OF THE CALCULATIONS

Below, we present the results obtained by numerically solving Eq. (7) for two possible regularizations ($\beta = 2$ versus $\beta = 4$). The data in Table 1 illustrate the convergence of Zeldovich's method over a broad interval of widths Γ. In order to compute Γ with a relative error of 10^{-4}, it is necessary, as a rule, to reach parameter values of $\alpha \le 10^{-6}$–10^{-7}. Table 2 demonstrates that the results are independent of the regularization method. Moreover, the correctness of the results given in Tables 1 and 2 is confirmed by the calculation of the shifts and widths of levels by perturbation theory [9] at the same values of the parameters K_0 and γ, in which case four to six terms in the expansion of the integral in (6) in the field strength prove to be sufficient.

For a few values of the Keldysh parameter, the calculated level width Γ as a function of $1/K_0$ is shown in Fig. 1. The dashed curves represent the results for the level width in the semiclassical approximation ($\tilde{\Gamma}$) [10–12]. It is valid for $K_0 \gg 1$ if $\gamma \le 1$ or for $K_0 \gg 2\ln\gamma$ if $\gamma \gg 1$. Under such conditions, the method of steepest descent can be used to calculate the width in question. With allowance for the shift of the level, we have [13]

$$\frac{\tilde{\Gamma}}{\kappa_0^2} = \frac{\gamma}{4\tau_0} [\cosh(2\tau_0) - 1 - \gamma^2]^{-1/2} \times \exp\{-2K_0 [f(\gamma) + \tau_0 \delta]\}, \quad (9)$$

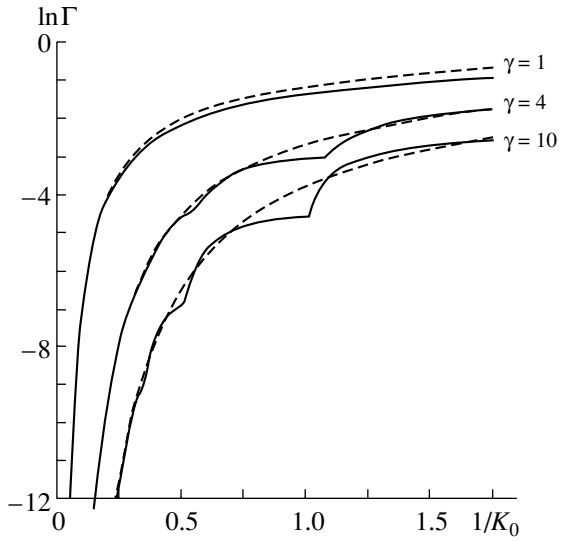

Fig. 1. Level width Γ as a function of $1/K_0 = 2\omega$ (Here, we set $\kappa_0 = 1$): (solid curves) results of a numerical calculation on the basis of Eq. (7) and (dashed curves) results obtained in the semiclassical approximation ($\tilde{\Gamma}$) on the basis of Eq. (9). The values of the Keldysh parameter γ are given on the curves; the scale along the ordinate is logarithmic.

where δ specifies the shift of the level [see Eq. (5)],

$$f(\gamma) = 2\tau_0(1 + \gamma^{-2}) - \gamma^{-2} \sinh(2\tau_0), \quad (10)$$

and τ_0 satisfies the equation

$$\frac{\sinh(2\tau_0)}{\tau_0} - \frac{\sinh^2 \tau_0}{\tau_0^2} = 1 + \gamma^2. \quad (11)$$

We note that the saddle point in the integral in (6) is $u_0 = -i\tau_0$, where τ_0 is the total "imaginary" time of the subbarrier motion of an electron [12]. Under the conditions of applicability of the semiclassical approximation, a large number of ionization channels contribute to the total level width, so that the role of each individual channel is insignificant. As the parameter γ increases, there appears a structure that is associated with the presence of individual ionization channels. One can clearly see this in Fig. 2, which shows $q = \Gamma/\tilde{\Gamma}$ as a function of γ.[2)] It turned out that the regularization according to (8) is inapplicable near the threshold of n-photon ionization—that is, under the condition

$$I + \mathcal{E}^2/2\omega^2 \approx n\omega. \quad (12)$$

Let us discuss reasons for which Zeldovich's method becomes inapplicable as one approaches the threshold of n-photon ionization.

[2)] The results set forth below were partly announced in [14].

Table 2. Comparison of the results produced by two regularization methods

$\gamma = 3, K_0 = 3$					
$\beta = 2$			$\beta = 4$		
α	$\delta \times 10^4$	$\eta \times 10^6$	α	$\delta \times 10^4$	$\eta \times 10^6$
1.0(−4)	8.2194	3.7913	1.0(−6)	8.2034	3.7479
2.5(−5)	8.2139	3.7465	1.0(−7)	8.2111	3.7279
1.56(−6)	8.2124	3.7354	1.0(−8)	8.2119	3.7313
3.91(−7)	8.2120	3.7319	1.0(−9)	8.2120	3.7316
$\alpha \to 0$	8.2120	3.7316	1.0(−10)	8.2120	3.7316
$\gamma = 0.5, K_0 = 1.1$					
$\beta = 2$			$\beta = 4$		
α	$\delta \times 100$	$\eta \times 10$	α	$\delta \times 100$	$\eta \times 10$
3.6(−3)	6.8605	1.1537	1.0(−4)	6.7616	1.1457
2.03(−3)	6.8667	1.1504	1.0(−5)	6.7605	1.1461
9.0(−4)	6.7854	1.1480	1.0(−6)	6.7604	1.1461
2.25(−4)	6.7666	1.1466	1.0(−7)	6.7604	1.1461
$\alpha \to 0$	6.7604	1.1463	1.0(−8)	6.7604	1.1461

Note: Quoted in this table are the relative shifts δ and the relative widths η of a quasistationary level ($\kappa_0 = 1$) according to calculations with the aid of the regulator in (8) at $\beta = 2$ and $\beta = 4$.

4. APPLICABILITY LIMITS OF ZELDOVICH'S METHOD

Let us consider the integral

$$J(\nu) = \int_0^\infty \frac{du}{u^{3/2}}(1 - e^{-i\nu u}) = \sqrt{4i\pi\nu}, \qquad (13)$$

which is a simplified version of that in (6) and which is convergent in the lower half-plane $\mathrm{Im}\nu \le 0$. Introducing regularization according to Zeldovich,

$$J = \lim_{\alpha \to +0} J_\alpha, \qquad (14)$$

$$J_\alpha(\nu) = \int_0^\infty \frac{du}{u^{3/2}}(1 - e^{-(i\nu u + \alpha u^2)}),$$

and performing integration by parts, we obtain

$$J_\alpha(\nu) = \sqrt{4\pi i\nu}\left[d_{1/2}(z) + \frac{1}{2z^2}d_{3/2}(z)\right], \qquad (15)$$

where

$$d_s(z) = z^s \exp(z^2/4)D_{-s}(z), \quad z = \frac{i\nu}{2\alpha}, \qquad (16)$$

and $D_{-s}(z)$ is a Weber parabolic cylinder function. Taking into account the asymptotic behavior [15] of Weber functions for $z \to \infty$, we arrive at ($\nu = \nu_1 + i\nu_2$)

$$J_\alpha(\nu) = \sqrt{4\pi i\nu}\left[1 - \frac{16\alpha}{\nu^2} + \mathrm{sign}(\nu_1)\theta(\nu_2 - |\nu_1|)\frac{i\alpha}{\sqrt{2}\nu^2}e^{-\frac{\nu^2}{4\alpha}}\right], \qquad (17)$$

where $\theta(x)$ is the Heaviside step function. If $\nu_1^2 > \nu_2^2$, then relation (13) follows from the above in the limit $\alpha \to +0$. But if $\nu_2 > |\nu_1|$, the last term in (17) grows exponentially, with the result that $J_\alpha(\nu)$ does not have a finite limit, this being due to the Stokes phenomenon, which is well known in the theory of asymptotic expansions. The expansion in the vicinity of a Stokes line requires a dedicated consideration (in this connection, see [16]).

Thus, we conclude that, for a quasistationary state characterized by a momentum $k = k_1 - ik_2$, Zeldovich's recipe is applicable if

$$|k_1| > k_2; \qquad (18)$$

that is, if the width of the level in question is less than the spacing between this level and the threshold. The last condition, which was not highlighted in [1, 2], is usually satisfied with a rather wide margin. At the

Table 3

$\beta = 2, a = 0.1$				
α	$\mathrm{Im}J_\alpha$			
	$\psi = 0$	$\psi = \pi/8$	$\psi = \pi/4$	$\psi = 3\pi/8$
6.25(−2)	0.3595	0.3505	0.2822	0.1584
1.56(−2)	0.4990	0.5140	0.4407	0.2610
3.91(−3)	0.6580	0.7470	0.7487	0.5341
4.88(−4)	0.7809	0.9318	0.9977	2.0221
6.10(−5)	0.7908	0.9313	1.0440	−3.261(9)
1.53(−5)	0.7917	0.9315	3.0408	4.001(47)
$\alpha \to 0$	0.7919	0.9322	−	−
$\beta = 4, a = 1.0$				
α	$\mathrm{Im}J_\alpha$			
	$\psi = 0$	$\psi = \pi/16$	$\psi = \pi/8$	$\psi = 3\pi/4$
6.25(−2)	2.3598	2.5904	2.7864	2.9084
1.56(−2)	2.5346	2.8482	3.1937	3.9480
3.91(−3)	2.5674	2.8800	3.2611	4.9011
4.88(−4)	2.4965	2.6988	2.7681	−0.3063
6.10(−5)	2.5005	2.7305	2.8520	−5.5047
1.53(−5)	2.5003	2.7333	2.8996	−6.8222(1)
$\alpha \to 0$	2.5003	2.7336	−	−

Note: Given in this table is the imaginary part of the integral in (14) for various values of the argument $\nu = a\exp(i\psi)$ that lie in the upper half-plane of the complex variable ν ($\psi \geq 0$). The boundaries of the region of convergence ($\psi = \pi/4$ at $\beta = 2$ and $\psi = \pi/8$ at $\beta = 4$) are consistent with (19).

same time, there can arise, in dealing with a dynamical Stark effect in a strong field, cases in which the inequality in (18) is violated, with the result that Zeldovich's method becomes inapplicable. In particular, precisely this situation is realized in solving Eq. (4) in the vicinity of ionization thresholds, so that it is impossible to construct, with the aid of Zeldovich's regularization, an analytic continuation of the integral to the region $\mathrm{Im}\epsilon > 0$.

This brings about the question of whether it is advisable to employ, in (14), regulators that decrease faster at infinity—for example, $R_4 = \exp(-\alpha u^4)$. It turns out that this is not so, however. A numerical analysis of solutions to Eq. (14) reveals that, although the rate of convergence in α increases upon going over to the regulator R_4, the region of applicability of the method shrinks: the constraint $k_2 < 0.41|k_1|$ (see Table 3) takes the place of (18). For a regulator of the general form (8), there is convergence within the angle

$$k_2 < |k_1|\tan\frac{\pi}{2\beta}, \qquad \beta > 1, \tag{19}$$

(see Appendix 2). For $\beta \to \infty$—that is, for $R_\infty = \exp(-\alpha e^u)$, for example—regularization is inapplicable for any $k_2 > 0$. As the simplest example, we consider the function

$$F(\nu) = \frac{1}{\nu} = i\int_0^\infty e^{-i\nu u}du, \quad \mathrm{Im}\nu < 0, \tag{20}$$

and an "exponential" regularization of this integral in the form

$$F_\alpha(\nu) = i\int_0^\infty \exp\left[-\left(i\nu u + \alpha e^u\right)\right]du \tag{21}$$
$$= i\alpha^{i\nu}\Gamma(-i\nu, \alpha), \qquad \mathrm{Re}\alpha > 0,$$

where $\Gamma(z, \alpha)$ is an incomplete gamma function. By

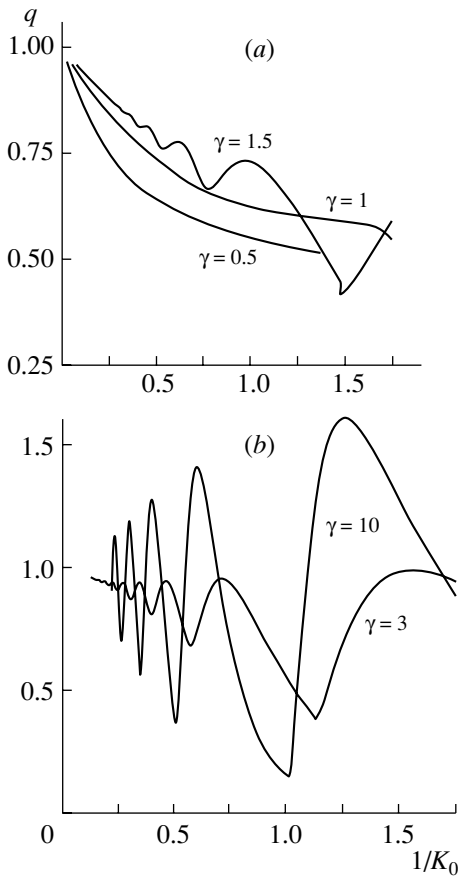

Fig. 2. Ratio $q = \Gamma/\tilde{\Gamma}$ as a function of $1/K_0$ (a) at $\gamma = 1.5$, 1, and 0.5 and (b) at $\gamma = 10$ and 3.

using the expansion [15]

$$\Gamma(-i\nu, \alpha) = \Gamma(-i\nu) - \sum_{n=0}^{\infty} \frac{(-1)^n \alpha^{n-i\nu}}{n!(n-i\nu)}, \qquad (22)$$
$$\nu \neq 0, -i, -2i, \ldots,$$

we find from (21) that

$$F_\alpha(\nu) = \frac{1}{\nu} + i\theta(\mathrm{Im}\nu)\alpha^{i\nu}\Gamma(-i\nu), \qquad (23)$$

whence one can see that the regularization used can be removed only for $\mathrm{Im}\nu < 0$. Thus, an excessive regularization of the integral in (20) does not lead to a solution of the problem at all: the limit of F_α for $\alpha \to +0$ exists only at $\mathrm{Im}\nu < 0$—that is, in the region where the function being considered is specified by the nonregularized integral.

5. CONCLUSION

The regularization method considered above was proposed by Zeldovich as far back as 1960. Although, in atomic and nuclear physics, there were, even at that time, many diversified problems that called for developing a mathematical formalism for the theory of quasistationary states,[3)] attempts at applying Zeldovich's method to specific physics problems were not undertaken, to the best of our knowledge, for a rather long period of time. In all probability, this was because a specific implementation of the procedure for regularizing integrals divergent exponentially at infinity required considerable computational means that were not available at that time. By now, the situation has changed radically: an ordinary PC is sufficient for obtaining the numerical results quoted in the present article. It has been shown above that Zeldovich's method, as well as its natural extension specified by Eq. (8), is quite efficient even beyond perturbation theory. Only upon introducing regularization does the basic Eq. (4) acquire physical meaning. In this connection, it is interesting to draw an analogy with quantum field theory, where amplitudes, matrix elements, and other similar quantities do not have unambiguous physical meaning unless one indicates the way of their regularization. In field theory, however, Feynman integrals suffer from a power-law or a logarithmic divergence, while, in Eqs. (4) and (6), the divergence is exponential. Nonetheless, Zeldovich's method is quite operative in that case as well.

In conclusion, we would like to indicate that problems in which one could employ Zeldovich's regularization method include those of Stark and Zeeman effects in a strong applied field and that of negative-ion photodecay. The equations for the complex-valued energy of a level associated with a delta-function potential in a constant electric and a constant magnetic field were derived in [18, 19]; the analogous equations for the case of crossed fields were obtained in [20]. These equations have a form similar to that in (4), the integrals involved, which are divergent at the upper limit, requiring regularization. The first terms of the expansions of E_r and Γ in a weak field were found in those studies; however, the region of a strong field has yet to be explored. It would be of interest to analyze the possibility of applying Zeldovich's method to these problems.

ACKNOWLEDGMENTS

This work was supported in part by the Russian Foundation for Basic Research (project nos. 00-02-16354, 03-02-17112, and 01-02-16850).

APPENDIX 1

For the shift of a level and its width, Tables 1 and 2 give values that are the limiting ones ($\alpha \to +0$) for Zeldovich's procedure specified by Eqs. (1)

[3)] In this connection, see, for example, [17].

and (8) and which correspond to the final result. In calculating them, we have performed an extrapolation by the formulas

$$f(0) = 3[f(h) - f(2h)] + f(3h),$$

$$f(0) = \frac{1}{3}[8f(h) - 6f(2h) + f(4h)],$$

and

$$f(0) = 4f(h) - 6f(2h) + 4f(3h) - f(4h),$$

whose order of precision is h^2 and h^3. The step h here was chosen in the form $h = \sqrt{\alpha}$, where α is the parameter in (8). We note that this specific choice of extrapolation step is not significant for the convergence of the method.

APPENDIX 2

Here, we will discuss the derivation of condition (19). The normalization integral N, which enters into Zeldovich's perturbation theory, is formed at the upper limit. In view of this, we consider the integral

$$I = \int_0^\infty \exp(2ikr)dr = -\frac{1}{2ik}, \qquad (A.1)$$

which is convergent in the upper half-plane $\mathrm{Im}k > 0$. However, the inequality $\mathrm{Im}k < 0$ always holds for quasistationary states, so that the integral diverges. In order to impart unambiguous meaning to this integral, we consider Zeldovich's procedure, taking a regulator in the form (8):

$$I = \lim_{\alpha\to+0} I_\alpha, \qquad (A.2)$$

$$I_\alpha = \int_0^\infty \exp\{-\alpha r^\beta + 2ikr\}dr.$$

It identically follows that

$$I_\alpha = -\frac{1}{2ik}[1 - \phi(z,\rho)], \qquad (A.3)$$

where

$$\phi(z,\rho) = \int_0^\infty \exp(-t + zt^\rho)dt \qquad (A.4)$$

$$= \sum_{n=0}^\infty \frac{\Gamma(n\rho+1)}{\Gamma(n+1)} z^n,$$

$z = 2ik\alpha^{-\rho}$, and $\rho = 1/\beta$, $0 \le \rho < 1$. In particular, we have $\phi(z,0) = \exp z$ and $\phi(z,1) = (1-z)^{-1}$.

Applying the method of steepest descent to (A.4), we find, apart from a preexponential factor, that

$$\phi(z,\rho) \sim \exp(c_\rho z^{1/(1-\rho)}), \qquad (A.5)$$

with $c_\rho = (1-\rho)\rho^{\rho/(1-\rho)}$, whence one can see that, for $\alpha \to +0$, $\phi \to \infty$ if $\arg z < \frac{\pi}{2}(1-\rho)$ and $\phi \to 0$ if $\arg z > \frac{\pi}{2}(1-\rho)$. Therefore, I_α has the correct limit (A.1) only in the second case, which, in the k plane, corresponds to the angle

$$-\frac{\pi}{2\beta} < \arg k < 0. \qquad (A.6)$$

It can easily be seen that the condition in (A.6) is equivalent to (19). Although this condition was obtained for a particular example, it is of rather general importance, which is confirmed by numerical calculations of the width Γ. In Fig. 2 from [14], characteristic discontinuities on the curves representing $\Gamma(F,\omega)$ correspond to regions in the vicinity of ionization thresholds. Within these, rather narrow, regions, Zeldovich's regularization method is not applicable.

The regularization method proposed in [1] corresponds to $\beta = 2$. In this case, the integral in (A.2) can be calculated exactly. The result is

$$I_\alpha = \frac{1}{2}\sqrt{\frac{\pi}{\alpha}} \exp\left(\frac{k^2}{\alpha}\right) \mathrm{erfc}\left(-\frac{ik}{\sqrt{\alpha}}\right), \qquad (A.7)$$

where $\mathrm{erfc}z = \frac{2}{\sqrt{\pi}}\int_z^\infty \exp(-t^2)dt$. With allowance for the well-known asymptotic formula (see, for example, [15]), we then obtain

$$\lim_{\alpha\to+0} I_\alpha = \begin{cases} -1/(2ik), & -\pi/4 < \arg k < 0, \\ \infty, & \arg k < -\pi/4. \end{cases} \qquad (A.8)$$

In practice, the condition of applicability of Zeldovich's method, $-\pi/4 < \arg k < 0$, is usually satisfied (for $\Gamma \ll E_r$) in all cases, with the exception of the special case of quasistationary states close to the threshold. We note that, in [1, 2], this condition was not indicated explicitly, although it follows from an analysis of the formulas given in [2, p. 323 of the Russian edition] (in all probability, the authors of [2] did not take into account the possibility of a change in the asymptotic behavior of an analytic function upon the traversal of a Stokes line).

As the parameter β grows, the strength of the regulator in (8) becomes greater, but the region of applicability of the regularization method shrinks concurrently [in the limit $\beta \to \infty$, it disappears completely; see formulas (21)–(23)]. To some extent, this resembles the situation that occurs in the theory of divergent series: there exist powerful methods [21] that make it possible to sum individual rapidly divergent series, but they fail when applied to the series $1 - 1 + 1 - 1 + \ldots = 1/2$, which is very weakly divergent.[4)]

[4)] In mathematics, this fact is expressed in terms of theorems of the Tauber type [21].

For the sum s of this series, it is natural to take the limit

$$s = \lim_{x\to 1} \sum_{n=0}^{\infty} (-1)^n x^{\lambda_n}, \qquad (A.9)$$

where $0 < \lambda_0 < \lambda_1 < \lambda_2 < \ldots$ and $\lambda_n \to \infty$ for $n \to \infty$. For $\lambda_n = n$ (Abel's method) and $\lambda_n = n^k$ with $k > 0$, this yields $s = 1/2$. If, however, one chooses a faster increasing sequence, $\lambda_n = a^n$ with $a > 1$, then the sum in (A.9) oscillates for $x \to 1$ without tending to a specific limit (see Subsection 4.10 in [21]), and this situation is quite typical.

REFERENCES

1. Ya. B. Zel'dovich, Zh. Éksp. Teor. Fiz. **39**, 776 (1960) [Sov. Phys. JETP **12**, 542 (1960)].
2. A. I. Baz, Ya. B. Zeldovich , and A. M. Perelomov, *Scattering, Reactions, and Decays in Nonrelativistic Quantum Mechanics* (Nauka, Moscow, 1971; Israel Program for Scientific Translations, Jerusalem, 1966).
3. F. V. Bunkin and A. M. Prokhorov, Zh. Éksp. Teor. Fiz. **46**, 1090 (1964) [Sov. Phys. JETP **19**, 739 (1964)].
4. Ya. B. Zel'dovich, Zh. Éksp. Teor. Fiz. **51**, 1492 (1966) [Sov. Phys. JETP **24**, 1006 (1967)].
5. V. I. Ritus, Zh. Éksp. Teor. Fiz. **51**, 1544 (1966) [Sov. Phys. JETP **24**, 1041 (1967)].
6. I. J. Berson, J. Phys. B **8**, 3078 (1975).
7. N. L. Manakov and L. P. Rappoport, Zh. Éksp. Teor. Fiz. **69**, 842 (1975) [Sov. Phys. JETP **42**, 430 (1975)].
8. L. V. Keldysh, Zh. Éksp. Teor. Fiz. **47**, 1945 (1964) [Sov. Phys. JETP **20**, 1307 (1964)].
9. N. L. Manakov and A. G. Fainshtein, Teor. Mat. Fiz. **48**, 385 (1981).
10. A. I. Nikishov and V. I. Ritus, Zh. Éksp. Teor. Fiz. **50**, 255 (1966) [Sov. Phys. JETP **23**, 168 (1966)].
11. A. M. Perelomov, V. S. Popov, and M. V. Terent'ev, Zh. Éksp. Teor. Fiz. **50**, 1393 (1966) [Sov. Phys. JETP **23**, 924 (1966)].
12. A. M. Perelomov, V. S. Popov, and M. V. Terent'ev, Zh. Éksp. Teor. Fiz. **51**, 309 (1966) [Sov. Phys. JETP **24**, 207 (1967)].
13. S. P. Andreev, B. M. Karnakov, V. D. Mur, and V. A. Polunin, Zh. Éksp. Teor. Fiz. **86**, 866 (1984) [Sov. Phys. JETP **59**, 506 (1984)].
14. V. D. Mur, S. G. Pozdnyakov, V. S. Popov, and S. V. Popruzhenko, Pis'ma Zh. Éksp. Teor. Fiz. **75**, 294 (2002) [JETP Lett. **75**, 249 (2002)].
15. I. S. Gradshtein and I. M. Ryzhik, *Tables of Integrals, Series, and Products* (Fizmatgiz, Moscow, 1962).
16. A. I. Nikishov and V. I. Ritus, Zh. Éksp. Teor. Fiz. **105**, 769 (1994) [JETP **78**, 411 (1994)].
17. A. I. Baz', Appendix in the Russian Translation of E. Titmarsh, *Eigenfunction Expansion Associated with Second-Order Differential Equations* (Inostrannaya Literatura, Moscow, 1961), Vol. II.
18. Yu. N. Demkov and G. F. Drukarev, Zh. Éksp. Teor. Fiz. **47**, 918 (1964) [Sov. Phys. JETP **20**, 614 (1964)].
19. Yu. N. Demkov and G. F. Drukarev, Zh. Éksp. Teor. Fiz. **49**, 257 (1965) [Sov. Phys. JETP **22**, 182 (1966)].
20. Yu. N. Demkov and B. S. Monozon, Zh. Éksp. Teor. Fiz. **61**, 956 (1971) [Sov. Phys. JETP **34**, 509 (1971)].
21. G. H. Hardy, *Divergent Series* (Oxford Univ. Press, Oxford, 1967).

Translated by A. Isaakyan

Physics of Atomic Nuclei, Vol. 66, No. 11, 2003, pp. 1972–1988. From Yadernaya Fizika, Vol. 66, No. 11, 2003, pp. 2022–2038.

ELEMENTARY PARTICLES AND FIELDS
Theory

B-Meson Physics: CP Violation and Semileptonic Decays*

I. M. Narodetskiĭ**

Institute of Theoretical and Experimental Physics,
Bol'shaya Cheremushkinskaya ul. 25, Moscow, 117259 Russia

Received February 11, 2003

Abstract—The paper represents a review of our present knowledge on the phenomenology of weak decays of quarks and their role in the determination of the parameters of the Standard Model. Specifically, we focus on CP violation in B decays and the determination of the Cabibbo–Kobayashi–Maskawa matrix element V_{cb} from exclusive and inclusive semileptonic B decays. We also briefly discuss phenomenological applications concerning the electron energy spectra in inclusive semileptonic B and B_c decays.

1. INTRODUCTION

The goal of B physics is to test precisely the flavor structure of the Standard Model (SM), i.e., the Cabibbo–Kobayashi–Maskawa (CKM) [1] description of quark mixing and CP violation. Flavor physics played an important role in the development of the SM. For a long time, the only experimental evidence for CP violation came from the kaon sector: $|\epsilon_K| = (2.28 \pm 0.02) \times 10^{-3}$, $\epsilon/\epsilon' = (1.73 \pm 0.18) \times 10^{-3}$. The smallness of K^0–$\bar{K}^0$ mixing led to the GIM mechanism and calculation of the c-quark mass before it was discovered [2]. The existence of CP violation in neutral-kaon decay provoked the hypothesis of a third generation before its experimental discovery. The large B^0–$\bar{B}^0$ mixing was the first evidence for a very large top-quark mass. Recently, one has had experimental evidence of CP violation in the B sector: $\sin(2\beta) = 0.75 \pm 0.09_{\rm stat} \pm 0.04_{\rm syst}$ (BaBar Collaboration [3]); $\sin(2\beta) = 0.99 \pm 0.14_{\rm stat} \pm 0.06_{\rm syst}$ (Belle Collaboration [4]).

In this paper, we review the phenomenology of weak decays of heavy quarks. Section 2 is focused on CP violation in B decays. In Section 3, the determination of the V_{cb} matrix element from semileptonic decays of B mesons is reviewed. Some phenomenological applications are considered in Section 4. We do not attempt to give complete references to all related literature. By now, there are excellent lectures and minireviews that cover the subjects in great depth [5–8]. We refer to these for more details and for more complete references to the original literature relevant to Sections 2 and 3.

2. CP VIOLATION IN B MESON DECAYS

The SM provides us with a parametrization of CP violation but does not explain its origin. In fact, CP violation may occur in three sectors of the SM: (i) in the quark sector via the phase of the CKM matrix, (ii) in the lepton sector via the phases of the neutrino mixing matrix, and (iii) in the strong interactions via the parameter $\theta_{\rm QCD}$.

The nonobservation of CP violation in strong interactions is a mystery whose explanation requires physics beyond the SM (such as a Peccei–Quinn symmetry and axions). CP violation in the neutrino sector has not yet been explored experimentally. CP violation in the quark sector has been studied in some detail and is the subject of this section.

2.1. CKM Matrix

The interactions between the quarks and gauge bosons in the SM are illustrated in Fig. 1, where the vertices (a), (b, c), and (d) refer to weak, electromagnetic, and strong interactions, respectively. The vertex for the charged-current interaction, in which quark flavor i changes to j, is depicted in Fig. 1a and has the Feynman rule

$$i\frac{g_2}{2\sqrt{2}}V_{ij}\gamma^\mu(1-\gamma^5), \qquad (1)$$

where g_2 is the coupling constant of the $SU(2)_L$ gauge group and V_{ij} is the ij element of the CKM matrix. Equation (1) illustrates the $V-A$ structure of the charged-current interactions.

Assuming the SM with three generations, the CKM matrix $V_{\rm CKM}$ is a unitary 3×3 one, relating the

*This article was submitted by the author in English.

**e-mail: naro@heron.itep.ru

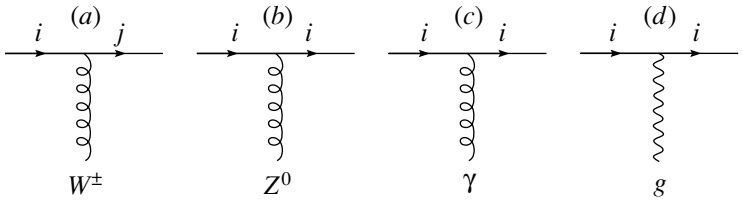

Fig. 1. Quark interactions with gauge bosons. The indices i and j correspond to the different flavors ($i = u, c, t; j = d, s, b$).

weak and mass eigenstates:

$$\begin{pmatrix} d' \\ s' \\ b' \end{pmatrix} = \begin{pmatrix} V_{ud} & V_{us} & V_{ub} \\ V_{cd} & V_{cs} & V_{cb} \\ V_{td} & V_{ts} & V_{tb} \end{pmatrix} \begin{pmatrix} d \\ s \\ b \end{pmatrix}. \qquad (2)$$

The general parametrization of V_{CKM} in terms of four parameters θ_{ij} ($ij = 12, 13, 23$) and δ_{13} recommended by the Particle Data Group [9] is

$$\begin{pmatrix} c_{12}c_{13} & s_{12}c_{13} & s_{13}e^{-i\delta_{13}} \\ -s_{12}c_{23} - c_{12}s_{23}s_{13}e^{i\delta_{13}} & c_{12}c_{23} - s_{12}s_{23}s_{13}e^{i\delta_{13}} & s_{23}c_{13} \\ s_{12}s_{23} - c_{12}c_{23}s_{13}e^{i\delta_{13}} & -c_{12}s_{23} - s_{12}c_{23}s_{13}e^{i\delta_{13}} & c_{23}c_{13} \end{pmatrix}, \qquad (3)$$

where $c_{ij} = \cos\theta_{ij}$ and $s_{ij} = \sin\theta_{ij}$, and δ_{13} is the CP-violating phase parameter.

With only two families, e.g., in a world without beauty (or t quarks), V_{CKM} can always be reduced to a real form, so that CP is necessarily conserved. In case of three families, one can introduce the phase-convention-invariant form

$$\mathrm{Im}(V_{ij}V_{kl}V_{il}^*V_{kj}^*) = J\sum_{m,n=1}^{3}\varepsilon_{ikm}\varepsilon_{jln}, \qquad (4)$$

where J is the Jarlskog invariant [10]:

$$J = c_{12}c_{23}c_{13}^2 s_{12}s_{23}s_{13}\sin\delta_{13}. \qquad (5)$$

CP violation is proportional to J and is not zero if $\delta_{13} \neq 0$.

2.2. Current Experimental Knowledge of the CKM Matrix

Before continuing, we briefly review our current experimental knowledge of each of the CKM magnitudes. The results are taken from the Particle Data Group [9].

First, consider the submatrix describing mixing among the first two generations. The parameter $|V_{ud}|$ is measured by studying the rates for nuclear β decay. Here, the isospin symmetry of the strong interactions is used to control the nonperturbative dynamics, since the operator $\bar{d}\gamma^\mu(1-\gamma^5)u$ is a partially conserved current associated with a generator of chiral $SU(2)_L \times SU(2)_R$. The current data yield

$$|V_{ud}| = 0.9734 \pm 0.0008, \qquad (6)$$

so $|V_{ud}|$ is known at the level of 0.1%. The parameter $|V_{us}|$ is measured via $K \to \pi\ell\bar{\nu}_\ell$ and $\Lambda \to p\ell\bar{\nu}_\ell$. Here, chiral $SU(3)_L \times SU(3)_R$ must be used in the hadronic matrix elements, since a strange quark is involved. Because the m_s corrections are larger, $|V_{us}|$ is only known to 1%:

$$|V_{us}| = 0.2196 \pm 0.0023. \qquad (7)$$

The CKM matrix elements involving the charm quark are not so well measured. One way to extract $|V_{cs}|$ is to study the decay $D \to K\ell^+\nu_\ell$. In this case, there is no symmetry by which one can control the matrix element $\langle K|\bar{s}\gamma^\mu(1-\gamma^5)c|D\rangle$, since flavor $SU(4)$ is badly broken. One is forced to resort to models for these matrix elements. The reported value is

$$|V_{cs}| = 0.996 \pm 0.013. \qquad (8)$$

The error estimate should probably be taken to be substantially larger. An alternative is to measure V_{cs} from inclusive processes at higher energies. For example, one can study the branching fraction for $W^+ \to c\bar{s}$, which can be computed using perturbative QCD. The result of a preliminary analysis is

$$|V_{cs}| = 1.00 \pm 0.13, \qquad (9)$$

consistent with the model-dependent measurement. The error in (9) is largely experimental and is unpolluted by hadronic physics.

Similarly, one extracts $|V_{cd}|$ from deep-inelastic neutrino scattering, using the process $\nu_\mu + d \to c + \mu^-$. This inclusive process may be computed perturbatively in QCD, leading to a result with accuracy at the level of 10%,

$$|V_{cd}| = 0.224 \pm 0.016. \quad (10)$$

The elements of V_{ij} involving the third generation are, for the most part, harder to measure accurately. The branching ratio for $t \to b\ell^+\nu_\ell$ can be analyzed perturbatively, but the experimental data are not very good. If one imposes the unitarity constraint $|V_{td}|^2 + |V_{ts}|^2 + |V_{tb}|^2 = 1$ (see below), the present bound on $|V_{tb}|$ is

$$|V_{tb}| = 0.99 \pm 0.15. \quad (11)$$

There are as yet no direct extractions of $|V_{td}|$ or $|V_{ts}|$. One can use the experimental data for the ratio $\mathrm{BR}(B \to X_s\gamma)/\mathrm{BR}(B \to X_c\ell\nu_\ell)$ and the theoretical prediction for $\mathrm{BR}(B \to X_s\gamma)$ in order to determine directly the combination $|V_{tb}V_{ts}^*|/|V_{cb}|$. In this way, averaging the CLEO and ALEPH data [11, 12], one obtains (for details, see [13])

$$\frac{|V_{ts}^* V_{tb}|}{|V_{cb}|} = 0.93 \pm 0.10, \quad (12)$$

where all the errors were added in quadrature. Using $|V_{tb}|$ from (11) and $|V_{cb}| = (40.6 \pm 1.1) \times 10^{-3}$ extracted from semileptonic B decays (see Section 3), one obtains

$$|V_{ts}| = 0.038 \pm 0.07. \quad (13)$$

This is probably the most direct determination of this CKM matrix element. With an improved measurement of $\mathrm{BR}(B \to X_s\gamma)$ and V_{tb}, one expects to reduce the present error on $|V_{ts}|$ by a factor of 2 or even more.

This leaves us with the matrix elements V_{ub} and V_{cb}, for which we need an understanding of B-meson decay. This issue will be discussed in Section 3.

2.3. The Wolfenstein Parametrization

The parametrization (3) is general, but awkward to use. For most practical purposes, it is sufficient to use the simpler, but approximate, Wolfenstein parametrization [14], which, following the observed hierarchy between the CKM matrix elements, expands the CKM matrix in terms of the four parameters

$$s_{12} = \lambda, \quad s_{23} = A\lambda^2, \quad s_{13}e^{-i\delta_{13}} = A\lambda^3(\rho - i\eta), \quad (14)$$

with λ being the expansion parameter. In terms of these parameters, one obtains the following to $\mathcal{O}(\lambda^6)$ terms inclusive [15]

$$V_{ud} = 1 - \frac{1}{2}\lambda^2 - \frac{1}{8}\lambda^4, \quad V_{us} = \lambda + \mathcal{O}(\lambda^7), \quad (15)$$

$$V_{cd} = -\lambda + \frac{1}{2}A^2\lambda^5[1 - 2(\rho + i\eta)], \quad (16)$$

$$V_{cs} = 1 - \frac{1}{2}\lambda^2 - \frac{1}{8}\lambda^4(1 + 4A^2),$$

$$V_{cb} = A\lambda^2 + \mathcal{O}(\lambda^8), \quad V_{ub} = A\lambda^3(\rho - i\eta), \quad (17)$$

$$V_{ts} = -A\lambda^2 + \frac{1}{2}A\lambda^4[1 - 2(\rho + i\eta)], \quad (18)$$

$$V_{td} = A\lambda^3(1 - \rho - i\eta), \quad V_{tb} = 1 - \frac{1}{2}A^2\lambda^4.$$

The CKM matrix can be written, in the Wolfenstein parametrization, as

$$V_{\mathrm{CKM}} = \begin{pmatrix} 1 - \lambda^2/2 & \lambda & A\lambda^3(\rho - i\eta) \\ -\lambda & 1 - \lambda^2/2 & A\lambda^2 \\ A\lambda^3(1 - \rho - i\eta) & -A\lambda^2 & 1 \end{pmatrix}. \quad (19)$$

The terms that are neglected are of $\mathcal{O}(\lambda^4)$. This parametrization corresponds to a particular choice of phase convention that eliminates as many phases as possible and puts the one remaining complex phase in the matrix elements V_{ub} and V_{td}.

The parameter λ is known with good precision:

$$\lambda = \sin\theta_{12} = 0.2237 \pm 0.0033. \quad (20)$$

The rate of the allowed $b \to c$ decay leads to a determination of the combination $A\lambda^2$:

$$A\lambda^2 = V_{cb} = (41.0 \pm 1.6) \times 10^{-3}. \quad (21)$$

The problem of determining ρ and η is best seen in light of the unitarity relation.

2.4. The Unitarity Triangle

The unitarity of the CKM matrix implies various relations between its elements:

$$\sum_k V_{ij}V_{kj}^* = \delta_{ij}. \quad (22)$$

The *unitarity triangles* are geometrical representations in the complex plane of the six Eqs. (22) with $i \neq k$. It is a trivial fact that any relationship of the form of a sum of three complex numbers equaling zero can be drawn as a closed triangle (see Fig. 2).

All the unitarity triangles have the same area, $J/2$. However, while the triangles have the same area, they

are of very different shapes: e.g., the ds triangle has two sides of order λ and one of order λ^5, while the sb triangle has larger sides of order λ^2 and the small side of order λ^5, giving an angle of order λ^2. It would be very difficult to measure the area of such triangles. This leaves us with the bd triangle corresponding to the relation

$$V_{ub}V_{ud}^* + V_{cb}V_{cd}^* + V_{tb}V_{td}^* = 0. \quad (23)$$

This relation is phenomenologically especially interesting as it simultaneously involves the elements V_{ub}, V_{cb}, and V_{td}, which are under extensive discussion at present. To an excellent accuracy, $V_{cd}^*V_{cb}$ is

$$V_{cd}^*V_{cb} = A\lambda^3 + \mathcal{O}(\lambda^7). \quad (24)$$

Rescale all terms in (23) by $A\lambda^3$ and put the vector $V_{cd}^*V_{cb}$ on the real axis. The coordinates of the remaining vertex correspond to the ρ and η parameters or, in an improved version [15], to $\bar{\rho} = (1 - \lambda^2/2)\rho$ and $\bar{\eta} = (1 - \lambda^2/2)\eta$. The corresponding triangle is shown in Fig. 3.

The angles α, β, and γ (also known as, respectively, ϕ_2, ϕ_1, and ϕ_3) are defined as follows:

$$\alpha = \arg\left(-\frac{V_{td}^*V_{tb}}{V_{ud}^*V_{ub}}\right), \quad (25)$$

$$\beta = \arg\left(-\frac{V_{cd}^*V_{cb}}{V_{td}^*V_{tb}}\right), \quad \gamma = \arg\left(-\frac{V_{ud}^*V_{ub}}{V_{cd}^*V_{cb}}\right).$$

The lengths R_u and R_t are

$$R_u = |\rho + i\eta| = \left|\frac{V_{ud}^*V_{ub}}{V_{cd}^*V_{cb}}\right|, \quad (26)$$

$$R_t = |1 - \rho - i\eta| = \left|\frac{V_{td}^*V_{tb}}{V_{ud}^*V_{ub}}\right|.$$

Since the area of the unitarity triangle is $\eta/2$, a nonflat triangle implies CP violation. The form of the unitarity triangle can be determined by measurements of CP-conserving quantities.

The length of one side, $|\rho + i\eta|$, is extracted from the determination of V_{ub}, e.g., from the rates of the forbidden $b \to u$ semileptonic transitions. The other side, $|1 - \rho - i\eta|$ is proportional to the mass difference $\Delta m_d = m_{B_d^0} - m_{\bar{B}_d^0}$. The latter is determined from the oscillation of B_d^0 mesons, which are dominated by graphs with virtual top quarks (see Fig. 4). These determinations (schematically shown in Fig. 5) point to a nonflat triangle, i.e., to the presence of a certain amount of CP violation.

Recall that, in the SM, the transitions $B_q \to \bar{B}_q$, $q = d, s$, are due to the box diagrams involving two W bosons and two up-type quarks, as is the case for K^0–$\bar{K}^0$ mixing. However, the long-range interactions arising from intermediate virtual states are negligible for the neutral-B-meson systems, because the large B mass is off the region of hadronic resonances. The calculation of the dispersive M_{12} and absorptive Γ_{12} parts of the box diagrams yields the following predictions for the off-diagonal element of the mass and decay matrices [16]:

$$M_{12} = -\frac{G_F^2 m_W^2 \eta_B m_{B_q} B_{B_q} f_{B_q}^2}{12\pi^2} S_0(m_t^2/m_W^2) \times (V_{tq}^*V_{tb})^2, \quad (27)$$

$$\Gamma_{12} = \frac{G_F^2 m_b^2 \eta'_B m_{B_q} B_{B_q} f_{B_q}^2}{8\pi}\left[(V_{tq}^*V_{tb})^2 + V_{tq}^*V_{tb}V_{cq}^*V_{cb}\mathcal{O}\left(\frac{m_c^2}{m_b^2}\right) + (V_{cq}^*V_{cb})^2\mathcal{O}\left(\frac{m_c^4}{m_b^4}\right)\right], \quad (28)$$

where G_F is the Fermi constant, m_W is the W boson mass, m_i is the mass of quark i, and m_{B_q} is the B_q-meson mass. The factor f_{B_q} is the vacuum-to-one-meson matrix element of the axial current, which arises in the naive approximation obtained by splitting the matrix element into two-quark terms and inserting the vacuum state between them. This is known as the vacuum-insertion approximation. The quantity B_{B_q} is simply the correction factor between that approximate answer and the true answer. It can be estimated in various model calculations.

The known function $S_0(x_t)$ can be approximated very well with [17]:

$$S_0(x_t) = 0.784x_t^{0.76}. \quad (29)$$

The QCD corrections η_B and η'_B are on the order of unity. The only nonnegligible contributions to M_{12} and Γ_{12} are from box diagrams involving two top quarks.

Many B^0–$\bar{B}^0$ oscillation analyses have been performed by the different collaborations (for the complete list of references, see [18]). The aim of these analyses is to measure the mass difference

$$\Delta m_d \equiv m_H - m_L, \quad (30)$$

where the H and L stand for heavier and less heavy B mesons. Although a variety of different techniques have been used, the individual Δm_d results obtained at high-energy colliders have remarkably similar precision. Their average is compatible with the recent and more precise measurements from asymmetric B factories. Before being combined, the measurements are adjusted on the basis of a common set of input values, including the b-hadron lifetimes and fractions. Combining all published measurements, the Particle Data Group [9] quotes the value of

$$\Delta m_d = 0.489 \pm 0.005_{\text{stat}} \pm 0.007_{\text{syst}}\ \text{ps}^{-1}. \quad (31)$$

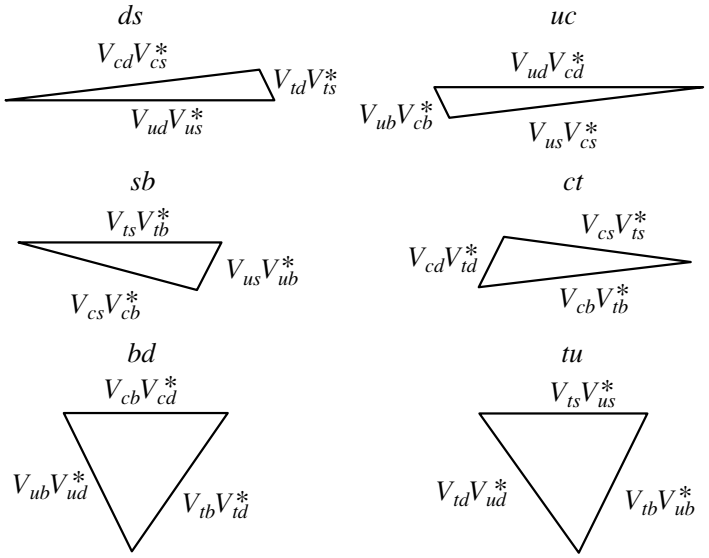

Fig. 2. Six unitarity triangles.

An example of a recent global analysis of the unitarity triangle, combining measurements of $|V_{cb}|$ and $|V_{ub}|$ in semileptonic B decays, $|V_{td}|$ in B–$\bar{B}$ mixing, and the CP-violating phase of V_{td}^2 in K–$\bar{K}$ mixing and $B \to J/\psi K$ decays, is given, e.g., in [19]. The values obtained at 95% confidence level are

$$\bar{\rho} = 0.21 \pm 0.12, \quad \bar{\eta} = 0.38 \pm 0.11. \tag{32}$$

The corresponding results for the angles of the unitarity triangle are

$$\sin(2\beta) = 0.74 \pm 0.14, \tag{33}$$
$$\sin(2\alpha) = -0.14 \pm 0.57, \quad \gamma = 62^\circ \pm 15^\circ.$$

These studies have established the existence of the CP-violating phase in the top sector of the CKM matrix, i.e., the fact that $\mathrm{Im}(V_{td}^2) \propto \bar{\eta} \neq 0$.

2.5. sin(2β) Measurements

The parameter $\sin(2\beta)$ is directly accessible through a study of CP violation in the "golden decay mode" of B^0 mesons,

$$(B_d^0 \text{ or } \bar{B}_d^0) \to J/\psi K_S. \tag{34}$$

The "golden" character of $B_d^0 \to J/\psi K_S$ derives from the fact that the final state is a CP eigenstate and that this decay mode is dominated by a CP-conserving tree diagram. Any CP violation observed in this mode must, to an excellent approximation, be attributed to B_d^0–$\bar{B}_d^0$ mixing. As stated above, the transitions B_d^0–$\bar{B}_d^0$ are described, in the lowest order, by a single box diagram involving two W bosons and two up-type quarks. The phase of the box diagram is easily seen to be $\exp(2i\beta)$. Therefore, measurement of CP-violation effects in this decay mode can be directly interpreted as a measurement of the β angle in the unitarity triangle.

In decays of neutral B mesons into a CP eigenstate f_{CP}, an observable CP asymmetry can arise from the interference of the amplitudes for decays with and without B–$\bar{B}$ mixing, i.e., from the fact that the amplitudes for $B^0 \to f_{CP}$ and $B^0 \to \bar{B}^0 \to f_{CP}$ must be added coherently. The resulting time-

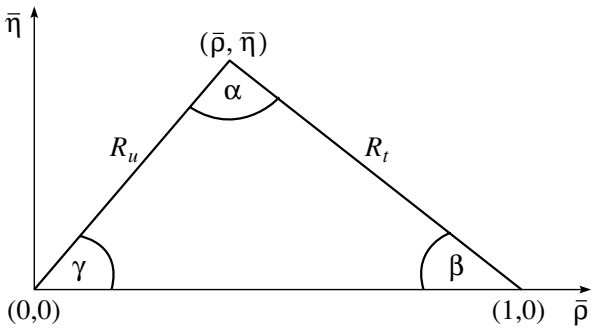

Fig. 3. Unitarity triangle corresponding to Eq. (23).

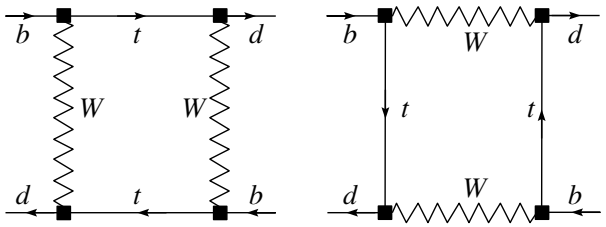

Fig. 4. SM box diagrams including B^0–$\bar{B}^0$ mixing.

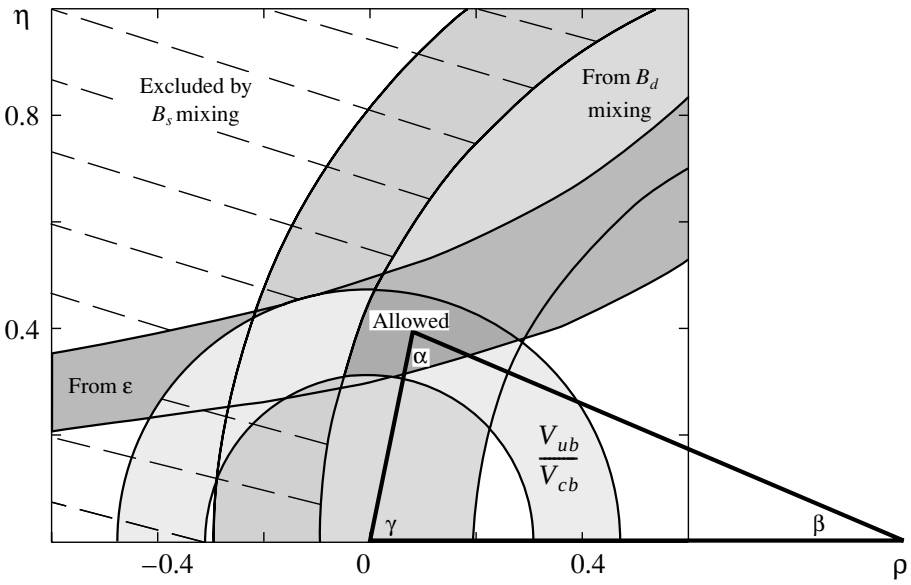

Fig. 5. Schematic determination of the unitarity triangle.

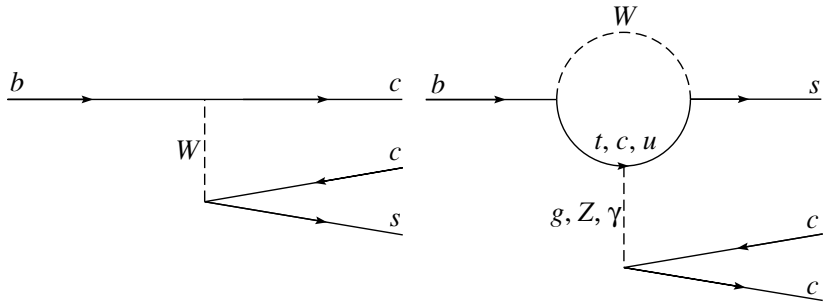

Fig. 6. Tree and penguin topologies in $B \to J/\psi K_S$ decays.

dependent asymmetry is given by

$$A_{CP}(t) = \frac{\Gamma(\bar{B}^0(t) \to f_{CP}) - \Gamma(B^0(t) \to f_{CP})}{\Gamma(\bar{B}^0(t) \to f_{CP}) + \Gamma(B^0(t) \to f_{CP})} \tag{35}$$

$$= \frac{2\mathrm{Im}(\hat{\lambda})}{1+|\hat{\lambda}|^2}\sin(\Delta m_d t) - \frac{1-|\hat{\lambda}|^2}{1+|\hat{\lambda}|^2}\cos(\Delta m_d t),$$

where

$$\hat{\lambda} = e^{i\phi_d}\bar{A}/A, \tag{36}$$

ϕ_d being the B–$\bar{B}$ mixing phase (which in the SM equals -2β) and $A(\bar{A})$ denoting the $B^0(\bar{B}^0) \to f_{CP}$ decay amplitude. If the amplitude is dominated by a single weak phase ϕ_A, then $|\hat{\lambda}| \simeq 1$ and

$$A_{CP}(t) \simeq \eta_{f_{CP}} \sin(\phi_d - 2\phi_A)\sin(\Delta m_d t), \tag{37}$$

where $\eta_{f_{CP}} = \pm 1$ is the CP signature of the final state.

The decay $B \to J/\psi K_S$ (for which $\eta_{J/\psi K_S} = -1$) is based on $b \to c\bar{c}s$ transitions, which in the SM can proceed via tree or penguin topologies, as shown in Fig. 6. To an excellent approximation, the decay amplitude for this process is real. A weak phase is introduced only through components of the up- and top-quark penguin diagrams that are strongly CKM suppressed. Parametrically, the "penguin pollution" to the weak phase from these effects is of order

$$\phi_A \sim \lambda^2(P/T) \sim 1\%, \tag{38}$$

where $P/T \sim 0.2$ is the tree-to-penguin ratio. Then, neglecting ϕ_A, one obtains

$$A_{CP}(t) \simeq \sin(2\beta)\sin(\Delta m_d t) \tag{39}$$

with an accuracy of about 1%.

The results obtained by the Belle and BaBar experiments are in reasonable agreement between themselves. Combining the Belle and BaBar results with earlier measurements by CDF at Fermilab ($0.79^{+0.41}_{-0.44}$) and ALEPH and OPAL at CERN

$(0.84^{+0.82}_{-1.04} \pm 0.16)$ gives the "world average"

$$\sin(2\beta_{J/\psi K_S}) = 0.734 \pm 0.054. \quad (40)$$

The discovery of CP violation in the B system, as reported by the BaBar and Belle Collaborations, is a triumph for the SM. There is now compelling evidence that the phase of the CKM matrix correctly explains the pattern of CP-violating effects in mixing and weak decays of kaons and charm and beauty hadrons. Specifically, the CKM mechanism explains why CP violation is a small effect in $K-\bar{K}$ mixing (ϵ_K) and $K \to \pi\pi$ decays (ϵ'/ϵ), why CP-violating effects in tree level D decays are below the sensitivity of present experiments, and why CP violation is small in $B-\bar{B}$ mixing (ϵ_B) but large in the interference of mixing and decay in $B \to J/\psi K_S$ ($\sin(2\beta_{J/\psi K})$).

The significance of the $\sin(2\beta_{J/\psi K})$ measurement is that, for the first time, a large CP asymmetry has been observed, proving that CP is not an approximate symmetry of nature. Rather, the CKM phase is, very likely, the dominant source of CP violation in low-energy flavor-changing processes. This opens a new era in which the model is expected to be scrutinized through a variety of other B and B_s decay asymmetries. Impressive progress has already been made in search for asymmetries in several hadronic B decays, including $B^0 \to \pi^+\pi^-$, $B^{0,\pm} \to K\pi$, and $B^\pm \to DK^\pm$. Current measurements are approaching the level of tightening bounds on the CP-violating phase γ. These and forthcoming measurements of B_s decays will enable a cross-check of the CKM model.

3. V_{cb} DETERMINATION

As discussed in Section 2, $|V_{cb}|$ sets the overall scale for the lengths of the sides, and $|V_{ub}|$ determines the length of one side. Precise determinations of both are needed to complement the measurement of the angles of the unitarity triangle. These matrix elements are measured from semileptonic B decays. In this section, we will discuss exclusive semileptonic decays of B mesons, in which the b quark decays into a c quark, and from which one can determine the $|V_{cb}|$ elements of the CKM matrix. In principle, $|V_{cb}|$ can be studied in any weak decay mediated by the W boson. Semileptonic decays offer the advantage that the leptonic current is calculable and QCD complications only arise in the hadronic current. Unlike hadronic decays, there are no final-state interactions. One still needs some understanding of the strong interaction. Some approaches offer detailed predictions for the QCD dynamics in heavy-quark decays. These predictions allow measurement of $|V_{cb}|$ with reasonable precision.

3.1. $B \to D^*\ell\nu$ and $B \to D\ell\nu$ Decays

The exclusive $|V_{cb}|$ determination is obtained through studying $B \to D^*\ell\nu$ and $B \to D\ell\nu$ decays. These decays have been studied in experiments performed at the $\Upsilon(4S)$ c.m. energy (CLEO [20], Belle [21]) and at the Z^0 c.m. energy at LEP (ALEPH [22], DELPHI [23], and OPAL [24]).

3.1.1. Kinematics. The hadronic form factors for semileptonic decays are defined as the Lorentz-invariant functions arising in the covariant decomposition of matrix elements of the vector and axial currents. It is conventional to parametrize these matrix elements by a set of scalar form factors. The most appropriate to the heavy-quark limit is the set of form factors $h_i(w)$, which are defined separately for the vector and axial currents:

$$\langle D(v')|\bar{c}\gamma^\mu b|B(v)\rangle = h_+(w)(v+v')^\mu + h_-(w)(v-v')^\mu, \quad (41)$$

$$\langle D(v')|\bar{c}\gamma^\mu\gamma^5 b|B(v)\rangle = 0, \quad (42)$$

$$\langle D^*(v',\epsilon)|\bar{c}\gamma^\mu b|B(v)\rangle = h_V(w)i\varepsilon^{\mu\nu\alpha\beta}\epsilon^*_\nu v'_\alpha v_\beta, \quad (43)$$

$$\langle D(v')|\bar{c}\gamma^\mu\gamma^5 b|B(v)\rangle = h_{A_1}(w)(w+1)\epsilon^{*\mu} - \epsilon^* v[h_{A_2}(w)v^\mu + h_{A_3}(w)v'^\mu], \quad (44)$$

where meson states are denoted as $|P(v)\rangle$ for a pseudoscalar state and $|V(v,\varepsilon)\rangle$ for a vector state, where v is the 4-velocity of a state and ε is the polarization vector, and $w = v \cdot v'$ is the velocity transfer which is linearly related to q^2, the invariant mass of W. Other linear combinations are also found in the literature.

In the case of heavy-to-heavy transitions, in the limit in which the active quarks have infinite mass, all the form factors are given in terms of a single function $\mathcal{F}(w)$, the Isgur–Wise form factor [25]:

$$h_+(w) = h_V(w) = h_{A_1}(w) = h_{A_3}(w) = \mathcal{F}(w), \quad h_-(w) = h_{A_2}(w) = 0. \quad (45)$$

In the realistic case of finite quark masses, these relations are modified: each form factor depends separately on the dynamics of the process.

3.1.2. The decay $B \to D^*\ell\nu$ in heavy-quark effective theory (HQET). HQET (see, e.g., [26]) predicts that the differential partial decay width for $B \to D^*\ell\nu$, $d\Gamma/dw$, is related to V_{cb} through an equation

$$\frac{d\Gamma}{dw}(B \to D^*\ell\nu) = \frac{G_F^2|V_{cb}|^2}{48\pi^3}\mathcal{K}(w)\mathcal{F}^2_{D^*}(w), \quad (46)$$

where $\mathcal{K}_{D^*}(w)$ is a known phase-space factor

$$\mathcal{K}(w) = (m_B - m_{D^*})^2 m^3_{D^*}\sqrt{w^2-1}(w+1)^2 \quad (47)$$

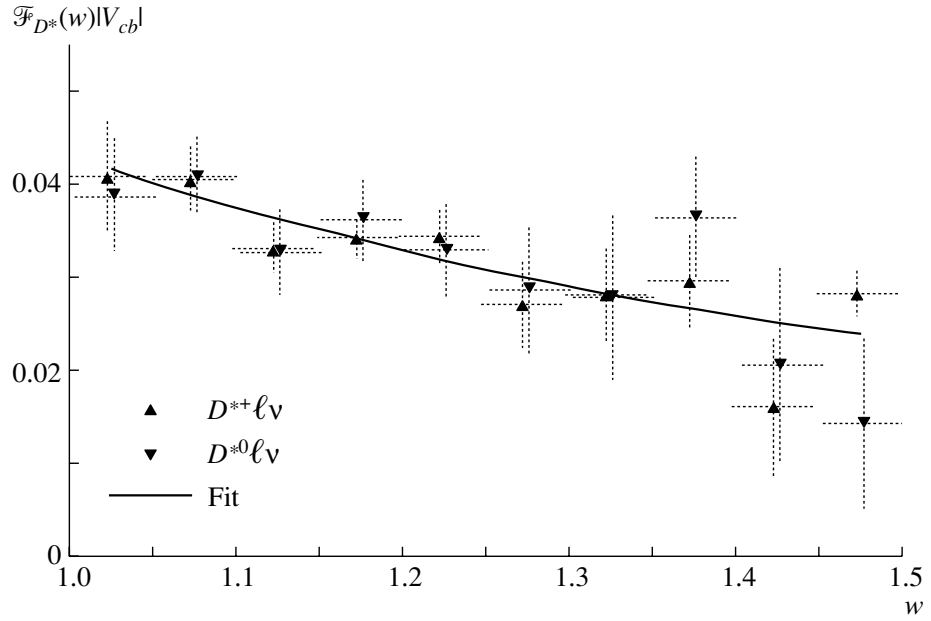

Fig. 7. Overlay of $\mathcal{F}_{D^*}(w)|V_{cb}|$, where the points are $B \to D^*\ell\nu$ data [8].

$$\times \left[1 + \frac{4w}{w+1}\frac{m_B^2 - 2wm_Bm_{D^*} + m_{D^*}^2}{(m_B - m_{D^*})^2}\right].$$

The function $\mathcal{F}_{D^*}(w)$ is the form factor for the B to D^* transition, i.e., the Isgur–Wise function combined with perturbative and power corrections.

The precision with which V_{cb} can be extracted is limited by the theoretical uncertainties in the evaluation of these corrections. In the infinite quark mass limit at the kinematical point, where D^* is at rest in the B rest frame, the wave function overlap is 1, i.e., $\mathcal{F}_{D^*}(1) = 1$. There are several different corrections to the infinite mass value $\mathcal{F}_{D^*}(1) = 1$:

$$\mathcal{F}_{D^*}(1) = \eta_{\rm QED}\eta_A\left[1 + \delta_{1/m_Q^2} + \ldots\right], \quad Q = c, b. \tag{48}$$

The correction $\mathcal{O}(1/m_Q)$ vanishes by virtue of Luke's theorem [27]. QED corrections $\eta_{\rm QED} \approx 1.007$, up to leading logarithms. QCD radiative corrections to two loops give $\eta_A = 0.960 \pm 0.007$. Different estimates of the $1/m_Q^2$ corrections yield

$$1 + \delta_{1/m_Q^2} = 0.91 \pm 0.04. \tag{49}$$

The analytical expression of $\mathcal{F}_{D^*}(w)$ is not known a priori, and this introduces an additional uncertainty in the determination of $\mathcal{F}_{D^*}(1)|V_{cb}|$. In an experiment, one measures the decay rate as function of w and extrapolates to $w = 1$. As the kinematically allowed range of w is small ($w \in [1.0, 1.5]$), the form factor is approximated as a Taylor expansion around $w = 1$:

$$\mathcal{F}_{D^*}(w) = \mathcal{F}_{D^*}(1)(1 + (w-1)\rho^2 + c(w-1)^2). \tag{50}$$

Figure 7 shows the latest CLEO measurement [20] of $\mathcal{F}_{D^*}|V_{cb}|$ as a function of w. The results of the fits of the latest experiments are given in Table 1. Averaging the data, one gets

$$\mathcal{F}_{D^*}(1)|V_{cb}| = (38.3 \pm 1.0) \times 10^{-3}. \tag{51}$$

This gives the most updated value quoted from [8]

$$|V_{cb}| = (42.1 \pm 1.1_{\rm exp} \pm 1.9_{\rm th}) \times 10^{-3}. \tag{52}$$

3.2. $B \to D\ell\nu$

The decay $B \to D\ell\nu$ can be analyzed in the same way as $B \to D^*\ell\nu$ decay. The differential decay rate for $B \to D\ell\nu$ decay is

$$\frac{d\Gamma}{dw} = \frac{G_{\rm F}^2|V_{cb}|^2}{48\pi^3}(m_B + m_D)^2 \tag{53}$$

Table 1. Experimental results after the correction to common inputs and world average (for details, see [8]); ρ^2 is the slope of the form factor at zero recoil as defined in (50)

Experiment	$\lvert V_{cb}\rvert \times 10^3$	ρ^2
CLEO [20]	$43.3 \pm 1.3 \pm 1.8$	$1.61 \pm 0.09 \pm 0.21$
Belle [21]	$36.0 \pm 1.9 \pm 1.8$	$1.45 \pm 0.16 \pm 0.20$
ALEPH [22]	$33.8 \pm 2.1 \pm 1.6$	$0.74 \pm 0.25 \pm 0.41$
DELPHI [23]	$36.1 \pm 1.4 \pm 2.5$	$1.42 \pm 0.14 \pm 0.37$
OPAL [24]	$38.5 \pm 0.9 \pm 1.8$	$1.35 \pm 0.12 \pm 0.31$

$$\times m_D^3(w^2-1)^{3/2}\mathcal{F}_D^2(w),$$

where we assume different form factors $\mathcal{F}_D(w)$. The precision with which $|V_{cb}|$ can be determined is not as good because of a smaller branching fraction, larger backgrounds, and an additional kinematic suppression factor w^2-1 [compare Eqs. (47) and (53)]. Nonetheless, it provides complementary information and provides a test of HQET predictions for the relationships between the form factors for semileptonic decays $B \to D$ and $B \to D^*$.

Theoretical predictions for $\mathcal{F}_D(1)$ are consistent: 1.03 ± 0.07 [28] and 0.98 ± 0.7 [29]. A quenched lattice calculation gives $\mathcal{F}_D(1) = 1.058^{+0.020}_{-0.017}$ [30]. Using $\mathcal{F}_D(1) = 1.0 \pm 0.07$, the Particle Data Group [9] quotes the value

$$|V_{cb}| = (41.3 \pm 4.0_{\rm exp} \pm 2.9_{\rm th}) \times 10^{-3}, \qquad (54)$$

consistent with (52). CLEO has also measured $b \to u\ell\nu$ decays, which are sensitive to $|V_{ub}|$. Experimentally, such measurements are difficult due to large backgrounds from the CKM-favored $b \to c\ell\nu$ decays.

3.3. Inclusive Semileptonic Decays

Alternatively, $|V_{cb}|$ can be extracted from measuring inclusive semileptonic decay $B \to X_c\ell\nu$. For beauty hadrons with $m_b \gg \Lambda_{\rm QCD}$ or $\bar{\Lambda}$, where $\Lambda_{\rm QCD}$ is a QCD scale and $\bar{\Lambda}$ is a QCD related scale of order of 400 MeV [see Eq. (58) below], one can use an operator product expansion (OPE) [31] combined with HQET [26]. The spectator model decay rate is the leading term in an OPE expansion controlled by the parameter $\bar{\Lambda}/m_b$. Nonperturbative corrections to the leading approximation arise only to order $1/m_b^2$. The key issue in this approach is the ability to separate nonperturbative corrections, which can be expressed as a series in powers of $1/m_b$, and perturbative corrections, expressed in powers of α_s. Quark–hadron duality is an important ab initio assumption in these calculations [32]. An unknown correction may be associated with this assumption [33]. Arguments supporting a possible sizeable source of errors related to the assumption of quark–hadron duality have been proposed [34]. This issue needs to be resolved with further measurements.

The OPE result for inclusive decay width $\Gamma_{\rm SL}$ reads

$$\Gamma_{\rm SL} = \frac{G_{\rm F}^2 m_b^5}{192\pi^3}\left(1 - a_1\frac{\alpha_s}{\pi} - a_2\left(\frac{\alpha_s}{\pi}\right)^2 + \dots\right) \qquad (55)$$
$$\times\left(\left(1+\frac{\lambda_1}{2m_b^2}\right)f(\rho) + \frac{\lambda_2}{2m_b^2}g(\rho) + \dots\right),$$

where α_s is the QCD coupling constant; $a_1 = 1.54$ and $a_2 = 1.43\beta_0$ (β_0 is the beta function) are coefficients of the perturbative expansion; $m_b(\mu)$ and $m_c(\mu)$ are short-scale quark masses (in particular, $m_b(\mu \sim 1\ {\rm GeV}) = 4.58 \pm 0.09\ {\rm GeV}$); and $f(\rho)$ and $g(\rho)$ are known as parton phase-space factors,

$$f(\rho) = 1 - 8\rho + 8\rho^3 - \rho^4 - 12\rho^2\log\rho, \qquad (56)$$

$$g(\rho) = -9 + 24\rho - 72\rho^2 + 72\rho^3 \qquad (57)$$
$$- 15\rho^4 - 36\rho^2\log\rho,$$

with $\rho = m_c^2/m_b^2$.

The parameters λ_1 and λ_2 are matrix elements of the HQET expansion, which have the following intuitive interpretations: λ_1 is proportional to the kinetic energy of the b quark in the B meson and λ_2 is the energy of the hyperfine interaction of the b quark spin and the light degrees of freedom in the meson. The third HQET parameter, $\bar{\Lambda}$, representing the energy of the light degrees of freedom, is introduced to relate the b-quark and B-meson masses through the expression

$$m_b = \bar{m}_B - \bar{\Lambda} + \frac{\lambda_1}{2m_b}, \qquad (58)$$

where $\bar{m}_B$ is the spin-averaged B-meson mass

$$\bar{m}_B = \frac{1}{4}(m_B + 3m_{B^*}) \qquad (59)$$

($\bar{m}_B = 5.313\ {\rm GeV}$). A similar relationship holds between the c-quark mass m_c and the spin-averaged charm-meson mass ($\bar{m}_D = 1.975\ {\rm GeV}$).

The parameter λ_2 can be extracted from the B^*-B mass splitting and found to be

$$\lambda_2 = 0.128 \pm 0.010\ {\rm GeV}^2, \qquad (60)$$

whereas the other parameters need more elaborate measurements. The aim of the new inclusive analyses is to determine λ_1 and $\bar{\Lambda}$ from experiment and thereby decrease the theoretical uncertainty which comes when extracting $|V_{cb}|$ from $\Gamma_{\rm SL}$.

The first stage of this experimental program has been completed recently. The CLEO collaboration has measured the shape of the photon spectrum in $b \to s\gamma$ inclusive decays [35]. Its first moment, giving the average energy of the γ emitted in this transition, is related to the b-quark mass. This corresponds to the measurement of the parameter

$$\bar{\Lambda} = +0.35 \pm 0.07 \pm 0.10\ {\rm GeV}. \qquad (61)$$

For semileptonic decays $B \to X_c\ell\nu$, two methods to determine $\bar{\Lambda}$ and λ_1 are known. The first method measures the first and second hadronic mass moments. The second method uses the measured shape

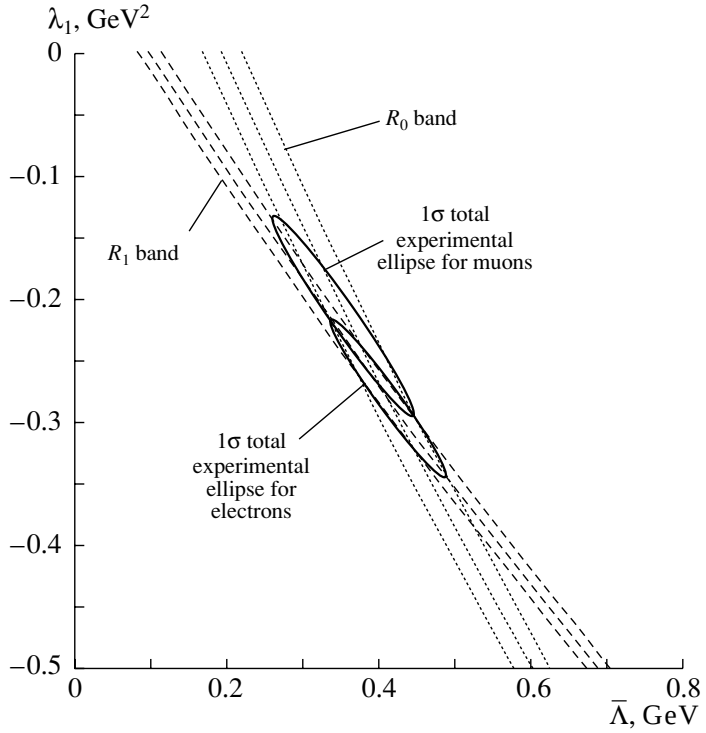

Fig. 8. Constraints on the HQET parameters λ_1 and $\bar{\Lambda}$ from measurements of the moments R_0 and R_1 [37].

of the lepton ($\ell = e, \mu$) energy spectrum to determine $\bar{\Lambda}$ and λ_1, through its energy moments, which are also predicted by HQET. The truncated moments with a lepton momentum cut $p_\ell = 1.5$ GeV

$$R_0 = \frac{\int\limits_{1.7} (d\Gamma_{\rm SL}/dE)dE}{\int\limits_{1.5} (d\Gamma_{\rm SL}/dE)dE}, \qquad (62)$$

$$R_1 = \frac{\int\limits_{1.5} E(d\Gamma_{\rm SL}/dE)dE}{\int\limits_{1.5} (d\Gamma_{\rm SL}/dE)dE} \qquad (63)$$

(E is the lepton energy) are employed to decrease sensitivity of the measurement to the secondary leptons from the cascade decays $b \to c/d\ell\nu$. The theoretical expressions for these moments [36] are evaluated by integrating over the lepton energy in the decay $b \to c\ell\bar{\nu}$ for the dominant Γ_c component. Constraints on $\bar{\Lambda}$ and λ_1 obtained from the CLEO measurements of R_0 and R_1 [37] are shown in Fig. 8. They correspond to

$$\bar{\Lambda} = 0.39 \pm 0.03_{\rm stat} \pm 0.06_{\rm syst} \pm 0.12_{\rm th}\ \text{GeV}, \quad (64)$$
$$\lambda_1 = -0.25 \pm 0.02_{\rm stat} \pm 0.05_{\rm syst} \pm 0.14_{\rm th}\ \text{GeV}.$$

Using the expression of the full semileptonic decay width given in Eq. (55), one can extract $|V_{cb}|$. For $\Gamma_{\rm SL}^{\rm exp} = (0.43 \pm 0.01) \times 10^{-10}$ MeV [8], assuming the validity of quark–hadron duality,

$$|V_{cb}| = (40.8 \pm 0.5_{\Gamma_{\rm SL}} \pm 0.4_{\lambda_1,\bar{\Lambda}} \pm 0.9_{\rm th}) \times 10^{-3}, \qquad (65)$$

where the first uncertainty is from the experimental value of the semileptonic width, the second uncertainty is from the HQET parameters (λ_1 and $\bar{\Lambda}$), and the third uncertainty is the theoretical one. Nonquantified uncertainties are associated with a possible quark–hadron duality violation.

3.4. Conclusions

At present, our knowledge of λ_1 and $\bar{\Lambda}$ limits the precision that we can achieve from inclusive semileptonic B decays. The aim of the new inclusive analyses is to determine λ_1 and $\bar{\Lambda}$ from experiment and thereby decrease the theoretical uncertainty that comes when extracting $|V_{cb}|$ from $\Gamma_{\rm SL}$. Each analysis alone provides two constraints, allowing a measurement of $\bar{\Lambda}$ and λ_1. Combining the two analyses overconstrains the theory parameters, thus allowing a test of the theoretical framework and experimental understanding of b-quark decays.

While experimental errors have reached a 1–2% level, the dominant uncertainties remain of theoretical

origin. High-precision tests of HQET, checks on possible violations of quark–hadron duality in semileptonic decays, and experimental determination of m_b, $m_b - m_c$, and λ_1 are needed to complete this challenging experimental program.

4. ELECTRON SPECTRA IN $B \to X_c \ell \nu$

Electron energy spectra in inclusive $B \to X_c \ell \nu$ decays can also be treated using OPE. The result (away from the endpoint of the spectrum) is that the inclusive differential decay width $d\Gamma/dE$ may be expanded in $\bar{\Lambda}/m_b$. The leading term (zeroth order in $\bar{\Lambda}/m_b$) is the free-quark decay spectrum, the subleading term vanishes, and the subsubleading term involves parameters from the heavy-quark theory, but should be rather small, as it is of order $(\Lambda/m_b)^2$.

However, the calculation of the lepton energy spectrum in OPE shows the appearance of singular distributions $\delta^{(n)}(E - m_b/2)$ near the endpoint, where $E = m_b/2$. The nonadequacy of the approach is also evident from the fact that, although $m_b/2$ is the largest lepton energy available for a free-quark decay, the physical endpoint corresponds to $E = m_B/2$. In these windows, bound-state effects, due to the Fermi motion of the heavy quark, become important and the $1/m_b$ expansion has to be replaced by an expansion in twist. To describe this region, one has to introduce a so-called shape function [38, 39], which, in principle, introduces a hadronic uncertainty. This is quite analogous to what happens for the structure function in deep-inelastic scattering in the region where the Bjorken variable $x_{\rm B} \to 1$. A model-independent determination of the shape function is not available at the present time; therefore, a certain model dependence in this region seems to be unavoidable unless lattice data become reasonably precise.

Two phenomenological approaches have been applied to describe strong interaction effects in the inclusive weak decays: the parton ACM model [40] amended to include the motion of the heavy quark inside the decaying hadron, and the "exclusive model" based on the summation of different channels, one by one [41]. The various light-front (LF) approaches to consideration of the inclusive semileptonic transitions were suggested in [42–45]. In [42, 43], the infinite momentum frame prescription $p_b = xP_B$ and, correspondingly, the floating b-quark mass $m_b^2(x) = x^2 M_B^2$ have been used. The transverse b-quark momenta were consequently neglected. In [45], the b-quark was considered as an on-mass-shell particle with the definite mass m_b, and the effects arising from the b-quark transverse motion in the $\bar{B}$ meson were included. The corresponding ansatz of [45] reduces to a specific choice of primordial LF distribution function $|\psi(\xi, p_\perp^2)|^2$, which represents the probability of finding the b quark carrying an LF fraction ξ and a transverse momentum squared $p_\perp^2 = |\mathbf{p}_\perp|^2$. As a result, a new parton-like formula for the inclusive semileptonic $b \to c, u$ width has been derived [45], which is similar to the one obtained by Bjorken *et al.* [46] in case of infinitely heavy b and c quarks.

4.1. ACM Model

The ACM model was originally developed to consider in detail the endpoint of the lepton spectrum in order to estimate a systematic error in modeling the full spectrum. It incorporates some of the corrections related to the fact that the decaying b quark is not free, but in a bound state. It was explicitly constructed to avoid mention of the b-quark mass. The model is extensively used in the analysis of the lepton energy spectrum in semileptonic decays. It reproduces very well numerically the shape of the semileptonic spectra, at least in their regular part.

The model treats the B meson with the mass m_B as consisting of the heavy b quark plus a spectator with fixed mass $m_{\rm sp}$; the latter usually represents a fitting parameter. The spectator quark has a momentum distribution $\Phi(\mathbf{p}^2)$ ($\mathbf{p}$ is its three-dimensional momentum). The momentum distribution is usually taken to be Gaussian: it is normalized so that

$$\int \Phi(\mathbf{p}^2) p^2 dp = 1. \tag{66}$$

The decay spectrum is determined by the kinematic constraints on the b quark. The energy-momentum conservation in the B-meson vertex implies that the b-quark energy

$$E_b = m_B - \sqrt{\mathbf{p}^2 + m_{\rm sp}^2}; \tag{67}$$

thus, the b quark cannot possess a definite mass. Instead, one obtains a "floating" b-quark mass

$$(m_b^f)^2 = m_B^2 + m_{\rm sp}^2 - 2m_B\sqrt{\mathbf{p}^2 + m_{\rm sp}^2}, \tag{68}$$

which depends on $\mathbf{p}^2$. The lepton spectrum is first obtained from the spectrum $d\Gamma_b^{(0)}(m_b^f, E)/dE$ of the b quark of invariant mass m_b^f (in the b-quark rest frame),

$$\frac{d\Gamma_b^{(0)}(m_b^f, E)}{dE} = \frac{G_{\rm F}^2 m_b^4}{48\pi^3}\frac{x^2(x_{\max} - x)^2}{(1-x)^3} \times [(1-x)(3-2x) + (1-x_{\max})(3-x)], \tag{69}$$

with $x = 2E_e/m_b$, $x_{\max} = 1 - \rho$, and $\rho = m_c^2/m_b^2$, then boosting back to the rest frame of the B meson

and averaging over the weight function $\Phi(\mathbf{p}^2)$:

$$\frac{d\Gamma_B}{dE} = \int\limits_0^{p_{\max}} dp p^2 \Phi(\mathbf{p}^2) \frac{(m_b^f)^2}{2pE_b} \int\limits_{E_-}^{E_+} \frac{dE'}{E'} \frac{d\Gamma_b^{(0)}(m_b^f, E')}{dE'}, \tag{70}$$

where E_b is given by (67), and the perturbative corrections are neglected for the moment. In Eq. (70),

$$p_{\max} = \frac{m_B}{2} - \frac{m_c^2}{2m_B - 4E}, \quad E_\pm = \frac{Em_b^f}{E_b \mp |\mathbf{p}|}. \tag{71}$$

In fact, the upper limit of integration in (70) is not E_+ but $\min(E_+, E_{\max})$, where

$$E_{\max} = \frac{m_B - m_{\rm sp}}{2} \left(1 - \frac{m_c^2}{(m_B - m_{\rm sp})^2}\right). \tag{72}$$

These expressions conclude the kinematical analysis in the ACM model.

4.2. B Meson on the Light Front

Similar to the ACM model, the LF quark model, treats the beauty meson as consisting of the heavy b quark plus a spectator quark. Both quarks have fixed masses, m_b and $m_{\rm sp}$, though. This is at variance with the ACM model, which has been introduced in order to avoid the notion of the heavy-quark mass at all. The calculation of the distribution over lepton energy in the LF approach does not require any boosting procedure but, instead, is based on the standard Lorentz-invariant kinematical analysis.

There are three independent kinematical variables in the inclusive phenomenology: the lepton energy E_ℓ; q^2, where $q = p_\ell + p_{\nu_\ell}$; and the invariant mass $M_X^2 = (p_B - q)^2$ of a hadronic state. Introducing the dimensionless variables $y = 2E_\ell/m_B$, $t = q^2/m_B^2$, and $s = M_X^2/m_B^2$, the differential decay rate for semileptonic B decay can be written as

$$\frac{d\Gamma_{\rm SL}}{dy} = \frac{G_{\rm F}^2 m_B^5}{64\pi^3} |V_{cb}|^2 \int\limits_0^{t_{\max}} dt \int\limits_{s_0}^{s_{\max}} ds \tag{73}$$

$$\times \left\{ tW_1 + \frac{1}{2}[y(1+t-s) - y^2 - t]W_2 + t\left[\frac{1+t-s}{2} - y\right] W_3 + \ldots \right\},$$

where the structure functions $W_i = W_i(s,t)$ appear in the decomposition of the hadronic tensor $W_{\alpha\beta}$ in Lorentz covariants. The ellipsis in (73) denotes the terms proportional to the lepton mass squared. The kinematical limits of integration can be found from the equation

$$\frac{s}{1-y} + \frac{t}{y} \le 1. \tag{74}$$

They are given by $0 \le y \le 1 - \rho$, where $\rho = m_c^2/m_b^2$, $s_{\max} = 1 + t - (y + t/y)$, and $t_{\max} = y[1 - \rho/(1 - y)]$.

In a parton model, inclusive semileptonic $B_c \to X_{Q'}\ell\nu_\ell$ decay is treated in a direct analogy to deep-inelastic scattering [45]. An approach is based on the hypothesis of quark–hadron duality. This hypothesis assumes that the inclusive decay probability into free quarks for which no reference to a particular hadronic state is needed equals one. The basic ingredient is the expression for the hadronic tensor $W_{\alpha\beta}$, which is given through the optical theorem by the imaginary part of the quark box diagram describing the forward scattering amplitude:

$$W_{\alpha\beta} = \int L_{\alpha\beta}^{(cb)}(p_b, p_c) \tag{75}$$

$$\times \delta[(p_b - q)^2 - m_c^2] \frac{|\psi(\xi, p_\perp^2)|^2}{\xi} \theta(\varepsilon_c) d\xi d^2 p_\perp,$$

where a quark tensor $L_{\alpha\beta}^{(cb)}(p_b, p_c)$ is defined as

$$L_{\alpha\beta}^{cb}(p_b, p_c) = \frac{1}{4} \sum_{\rm spins} \bar{u}_c O_\alpha u_b \cdot \bar{u}_b O_\beta^+ u_c \tag{76}$$

$$= 2(p_{c\alpha} p_{b\beta} + p_{c\beta} p_{b\alpha} - g_{\alpha\beta}(p_c p_b) + i\epsilon_{\alpha\beta\gamma\delta} p^{c\gamma} p^{b\delta}),$$

$g_{\alpha\beta}$ is the metric tensor, and the factor $1/\xi$ in Eq. (75) comes from the normalization of the B-meson vertex [47].

Equation (75) amounts to averaging the perturbative decay distribution over motion of a heavy quark governed by the distribution function $|\psi(\xi, p_\perp^2)|^2$. In this respect, the approach is similar to the parton model in deep-inelastic scattering, although it is not really a parton model in its standard definition. The normalization condition reads

$$\pi \int\limits_0^1 d\xi \int dp_\perp^2 |\psi(\xi, p_\perp^2)|^2 = 1. \tag{77}$$

The function $\theta(\varepsilon_c)$, where ε_c is the c-quark energy, is inserted in Eq. (75) for consistency with the use of the valence LF wave function to calculate the b-quark distribution in the B meson.

The endpoint for the quark decay spectrum is

$$y_{\max}^b = (m_b/m_B)(1 - m_c^2/m_b^2), \tag{78}$$

whereas the physical endpoint is

$$y_{\max} = 1 - m_D^2/m_B^2, \tag{79}$$

where m_D is the D-meson mass. The endpoint for the LF electron spectrum is in fact not $y_{\max}$, but

$$y_{\max}^{\mathrm{LF}} = 1 - m_c^2/m_B^2. \quad (80)$$

This is the direct consequence of the $p_\perp^2$ integration in Eq. (75) [45]. Note that $y_{\max}^{\mathrm{LF}}$ coincides with $y_{\max}^{\mathrm{ACM}}$ with accuracy $\sim m_{\mathrm{sp}}/m_B$. For $m_c \sim 1.5$ GeV, the difference between $y_{\max}^{\mathrm{LF}}$ and $y_{\max}$ is on the order of 10^{-2}.

4.3. The Distribution Function of the b Quark

An explicit representation for the B-meson Fock expansion in QCD is not known. A priori, there is no connection between equal-time (ET) wave function $w(\mathbf{k}^2)$ of a constituent quark model and LF wave function $\psi(\xi, p_\perp^2)$. The former depends on the c.m. momentum squared $k^2 = |\mathbf{k}|^2$, while the latter depends on the LF variables ξ and $p_\perp^2$. However, there is a simple operational connection between ET and LF wave functions [48]. This is a model-dependent enterprise, but it has its close equivalent in studies of electron spectra using the ACM model. The idea is to find a mapping between the variables of the wave functions that will turn a normalized solution $w(\mathbf{k}^2)$ of the ET equation of motion into a normalized solution $\psi(\xi, p_\perp^2)$ of the different-looking LF equation of motion. That will allow us to convert the ET wave function, and all the labor behind it, into a usable LF wave function. This procedure amounts to a series of reasonable (but naive) guesses about what the solution of a relativistic theory involving confining interactions might look like.

Specifically, one converts from ET to LF momenta by leaving the transverse momenta unchanged, $\mathbf{k}_\perp = \mathbf{p}_\perp$, and letting

$$p_{iz} = \frac{1}{2}(p_i^+ - p_i^-) = \frac{1}{2}\left(p_i^+ - \frac{p_{i\perp}^2 + m_i^2}{p_i^+}\right) \quad (81)$$

for both the b quark ($i = b$) and the quark-spectator ($i = \mathrm{sp}$). Here, $p_i^\pm = p_{i0} \pm p_{iz}$ with $\sum p_i^+ = p_B^+ = m_B$ (in the B-meson rest frame).

In what follows, we identify $\Phi(\mathbf{k}^2) = |w(\mathbf{k}^2)|^2$ with the Gaussian distribution

$$\Phi(\mathbf{k}^2) = \frac{4}{\sqrt{\pi} p_{\mathrm{F}}^3} \exp\left(-\frac{\mathbf{k}^2}{p_{\mathrm{F}}^2}\right). \quad (82)$$

Then,

$$|\psi(\xi, p_\perp^2)|^2 = \frac{4}{\sqrt{\pi} p_{\mathrm{F}}^3} \exp\left(-\frac{p_\perp^2 + p_z^2}{p_{\mathrm{F}}^2}\right) \left|\frac{\partial p_z}{\partial \xi}\right|, \quad (83)$$

where

$$p_z(\xi, p_\perp^2) = \frac{1}{2}\left((1-\xi)m_B - \frac{p_\perp^2 + m_{\mathrm{sp}}^2}{(1-\xi)m_B}\right), \quad (84)$$

$$\left|\frac{\partial p_z}{\partial \xi}\right| = \frac{1}{2}\left(m_B + \frac{p_\perp^2 + m_{\mathrm{sp}}^2}{(1-\xi)^2 m_B}\right). \quad (85)$$

The calculation of the structure functions $W_i(t, s)$ in the LF parton approximation is straightforward. The result is

$$W_i(t,s) = \int w_i(s,t,\xi) \quad (86)$$
$$\times\, \delta[(p_b - q)^2 - m_c^2] \frac{|\psi(\xi, p_\perp^2)|^2}{\xi} \theta(\varepsilon_c) d\xi d^2 p_\perp,$$

where the structure functions $w_i(s, t, \xi)$ are analogs of $W_i(s, t)$ in (73) for the free-quark decay and can be easily calculated using Eq. (76) {see, e.g., Eqs. (A.8) of [45]}. Equation (86) differs from the corresponding expressions of [42] and [43] by the nontrivial dependence on $p_\perp^2$ which enters both $|\psi(\xi, p_\perp^2)|^2$ and the argument of the δ function. For further details, see [45].

4.4. The Choice of m_b

An important technical issue that appears in the problem is the definition of the quark mass m_b. The semileptonic decay rate is proportional to m_b^5; thus, any uncertainty in the definition of heavy-quark mass transfers into a huge uncertainty in the predicted rate. The problem is to find a definition consistent with that of HQET.

In the ACM model, it is known [49, 50] that, once Γ_{ACM} is expressed in terms of $m_b^{\mathrm{ACM}} = \langle m_b^f \rangle$ [which is nothing but the floating mass $m_b^f(\mathbf{p}^2)$ of Eq. (68) averaged over the distribution $\Phi(\mathbf{p}^2)$], the correction to first order in $1/m_b$ both to the inclusive semileptonic width and to the regular part of the lepton spectrum can be absorbed into the definition of the quark mass, in full agreement with the general statement of the absence of the $1/m_b$ correction in total width.

The choice of m_b in the LF approach was first addressed in the context of the LF model for $b \to s\gamma$ transitions [51]. It was shown that the LF model can be made to agree with HQET, provided m_b^{LF} is defined from the requirement of the vanishing of the first moment of the distribution function. This condition coincides with that used in HQET to define the pole mass of the b quark. In this way, one avoids an otherwise large (and model-dependent) correction of order $1/m_b$, but at the expense of introducing the shift in the constituent quark mass, which largely

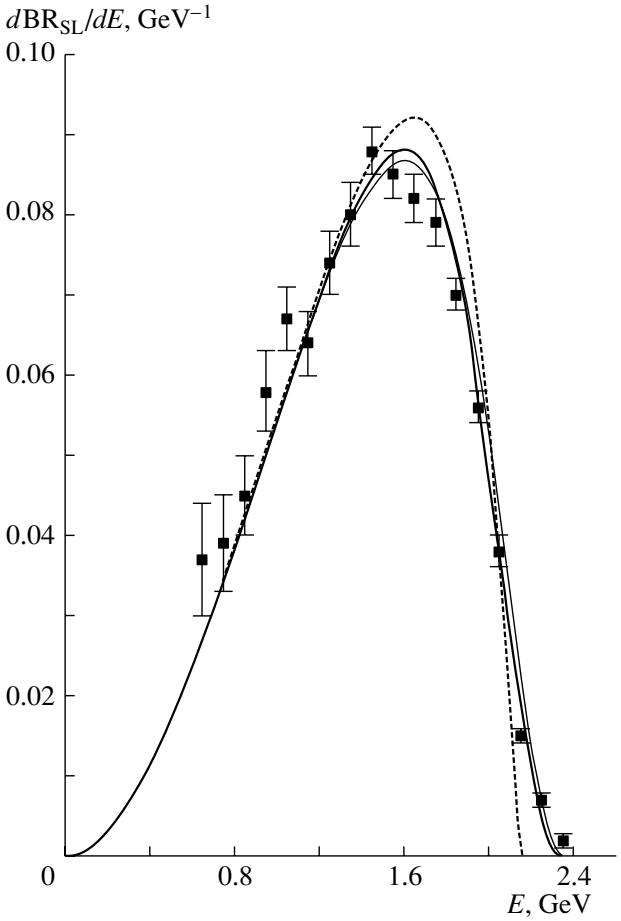

Fig. 9. The predicted electron energy spectrum [52] compared with the CLEO data [53]. The calculation uses $p_{\mathrm{F}} = 0.4$ GeV, $m_b = 4.8$ GeV, $m_c = 1.5$ GeV, and $\alpha_s = 0.25$ for the perturbative corrections. Thick solid curve is the LF result, thin solid curve is the ACM result, and dashed curve refers to the free-quark decay. The spectra are normalized to 10.16, 10.23, and 10.37%, respectively; $|V_{cb}| = 0.042$.

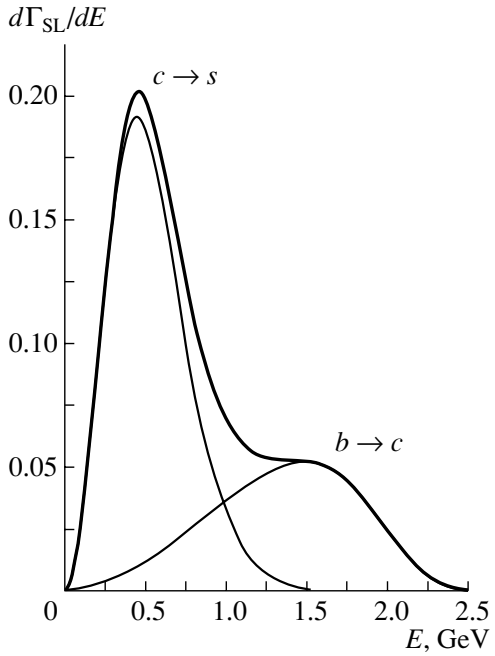

Fig. 10. The electron energy spectrum in semileptonic B_c decays [55]. The calculation uses $p_{\mathrm{F}} = 0.92$ GeV, $m_b = 5.0$ GeV, $m_c = 1.5$ GeV, and $\alpha_s = 0.25$ for the perturbative corrections.

compensates the bound-state effects. It has also been demonstrated that the values of m_b^{LF} found by this procedure agree well with the average values $\langle m_b^f \rangle$ in the ACM model. Accepting the identification $m_b^{\mathrm{LF}} = m_b^{\mathrm{ACM}}$, a similar agreement, but for the semileptonic $b \to c$ decays, has been found in [52].

4.5. Electron Energy Spectra: LF Model vs. ACM Model

In Table 2, for various values of p_{F}, the values of the total semileptonic width for the free quark with the mass $m_b = \langle m_b^f \rangle$ and the B-meson semileptonic widths calculated using the LF and ACM approaches, respectively, are given. In the last two columns are shown the fractional deviations $\delta = \Delta\Gamma_{\mathrm{SL}}/\Gamma_{\mathrm{SL}}^b$ (in percent) between the semileptonic widths determined in the LF and ACM models and that of the free quark. The agreement between the LF and ACM approaches is excellent for small p_{F}. This agreement is seen to break down at $p_{\mathrm{F}} \geq 0.4$ GeV, but even for $p_{\mathrm{F}} \sim 0.5$ GeV, the difference between the ACM and LF inclusive widths is still small and is of the order of a percent level.

Figure 9 shows the three theoretical curves for the electron spectrum in inclusive $B \to X_c \ell \nu_\ell$ decays for the LF, ACM, and free-quark models. This is a direct calculation of the spectrum and not a χ^2 fit. A more detailed fit can impose a constraint on the distribution function and the mass of the charm quark. Such a fit should also account for detector resolution. The overall normalization of the electron energy spectra,

$$\mathrm{BR}_{\mathrm{LF}} = 10.16\%, \qquad \mathrm{BR}_{\mathrm{ACM}} = 10.23\%, \qquad \mathrm{BR}_{\mathrm{free}} = 10.37\%, \tag{87}$$

is in agreement with the experimental finding [53] $\mathrm{BR}_{\mathrm{SL}} = (10.49 \pm 0.17 \pm 0.43)\%$.

The calculations implicitly include the $\mathcal{O}(\alpha_s)$ perturbative corrections arising from gluon bremsstrahlung and one-loop effects, which modify the electron energy spectra at the partonic level (see, e.g., [54] and references therein). It is customary to define a correction function $G(x)$ to the electron spectrum

Table 2. Comparison of the LF and ACM results {in all cases, $m_{sp} = 0.15$ GeV, $m_c = 1.5$ GeV, and the radiative corrections are neglected; a momentum distribution of the b quark is taken in the standard Gaussian form (82) with the Fermi momentum p_F; $|V_{cb}| = 0.04$; experimental results are after the correction to common inputs and world average—for details, see [8]}

p_F, GeV	$\langle m_b^f \rangle$, GeV	Γ_{SL}^b, ps^{-1}	Γ_{SL}^{ACM}, ps^{-1}	Γ_{SL}^{LF}, ps^{-1}	δ^{ACM}, %	δ^{LF}, %
0.1	5.089	0.1007	0.1005	0.1005	0.2	0.2
0.2	5.004	0.0906	0.0902	0.0901	0.4	0.5
0.3	4.905	0.0799	0.0792	0.0789	0.9	1.2
0.4	4.800	0.0696	0.0688	0.0682	1.1	2.0
0.5	4.692	0.0602	0.0592	0.0584	1.7	3.0

$d\Gamma_b^{(0)}$ calculated in the tree approximation for the free-quark decay through

$$\frac{d\Gamma_b}{dx} = \frac{d\Gamma_b^{(0)}}{dx}\left(1 - \frac{2\alpha_s}{3\pi}G(x)\right), \qquad (88)$$

where $x = 2E/m_b$. The function $G(x)$ contains the logarithmic singularities $\sim \ln^2(1-x)$, which for $m_c = 0$ appear at the quark-level endpoint $x_{max} = 1$. This singular behavior at the endpoint is clearly a signal of the inadequacy of the perturbative expansion in this region. The problem is solved by taking into account the bound-state effects. Since the radiative corrections must be convoluted with the distribution function, the endpoints of the perturbative spectra are extended from the quark level to the hadron level and the logarithmic singularities are eliminated.

4.6. B_c Decays

Our last example is the electron energy spectrum in the semileptonic decays of the B_c meson [55]. The semileptonic width consists of two contributions, $\Gamma_{SL} = \Gamma_{SL}^b + \Gamma_{SL}^c$, which are, respectively, $b \to \bar{c}W^+$ with the c quark as the spectator and $\bar{c} \to \bar{s}W^-$ with the b quark as the spectator. Since these processes lead to the different final states, their amplitudes do not interfere. In the simplest view, b and $\bar{c}$ are free, and the total semileptonic width is just the sum of the b and $\bar{c}$ semileptonic widths, with c decay dominating. Approximating this by $\Gamma_{SL}(B_c) = \Gamma_{SL}(B) + \Gamma_{SL}(D)$ yields $\Gamma_{SL}(B_c) \sim 0.22$ ps^{-1}. This estimate is modified by strong interaction effects.

Figure 10 shows the lepton energy spectrum in the decay $B_c \to Xe\nu_e$. This calculation uses the quark masses $m_b = 5$ GeV and $m_c = 1.5$ GeV as was chosen in [56]. The free-quark semileptonic widths are $\Gamma_{SL}^{c,free} = 0.218$ ps^{-1} and $\Gamma_{SL}^{b,free} = 0.090$ ps^{-1}. The Fermi momentum p_F is chosen as $p_F = 0.92$ GeV, corresponding to the Isgur–Scora model. Like the OPE formalism, the LF approach leads to a reduction of the free-quark decay rates caused by binding, but the bound-state corrections for the $c \to s$ semileptonic rate is sizeably larger, $\Gamma_{SL}(B_c) = 0.18$ ps^{-1},

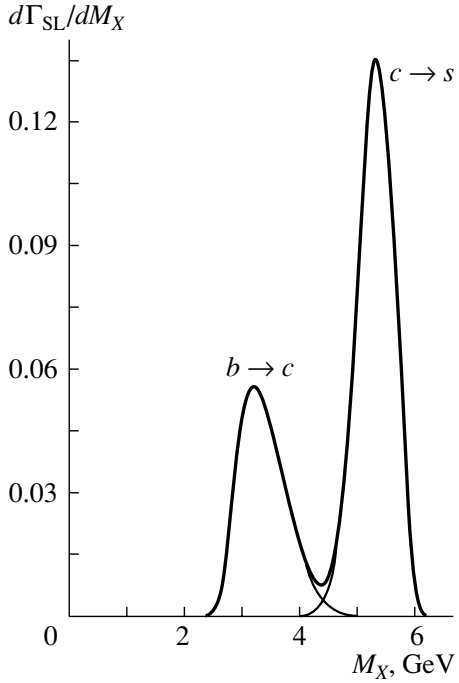

Fig. 11. The hadronic mass distribution spectrum in semileptonic B_c decays. The values of the parameters are the same as in Fig. 10.

than those reported in [56]. The result of [56] would correspond to a rather soft B_c wave function with $p_F \sim 0.5$ GeV, which seems to be excluded by existing constituent quark models.

Finally, we note that the theoretical results for the electron spectrum can be translated into predictions for the hadronic mass spectrum. In Fig. 11, we show the invariant mass distribution of the hadrons recoiling against $\ell\nu$. The LF predictions for hadronic mass spectra must be understood in the sense of quark–hadron duality. The true hadronic mass spectrum may have a resonance structure that looks rather different from our inclusive predictions. Inclusive calculations predict a continuum that is given by the inclusive spectrum and is dual to a large number of overlapping resonances.

ACKNOWLEDGMENTS

This work was supported in part by NATO, grant no. PST.CLG.978710.

REFERENCES

1. N. Cabibbo, Phys. Rev. Lett. **10**, 531 (1963); M. Kobayashi and T. Maskawa, Prog. Theor. Phys. **49**, 652 (1973).
2. S. Glashow, J. Iliopoulos, and L. Maiani, Phys. Rev. D **2**, 1285 (1970).
3. B. Aubert *et al.* (BaBar Collab.), hep-ex/0203007.
4. K. Abe *et al.* (Belle Collab.), Phys. Rev. D **66**, 032007 (2002).
5. E. Quinn, *B Physics and CP Violation, Lectures given at Particle Physics School, ICTP, Trieste, 2001*; hep-ph/0111177.
6. Y. Nir, *Heavy Flavor Physics* (St. Andrews, 2001), p. 147; hep-ph/0109090.
7. M. Neubert, hep-ph/0110301; Y. Nir, hep-ph/0208080; A. Buras, hep-ph/0210291.
8. M. Artuso and E. Barberio, Phys. Rev. D **66** (1-1) (2002); hep-ph/0205163.
9. K. Hagiwara *et al.* (Particle Data Group), Phys. Rev. D **66**, 010001 (2002).
10. C. Jarlskog, Phys. Rev. Lett. **55**, 1039 (1985).
11. S. Ahmed *et al.* (CLEO Collab.), hep-ex/9908022.
12. R. Barate *et al.* (ALEPH Collab.), Phys. Lett. B **429**, 169 (1998).
13. C. Greub and T. Hurth, Nucl. Phys. B (Proc. Suppl.) **74**, 247 (1999); hep-ph/9809468.
14. L. Wolfenstein, Phys. Rev. Lett. **51**, 1945 (1983).
15. A. J. Buras, M. E. Lautenbacher, and G. Ostermaier, Phys. Rev. D **50**, 3433 (1994); hep-ph/9403384.
16. A. J. Buras, W. Slominski, and H. Steger, Nucl. Phys. B **245**, 369 (1984).
17. A. J. Buras and R. Fleishner, in *Heavy Flavors II*, Ed. by A. J. Buras and M. Linder (World Sci., Singapore, 1998).
18. O. Schneider, see [9]; hep-ph/0206171.
19. A. Höcker, H. Lacker, S. Laplace, and F. Le Diberder, Eur. Phys. J. C **21**, 225 (2001).
20. R. A. Briers *et al.* (CLEO Collab.), LNS Preprint CLNS 01-1776 (2002); hep-ex/0203032.
21. K. Abe *et al.* (Belle Collab.), Phys. Lett. B **526**, 247 (2002); hep-ex/0111060.
22. D. Buskulic *et al.* (ALEPH Collab.), Phys. Lett. B **395**, 373 (1997).
23. P. Abreu *et al.* (DELPHI Collab.), Phys. Lett. B **510**, 55 (2001).
24. G. Abbiendi *et al.* (OPAL Collab.), Phys. Lett. B **482**, 15 (2000).
25. N. Isgur and M. B. Wise, Phys. Lett. B **232**, 113 (1989); **237**, 527 (1990).
26. M. Neubert and M. B. Wise, *Heavy-Quark Physics* (Cambridge Univ. Press, Cambridge, 2000).
27. M. Luke, Phys. Lett. B **252**, 447 (1990).
28. D. Scora and N. Isgur, Phys. Rev. D **52**, 2783 (1995).
29. Z. Ligeti, Y. Nir, and M. Neubert, Phys. Rev. D **49**, 1302 (1994).
30. S. Hashimoto *et al.*, Phys. Rev. D **61**, 014502 (2000).
31. I. Bigi, M. Shifman, and N. G. Uraltsev, Annu. Rev. Nucl. Part. Sci. **47**, 591 (1997).
32. I. I. Bigi and N. G. Uraltsev, Int. J. Mod. Phys. A **16**, 5201 (2001).
33. G. Buchalla, hep-ph/0202092, and references therein.
34. N. Isgur, Phys. Lett. B **448**, 111 (1999).
35. S. Chen *et al.* (CLEO Collab.), hep-ex/0108032.
36. M. Gremm and A. Kapustin, Phys. Rev. D **55**, 6924 (1997); hep-ph/9603448.
37. R. A. Briere *et al.* (CLEO Collab.), hep-ex/0209024.
38. I. Bigi *et al.*, Int. J. Mod. Phys. A **9**, 2467 (1994).
39. M. Neubert, Phys. Rev. D **49**, 3392, 4623 (1994).
40. G. Altarelli, N. Cabibbo, G. Corbo, *et al.*, Nucl. Phys. B **202**, 512 (1982).
41. N. Isgur *et al.*, Phys. Rev. D **39**, 799 (1989).
42. C. H. Jin, M. F. Palmer, and E. A. Paschos, Phys. Lett. B **329**, 364 (1994); C. H. Jin and E. A. Paschos, in *Proc. of the Int. Symp. on Heavy Flavor and Electroweak Theory, Beijing, China, 1995,* Ed. by C. H. Chang and C. S. Huang (World Sci., Singapore, 1996), p. 132.
43. V. L. Morgunov and K. A. Ter-Martirosyan, Yad. Fiz. **59**, 1243 (1996) [Phys. At. Nucl. **59**, 1221 (1996)].
44. I. L. Grach, I. M. Narodetskii, S. Simula, and K. A. Ter-Martirosyan, Nucl. Phys. B **592**, 227 (1997).
45. S. Kotkovsky, I. M. Narodetskii, S. Simula, and K. A. Ter-Martirosyan, Phys. Rev. D **60**, 114024 (1999).
46. J. Bjorken, I. Dunietz, and M. Taron, Nucl. Phys. B **371**, 111 (1992).
47. N. B. Demchuck, I. L. Grach, I. M. Narodetskii, and S. Simula, Yad. Fiz. **59**, 2235 (1996) [Phys. At. Nucl. **59**, 2152 (1996)].
48. F. Coester, Prog. Part. Nucl. Phys. **29**, 1 (1992).
49. L. Randall and R. Sundrum, Phys. Lett. B **312**, 148 (1993).
50. I. Bigi, M. Shifman, N. Uraltsev, and A. Vainstein, Phys. Lett. B **328**, 431 (1994).

51. Y.-Y. Keum, P. Yu. Kulikov, I. M. Narodetskii, and H. S. Song, Phys. Lett. B **471**, 72 (1999).
52. I. L. Grach, P. Yu. Kulikov, and I. M. Narodetskii, Pis'ma Zh. Éksp. Teor. Fiz. **73**, 359 (2001) [JETP Lett. **73**, 317 (2001)].
53. B. Barish *et al.* (CLEO Collab.), Phys. Rev. Lett. **76**, 1570 (1996).
54. M. Jezabek and J. H. Kühn, Nucl. Phys. B **320**, 20 (1989).
55. A. Datta *et al.* (in press).
56. M. Beneke and G. Buchalla, Phys. Rev. D **53**, 4991 (1996).

Physics of Atomic Nuclei, Vol. 66, No. 11, 2003, pp. 1989–1993. From Yadernaya Fizika, Vol. 66, No. 11, 2003, pp. 2039–2043.

ELEMENTARY PARTICLES AND FIELDS
Theory

Isospin Violation in Mixing and Decays of ρ and ω Mesons*

Ya. I. Azimov

Petersburg Nuclear Physics Institute, Russian Academy of Sciences, Gatchina, 188300 Russia

Received January 17, 2003

Abstract—The influence of isospin-violating (ρ^0, ω) mixing is discussed for any pair of decays of ρ^0, ω into the same final state. It is demonstrated, in analogy to the CP violation in neutral kaon decays, that isospin violation can manifest itself in various forms: direct violation in amplitudes and/or violation due to mixing. In addition to the known decays $(\rho^0, \omega) \to \pi^+\pi^-$ and $(\rho^0, \omega) \to \pi^0\gamma$, the pair of decays to e^+e^- and the whole set of radiative decays with participation of ρ^0, ω (in initial or final states) are also shown to be useful and promising for studies. Existing data on these decays agree with the universal character of the mixing parameter and indirectly support enhancement of $\rho^0 \to \pi^0\gamma$ in respect to $\rho^\pm \to \pi^\pm\gamma$. Future precise measurements will allow one to separate different forms of isospin violation and elucidate their mechanisms.

1. INTRODUCTION

It is widely known that isospin symmetry is violated. But nobody knows why and how it is violated. There are at least two possible sources of the violation:

(1) QED does not respect the isospin, since different members of any isomultiplet always have different electric charges. As a result, the photon can be considered as a two-component object with isospins $I = 0, 1$. Therefore, the presence of photons, real or virtual, inevitably spoils the symmetry. The corresponding effect for processes without real photons is expected to be $\mathcal{O}(\alpha)$ in the amplitude.

(2) QCD can also violate isospin, due to different properties of u and d quarks. Most popular here are references to different quark masses, but other properties, not always directly related to masses, may also be efficient (as examples, I can mention magnetic moments or difference of quark wave functions inside hadrons). Estimates of the expected effect in such approaches are rather ambiguous.

Experiments demonstrate isospin violation (e.g., hadron mass differences) mostly at the relative level of order 10^{-2} or less. This does not even allow one to discriminate between the two above mechanisms. Thus, further studies, both theoretical and experimental, are necessary to elucidate the underlying physics.

A favorable site for such studies may be provided by mixing of ρ^0 and ω mesons, where some enhancement becomes possible due to $M_\omega \approx M_\rho$. A well- and long-known example is the decay $\omega \to \pi^+\pi^-$. The isospin symmetry totally forbids it (initial $I = 0$, final $I = 1$), but the mixing opens the cascade transition $\omega \to \rho^0 \to \pi^+\pi^-$. The resulting branching ratio achieves 2% [1], instead of $\mathcal{O}(\alpha^2)$.

A more recent example of possible manifestation of the mixing is given by decays $\rho \to \pi\gamma$. There is experimental evidence for enhancement of the neutral decay in respect to the charged one (see [1]; the exact value is still uncertain, as evident from comparison of the corresponding numbers in the neighboring issues of Particle Data Group [1, 2]). Meanwhile, the isospin conservation admits only the isoscalar photon component to participate in those decays, and so probabilities for $\rho^0 \to \pi^0\gamma$ and $\rho^\pm \to \pi^\pm\gamma$ were expected to be the same. Their inequality (either enhancement or suppression of the neutral decay) may emerge from contribution of the cascade $\rho^0 \to \omega \to \pi^0\gamma$, which is impossible for the charged decay (see [3] and references therein).

In a recent paper [4], I suggested broadening the set of decays under consideration, since any pair of decays $\omega, \rho^0 \to$ (the same final state) should be sensitive to the (ρ, ω) mixing. This talk gives a brief presentation of ideas and results of the paper [4].

2. VECTOR MESON MIXING

Let us begin with bare states $\omega^{(0)}$ and $\rho^{(0)}$. They have bare (complex) masses

$$M_\omega^{(0)} = m_\omega^{(0)} - \frac{i}{2}\Gamma_\omega^{(0)}, \quad M_\rho^{(0)} = m_\rho^{(0)} - \frac{i}{2}\Gamma_\rho^{(0)}$$

*This article was submitted by the author in English.

1063-7788/03/6611-1989$24.00

and bare propagators

$$[D_\omega^{(0)}(k^2)]_{\mu\nu} = \frac{g_{\mu\nu} - \dfrac{k_\mu k_\nu}{M_\omega^{(0)2}}}{k^2 - M_\omega^{(0)2}}, \qquad (1)$$

$$[D_\rho^{(0)}(k^2)]_{\mu\nu} = \frac{g_{\mu\nu} - \dfrac{k_\mu k_\nu}{M_\rho^{(0)2}}}{k^2 - M_\rho^{(0)2}}.$$

Mixing arises if there exist transitions $\omega^{(0)} \to \rho^{(0)}$ and $\rho^{(0)} \to \omega^{(0)}$. Corresponding transition vertices may be described by transition amplitudes $G_{\omega\rho}$ and $G_{\rho\omega}$, respectively.[1)] Summation over all mutual transitions provides four different propagators for bare states:

$$D_{\rho\rho}(k^2), \quad D_{\rho\omega}(k^2), \quad D_{\omega\rho}(k^2), \quad D_{\omega\omega}(k^2),$$

which describe all reciprocal transformations of $\rho^{(0)}$ and $\omega^{(0)}$. Together they may be considered as a 2×2 matrix propagator. Its diagonalization picks out physical propagators $D_\omega(k^2)$ and $D_\rho(k^2)$ with physical masses

$$M_\omega^2 = M^2 + K\delta M^2, \quad M_\rho^2 = M^2 - K\delta M^2, \quad (2)$$

where

$$\delta M^2 = \frac{M_\omega^{(0)2} - M_\rho^{(0)2}}{2}, \quad M^2 = \frac{M_\omega^{(0)2} + M_\rho^{(0)2}}{2},$$
$$K = \sqrt{1 + \tilde{G}_{\rho\omega}\tilde{G}_{\omega\rho}},\ \tilde{G}_{\rho\omega} = \frac{G_{\rho\omega}}{\delta M^2},\ \tilde{G}_{\omega\rho} = \frac{G_{\omega\rho}}{\delta M^2}.$$

Now, we can consider a process $i \to f$ where ρ^0 and/or ω appear as the intermediate states. Its amplitude in terms of bare states is

$$A_{if} = A_{i\rho}^{(0)} D_{\rho\rho} A_{\rho f}^{(0)} + A_{i\rho}^{(0)} D_{\rho\omega} A_{\omega f}^{(0)} \qquad (3)$$
$$+ A_{i\omega}^{(0)} D_{\omega\omega} A_{\omega f}^{(0)} + A_{i\omega}^{(0)} D_{\omega\rho} A_{\rho f}^{(0)},$$

where $A_{i\rho}^{(0)}$ and $A_{i\omega}^{(0)}$ are production amplitudes for bare $\rho^{(0)}$ and $\omega^{(0)}$ states, while $A_{\rho f}^{(0)}$ and $A_{\omega f}^{(0)}$ are their decay amplitudes. The whole amplitude may be rewritten in terms of physical states in the simple form

$$A_{if} = A_{i\rho} D_\rho A_{\rho f} + A_{i\omega} D_\omega A_{\omega f}, \qquad (4)$$

where the physical propagators $D_\rho(k^2)$ and $D_\omega(k^2)$ are used together with the physical amplitudes

$$A_{i\rho} = \sqrt{\frac{K+1}{2K}} \left(A_{i\rho}^{(0)} - A_{i\omega}^{(0)} \frac{\tilde{G}_{\omega\rho}}{K+1} \right), \qquad (5)$$

$$A_{i\omega} = \sqrt{\frac{K+1}{2K}} \left(A_{i\omega}^{(0)} + A_{i\rho}^{(0)} \frac{\tilde{G}_{\rho\omega}}{K+1} \right)$$

for the ρ^0- and ω-meson production and

$$A_{\rho f} = \sqrt{\frac{K+1}{2K}} \left(A_{\rho f}^{(0)} - \frac{\tilde{G}_{\rho\omega}}{K+1} A_{\omega f}^{(0)} \right), \qquad (6)$$

$$A_{\omega f} = \sqrt{\frac{K+1}{2K}} \left(A_{\omega f}^{(0)} + \frac{\tilde{G}_{\omega\rho}}{K+1} A_{\rho f}^{(0)} \right)$$

for the meson decays.

The picture of mixed $\rho^{(0)}$ and $\omega^{(0)}$ states is similar to the well-known picture of mixing for K^0 and $\bar{K}^0$, as described by Lee, Oehme, and Yang [5]. It corresponds to diagonalization of the mass-squared matrix of the (ρ, ω) system

$$\mathcal{M}^2 = \begin{pmatrix} M_\rho^{(0)2} & G_{\omega\rho} \\ G_{\rho\omega} & M_\omega^{(0)2} \end{pmatrix} \qquad (7)$$

(and its matrix propagator $\mathcal{D} = (k^2 - \mathcal{M}^2)^{-1}$) in the form

$$\mathcal{M}^2 = \sqrt{\frac{K+1}{2K}} \begin{pmatrix} 1 & \dfrac{\tilde{G}_{\omega\rho}}{K+1} \\ -\dfrac{\tilde{G}_{\rho\omega}}{K+1} & 1 \end{pmatrix} \begin{pmatrix} M_\rho^2 & 0 \\ 0 & M_\omega^2 \end{pmatrix} \qquad (8)$$
$$\times \sqrt{\frac{K+1}{2K}} \begin{pmatrix} 1 & -\dfrac{\tilde{G}_{\omega\rho}}{K+1} \\ \dfrac{\tilde{G}_{\rho\omega}}{K+1} & 1 \end{pmatrix}.$$

The bare states $|\rho^{(0)}\rangle$ and $|\omega^{(0)}\rangle$ appear to be analogs of flavor states $|K^0\rangle$ and $|\bar{K}^0\rangle$, while the physical states

$$|\rho\rangle = N_\rho \left(|\rho^{(0)}\rangle - \frac{\tilde{G}_{\rho\omega}}{K+1} |\omega^{(0)}\rangle \right), \qquad (9)$$

$$|\omega\rangle = N_\omega \left(\frac{\tilde{G}_{\omega\rho}}{K+1} |\rho^{(0)}\rangle + |\omega^{(0)}\rangle \right)$$

play the role of $|K_S\rangle$ and $|K_L\rangle$ [compare with expressions (6); N_ρ and N_ω are normalizing factors]. The essential difference, however, is the nonvanishing δM^2, which would imply CPT violation in the case of $(K^0\bar{K}^0)$. As for the neutral kaons, there is a possibility of rephasing for $\rho^{(0)}$ and $\omega^{(0)}$. T invariance makes it possible to fix their phases so that

$$\tilde{G}_{\rho\omega} = \tilde{G}_{\omega\rho} \equiv \tilde{G}.$$

An analogy between the two systems would be more evident if one could observe oscillating time distributions of ρ and ω decays. This is, however, quite unrealistic, and we can study only time-integrated

[1)] See [4] for more detailed description of the vertices.

double-pole distributions in k^2. A more detailed discussion of similarity and difference between (ρ^0,ω) and $(K^0,\bar{K}^0)$ may be found in [4]. I would like, nevertheless, to mention here one unfamiliar point: while the bare states are orthogonal, the physical (ρ^0,ω) states are orthogonal only if $\tilde{G}$ is real.

3. MIXING AND ISOSPIN VIOLATION IN DECAYS

Symmetry violations in decays of neutral kaons are known to reveal themselves in two forms: mixing violation, manifested in mixing parameters of eigenstates; and direct violation, seen as a property of one or another particular amplitude for kaon decays. Isospin violation for the (ρ,ω) system may also have two forms. It can be direct violation, seen in production or decay amplitudes for bare states; or it can be mixing violation due to dimensionless parameters $\tilde{G}_{\rho\omega}$ and $\tilde{G}_{\omega\rho}$. Existing experience allows one to expect relative effects in amplitudes ~ 0.01 for the direct violation, while $|\tilde{G}|$ might be up to 0.1. This apparent enhancement of $\tilde{G}$ arises due to the denominator δM^2, which is small at the hadron mass scale. Nevertheless, the difference is not very strong, and future accurate description may require accounting for both kinds of isospin violation.

Let us compare a pair of decays $(\omega,\rho^0)\to f$ with the same final state. The ratio of their amplitudes is

$$a_{\omega/\rho^0 f}\equiv\frac{A_{\omega f}}{A_{\rho f}}=a^{(0)}_{\omega/\rho^0 f} \times\left(1+\frac{\tilde{G}}{(K+1)a^{(0)}_{\omega/\rho^0 f}}\right)\left(1-\frac{\tilde{G}a^{(0)}_{\omega/\rho^0 f}}{K+1}\right)^{-1}, \tag{10}$$

where we assume T invariance and define

$$a^{(0)}_{\omega/\rho^0 f}\equiv\frac{A^{(0)}_{\omega f}}{A^{(0)}_{\rho f}}.$$

Now, neglecting the difference of phase spaces in the decays, we can easily describe the measurable quantity

$$r_{\omega/\rho^0 f}\equiv\frac{\Gamma(\omega\to f)}{\Gamma(\rho^0\to f)}=|a_{\omega/\rho^0 f}|^2. \tag{11}$$

Each pair of decays has its own parameter $a^{(0)}_{\omega/\rho^0 f}$, while $\tilde{G}$ is universal.

For decays $(\omega,\rho^0)\to\pi^+\pi^-$, we can assume the absence of direct isospin violation, i.e., take $a^{(0)}_{\omega/\rho^0(2\pi)}\to 0$, and obtain the simple relation

$$r_{\omega/\rho^0(2\pi)}\equiv\frac{\Gamma(\omega\to 2\pi)}{\Gamma_\rho}=\frac{1}{4}|\tilde{G}|^2, \tag{12}$$

where deviation of K from unity has been neglected. On the basis of the tables from [1], it gives

$$|\tilde{G}|=(6.2\pm 0.5)\times 10^{-2}. \tag{13}$$

Large variation of this quantity when it is extracted from the consequent issues of the Particle Data Group [1, 2] shows that the realistic error should be taken at least a factor of 2 higher.

Photonic decays $(\omega,\rho^0)\to\pi^0\gamma,\eta\gamma,e^+e^-$ and $\eta'\to(\omega,\rho^0)\gamma$ contain a real or virtual photon and have, therefore, nonvanishing direct isospin violation. It can be assumed, however, to have a very simple form based on the structure of the photon coupling to light quarks:

$$e_u\bar{u}u+e_d\bar{d}d=\frac{e_u+e_d}{\sqrt{2}}\frac{\bar{u}u+\bar{d}d}{\sqrt{2}}+\frac{e_u-e_d}{\sqrt{2}}\frac{\bar{u}u-\bar{d}d}{\sqrt{2}}.$$

Evidently, the effective isovector charge is 3 times more than the isoscalar one. We can use this fact together with an additional assumption that the $\bar{u}u$ and $\bar{d}d$ components of the mesons produce the same matrix elements (and, therefore, do not manifest any true direct violation of isospin). Then, for the ratios

$$r_{\eta'\rho^0/\omega}\equiv\frac{\Gamma(\eta'\to\rho^0\gamma)}{\Gamma(\eta'\to\omega\gamma)},\quad r_{\rho^0/\omega\eta}\equiv\frac{\Gamma(\rho^0\to\eta\gamma)}{\Gamma(\omega\to\eta\gamma)},$$
$$r_{\rho^0/\omega(ee)}\equiv\frac{\Gamma(\rho^0\to e^+e^-)}{\Gamma(\omega\to e^+e^-)},$$

we obtain the same expression

$$r=9\left|\frac{1-\frac{1}{6}\tilde{G}}{1+\frac{3}{2}\tilde{G}}\right|^2. \tag{14}$$

A given value of r corresponds to a circle in the complex plane of $\tilde{G}$, which should intersect another circle, related to Eq. (12), and determine $\tilde{G}$ up to the sign of $\mathrm{Im}\tilde{G}$.

Data of tables [1] provide the values

$$r_{\eta'\rho^0/\omega}=9.74\pm 1.05,\quad r_{\rho^0/\omega\eta}=10.3\pm 2.6, \tag{15}$$
$$r_{\rho^0/\omega(ee)}=11.42\pm 0.42,$$

which do not contradict each other. Experimental errors transform all the corresponding circles into circular bands shown in the figure. Though the errors are large, the picture looks consistent with the value of $\tilde{G}$ being universal for various decays and having $\mathrm{Re}\tilde{G}<0$.

In the same approach, we can write

$$r_{\rho^0/\rho^\pm\pi}\equiv\frac{\Gamma(\rho^0\to\pi^0\gamma)}{\Gamma(\rho^\pm\to\pi^\pm\gamma)}=\left|1-\frac{3}{2}\tilde{G}\right|^2, \tag{16}$$

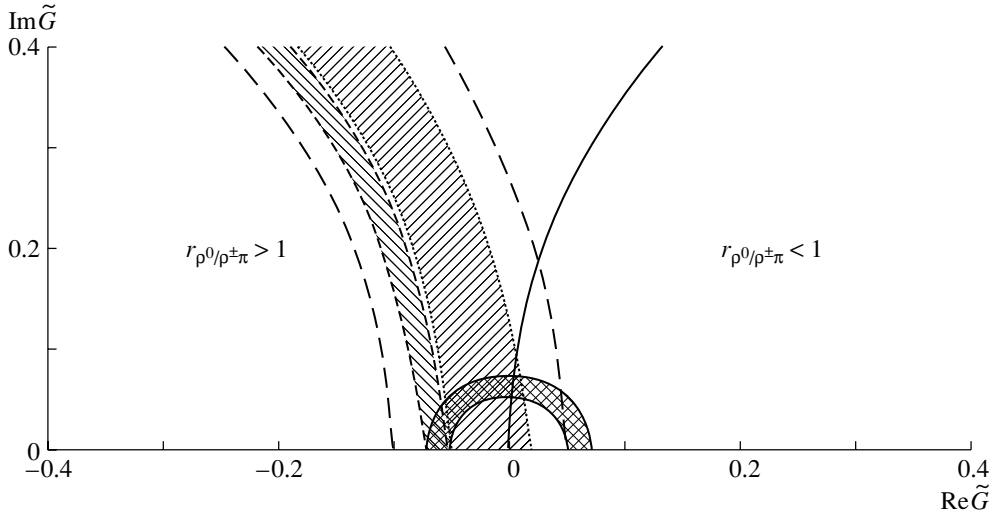

Properties of various (ρ^0, ω)-decay pairs as seen on the complex plane of $\tilde{G}$ when using values (15). The long-dashed uncovered band is for $(\rho^0, \omega) \to \eta\gamma$; the short-dashed band with left-inclined hatching is for $(\rho^0, \omega) \to e^+e^-$; the dotted band with right-inclined hatching is for $\eta' \to (\rho^0, \omega)\gamma$. The solid ring with double hatching is for $(\omega, \rho) \to \pi\pi$, Eq. (13) with the doubled error. The area to the left/right of the solid line corresponds to $r_{\rho^0/\rho^\pm\pi}$ more/less than unity, i.e., to enhancement/suppression of $\rho^0 \to \pi^0\gamma$ in respect to $\rho^\pm \to \pi^\pm\gamma$.

which shows that interference of direct and cascade contributions may either suppress or enhance the neutral radiative decay. $\mathrm{Re}\tilde{G} < 0$ leads to enhancement of the neutral-vs.-charged decay, in agreement with experimental evidence [1]. This demonstrates both the role of mixing in pairs of (ρ^0, ω) decays and the consistency of the discussed approach to description of the isospin violation.

The considered photonic decays can be easily described in the framework of the additive quark model. Its simplest form provides exactly the same expression as in Eq. (14). To check that they have a more general meaning, we can consider many-particle decays $(\rho^0, \omega) \to \pi^0\pi^0\gamma$, which are not easy for application of the additive quark model. However, we can use the fact of "isotopic separation" in these decays: only the isovector (isoscalar) component of the photon would participate in the decay of ρ^0 (ω) in the absence of some additional isospin violation because of mixing or any direct effects. Therefore, the quantity

$$r_{\rho^0/\omega(\pi\pi)} \equiv \frac{\Gamma(\rho^0 \to \pi^0\pi^0\gamma)}{\Gamma(\omega \to \pi^0\pi^0\gamma)} \qquad (17)$$

should satisfy the same Eq. (14). Experimentally [1], $r_{\rho^0/\omega(\pi\pi)} \approx 11$. The uncertainty is still large, but we see just the expected tendency ($r_{\rho^0/\omega(\pi\pi)}$ seems to be higher than the unmixed numerical value of 9).

Up to now, we have neglected any really direct violation of the isospin symmetry. In photonic decays, this meant that the arising matrix elements were assumed to be the same for u and d components of the mesons, and violation emerged only due to the difference of e_u and e_d. However, the slight difference of $r_{\eta'\rho^0/\omega}$ and $r_{\rho^0/\omega(ee)}$ may be viewed as evidence for the existence of some additional direct violation, giving different matrix elements for the u and d components. Other possible evidence for such violation comes from the ratio

$$r_{\omega/\rho^\pm\pi} \equiv \frac{\Gamma(\omega \to \pi^0\gamma)}{\Gamma(\rho^\pm \to \pi^\pm\gamma)}, \qquad (18)$$

which experimentally [1] equals 10.9 ± 1.3. This exceeds the expectation based on the expression

$$r_{\omega/\rho^\pm\pi} = 9\left|1 + \frac{1}{6}\tilde{G}\right|^2, \qquad (19)$$

with $\tilde{G}$ satisfying Eq. (13) and having $\mathrm{Re}\tilde{G} < 0$. Sources of additional (direct) violations are still to be discussed.

4. CONCLUSION

The above examples demonstrate that the (ρ, ω) mixing reveals itself not only in decays $\omega \to \pi^+\pi^-$ and $\rho^0 \to \pi^0\gamma$. It also affects all pairs of decays of ρ^0, ω to the same final state and decays of heavier particles with production of ρ^0, ω.

Though the current precision is still insufficient for firm conclusions, existing data on radiative decays of (ρ^0, ω) and decays to e^+e^- are shown to agree with the regular, correlated manner expected for the influence of mixing. The whole set of decays gives

additional indirect support for enhancement of $\rho^0 \to \pi^0\gamma$ in comparison with $\rho^\pm \to \pi^\pm\gamma$.

Future, more precise measurements of those and other decays will help to separate isospin violation due to (ρ, ω) mixing from direct violation in various processes and to study them in detail. This will allow one to pick out the underlying physics and construct adequate models for isospin violation.

ACKNOWLEDGMENTS

The work was supported in part by the Russian Foundation for Basic Research (project no. 00-15-96610).

REFERENCES

1. K. Hagiwara *et al.*, Phys. Rev. D **66**, 010001 (2002).
2. D. E. Groom *et al.*, Eur. Phys. J. C **15**, 1 (2000).
3. M. Benayoun and H. B. O'Connell, Eur. Phys. J. C **22**, 503 (2001).
4. Ya. I. Azimov, Eur. Phys. J. A **16**, 209 (2003); hep-ph/0209153.
5. T. D. Lee, R. Oehme, and C. N. Yang, Phys. Rev. **106**, 340 (1957).

Physics of Atomic Nuclei, Vol. 66, No. 11, 2003, pp. 1994–2016. From Yadernaya Fizika, Vol. 66, No. 11, 2003, pp. 2044–2066.

ELEMENTARY PARTICLES AND FIELDS
Theory

High-Energy Hadronic Interactions (20 Years of the Quark–Gluon Strings Model)*

A. B. Kaidalov**

Institute for Theoretical and Experimental Physics,
Bol'shaya Cheremushkinskaya ul. 25, Moscow, 117259 Russia

Received January 22, 2003; in final form, May 14, 2003

Abstract—The approach to high-energy hadronic interactions based on the $1/N$ expansion in QCD and the string model of hadrons is reviewed. The Quark–Gluon Strings Model (QGSM) is discussed in detail. Applications of the QGSM to the multiparticle production at high energies are considered. It is shown that the model gives a perfect description of many aspects of hadronic interactions: diffractive processes, multiplicity distributions, correlations, and inclusive spectra of different particles in a broad energy region. It is pointed out that predictions of the model are in good agreement with data from hadronic colliders. Recent applications of the approach to small-x physics and heavy-ion collisions are reviewed.

1. INTRODUCTION

Quantum chromodynamics (QCD) is a real candidate for a theory of strong interactions. Asymptotic freedom of QCD makes it possible to apply perturbation theory to processes with large momentum transfer, and predictions of perturbative QCD for these processes are in good agreement with experimental data. On the other hand, large-distance phenomena, where the coupling constant is not small and nonperturbative effects are important, still present a problem for the theory. It is very important to understand QCD in this large-distance domain. Processes with small momentum transfer, which give a dominant contribution to high-energy hadronic interactions, provide a natural testing ground for theoretical ideas and QCD-based models of large-distance dynamics.

In this paper, I shall review the approach to high-energy hadronic interactions based on the Reggeon calculus and $1/N$ expansion in QCD [1–4]. Extra dynamical input is provided by the color-tube or string models [6–9], which are closely related to the space-time picture of interaction in $1/N$ expansion. The existence of stringlike configurations of gluonic fields is confirmed by lattice calculations.

The powerful method of Reggeon theory, based on analyticity and unitarity, has been developed for description of soft hadronic interactions at high energies. In this review, I shall show how to incorporate the QCD-based models into this general scheme. As a result, many relations between parameters of Reggeon theory are established. A model based on these ideas was developed about 20 years ago in ITEP by K.A. Ter-Martirosyan and myself [10–16] and is called the Quark–Gluon Strings Model (QGSM). A similar Dual Parton Model (DPM) has been developed independently by Capella *et al.* [17, 18] and there are many important contributions to this field by other authors [19–23]. A more complete list of references can be found in the reviews [18, 24].

This approach has been applied to many different problems of strong interactions: hadronic mass spectrum [14], widths of resonances [15], relations between the total cross sections, residues of Regge poles [15], behavior of hadronic form factors [10], and multiparticle production at high energies [12, 13, 16, 25, 26]. Here, I shall concentrate mainly on the subject of multiparticle production in hadronic collisions with an emphasis on the main predictions of the QGSM and DPM models, their successes and problems. Applications of this approach to new areas of small-x physics and heavy-ion collisions at very high energies will be also discussed.

The Pomeron is the main object of the Reggeon approach to high-energy hadronic interactions. In the first part of this paper, I shall discuss the properties of $1/N$ expansion in QCD and its relation to the dynamics of Reggeons and of the Pomeron. A review of the main properties of the QGSM will be given in Section 3, and comparison of its prediction with experimental data on high-energy hadronic interactions in Section 4. The role of interactions between Pomerons and the relation of these interactions to

*This article was submitted by the author in English.

**e-mail: kaidalov@heron.itep.ru

a large-mass diffractive production is discussed in Section 5.

In Section 6, I shall apply the formalism to interactions of virtual photons with nucleons and nuclei. A qualitative picture of diffractive dissociation of a virtual photon will be described and a model based on this picture and methods of Reggeon theory will be formulated. This model gives a unified description of both structure functions of the proton in a broad region of virtualities Q^2 and diffractive dissociation of a virtual photon in this region. The model leads to definite predictions for shadowing of nuclear structure functions.

Section 7 is devoted to heavy-ion collisions. I shall emphasize the importance of shadowing effects in heavy-ion collisions. It will be shown how these effects modify predictions of the Glauber model for inclusive spectra and particle densities at very high energies.

The main conclusions of the review are formulated in Section 8.

2. $1/N$ EXPANSION AND THE POMERON IN QCD

A nonperturbative method that can be used in QCD for description of large-distance dynamics is the $1/N$ expansion (or topological expansion) [1–3].

In this approach, the quantities $1/N_c$ [1] or $1/N_{\rm lf}$ [2, 3] (N_c is the number of colors and $N_{\rm lf}$ is the number of light flavors) are considered as small parameters and amplitudes and Green's functions are expanded in terms of these quantities. In QCD, $N_c = 3$ and $N_{\rm lf} \simeq 3$ and the expansion parameter does not look small enough. However, in most cases, the expansion parameter is $1/N_c^2 \sim 0.1$.

In the formal limit $N_c \to \infty$ ($N_{\rm lf}/N_c \to 0$), QCD has many interesting properties and has been intensively studied theoretically. There is hope of obtaining an exact solution of the theory in this limit (two-dimensional QCD has been solved in the limit $N_c \to \infty$). However, this approximation is rather far from reality, as resonances in this limit are infinitely narrow ($\Gamma \sim 1/N_c$). The case when the ratio $N_f/N_c \sim 1$ is fixed and the expansion in $1/N_f$ (or $1/N_c$) is carried out [2, 3] seems more realistic.

This approach is sometimes called the topological expansion, because the given term of this expansion corresponds to an infinite set of Feynman diagrams with definite topology. It should be emphasized that $1/N$ expansion should be applied to Green's functions or amplitudes for white states.

The first term of the expansion corresponds to the planar diagrams of the type shown in Fig. 1 for the binary reaction. These diagrams always have as border lines the valence quarks of the colliding hadrons. At high energies, they should correspond to exchanges by secondary Regge poles $\alpha_{\rm R}(\rho, A_2, \omega, \dots)$ "made of" light quarks. The s-channel cutting of the planar diagram of Fig. 1*a* is shown in Fig. 1*b*. Here and in the following, we do not show internal lines of gluons and quark loops. This diagram corresponds to a multiparticle production, which has the same properties as in the multiperipheral model. Let us note that the planar diagrams correspond to annihilation of a valence quark and an antiquark, belonging to colliding hadrons.

It is necessary to take into account that $1/N$ is the dynamical expansion. This means that it can work better in some regions of kinematical variables, while in some kinematical limits its convergence can be worse. For example, in the case of $2 \to 2$ amplitude, which is a function of two variables s, t, the $1/N$ expansion becomes more accurate as t increases in the positive-t region [27], while at high energies one should consider several terms of the topological expansion. The last point we shall discuss in detail in this paper.

The topological classification of diagrams in QCD leads to many relations between parameters of the Reggeon theory, hadronic masses, widths of resonances, and total cross sections (for a review, see [26]). All these relations are in good agreement with experiment.

A contribution of the planar diagrams to the total cross section decreases with energy as $1/s^{1-\alpha_{\rm R}(0)} \approx 1/\sqrt{s}$. This decrease is connected to the fact that quarks have spin $1/2$ and, in the lowest order of perturbation theory, an exchange by two quarks in the t channel leads to the behavior of the cross section $\sigma \sim 1/s$, which corresponds to the intercept $\alpha_{\rm R}(0) = 0$. Interaction between quarks should lead to an increase in the intercept to the observed value $\alpha_{\rm R}(0) \approx 0.5$.

A calculation of Regge trajectories in QCD is a difficult problem, even for planar diagrams. It was considered in papers [28] using the method of Wilson loop path integral [29]. It was shown that, under a reasonable assumption about large-distance dynamics [minimal area law for Wilson loop at large distances, confirmed by numerous lattice data, $\langle W \rangle \sim \exp(-\sigma S_{\rm min})$ (σ is the string tension)], it is possible to calculate the spectrum of $q\bar{q}$ states. The resulting spectrum for light quarks with a good accuracy is described by a very simple formula

$$\frac{M^2}{2\pi\sigma} = L + 2n_r + c_1, \qquad (1)$$

where M is the mass of the state, and L and n_r are orbital and radial quantum numbers. This spectrum

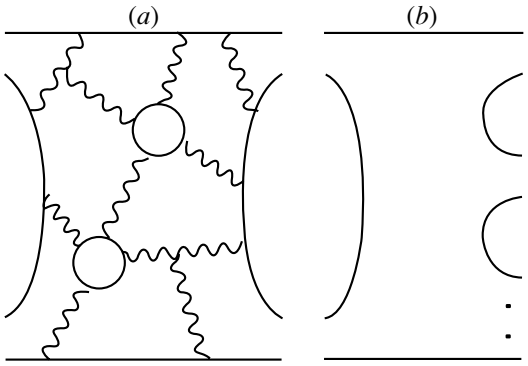

Fig. 1. (*a*) Planar diagrams for a binary reaction; (*b*) *s*-channel cuttings of planar diagrams (*a*). Full lines denote quarks; wavy lines, gluons.

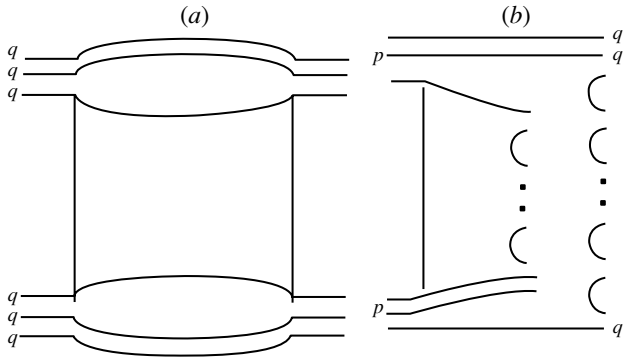

Fig. 2. (*a*) Cylinder-type diagrams and (*b*) cuttings of these diagrams in the *s* channel.

corresponds to an infinite set of linear Regge trajectories similar to the one of dual and string models.

In [28], spin effects have not been taken into account. Realistic calculations of masses of hadrons, which take into account spin effects, perturbative interactions at small distances, and quark loops, have been carried out recently [30]. The resulting Regge trajectories are in good agreement with experiment.

There are diagrams for elastic scattering or reactions without quantum-number exchange in the t channel, shown in Fig. 2*a*, where the valence quarks of colliding hadrons are conserved in the process of interaction. These are so-called cylinder-type diagrams and their s-channel cuttings correspond to the multiparticle production configurations, shown in Fig. 2*b*. These configurations correspond to production of two chains of particles, and each chain has the same structure as the one shown for the planar diagram of Fig. 1*b*. From the t-channel point of view, the cylinder diagrams are due to exchange by gluons in the t channel. It is usually assumed that these diagrams lead to the Pomeron pole. From the topological classification point of view, the cylinder diagrams correspond to a sphere with two boundaries given by the valence quark lines of colliding hadrons.

It is very important to calculate the Pomeron trajectory in QCD. Perturbative calculations of the Pomeron in QCD were carried out by Lipatov and collaborators [31] (BFKL Pomeron) many years ago. The Pomeron is related to a sum of ladder-type diagrams with exchange of Reggeized gluons. Reggeization of gluons (as well as quarks) is an important property of QCD (at least, in perturbation theory). In the leading approximation of perturbation theory, an expression for the intercept of the Pomeron $\alpha_{\mathrm{P}}(0)$ is [31]

$$\Delta \equiv \alpha_{\mathrm{P}}(0) - 1 = \frac{4N_c \ln 2}{\pi}\alpha_s. \qquad (2)$$

In this approximation (for the QCD coupling constant, $\alpha_s \approx 0.2$), $\Delta \approx 0.5$. NLO corrections have been calculated recently [32] and strongly decrease LO results for Δ. The value of Δ depends on the choice of renormalization scheme and renormalization scale. The choice of a physical (BLM) scheme leads to stable results for $\Delta \approx 0.17$, which practically does not depend on virtuality of a process [33].

An influence of the nonperturbative effects on the Pomeron trajectory and relation to the spectrum of glueballs was considered in [34, 35], using the method of Wilson loop path integral discussed above for the case of $q\bar{q}$ Regge poles.

In the approximation where the spin effects and quark loops are neglected, the spectrum of two-gluon glueballs is determined by the expression for the Wilson loop at large distances given above with the only difference that the string tension ($\sigma \equiv \sigma_{\mathrm{fund}}$) for the $q\bar{q}$ system is changed to σ_{adj} string tension for the gg system. Thus, the mass spectrum for glueballs is given by Eq. (1) with the change $\sigma \to \sigma_{\mathrm{adj}}$.

The value of σ_{adj} can be found from the string tension σ_{fund} of the $q\bar{q}$ system, multiplying it by 9/4, as follows from Casimir scaling observed on the lattices. Taking the experimental Regge slope for mesons $\alpha' = 0.89\ \mathrm{GeV}^{-2}$, one obtains $\sigma_{\mathrm{fund}} = 0.18\ \mathrm{GeV}^2$ and $\sigma_{\mathrm{adj}} \approx 0.40\ \mathrm{GeV}^2$.

The calculated spectrum of glueballs [35] is in perfect agreement with the results of lattice calculations. The glueball Regge trajectory is close to $q\bar{q}$ Regge trajectories f, f' in the region of small t. In this region, a mixing between gluonic and $q\bar{q}$ Regge trajectories is important. The mixing effects and account of small distances by QCD perturbation theory allow one to obtain a phenomenologically acceptable intercept of the Pomeron trajectory and lead to an interesting pattern of vacuum trajectories in the positive-t region [35]. I would like to emphasize that, in this approach, the "hard" and "soft" Pomerons are mixed.

The equation for the Pomeron singularity contains both nonperturbative effects and perturbative dynamics. Thus, the resulting "physical" pole is a state due to both "soft" and "hard" interactions. The Pomeron in QCD has a very rich and interesting structure.

Regge poles are not the only singularities in the complex angular momentum plane. Exchange of several Reggeons in the t channel leads to moving branch points (or Regge cuts) in the complex angular momentum j plane. Contributions of these singularities to scattering amplitudes $T_n(s,0) \sim s^{1+n\Delta}$ are especially important at high energies for $\Delta > 0$. The whole series of n-Pomeron exchanges should be summed. An account of these multi-Pomeron exchanges in the t channel leads to unitarization of scattering amplitudes. The Gribov Reggeon diagram technique [36] allows one to calculate contributions of Regge cuts to scattering amplitudes.

From the point of view of $1/N$ expansion, n-Pomeron exchange contributions correspond to more complicated topologies with "handles." Thus, each topological class of surfaces is characterized by a given number of boundaries (n_b) and handles (n_h). Topological expansion allows one to give a complete classification of diagrams and to determine their dependence on the parameter $1/N$. The diagrams of a given topological class have the following dependence on $1/N$:

$$T_{n_b,n_h} \sim (1/N)^{n_b+2n_h}. \qquad (3)$$

Thus, the contribution of planar diagram ($n_b = 1$, $n_h = 0$) to the scattering amplitude is $\sim 1/N$, the cylinder-diagram ($n_b = 2$, $n_h = 0$) contribution is $\sim(1/N)^2$, and the amplitude for the diagram of two-Pomeron exchange ($n_b = 2$, $n_h = 1$) is $\sim(1/N)^4$. Equation (3) is valid for four-point functions (amplitudes). For amplitudes with a larger number of hadrons, one should take into account that each extra external hadronic state introduces a factor $1/\sqrt{N}$ due to normalization of its wave function.

Note that the ratio of the cylinder to the planar diagram is $\sim 1/N$; however, for the amplitudes with vacuum quantum numbers in the t channel, the cylinder-type diagrams will dominate at high energies, because this ratio increases as $s^{\alpha_P(0)-\alpha_R(0)}$ as energy increases. This is one of the manifestations of the dynamical character of the $1/N$-expansion mentioned above. In many cases, the type of process (and the number of boundaries) is fixed by the quantum numbers in the t channel. In these cases, the expansion is in the number of handles and, according to Eq. (3), the expansion parameter is $(1/N)^2$, as was mentioned above.

3. QUARK–GLUON STRINGS MODEL

The topological or $1/N$ expansion discussed in the previous section gives a useful classification of all QCD diagrams. It becomes especially predictive if a definite spacetime picture for these diagrams is given.

The process of hadronic interactions at high energies can be related to production of new objects—color tubes or strings [24]. It is necessary to consider separately two cases, corresponding to (1) the processes with annihilation of valence quarks of the colliding hadrons, corresponding to the planar diagrams of $1/N$ expansion, and (2) the processes of diffraction type, where the valence quarks are conserved, connected to the cylinder-type diagrams.

In the first case after an interaction and annihilation of valence quarks, the color-tube configuration is produced and, after some time, decays to two similar configurations by production of $q\bar{q}$ from the vacuum. This process repeats until many white $q\bar{q}$ states—hadrons—are produced. The time needed for production of a hadron with momentum p is $\tau \sim p/m^2$, so in the c.m.s. the fastest hadrons, which contain the spectator quarks q_a and $\bar{q}_b$, will be produced last. Each produced q and $\bar{q}$ have small relative momenta in their rest system or small rapidity differences. As a result, due to Lorentz invariance of the picture, finally produced hadrons at high energies will be uniformly distributed in the rapidity and will have limited transverse momenta—the same characteristics as in multiperipheral models.

The total cross section of the process of particle production with $\bar{q}_a q_b$ annihilation $\sigma_{ab}^{(\mathrm{ann})}$ can be expressed in terms of the probabilities $w(y_q)$ of finding in the fast moving hadron a quark with a given rapidity y_q or the momentum ratio x_q. These variables are connected by the relation $y_q = \ln(2p_0 x_q/m_{\perp q})$, where p_0 is the momentum of the hadron and $m_{\perp q}$ is the transverse mass of the quark. The function $w(y_q)$ depends on the invariants—rapidity differences $\Delta y = \bar{y}_q - y_q \simeq y_a - y_q$, where $\bar{y}_q$ is the mean value of rapidity of the quark in the fast moving hadron. This difference can also be written as $\bar{y}_q - y_q = \ln(\bar{x}_q/x_q)$, where $\bar{x}_q$ is the mean fraction of the initial hadron momentum carried by the valence quark q.

The cross section $\sigma_{ab}^{(\mathrm{ann})}$ can be written as the product of probabilities of finding in a given system the valence antiquark $\bar{q}_a$ and the quark q_b with close rapidities, as only such pairs annihilate with large cross section $\sigma_0 \sim 1/m^2$:

$$\sigma_{ab}^{(\mathrm{ann})}(s) = w(y_a - y_{\bar{q}_a}) w(y_{q_b} - y_b)\sigma_0. \qquad (4)$$

The result evidently should not depend on the choice of the reference frame—on the value of $y_{\bar{q}_a} \simeq y_{q_b}$. The

only function that satisfies this condition at large Δy is

$$w(\Delta y) = C\exp(-\beta\Delta y). \quad (5)$$

Thus, the probability of finding in a fast hadron a slow valence quark with the rapidity strongly different from the rapidity of a hadron decreases exponentially with Δy. The cross section $\sigma_{ab}^{(\mathrm{ann})}$ has the following energy dependence at large s ($y_a - y_b = \ln(s/(m_a m_b))$):

$$\sigma_{ab}^{(\mathrm{ann})}(s) \sim \exp\left[-\beta(y_a - y_b)\right] \sim 1/s^{\beta}. \quad (6)$$

The cross section has a power-law decrease as energy increases. Comparing this behavior with the Regge dependence $\sigma_{ab}^{(\mathrm{ann})}(s) \sim 1/s^{1-\alpha_{\mathrm{R}}(0)}$, corresponding to the exchange of Regge poles α_{R}, we conclude that the constant β, which characterizes the behavior of the valence quark distributions at $\Delta y \gg 1$ or $x \to 0$, is equal to $1 - \alpha_{\mathrm{R}}(0)$.

Analogous considerations in the impact-parameter $\mathbf{b}$ space lead to the following equation for the quark distribution $w(\Delta y, \Delta\mathbf{b})$:

$$\int d^2 b_q w(y_a - y_q, \mathbf{b}_a - \mathbf{b}_q) w(y_q - y_b, \mathbf{b}_q - \mathbf{b}_b) \quad (7)$$
$$= c w(y_a - y_b, \mathbf{b}_a - \mathbf{b}_b).$$

The solution to this integral equation has the form

$$w(\Delta y, \Delta\mathbf{b}) = \frac{c\exp(-\beta\Delta y)}{4\pi\alpha'\Delta y}\exp\left[-\frac{(\Delta\mathbf{b})^2}{4\alpha'\Delta y}\right]. \quad (8)$$

Equation (8) leads to the characteristic Regge behavior for total cross section $\sigma_{ab}^{(\mathrm{ann})}(s, \mathbf{b})$ in the impact-parameter space, and the parameters β and α' are connected to the intercept and the slope of Regge trajectories α_{R}:

$$\beta = 1 - \alpha_{\mathrm{R}}(0), \quad \alpha' = \alpha'_{\mathrm{R}}(0). \quad (9)$$

Expression (8) can be interpreted as a result of a random walk (diffusion) in the impact-parameter space of a valence quark with a probability decreasing with Δy.

Thus, in this model, the distributions of valence quarks at small x are determined by the parameters of the secondary (α_{R}) Regge poles.

In the process of string (color tube) breaking, the probability of producing only two final hadrons is small at large energies (the mean number of produced hadrons is proportional to $\ln s$). For example, in the process $\pi^+\pi^- \to \pi^0\pi^0$, the valence $u\bar{u}(d\bar{d})$ quarks of π^+ and π^- annihilate, and then the color tube is formed. It breaks later with $d\bar{d}(u\bar{u})$ production from the vacuum, which together with the quark spectators produces the final π^0 mesons. Using the t invariance (for this example, it is also possible to use isospin invariance), it is easy to see that the probability of the string breaking with production of only two final pions with rapidity difference Δy $w_{\pi\pi}(\Delta y) = \sigma_{\pi^+\pi^-\to\pi^0\pi^0}/\sigma_{\pi^+\pi^-}^{(\mathrm{ann})}$ has the form of Eq. (8) with $\beta = 1 - \alpha_\rho(0)$. In the reaction $\pi^+\pi^- \to K^+K^-$, an $s\bar{s}$ pair of quarks is produced under the string breaking, and comparing the amplitude of this process with the Regge dependence, we obtain

$$w_{K\bar{K}} = \frac{\sigma_{\pi^+\pi^-\to K\bar{K}}}{\sigma_{\pi^+\pi^-}^{(\mathrm{ann})}} \sim \frac{\exp\left[-2(1-\alpha_{K^*}(0))\Delta y\right]}{\Delta y\exp\left[-(1-\alpha_\rho(0))\Delta y\right]}. \quad (10)$$

In this case, $\beta = 1 - 2\alpha_{K^*}(0) + \alpha_\rho(0) = 1 - \alpha_\phi(0)$. The last equality is due to the relations between intercepts of Regge trajectories obtained in [14].

These results can be generalized [11] to the situations where the hadronic state produced in the process of the string fission has a large rapidity gap Δy between groups of particles. The probability of such a configuration is determined by Eq. (8), and the values of constants β and α' depend on the type of quark q_k.

Detailed models of string breaking have been developed [8] and are widely used now in Monte Carlo simulations of multiparticle production.

Let us consider now the inelastic interaction of hadrons in the case of cylinder-type diagrams, when the valence quarks of colliding hadrons do not annihilate. In this case, an interaction is determined by the gluonic exchanges, which lead to the color exchange between colliding hadrons. The main contribution in $1/N$ expansion is due to the exchange of the state with the quantum number of the color octet (as, for example, a single-gluon exchange). Note that, in this situation, contrary to the planar case, the valence quarks are in their average configuration and it is reasonable to assume that the probability of finding soft gluons in any reference frame is not small. This means that such cross section will not decrease with energy and corresponds to the assumption that the intercept of the Pomeranchuk pole $\alpha_{\mathrm{P}}(0) \geq 1$.

After the color exchange takes place, the colliding hadrons move in opposite directions (in c.m.s.) and are in the representation $\mathbf{8}$ of the group $SU(3)_c$. The configuration of the color field in this case in the large-N_c limit corresponds to the sum of two strings of the $q\bar{q}$ type considered above. These strings decay in the same manner as in the planar case, and the decays of these strings are independent (in the leading $1/N$ order). The only correlation between strings is that hadrons with close rapidities must have close values of impact parameters ($(\Delta\mathbf{b})^2 \sim 1/m^2$). This is, however, essential in order to provide the Regge pole nature for the Pomeron.

From the fact that there are two strings in the Pomeron case, we conclude that the density of produced hadrons at very high energy and in the central rapidity region in this case is twice as large as that in the planar case. The same follows from the comparison of the single-chain diagram of Fig. 1*b* with the two-chain diagram of Fig. 2*b*. Thus, the string model provides a simple picture of interaction for diagrams of $1/N$ expansion.

Consider now the processes of multiparticle production in more detail. The simplest process is the single-particle inclusive production $ab \to cX$. The inclusive distribution of hadrons for the planar diagrams of Fig. 1*b* can be written as

$$f_c^{(\mathrm{pl})} = \frac{1}{\sigma_{ab}^{(\mathrm{pl})}(s)} E_c \frac{d^3\sigma_c^{(\mathrm{pl})}}{d^3p_c} \qquad (11)$$
$$= F^c(y_{q_a} - y_c, y_c - y_{\bar{q}_b}, p_{\perp c}^2).$$

When $y_{q_a} - y_c$ or $y_c - y_{\bar{q}_b} \gg 1$, F^c does not depend on the corresponding variable. This is the consequence of the short-range nature of correlations in rapidity for the process of string decay. Thus, at high energies and in the fragmentation region of hadron a when $y_{q_a} - y_c \sim 1$ and $y_c - y_{\bar{q}_b} \gg 1$, the function F^c of Eq. (11) depends only on two variables and can be written in terms of the Feynman variable $x = p_{||}^c/p_{q_a} = p_{||}^c/p_a$:

$$f_c^{(\mathrm{pl})} = F^c(x, p_\perp^2) \equiv D_{q_a}^c(x, p_\perp^2)x. \qquad (12)$$

The function $D_{q_a}^c$ is the fragmentation function of the quark q_a to the hadron c. In the limit $x \to 0$, function F^c does not depend on x and $D_{q_a}^c = g^c(p_\perp^2)$. This corresponds to a uniform distribution of final hadrons in the central rapidity region.

The fastest hadrons usually contain the valence quark q_a, and it is possible to determine the behavior of the function D_q^c in the limit $x \to 1$, when there is a big rapidity gap $\Delta y \simeq \ln 1/(1-x)$. The probability of such a configuration is described by $w(\Delta y)d(\Delta y)$ with $\beta = 1 - \alpha_{kk}$ in Eq. (8) and $d(\Delta y) = dx/(1-x)$; index k denotes the type of exchanged quark. Coming from the impact parameter to the transverse momenta of hadrons, one obtains

$$D_{q_a}^c(x, p_\perp^2) = b(p_\perp^2)(1-x)^{\alpha_{ii}(0) - 2\alpha_{ik}(p_\perp^2)}, \qquad (13)$$
$$x \to 1.$$

The fragmentation functions satisfy the relation

$$\sum_c \int_0^1 D_q^c(x) x dx = 1, \qquad (14)$$

which follows from energy–momentum conservation. The behavior of fragmentation functions for different types of quarks and hadrons can be determined in the region $x \to 1$ [26]. This, together with the $1/x$ dependence for $x \to 0$ and the relations that follow from conservation of momentum [Eq. (14)], charge, strangeness, etc., strongly limits possible behavior of fragmentation functions.

Using planarity and the Kancheli–Mueller [37, 38] theorem, which relates inclusive cross sections to the discontinuity of the $ab\bar{c} \to ab\bar{c}$ forward scattering amplitude, it is possible to obtain many relations between inclusive particle spectra [24].

Consider now the case of the two-chain production mechanism of Fig. 2*b*. Here, the quarks that produce each chain have only a fraction of the energy of colliding hadrons. The final hadron c can be produced in each of the chains and its distribution should be the same as in the planar case. Thus, the inclusive distribution can be written as a sum of two terms—convolutions of the probabilities of having a string of a certain length in the rapidity and the functions F^c of Eq. (11), which characterize the distribution of hadrons produced in the process of string breaking:

$$f_c^{(\mathrm{cyl})}(y) = \frac{d\sigma_c^{(\mathrm{cyl})}}{\sigma^{(\mathrm{cyl})} dy_c} = \frac{1}{\sigma^{(\mathrm{cyl})}} \int d^2p_\perp \qquad (15)$$
$$\times E_c \frac{d^3\sigma_c^{(\mathrm{cyl})}}{d^3p_c} = \int\int\int d^2p_\perp dy_{q_a} dy_{\bar{q}_b} w^{q_a}(y_{q_a})$$
$$\times w^{\bar{q}_b}(y_{\bar{q}_b}) F^c(y_{q_a} - y_c, y_c - y_{\bar{q}_b}, p_\perp^2) + \mathrm{s.c.},$$

where s.c. denotes the analogous expression from the contribution of the second chain. The function $w^i(y_i)$ determines the probability that the end of the string, related to the quark i, has the rapidity y_i or the fraction of the momentum x_i.

At high energies and in the fragmentation region of the particle a, it is possible to write the inclusive spectrum in terms of the variable x:

$$f_c^{(\mathrm{cyl})} = \frac{\bar{x}}{\sigma^{(\mathrm{cyl})}} \frac{d\sigma_c^{(\mathrm{cyl})}}{dx} = \int_x^1 dx_q \phi_q^a(x_q) \qquad (16)$$
$$\times D_q^c\left(\frac{x}{x_q}\right)\frac{x}{x_q} + \mathrm{s.c.},$$

where $\bar{x} = E_c/p_a$ and the functions $\phi_q^a(x_q)$ are the distributions of "quarks" (ends of the strings) in hadron a. They are connected to the functions $w(y_q)$ introduced before by a relation $w(y_q)dy_q = \phi_q(x_q)dx_q$.

The ends of the strings corresponding to the valence quark and antiquark of the initial hadron carry the total momentum of the initial hadron: $\int_0^1 (\phi_q^a(x) +$

$\phi^a_{\bar{q}}(x))xdx = 1$. Using this condition and Eq. (16), it is easy to verify that inclusive cross sections satisfy the sum rule, which follows from the conservation of the momentum:

$$\sum_c \int_0^1 f_c^{(\mathrm{cyl})}(x)dx = 1. \quad (17)$$

The behavior of the valence quark distribution at $x \to 0$ follows from Eq. (6):

$$\phi^a_{q_i}(x) = \frac{w^{q_a}(\ln(\bar{x}/x))}{x} \sim x^{-\alpha_{ii}(0)}, \quad x \to 0. \quad (18)$$

The behavior at $x \to 1$ can be obtained if we take into account that, for $x_{q_i} \to 1$, the corresponding $\bar{q}_k$ is very slow:

$$\phi^a_{q_k}(x) \sim (1-x)^{-\alpha_{kk}(0)}, \quad x \to 1. \quad (19)$$

Let us note that the behavior of the "quark" distributions and fragmentation functions, given by Eqs. (18), (19), and (13), correspondingly, is valid only for the soft processes and are different from those valid in hard processes for pointlike quarks.

The behavior of inclusive distributions for cylinder diagrams in the limit $x \to 1$ follows from Eq. (16) and Eqs. (13), (19):

$$f_c^{(\mathrm{cyl})}(x) \sim (1-x)^{1-\alpha_{kk}-\alpha_{ll}} = (1-x)^{1-2\alpha_{kl}}, \quad x \to 1. \quad (20)$$

This expression corresponds to the triple-Regge asymptotics of inclusive spectra.

Equation (16) can be generalized to include dependence on transverse momenta of hadrons [39]. In this case, it is necessary to introduce an extra integration over transverse momentum of the end of the string.

It was assumed in the QGSM that the Pomeron corresponding to the cylinder-type diagrams is a simple pole with $\alpha_{\mathrm{P}}(0) > 1$. The value of $\alpha_{\mathrm{P}}(0)$ was determined from analysis of experimental data.

For such a "supercritical" Pomeron, higher terms of the topological expansion associated with exchange by several Pomerons in the t channel are also important. This is due to the fact that, though the exchange by n Pomerons is $\sim 1/(N^2)^n$, it is enhanced by the factor $(s)^{n\Delta}$. Thus, it is necessary to sum many terms of the topological expansion at very high energy. The s-channel discontinuities of these diagrams are related to processes of production of $2k$ ($k \le n$) chains of particles.

The AGK-cutting rules [40] make it possible to determine the cross sections for $2k$-chain (string) production (with any number of uncut Pomerons) if the contributions of all n-Pomeron exchanges to the forward elastic scattering amplitude are known. These contributions can be calculated using the Reggeon diagram technique [36]. In most calculations, diagrams of the eikonal type have been taken into account [18, 24]. The inelastic diffraction was taken into account in the "quasi-eikonal" approximation (for account of more complicated diagrams with interactions between Pomerons, see below). In this model, the cross sections of $2k$-chain production σ_k have the form [41]

$$\sigma_k(\xi) = \frac{\sigma_{\mathrm{P}}}{kz}\left[1 - \exp(-z)\sum_{i=0}^{k-1}\frac{z^i}{i!}\right], \quad k \ge 1, \quad (21)$$

where

$$\sigma_{\mathrm{P}} = 8\pi\gamma_{\mathrm{P}}\exp(\Delta\xi), \quad z = \frac{2C\gamma_{\mathrm{P}}}{R^2 + \alpha'_{\mathrm{P}}\xi}\exp(\Delta\xi),$$
$$\xi = \ln(s/s_0),$$

γ_{P} and R^2 are parameters that describe the Pomeron residue (see below). The quantity $C = 1.5$ takes into account modification of the eikonal approximation due to intermediate inelastic diffractive states.

The total interaction cross section in this model has the form

$$\sigma^{(\mathrm{tot})} = \sum_0^\infty \sigma_k(\xi) = \sigma_{\mathrm{P}} f\left(\frac{z}{2}\right), \quad (22)$$
$$f\left(\frac{z}{2}\right) = \sum_1^\infty \frac{(-z)^{n-1}}{n \cdot n!},$$

where $\sigma_0(\xi) = \sigma^{(\mathrm{el})} + \sigma^{(\mathrm{DD})}$ is the cross section of diffractive processes [(DD) denotes diffraction dissociation] and it is given by the formula

$$\sigma_0(\xi) = \sigma_{\mathrm{P}}\left[f\left(\frac{z}{2}\right) - f(z)\right]. \quad (23)$$

The simplest parametrization of the Pomeron exchange

$$T_{\mathrm{P}}(\xi, t) = \gamma_{\mathrm{P}}\exp[\alpha_{\mathrm{P}}(0)\xi + (R^2 + \alpha'_{\mathrm{P}}\xi)t] \quad (24)$$

has been used in Eqs. (21)–(23).

The parameters γ_{P}, R^2, Δ, and α'_{P} were determined from the fit to the experimental data on the total interaction cross sections and differential cross section of elastic pp and $p\bar{p}$ scattering at high energies [42, 43]. The most important quantities Δ and α'_{P} have the following values:

$$\Delta = 0.12\text{–}0.14, \quad \alpha'_{\mathrm{P}} = 0.2\text{–}0.25\ \mathrm{GeV}^{-2}. \quad (25)$$

It should be noted that the value of Δ becomes larger ($\Delta \approx 0.2$) if the interaction between Pomerons is taken into account [44] (see below).

For superhigh energies, when $\xi \gg 1$, $\sigma^{(\mathrm{tot})}(\xi)$ has a Froissart-type behavior

$$\sigma^{(\mathrm{tot})}(\xi) \simeq \frac{8\pi\alpha'_{\mathrm{P}}\Delta}{C}\xi^2. \tag{26}$$

This type of behavior for the total cross section is common to a broad class of models with $\alpha_{\mathrm{P}}(0) > 1$. The slope of the diffraction cone increases asymptotically also as ξ^2.

Inclusive cross sections and multiplicity distributions can be obtained in this approach by summing over hadronic production for all processes of $2k$-chain formation:

$$\frac{d\sigma_c}{dy_c} = \sum_0^\infty \sigma_k(\xi) f_c^k(\xi, y_c), \tag{27}$$

$$\sigma_N(\xi) = \sum_0^\infty \sigma_k(\xi) W_N^k(\bar{N}_k(\xi)), \tag{28}$$

where $f_c^k(\xi, y_c) = d\sigma_c^k/(\sigma_k dy_c)$ and W_N^k are rapidity and multiplicity distributions for $2k$-chain production with mean values $\bar{N}_k$. The term with $k = 0$ in Eqs. (27), (28) corresponds to the process of diffraction dissociation $\sigma^{(\mathrm{DD})}$.

The function f_c^1 has been considered above [Eqs. (15), (16)]. For an arbitrary configuration where there are both valence and "sea chains," functions $f_c^k(\xi, y_c)$ can be written in the form [16, 25] (we consider here, as an example, pp collisions, where valence chains connect the valence quark of one colliding proton with the diquark of another proton)

$$f_c^k(\xi, x) = a_c[f_q^{c,k}(x_+) f_{qq}^{c,k}(x_-) \tag{29}$$
$$+ f_{qq}^{c,k}(x_+) f_q^{c,k}(x_-) + 2(k-1) f_{q_{\mathrm{sea}}}^{c,k}(x_+) f_{\bar{q}_{\mathrm{sea}}}^{c,k}(x_-)],$$

where $x_\pm = \frac{1}{2}\left[\sqrt{x_\perp^2 + x^2} \pm x\right]$, $x_\perp = 2\bar{m}_\perp^c/\sqrt{s}$, $x_+ = \exp(y_c - y_c^{\max})$, and

$$f_i^{c,k}(x) = \int_x^1 dx_1 \phi_i^{a,k}(x_1) D_i'^c\left(\frac{x}{x_1}\right)\frac{x}{x_1}, \tag{30}$$
$$i = q, qq, q_{\mathrm{sea}}.$$

The first two terms in Eq. (29) correspond to chains connected to valence quarks and diquarks and generalize Eq. (16) to all values of rapidity. The function $D_i'^c(z)$, which enters Eq. (29), differs from the function $D_i^c(z)$ only by the constant a_c, which determines the density of hadrons of a given type produced in the central rapidity region in a single chain. The last term in Eq. (29) is due to extra chains connected to sea quarks.

From the discussion above, we know that, for a single-cylinder case, the distribution functions of quarks in pp collisions have the following behavior in the limits $x \to 0$ and $x \to 1$:

$$\phi_q^{p,1}(x) = \begin{cases} c_1 x^{-\alpha_{\mathrm{R}}(0)}, & x \to 0, \\ c_2(1-x)^{\alpha_{\mathrm{R}}(0) - 2\alpha_N(0)}, & x \to 1. \end{cases} \tag{31}$$

The $x \to 1$ behavior for a quark in a proton is determined by the $x \to 0$ behavior of a diquark. The last is related in this approach to the intercept of the qq–$\bar{q}\bar{q}$ trajectory, which in this approach is equal to $\alpha_{q\bar{q}}(0) - 2\alpha_{qqq}(0) = \alpha_{\mathrm{R}}(0) - 2\alpha_N(0)$, where $\alpha_{\mathrm{R}}(0) = 0.5$ and $\alpha_N(0) \simeq -0.5$ are the intercepts of bosonic and fermionic Regge trajectories.

The distributions $\phi_q^{p,k}(x)$ with $k > 1$ have the same behavior as $x \to 0$. This is connected to the fact that we consider the rescatterings with limited masses in the intermediate states, so the probabilities of having slow ends of sea chains must decrease as $x \to 0$. The distributions of the type $1/x$ at small x correspond to the "enhanced" diagrams with interactions between Pomerons, which are neglected in the "quasi-eikonal" model. For $x \to 1$, the distributions with $k > 1$ must be softer than for the case $k = 1$, because, if one quark takes all the momentum of the initial hadron, all other constituents must be soft. The probability of slowing each extra quark (antiquark) is $\sim x^{1-\alpha_{\mathrm{R}}(0)}$. Thus, $\phi_q^{p,k} \sim (1-x)^{\alpha_{\mathrm{R}}(0) - 2\alpha_N(0) + 2(1-\alpha_{\mathrm{R}}(0))(k-1)}$ as $x \to 1$.

Interpolation formulas have been used in the calculations [16, 25]. For example,

$$\phi_u^{p,k}(x_1) = C_u^k x_1^{-\alpha_{\mathrm{R}}(0)} \tag{32}$$
$$\times (1-x_1)^{\alpha_{\mathrm{R}}(0) - 2\alpha_N(0) + 2(1-\alpha_{\mathrm{R}}(0))(k-1)}.$$

The coefficients C_i^k are determined from the normalization condition:

$$C_u^k = \frac{\Gamma\left(2 - 2\alpha_N(0) + 2(1-\alpha_{\mathrm{R}}(0))(k-1)\right)}{\Gamma(1-\alpha_{\mathrm{R}}(0))\Gamma\left(\alpha_{\mathrm{R}}(0) - 2\alpha_N(0) + 2(1-\alpha_{\mathrm{R}}(0))(k-1) + 1\right)}. \tag{33}$$

The fragmentation functions $D_i^c(z)$ have been determined using the rules described above and interpolating between the $z \to 0$ and $z \to 1$ limits [26]. The function $D_u^{\pi^+}$, for example, was chosen in the form

$$zD_u^{\pi^+}(z) = a_\pi(1-z)^{-\alpha_R(0)+\lambda}, \quad (34)$$

where $\lambda = 2\alpha'_R\overline{p_{\perp\pi}^2} \approx 0.5$. Using such interpolation formulas for $D_i^c(z)$ and sum rules, which follow from conservation of momentum, charge, strangeness, etc., it is possible to determine the fragmentation functions of both quarks and diquarks for many types of hadrons in a full kinematical region [26]. Here, I give some examples:

$$zD_u^{\pi^-}(z) = a_\pi(1-z)^{-\alpha_R(0)+\lambda+2(1-\alpha_R(0))}, \quad (35)$$

$$zD_{uu}^{\pi^+}(z) = a_\pi(1-z)^{\alpha_R(0)-2\alpha_N(0)+\lambda}, \quad (36)$$

$$zD_u^{K^+}(z) = a_K(1-z)^{-\alpha_\phi(0)+\lambda}(1+a_{1K}z), \quad (37)$$

$$zD_u^{K^-}(z) = a_K(1-z)^{-\alpha_\phi(0)+\lambda+2(1-\alpha_R(0))}. \quad (38)$$

The constants a_π, a_K, and a_{1K} are equal to $a_\pi = 0.4$–0.44, $a_K = \frac{1}{8}a_\pi$, and $a_{1K} \simeq 2$.

Thus, in contrast to other models, where fragmentation functions are determined from experimental data, in QGSM practically all parameters are fixed theoretically. The inclusive spectra in this model automatically have the correct triple-Regge limit for $x \to 1$ and double-Regge limit for $x \to 0$ and satisfy all conservation laws.

4. COMPARISON WITH EXPERIMENT

After all the parameters of the Pomeranchuk pole have been determined from a fit to experimental data on the total cross sections of pp, $p\bar{p}$ interactions and the slope of the diffraction cone B in elastic pp scattering (Fig. 3), the predictions of the QGSM for different characteristics of multiparticle production at high energies contain practically no new free parameters. Note that the asymptotic regime, where both total cross sections and slopes of the diffraction cone increase as ξ^2, is achieved at extremely high energies $\sqrt{s} \sim 10^4$–10^5 GeV. It follows from Fig. 3 that the approximate linear dependence on ξ of the slope of the diffraction cone in elastic pp scattering observed at present energies will be modified in the LHC energy range. This theoretical prediction can be checked experimentally at LHC.

The model does not contain "odderon"-type singularities [45] with negative signature, which could lead to a difference of pp and $p\bar{p}$ scattering, so at energies $\sqrt{s} \geq 10^2$ GeV all characteristics of pp and $p\bar{p}$ interactions coincide. In the following, we shall often compare data on $p\bar{p}$ interactions at energies of present colliders with data on pp interactions at lower energies.

For a sum of all n-Pomeron exchange diagrams of the eikonal type (without interaction between Pomerons), there is a cancellation of their contributions to the single-particle inclusive spectra in the central rapidity region for $n \geq 2$ [40]. Thus, only the pole diagram contributes and inclusive spectra increase with energy as $f^a \sim (s/s_0)^\Delta$. This means, in particular, that an energy dependence of inclusive spectra in the central rapidity region gives more reliable information on the value of Δ than an energy dependence of $\sigma^{(\mathrm{tot})}$, where Pomeron cuts strongly modify energy dependence compared to the pole diagram.

Rapidity (and pseudorapidity) distributions of charged particles in pp ($p\bar{p}$) interactions at different energies are shown in Fig. 4. In the supercritical Pomeron theory with account of "nonenhanced" diagrams, which we consider now, inclusive cross sections $d\sigma_c/dy$ at very high energies and at $y \approx 0$ increase with energy as $(s/s_0)^\Delta$. It follows from Fig. 4 that the value of $\Delta = 0.12$–0.14 found from analysis of $\sigma^{(\mathrm{tot})}(s)$ [42, 43] is in perfect agreement with the rise of rapidity distributions with energy. Let us note that, in the intermediate energy region $\sqrt{s} \sim 10$ GeV, there is an important effect, connected with the fluctuations in rapidity of the ends of the strings, which leads to an extra increase in inclusive spectra in the central rapidity region [12].

An integral over a rapidity distribution gives an average multiplicity of charged hadrons $\langle N_{\mathrm{ch}} \rangle$. The model reproduces quite well both rapidity distributions and $\langle N_{\mathrm{ch}} \rangle$ at accessible energies. $\langle N_{\mathrm{ch}} \rangle$ increases with energy much faster than $\ln(s/s_0)$ and reaches values of about 100 charged particles in the LHC energy range.

The multiplicity distributions in the model are given according to Eq. (28) by a sum of contributions connected to a different number of cut Pomerons ($2k$ chains). Each of these contributions has a Poisson-like form (only short-range correlations inside chains), but their sum has a very peculiar dependence on energy. At energies $\sqrt{s} \leq 10^2$ GeV, different contributions overlap strongly. This leads to an approximate KNO scaling, i.e., dependence of the quantity $\Psi \equiv \langle N_{\mathrm{ch}} \rangle \sigma_{N_{\mathrm{ch}}}/\sigma^{(\mathrm{in})}$ on the variable $z = N_{\mathrm{ch}}/\langle N_{\mathrm{ch}} \rangle$ only. The model reproduces multiplicity distributions well at these energies [13]. The mean number of chains increases with energy (as $(s/s_0)^\Delta$) and the model predicts [13] the definite violation of KNO scaling. This prediction was confirmed by the experimental data at the S$p\bar{p}$S collider—Fig. 5. In

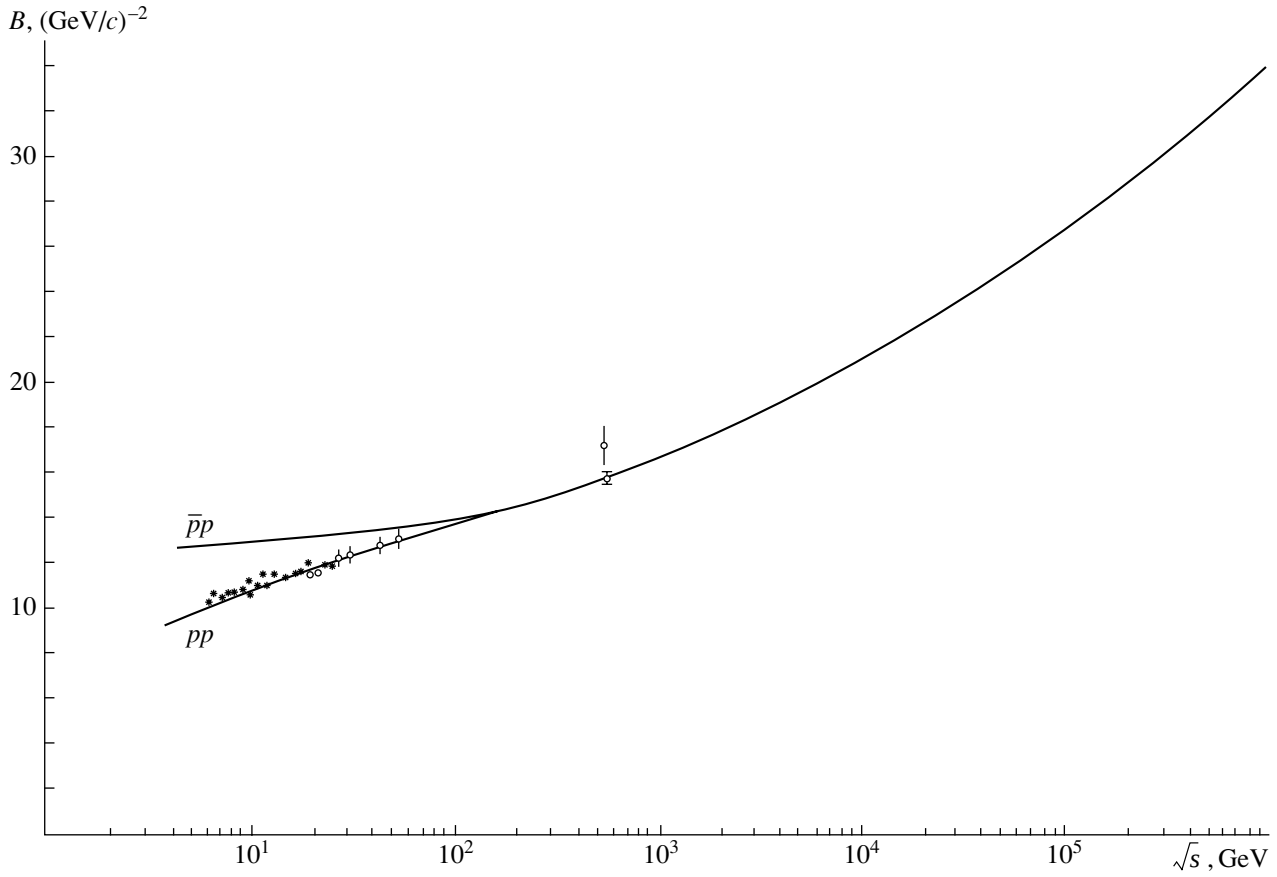

Fig. 3. Energy dependence of the diffraction cone slope B for elastic pp, $\bar{p}p$ scattering.

this figure, the multiplicity distribution at energy $\sqrt{s} = 10^5$ GeV is also shown. As energy increases, the maximum of the distribution in a variable $z = N_{\rm ch}/\langle N_{\rm ch}\rangle$ moves to the left and the distribution increases in the region of large z. It is interesting to note that, at superhigh energies $\sqrt{s} \sim 10^5$ GeV, different terms in the sum of Eq. (28) start to be separated and the distribution has the corresponding maxima and minima. At present energies $\sqrt{s} \sim 10^3$ GeV, only the first maximum and a "shoulder" start to appear. This prediction of a structure in multiplicity distributions at very high energies is consistent with experimental observations at existing colliders.

The model also reproduces well the semi-inclusive rapidity distributions and dependence of multiplicity distributions on rapidity [13, 16]—see Fig. 6. Thus, the study of multiplicity distributions not only confirms the multicomponent structure of the model, but also shows that the weights of different components $(\sigma_k/\sigma^{(\rm in)})$ are close to the predictions of the quasi-eikonal approximation.

Another consequence of the multi-Pomeron contributions is an existence of the long-range rapidity correlations. It leads, in particular, to a large and fast increasing with energy (as $(s/s_0)^{2\Delta}$) of the long-range part of the correlation function $C(y, 0)$ and to strong forward–backward correlations. For a single-Pomeron contribution, the correlations are of a short-range order in rapidity; however, due to the presence of several components with different densities of produced particles, the long-range correlations become important. In the case of the forward–backward correlations, for example, by increasing the number of particles in the forward hemisphere, we automatically increase the number of produced chains and thus increase the mean multiplicity of hadrons in the backward hemisphere. The dependence of the mean multiplicity of charged hadrons, produced in the backward hemisphere (rapidity region from -4 to -1), on the number of charged particles in the forward rapidity interval (from 1 to 4) is shown in Fig. 7. The model reproduces the nearly linear dependence of experimental data.

Let us consider now inclusive spectra of different hadrons at high energies. The QGSM makes it possible to calculate spectra for all values of the variable x [16]. Spectra of π^- and π^+ mesons in pp interactions are shown in Figs. 8*a* and 8*b*. Note that

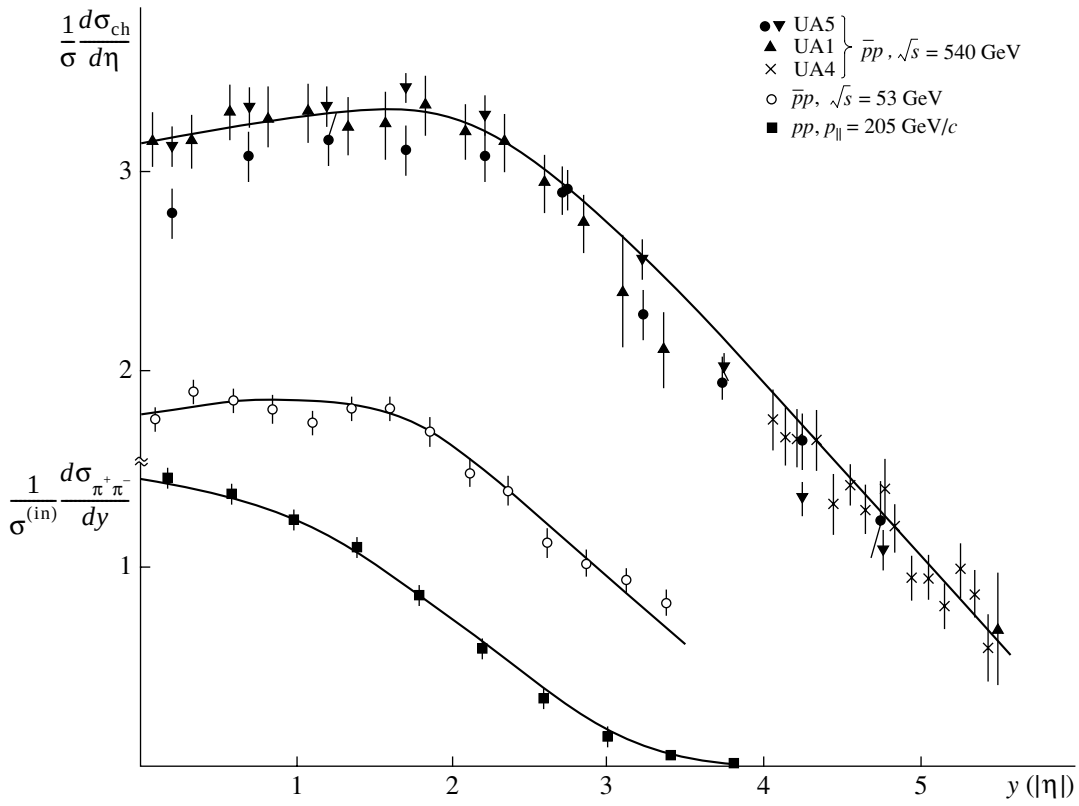

Fig. 4. Rapidity (pseudorapidity) distributions of charged particles and pions produced in pp ($p\bar{p}$) interactions at different energies.

the Feynman scaling is strongly violated in the region of small x. On the other hand, in the fragmentation region $x \geq 0.1$, a violation of scaling is rather weak. This has important implications for cosmic-ray experiments.

Predictions of the model for inclusive cross sections and mean multiplicities of $K^{\pm}$ and K^0_S mesons are presented in [25] and are in good agreement with experimental data. In the QGSM, the strange-quark suppression factor is predicted theoretically [26] and is confirmed by experimental data. The ratio of the mean multiplicities of kaons and pions increases with energy. This increase in the model is mainly due to the mass difference of kaons and pions, and the ratio tends to a constant value ≈ 0.12 asymptotically.

The spectra of protons and antiprotons and the corresponding theoretical curves [25] are shown in Fig. 9. The spectra of the protons have a clear "leading" behavior (distributed in the region $x \sim 1$) due to the fragmentation of diquarks, which have a distribution concentrated at x_{qq} close to 1. The antiprotons, on the contrary, are determined mainly by the "central" production in the valence chains and arise also from sea chains. Asymptotically, in the central region ($x \approx 0$), the spectra of protons and antiprotons should be equal (the same is true for all particles and antiparticles).

Another example of the "leading" behavior is the spectrum of Λ hyperons, shown in Fig. 10. The strange-quark suppression in the fragmentation function of the model is a function of z and is proportional to $(1-z)^{\alpha_\rho(0)-\alpha_\phi(0)}$ as $z \to 1$. This leads to a shift of the maximum of the spectrum for Λ to smaller values of x than for nonstrange baryons (like n or Δ isobar) in good agreement with experimental data.

Energy dependences of mean multiplicities for n, $\bar{p}$, and $\bar{\Lambda}$ are shown in Fig. 11.

The model was extended to the processes of charmed-particle production in [46]. The main problem here is a poor knowledge of the $c\bar{c}$ trajectory. The form of the x behavior and absolute normalization depend strongly on the intercept of the $c\bar{c}$ trajectory. In [46], two values of $\alpha_{c\bar{c}}(0)$ have been used: $\alpha_{c\bar{c}} = -2$, which follows from the mass spectrum under an assumption of linear trajectories, and $\alpha_{c\bar{c}} = 0$ from perturbative calculations. The nonperturbative value is preferable from analysis of recent data on Λ_c production. The model gives reasonable predictions for energy behavior of inclusive cross sections of heavy-particle production at superhigh energies and forms

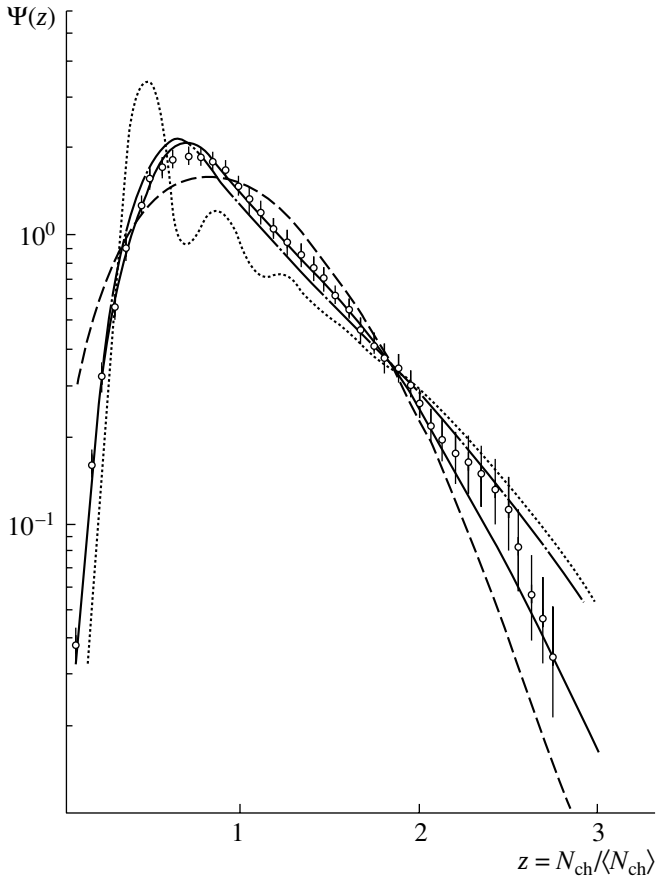

Fig. 5. KNO distributions in pp ($p\bar{p}$) interactions. The full curve is for $\sqrt{s} = 540$ GeV, the dotted curve is for $\sqrt{s} = 10^5$ GeV, the dash-dotted one is for $\sqrt{s} = 2 \times 10^3$ GeV, and the dashed one represents the data for $\sqrt{s} \sim 10$ GeV. The data at $\sqrt{s} = 540$ GeV are from UA5 group.

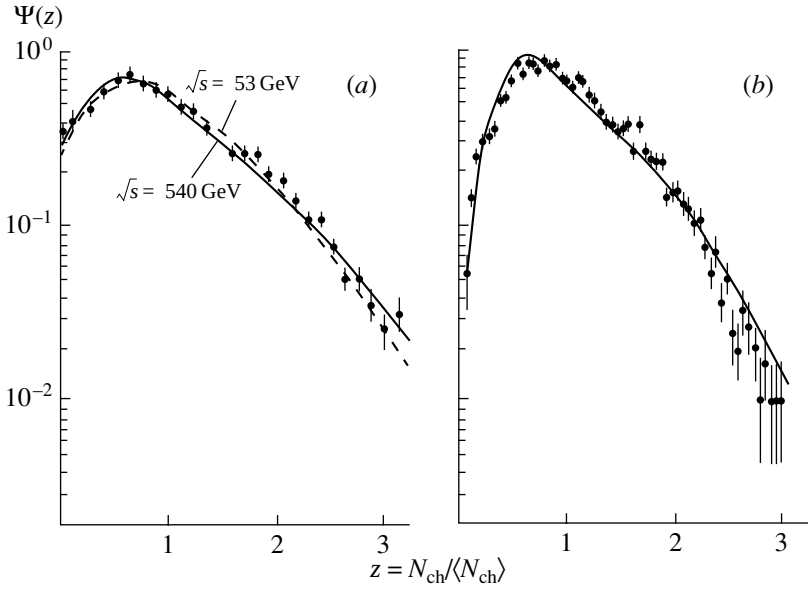

Fig. 6. Multiplicity distributions at $\sqrt{s} = 540$ GeV for different pseudorapidity intervals: (a) $|\eta| < 1.5$ (for comparison, the theoretical prediction for ISR energy $\sqrt{s} = 53$ GeV is indicated by the dashed curve) and (b) $|\eta| < 3.5$. The data are from UA1 group.

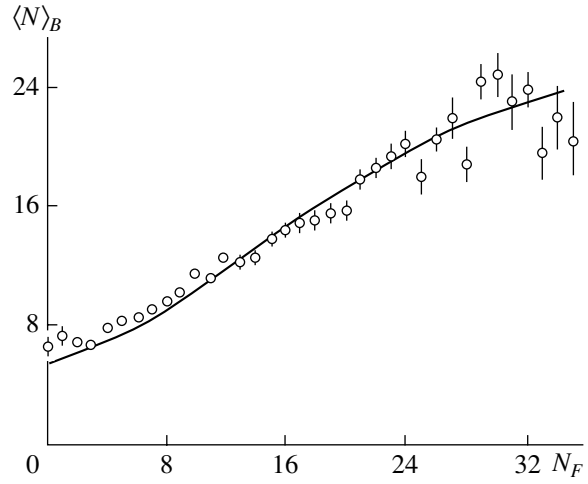

Fig. 7. Forward–backward correlations at $\sqrt{s} = 540$ GeV.

of inclusive spectra for different charmed particles [47, 48].

Thus, the QGSM gives a completely adequate description of a large amount of experimental data on multiparticle production at high energies. Monte Carlo realizations of the model also exist [49].

5. DIFFRACTIVE-PRODUCTION PROCESSES AND INTERACTIONS BETWEEN POMERONS

Diffractive production of particles at high energies, in the Regge pole model is described by the diagrams with Pomeron exchange. It is possible to have excitation of one of the colliding hadrons—single-diffraction dissociation (Fig. 12*a*)—or excitation of both initial particles—double-diffraction dissociation (Fig. 12*b*).

For all diffractive processes, there is a large rapidity gap between groups of produced particles. For example, for single-diffraction dissociation, there is a gap between the particle $1'$ and the rest system of hadrons. This rapidity gap $\Delta y \approx \ln(1/(1-x))$, where x is the Feynman variable of hadron $1'$. The mass of a diffractively excited state at large s can be large. The only condition for diffraction dissociation is $s_i \ll s$ ($i = 1, 2$ in Fig. 12). For large masses of excited states, $s_2 \approx (1-x)s$ and $\xi' = \ln(s/s_2) \approx \Delta y$.

The cross section for inclusive single-diffraction dissociation in the Regge pole model can be written in the following form:

$$\frac{d^2\sigma}{d\xi_2 dt} = \frac{(g_{11}(t))^2}{16\pi}|G_{\mathrm{P}}(\xi', t)|^2\sigma_{\mathrm{P2}}^{(\mathrm{tot})}(\xi_2, t), \qquad (39)$$

where $\xi_2 \equiv \ln(s_2/s_0)$ and $G_{\mathrm{P}}(\xi', t) = \eta(\alpha_{\mathrm{P}}(t)) \times \exp[(\alpha_{\mathrm{P}}(t)-1)\xi']$ is the Pomeron Green's function.

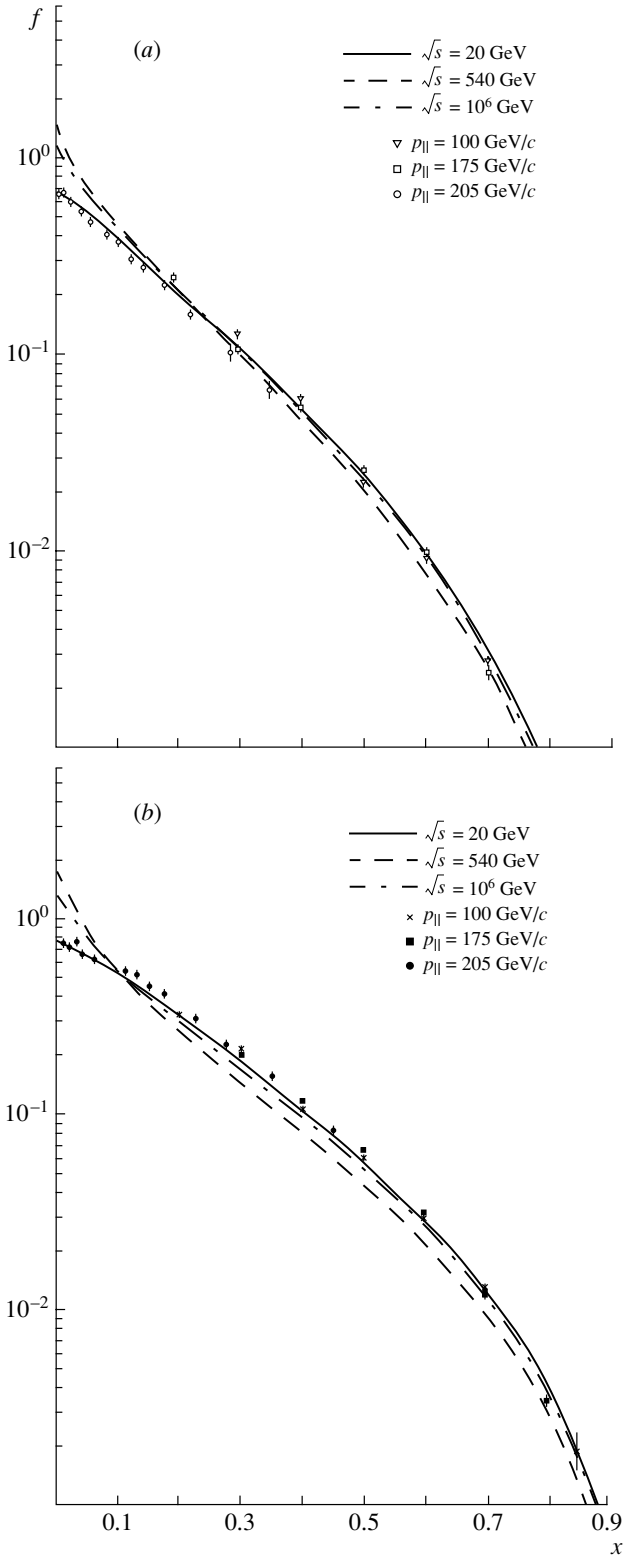

Fig. 8. Inclusive cross sections $f \equiv \frac{1}{\sigma^{(\mathrm{in})}} \int d^2p_\perp E d^3\sigma/d^3p$ for (*a*) π^- and (*b*) π^+ at various energies.

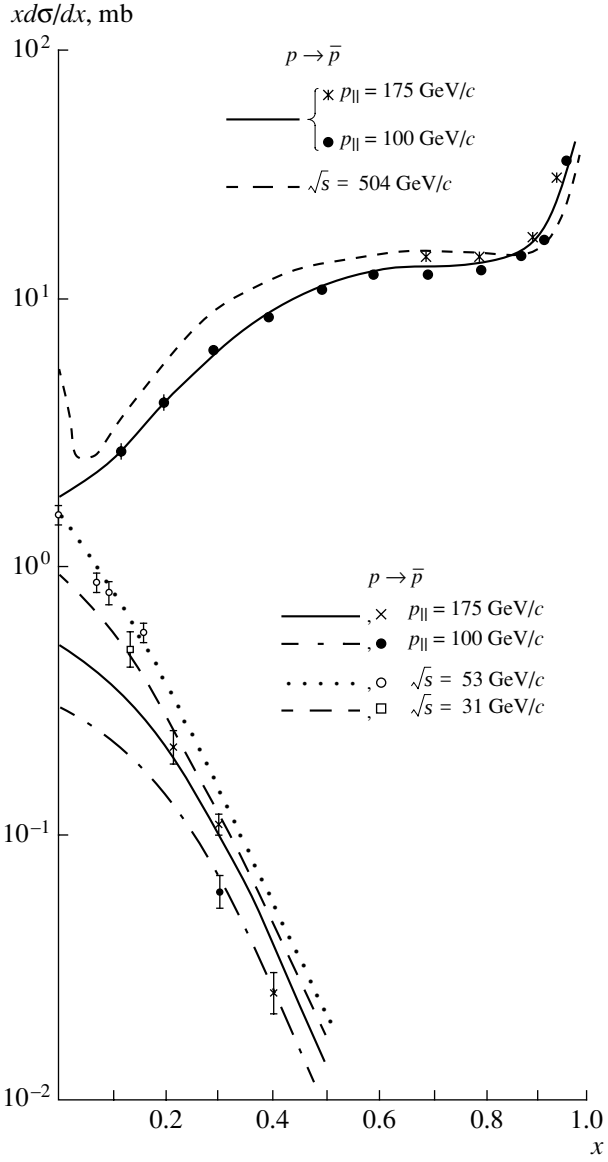

Fig. 9. Spectra of p and $\bar{p}$ in pp collisions. The short-dashed curve is the prediction for $\sqrt{s} = 540$ GeV.

The quantity $\sigma_{\mathrm{P2}}^{(\mathrm{tot})}(\xi_2, t)$ can be considered as the Pomeron–particle total interaction cross section [50]. Note that this quantity is not directly observable and it is defined by its relation to the diffraction production cross section [Eq. (39)]. This definition is useful, however, because at large s_2 this cross section has the same Regge behavior as usual cross sections:

$$\sigma_{\mathrm{P2}}^{(\mathrm{tot})}(s_2, t) = \sum_k g_{22}^k(0) r_{\mathrm{PP}}^{\alpha_k}(t) \left(\frac{s_2}{s_0}\right)^{\alpha_k(0)-1}, \quad (40)$$

where the $r_{\mathrm{PP}}^{\alpha_k}(t)$ is the triple-Reggeon vertex, which describes coupling of two Pomerons to Reggeon α_k.

In this kinematical region $s \gg s_2 \gg m^2$, the inclusive diffractive cross section is described by the triple-Regge diagrams (Fig. 13) and has the form

$$f^1 = \sum_k G_k(t)(1-x)^{\alpha_k(0)-2\alpha_{\mathrm{P}}(t)} \left(\frac{s}{s_0}\right)^{\alpha_k(0)-1}. \quad (41)$$

The Pomeron–proton total cross section and triple-Regge vertices $r_{\mathrm{PP}}^{\mathrm{P}}$, r_{PP}^{f} have been determined from analysis of experimental data of diffractive production of particles in hadronic collisions (see [51]).

In the eikonal-type models discussed above, the diffraction dissociation to the states with not overly large masses has been taken into account. Diffractive production of states with large masses is related to the diagrams with interactions between Pomerons. Neglect of these interactions in the first approximation is justified by a smallness of triple-Pomeron and four-Pomeron interaction vertices, found from analysis of diffractive processes [51]. However, at very high energies, it is necessary to include the diagrams with Pomeron interactions in order to have a self-consistent description of high-energy hadronic interactions, including large-mass diffractive production of particles. The main drawback of the original formulation of the QGSM and DPM models is an absence of "enhanced" diagrams with interactions between Pomerons. It was demonstrated in paper [44] that inclusion of these diagrams leads in many cases to predictions which are very close to the results of eikonal-type models; however, the value of the "bare" Pomeron intercept increases up to $\alpha_{\mathrm{P}}(0) \approx 1.2$. A model for multiparticle production with an account of the complete set of "enhanced" diagrams has yet to be formulated. We shall demonstrate below that an account of interactions between Pomerons is important for heavy-ion collisions at high energies and leads to effects which are seen experimentally at RHIC.

6. SMALL-x PHYSICS

In this section, it will be shown that the methods developed for analysis of high-energy hadronic interactions described above can be applied to physics of small-Bjorken variable x studied in deep-inelastic scattering. Experiments at HERA have found two extremely important properties of small-x physics: a fast increase in parton densities as x decreases [52, 53] and the existence of substantial diffractive production in deep-inelastic scattering (DIS) [54, 55].

In DIS, it is possible to study different asymptotic limits. For a virtuality of the photon $Q^2 \to \infty$ and $x = Q^2/(W^2 + Q^2) \sim 1$ ($W^2 = (p_{\gamma^*} + p_p)^2$), the usual QCD evolution equations can be applied and Q^2 dependence of the structure functions and distributions of partons can be predicted if an initial

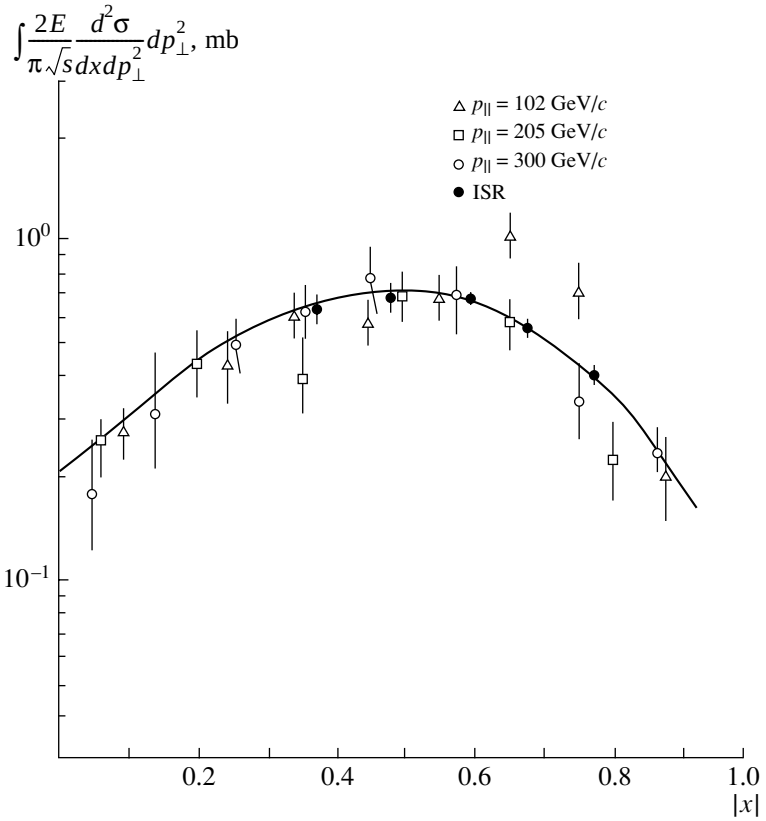

Fig. 10. Spectra of Λ hyperons in pp collisions. Theoretical curve is for $\sqrt{s} = 27.5$ GeV.

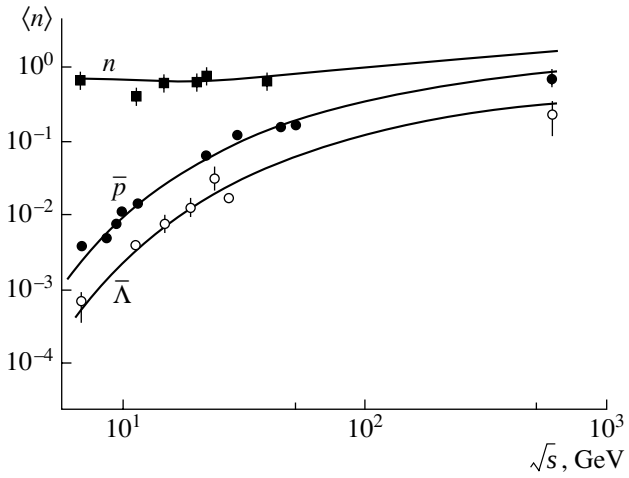

Fig. 11. Energy dependence of multiplicities of n, $\bar{p}$, and $\bar{\Lambda}$.

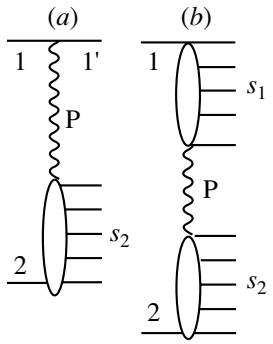

Fig. 12. Diagrams for diffractive production of hadrons in the Regge pole model.

condition for structure functions at $Q^2 = Q_0^2$ is formulated. On the other hand, if Q^2 is fixed and $x \to 0$ (or $\ln(1/x) \to \infty$), the asymptotic Regge limit is relevant. The most interesting question is: What is the behavior of DIS in the region where both $\ln(1/x)$ and $\ln Q^2$ are large? This is a transition region between perturbative and nonperturbative dynamics in QCD, and its study can give important information on the properties of confinement and its relation to the QCD perturbation theory. The asymptotic Regge limit in DIS can be related to the high-energy limit of hadronic interactions and is usually described in terms of the Pomeranchuk singularity.

6.1. Diffractive Processes in $\gamma^* p$ Interactions

A fast increase in $\sigma_{\gamma^* p}^{(\mathrm{tot})}$ as $W^2 \equiv s$ increases at large Q^2 observed experimentally [52, 53] raises a

question whether there are two different Pomerons—"soft" and "hard." From studies of the Pomeron in QCD [35], it follows that there are no theoretical reasons for such a situation and most probably the rightmost pole in the j plane is generated by both "soft" and "hard" dynamics. I shall assume that there is one ("physical") Pomeron pole with the same $\alpha_{\mathrm{P}}(0)$ as was determined from high-energy hadronic interactions with an account of many-Pomeron cuts. On the other hand, the effective intercept, which depends on the relative contribution of multi-Pomeron diagrams, can be different in different processes.

There are good reasons to believe that the fast increase in $\sigma^{(\mathrm{tot})}_{\gamma^* p}$ with energy in the HERA energy range will change to a slower increase at much higher energies. This is due to multi-Pomeron effects, which are related to shadowing in highly dense systems of partons, with eventual "saturation" of densities. This problem has a long history (for reviews, see [56]) and has been extensively discussed in recent years [57]. It is closely connected to the problem of the dynamics of very high energy heavy-ion collisions [58] (see below).

In [59], it was suggested that the increase in the effective intercept of the Pomeron, $\alpha_{\mathrm{eff}} = 1 + \Delta_{\mathrm{eff}}$, as Q^2 increases from zero to several GeV^2, is mostly due to a decrease in shadowing effects with increasing Q^2. A parametrization of the Q^2 dependence of $\Delta_{\mathrm{eff}}(Q^2)$,

$$\Delta_{\mathrm{eff}}(Q^2) = \Delta_0 \left(1 + \frac{2Q^2}{d + Q^2}\right),$$

such that $\Delta_{\mathrm{eff}} \approx 0.1$ for $Q^2 \approx 0$ (as in soft hadronic interactions) and $\Delta_{\mathrm{eff}} \approx 0.2$ (bare Pomeron intercept) for Q^2 of the order of few GeV^2, gives a good description of all existing data on $\gamma^* p$ total cross sections in the region of $Q^2 \leq 5$–10 GeV^2 [59, 60]. At larger Q^2, effects due to QCD evolution become important. Using the above parametrization as the initial condition in the QCD evolution equation, it is possible to describe the data in the whole region of Q^2 studied at HERA [59, 61].

As was emphasized above, the value of Δ_{eff} should depend not only on Q^2 but also on x and it should decrease as $x \to 0$. It is important to build an explicit model based on Reggeon theory, where all these effects will be incorporated.

This problem was investigated recently in [62], where the Reggeon approach was applied to the processes of diffractive $\gamma^* p$ interaction. It was emphasized in the previous section that, in the Reggeon calculus [36], the amount of rescatterings (or multi-Pomeron exchanges) is closely related to diffractive production. AGK cutting rules [40] allow one to calculate the cross section of inelastic diffraction if contributions of multi-Pomeron exchanges to the elastic-scattering amplitude are known. Thus, it is very important for self-consistency of theoretical models to describe not only total cross sections, but, simultaneously, inelastic diffraction. In particular, in the Reggeon calculus, the variation of Δ_{eff} with Q^2 is related to the corresponding variation of the ratio of diffractive to total cross sections. In [62], an explicit model for the contribution of rescatterings was constructed, which leads to the pattern of energy behavior of $\sigma^{(\mathrm{tot})}_{\gamma^* p}(W^2, Q^2)$ for different Q^2 described above. Moreover, it allows one to describe simultaneously diffraction production by real and virtual photons. In this model, it is possible to study quantitatively a regime of "saturation" of parton densities.

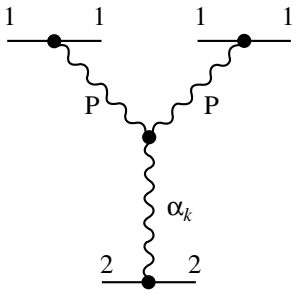

Fig. 13. Triple-Regge diagram.

Let us discuss briefly the qualitative picture of diffractive dissociation of a highly virtual photon at high energies. It is convenient to discuss this process in the laboratory frame, where the quark–gluon fluctuations of a photon live a long time $\sim 1/x$ (Ioffe time [63]). A virtual photon fluctuates first to a $q\bar{q}$ pair. There are two different types of configurations of such pair, depending on transverse distance between quarks (or $k_\perp$).

(a) Small-size configurations with $k_\perp^2 \sim Q^2$. These small dipoles ($r \sim 1/k_\perp \sim 1/Q$) have a small ($\sim r^2$) total interaction cross section with the proton.

(b) Large-size configurations with $r \sim 1/\Lambda_{\mathrm{QCD}}$ and $k_\perp \sim \Lambda_{\mathrm{QCD}} \ll Q$. They have a large total interaction cross section, but contribute with a small phase space at large Q^2, because these configurations are kinematically possible only if the fraction of longitudinal momentum carried by one of the quarks is very small: $x_1 \sim k_\perp^2/Q^2 \ll 1$. This configuration corresponds to the "aligned jet," introduced by Bjorken and Kogut [64].

Both configurations lead to the same behavior of $\sigma^{(\mathrm{tot})}_{\gamma^* p} \sim 1/Q^2$, but they behave differently in the process of the diffraction dissociation of a virtual photon [65, 66]. The cross section of such a process is proportional to a square of modulus of the corresponding diffractive amplitude, and for a small-size

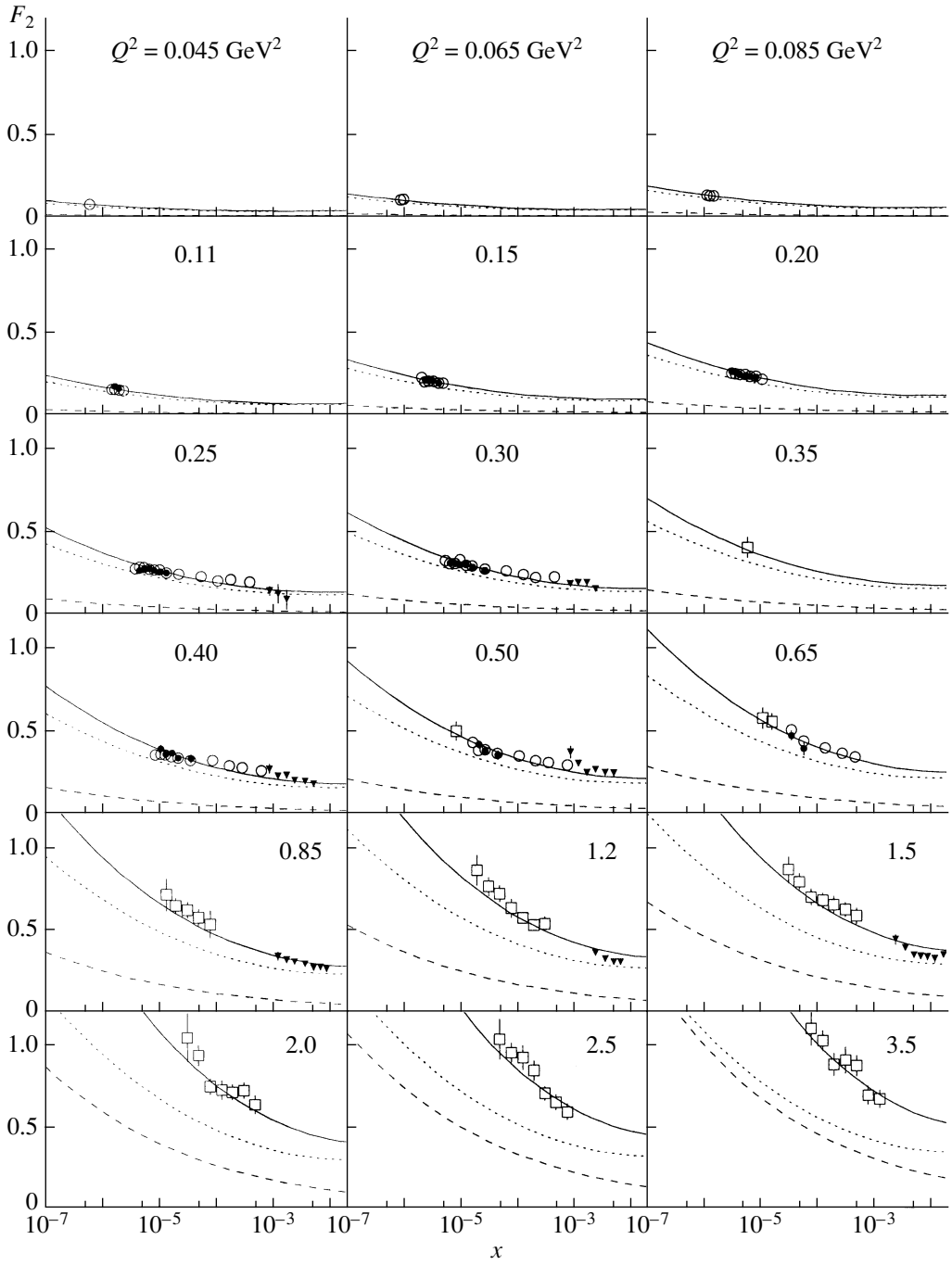

Fig. 14. Structure function F_2 as a function of x for different values of Q^2 compared with experimental data. Dashed curves denote small-distance contributions; dotted curves, large-distance contributions; full curves, their sum.

configuration, it is small ($\sim 1/Q^4$). For large-size configurations, smallness is only due to the phase space and the inclusive cross section for diffractive dissociation of a virtual photon decreases as $1/Q^2$, i.e., in the same way as the total cross section. This is true only for the total inclusive diffractive cross section, where characteristic masses of produced states are $M^2 \sim Q^2$. For exclusive channels with fixed mass (for example, production of vector mesons), the situation is different and these cross sections decrease faster than $1/Q^2$ at large Q^2.

Inclusive diffractive production of very large masses ($M^2 \gg Q^2$) can be described in the first approximation by triple-Regge diagrams [67]. From the point of view of the quark–gluon fluctuation of the fast photon, the triple-Pomeron contribution corresponds

to diffractive scattering of a very slow (presumably gluonic) parton, which has a small virtuality.

The model [62] uses the picture of diffraction dissociation of a virtual photon outlined above and is a natural generalization of models used for the description of high-energy hadronic interactions. The interaction of the small-size component in the wave function of a virtual photon is calculated using QCD perturbation theory. The main parameter of the model—intercept of the Pomeron—was fixed from a phenomenological study of these interactions discussed above ($\Delta_{\mathrm{P}} = 0.2$) and was found to give a good description of $\gamma^* p$ interactions in a broad range of Q^2 ($0 \le Q^2 < 10\,\mathrm{GeV}^2$). Another important parameter of the theory, the triple-Pomeron vertex, obtained from a fit to the data ($r^{(0)}_{\mathrm{PPP}}/g^{\mathrm{P}}_{pp}(0) \approx 0.1$) is also in reasonable agreement with the analysis of soft hadronic interactions [44, 67]. The description of the structure function F_2 as a function of x for different values of Q^2 (experimental data are from H1 [52], ZEUS [53]) is shown in Fig. 14. Diffraction dissociation of a virtual photon is usually represented as a function of Q^2, M^2 (or $\beta = Q^2/(M^2+Q^2)$), and $x_{\mathrm{P}} = x/\beta = (M^2+Q^2)/(W^2+Q^2)$. A description of HERA data on diffractive dissociation [55] in the model is shown in Figs. 15 and 16. The model can be used to predict structure functions and partonic distributions at higher energies or smaller x, which will be accessible for experiments at LHC.

6.2. Shadowing Effects for Nuclear Structure Functions

A study of the shadowing effects for structure functions of nuclei in the small-x region provides a stringent test of the Reggeon approach to the small-x problem. The shadowing effects are enhanced for nuclei ($\sim A^{1/3}$) and lead to deviations from A^1 behavior for structure functions of nuclei. The Glauber–Gribov [68, 69] approach to interactions of particles with nuclei makes it possible to calculate rescattering corrections for interaction of a virtual photon with a nucleus in terms of diffractive interaction of a photon with a nucleon, which was discussed above.

A contribution of a double-rescattering term to the $\sigma_{\gamma^* A}$ is directly expressed in terms of the differential cross section for a diffraction dissociation of a virtual photon in $\gamma^* N$ interactions,

$$\sigma^{(2)} = -4\pi \int d^2b T_A^2(b) \qquad (42)$$
$$\times \int dM^2 \frac{d\sigma^{(\mathrm{DD})}_{\gamma^* N}(t=0)}{dM^2 dt} F_A(t_{\min}),$$

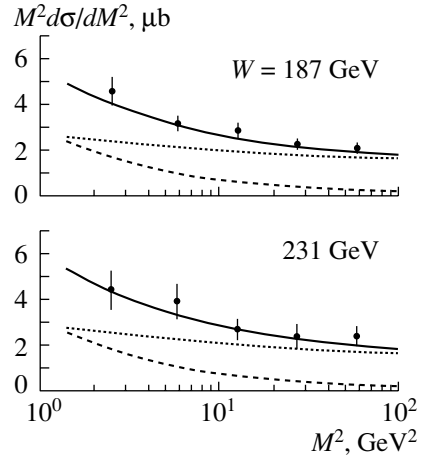

Fig. 15. M^2 distribution for diffraction dissociation of a photon at $Q^2 = 0$. Dotted and dashed curves denote PPP and PPR contributions, respectively.

where $F_A(t_{\min}) = \exp(R_A^2 t_{\min}/3)$; $t_{\min} \approx -m_N^2 x_{\mathrm{P}}^2$, $x_{\mathrm{P}} = 1 - x_p$; R_A is the nuclear radius; and $T_A(b)$ is the nuclear profile function ($\int d^2b T_A(b) = A$).

Higher order rescatterings are model-dependent, and in the generalized Schwimmer model [70], we obtain in the region of small x

$$F_{2A}/F_{2N} = \int d^2b \frac{T_A(b)}{1 + F(x,Q^2)T_A(b)} \qquad (43)$$

with

$$F(x,Q^2) = 4\pi \int dM^2 \left(d\sigma^{(\mathrm{DD})}_{\gamma^* N}(t=0)/dM^2 dt\right)$$
$$\times \left(F_A(t_{\min})/\sigma_{\gamma^* N}(x,Q^2)\right).$$

Theoretical predictions [71] based on Eq. (43) and the model for diffraction dissociation of [67] are in very good agreement with NMC data on nuclear structure functions at very small x [72]. We believe that this approach gives reliable predictions for nuclear shadowing effects in the region of smaller x not yet studied experimentally. This region will play an important role in dynamics of heavy-ion collisions at superhigh (LHC) energies.

7. HEAVY-ION COLLISIONS AT HIGH ENERGIES

7.1. High-Energy Nuclear Interactions

Let us consider first high-energy hadron–nucleus interactions. In the Glauber model, it is described by diagrams that look like successive rescatterings of an initial hadron on nucleons of the nucleus. However, as was emphasized by Gribov [69], the spacetime picture of the interaction at high energy $E > m_h \mu R_A$ (μ is a characteristic hadronic scale ~ 1 GeV) is completely

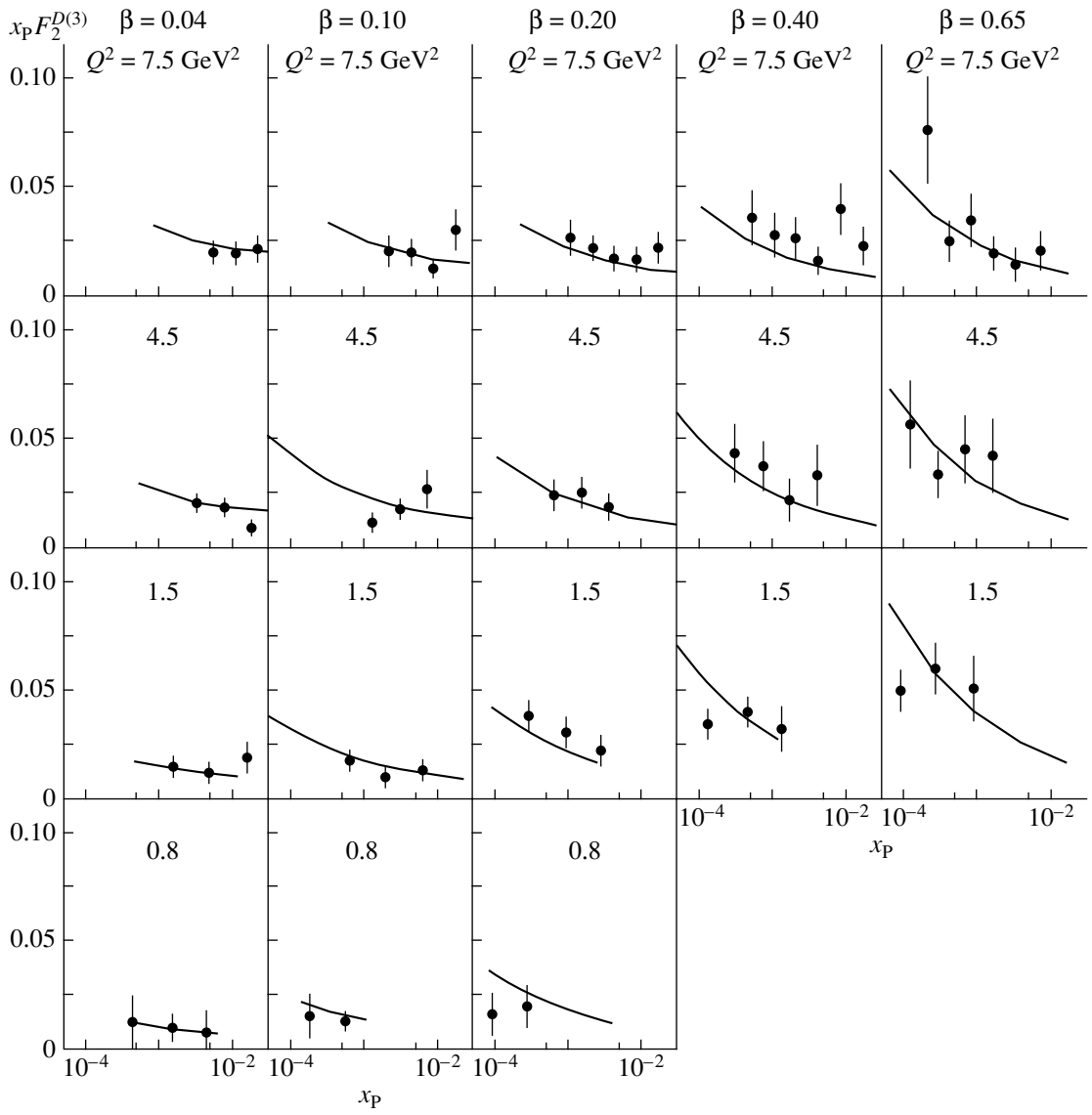

Fig. 16. The diffractive structure function $x_P F_2^{D(3)}$ as a function of x_P for fixed values of Q^2 and $\beta = Q^2/(Q^2 + M^2)$.

different from this simple picture. At high energy, there are coherent interactions of a fluctuation of the initial hadron with nucleons of the nucleus. The fluctuation is "prepared" long before its interaction with the nucleus. Nevertheless, the elastic hA amplitude can be written as a sum of the diagrams, with elastic rescatterings that give the same result as the Glauber model, plus all possible diffractive excitations of the initial hadron. At not overly high energies $E_L \sim 10^2$ GeV, these inelastic contributions lead to corrections to the Glauber approximation of 10–20% for the total hA cross section. However, at very high energies and for inclusive cross sections, this modification of the Glauber approximation is very important. The difference between the Glauber model and Gribov's theory is essential for understanding shadowing corrections for structure functions of nuclei, as was shown in the previous section, and for many aspects of multiparticle production on nuclei [73].

An important consequence of the spacetime structure of high-energy interactions of hadrons with nuclei is the AGK result [40], according to which, for inclusive cross sections, all rescatterings cancel, so that these cross sections are determined by the diagrams of the impulse approximation. Note, however, that this result, valid asymptotically in the central rapidity region, only applies to diagrams of the Glauber type, i.e., when masses of intermediate states in rescattering diagrams are limited and do not increase with energy. As a result, the inclusive cross section for the production of a hadron a is expressed, for a given impact parameter b, in terms of inclusive cross section

for hN interactions:

$$E\frac{d^3\sigma^a_{hA}(b)}{d^3p} = T_A(b)E\frac{d^3\sigma^a_{hN}}{d^3p}. \quad (44)$$

After integration over b, we get

$$E\frac{d^3\sigma^a_{hA}}{d^3p} = AE\frac{d^3\sigma^a_{hN}}{d^3p}. \quad (45)$$

The total and inelastic hA cross sections in the Glauber model can be easily calculated and are given for heavy nuclei by well-known expressions. For example,

$$\sigma^{(\mathrm{in})}_{hA} = \int d^2b(1-\exp(-\sigma^{(\mathrm{in})}_{hN}T_A(b)). \quad (46)$$

The situation for nucleus–nucleus collisions is much more complicated. There are no analytic expressions in the Glauber model for heavy-nucleus elastic-scattering amplitudes. The problem stems from a complicated combinatorics and from the existence of dynamical correlations related to "loop diagrams" [74, 75]. Thus, usually, an optical-type approximation [76, 77] and probabilistic models for multiple rescatterings [78] are used. For inclusive cross sections in AB collisions, the result of the Glauber approximation is very simple to formulate due to the AGK cancellation theorem. It is possible to prove, for an arbitrary number of interactions of nucleons of both nuclei [79], that all rescatterings cancel in the same way as for hA interactions. Thus, a natural generalization of Eq. (44) for inclusive spectra of hadrons produced in the central rapidity region in nucleus–nucleus interactions takes place in the Glauber approximation:

$$E\frac{d^3\sigma^a_{AB}(b)}{d^3p} = T_{AB}(b)E\frac{d^3\sigma^a_{NN}}{d^3p}, \quad (47)$$

where $T_{AB}(b) = \int d^2sT_A(\mathbf{s})T_B(\mathbf{b}-\mathbf{s})$, and A, B are atomic numbers of colliding nuclei. After integration over b, Eq. (47) gives

$$E\frac{d^3\sigma^a_{AB}}{d^3p} = ABE\frac{d^3\sigma^a_{NN}}{d^3p}. \quad (48)$$

The densities of charged particles can be obtained from Eqs. (47) and (48) by dividing them by the total inelastic cross section of nucleus–nucleus interaction. For example,

$$\frac{dn^{(\mathrm{ch})}_{AB}(b)}{dy} = \frac{T_{AB}(b)}{\sigma^{(\mathrm{in})}_{AB}}\frac{d\sigma^{(\mathrm{ch})}_{NN}}{dy} \quad (49)$$

and

$$\frac{dn^{(\mathrm{ch})}_{AB}}{dy} = \frac{AB}{\sigma^{(\mathrm{in})}_{AB}}\frac{d\sigma^{(\mathrm{ch})}_{NN}}{dy}. \quad (50)$$

Densities of charged hadrons $dn^{(\mathrm{ch})}/d\eta|_{\eta=0}$ in central Pb–Pb collisions at $\sqrt{s} = 130$ GeV

Glauber	With shadowing corrections	Experiment [82]
1200 ± 100	630 ± 120	$555 \pm 12 \pm 35$

In the following, we shall use these results to calculate particle densities in the central rapidity region at energies of RHIC and LHC. Reviews of applications of the Glauber–Gribov approach, $1/N$ expansion in QCD, and string model to processes of nucleus–nucleus interactions can be found in [18, 80].

7.2. Particle Densities in Heavy-Ion Collisions at Superhigh Energies

Now, we will address the question of particle densities in heavy-ion collisions.

Equation (50) for particle densities integrated over impact parameter (minimum bias events) can be rewritten as

$$\frac{dn^{(\mathrm{ch})}_{AB}}{dy} = n_{AB}\frac{dn^{(\mathrm{ch})}_{NN}}{dy}, \quad (51)$$

where $n_{AB} = AB\sigma^{(\mathrm{in})}_{NN}/\sigma^{(\mathrm{in})}_{AB}$. It corresponds to the average number of collisions in the Glauber model. For $A = B \gg 1$, n_{AB} behaves as $CA^{4/3}$ with $C \approx \sigma^{(\mathrm{in})}_{NN}/(4\pi R_0^2)(R_A = R_0A^{1/3})$. It is well known that Eqs. (47), (48), and (51) can be applied to hard processes, but in the Glauber approximation, they are valid for soft processes as well. We shall see below that, for both soft and hard processes, these equations have to be modified.

Using Eqs. (50) and (51), we obtain for Pb–Pb collisions at LHC at $y = 0$ the following numbers for minimum-bias events and central ($b < 3$ fm) collisions, respectively: $dn^{(\mathrm{ch})}/dy = 2100$ and $dn^{(\mathrm{ch})}/dy = 8500$.

Thus, the Glauber approximation predicts very large densities of charged hadrons in central heavy-ion collisions at LHC. However, are these predictions realistic? In order to answer this question, we will consider possible limitations of the Glauber approximation and also the corrections to the AGK cancellation theorem that are important at high energies.

There are two types of corrections to Eqs. (44) and (47).

(a) The effects due to energy–momentum conservation: the energy of the initial hadron is shared by "constituents" and each subcollision happens at smaller energy. These effects are very important in the fragmentation regions of colliding hadrons (or nuclei)

and reduce particle densities. For $y = 0$, this reduction decreases as $(1/s)^{1/4}$. It is very important at SPS energies and has some effect at RHIC; however, at LHC energies in the central rapidity region, this effect is small.

(b) Another dynamical effect is important at very high energies when diffractive production of very heavy hadronic states ($M^2 \gg m_N^2$) becomes possible. It is related to the triple-Pomeron interaction discussed above and corresponds to an interaction between Pomerons (strings in the string models of particle production). As the total and inelastic cross sections of hA and AB interactions at high energies are close to a black-disc limit due to Glauber-type diagrams, these extra interactions have a small influence on total cross sections. However, they are very important for inclusive spectra in the central rapidity region [73], where contributions of Glauber rescatterings cancel due to AGK rules.

Extra shadowing effects related to these interactions modify the A dependence of the Glauber approximation for inclusive spectra [Eqs. (44), (47)] in such a way that the behavior $d\sigma_{AB}/dy \sim AB$ of the Glauber approximation changes to $d\sigma_{AB}/dy \sim A^\alpha B^\alpha$, where $\alpha < 1$. For very strong interaction between Pomerons, $\alpha \to 2/3$. This limit leads to universal particle densities in pp, pA, and AB collisions. Due to a rather weak interaction between Pomerons even at LHC energies, the value of α is close to 0.9.

The problem of shadowing for inclusive spectra is not especially related to soft processes. The same interactions are relevant also for hard processes (production of jets or particles with large p_T, heavy quarks, large-mass lepton pairs, etc.). For hard processes, due to the QCD factorization theorem, inclusive spectra in nucleus–nucleus collisions are given by convolutions of hard cross sections with distributions of partons in the colliding nuclei. In these cases, interactions between Pomerons describe shadowing effects for nuclear structure functions (i.e., distributions of quarks and gluons in nuclei). Due to a coherence condition, these effects are important only in the region of very small x_i of partons ($x_i \ll 1/(R_A m_N)$). Thus, these effects are important only at very high energies, when $x_i \approx M_T/\sqrt{s}$ satisfy this condition. This condition in terms of x_i of partons coincides with the condition on diffractive production of large-mass states discussed above.

These effects were calculated in [81] in the same model, which was used above for description of the shadowing effects for nuclear structure functions. It was predicted that an account of extra shadowing due to interactions between Pomerons will lead to a decrease in particle densities compared to the Glauber model predictions by a factor ≈ 4 at LHC and by a factor ≈ 2 at RHIC energies. Comparison with first results from RHIC [82] is given in table. The experiment clearly shows a large deviation from the prediction of the Glauber approximation and demonstrates an importance of the shadowing effects for inclusive spectra of hadrons. This approach also reproduces the dependence of particle densities at RHIC on number of participants [83].

These results show that, already starting from RHIC energies, interactions between Pomerons (or strings) play an important role in the dynamics of heavy-ion collisions. On the other hand, characteristic values of partons $x_i \sim 10^{-2}$ at these energies and both experimental data on shadowing for nuclear structure functions [72] and their theoretical interpretation [71] show that we are very far from "saturation" in this region.

8. CONCLUSION

The results presented in this paper show that applications of $1/N$ expansion in QCD and string model to hadronic process allow one to understand many characteristic features of strong interactions. The Reggeon theory of high-energy interactions, based on analyticity and unitarity, becomes much more predictive, because there are many relations between parameters of this theory. As a result, it was possible to formulate a simple quark–gluon strings model that contains only a few parameters and gives a good description of many characteristics of multiparticle production at high energies. The model allows us to predict total cross sections, multiplicities, inclusive spectra of different particles, and other observables for energies of future colliders.

An important theoretical question is to prove directly from QCD the main assumption of this approach on the connection between planar diagrams and Regge behavior.

A challenging problem for high-energy hadronic physics and for this approach, in particular, is the nature of the Pomeron. The analysis of this problem in QCD with inclusion of both nonperturbative and perturbative effects shows that the Pomeron has a very rich dynamical structure.

The interactions between Pomerons are important at very high energies. They are essential in hadron–nucleus and especially in nucleus–nucleus collisions [73, 81], where approach to thermalization and conditions for quark–gluon plasma formation strongly depend on the strength of interactions between strings.

ACKNOWLEDGMENTS

I would like to thank K. Boreskov, A. Capella, V. Fadin, E.G. Ferreiro, O.V. Kancheli, V.A. Khoze, J.H. Koch, G. Korchemski, E. Levin, L.N. Lipatov, A. Martin, C. Merino, C.A. Salgado, Yu.A. Simonov, K.A. Ter-Martirosyan, and J. Tran Thanh Van for stimulating discussions.

This work is supported in part by grants from INTAS (grant no. 00-00366), NATO (grant no. PSTCLG-977275), and the Russian Foundation for Basic Research (project nos. 00-15-96786, 01-02-17383).

REFERENCES

1. G. 't Hooft, Nucl. Phys. B **72**, 461 (1974).
2. G. Veneziano, Phys. Lett. B **52B**, 220 (1974).
3. G. Veneziano, Nucl. Phys. B **117**, 519 (1976).
4. M. Ciafalloni, G. Marchesini, and G. Veneziano, Nucl. Phys. B **98**, 472 (1975).
5. A. Casher, J. Kogut, and L. Susskind, Phys. Rev. D **10**, 732 (1974).
6. X. Artru and G. Mennesier, Nucl. Phys. B **70**, 93 (1974).
7. A. Casher, H. Neuberger, and S. Nussinov, Phys. Rev. D **20**, 179 (1979).
8. B. Andersson, G. Gustafson, and C. Peterson, Phys. Lett. B **71B**, 337 (1977); Z. Phys. C **1**, 105 (1979).
9. E. G. Gurvich, Phys. Lett. B **87B**, 386 (1979).
10. A. B. Kaidalov, Pis'ma Zh. Éksp. Teor. Fiz. **32**, 494 (1980) [JETP Lett. **32**, 474 (1980)].
11. A. B. Kaidalov, Zh. Éksp. Teor. Fiz. **33**, 1369 (1981) [Sov. J. Nucl. Phys. **33**, 733 (1981)].
12. A. B. Kaidalov, Phys. Lett. B **116B**, 459 (1982).
13. A. B. Kaidalov and K. A. Ter-Martirosyan, Phys. Lett. B **117B**, 247 (1982).
14. A. B. Kaidalov, Z. Phys. C **12**, 63 (1982).
15. P. E. Volkovitskii and A. B. Kaidalov, Yad. Fiz. **35**, 1231 (1982) [Sov. J. Nucl. Phys. **35**, 720 (1982)]; Yad. Fiz. **35**, 1556 (1982) [Sov. J. Nucl. Phys. **35**, 909 (1982)].
16. A. B. Kaidalov and K. A. Ter-Martirosyan, Yad. Fiz. **39**, 1545 (1984) [Sov. J. Nucl. Phys. **39**, 979 (1984)]; **40**, 211 (1984) [**40**, 135 (1984)].
17. A. Capella *et al.*, Z. Phys. C **3**, 329 (1980); A. Capella and J. Tran Thanh Van, Phys. Lett. B **114B**, 450 (1982); Z. Phys. C **10**, 249 (1981).
18. A. Capella, U. Sukhatme, C.-I. Tan, and J. Tran Thanh Van, Phys. Rep. **236**, 225 (1994).
19. J. Dias de Deus and S. Jadach, Acta Phys. Pol. B **9**, 249 (1978).
20. G. Cohen-Tannoudji *et al.*, Phys. Rev. D **19**, 3397 (1979); **21**, 2699 (1980).
21. H. Minakata, Phys. Rev. D **20**, 1656 (1979).
22. P. Auranche and F. W. Bopp, Phys. Lett. B **114B**, 363 (1982); Z. Phys. C **13**, 459 (1982).
23. J. Ranft and S. Ritter, Z. Phys. C **20**, 347 (1983); Z. Phys. C **27**, 569 (1985).
24. A. B. Kaidalov, in *Proc. of the Int. Conf. on QCD at 200 TeV,* Ed. by L. Cifarelli and Yu. Dokshitzer (Plenum Press, New York, 1992), p. 1; Surv. High Energy Phys. **13**, 265 (1999).
25. A. B. Kaidalov and O. I. Piskunova, Yad. Fiz. **41**, 1278 (1985) [Sov. J. Nucl. Phys. **41**, 816 (1985)]; Z. Phys. C **30**, 145 (1985).
26. A. B. Kaidalov, Sov. J. Nucl. Phys. **45**, 902 (1987).
27. G. F. Chew and C. Rozenzweig, Phys. Rep. **41**, 26 (1978).
28. A. Dubin, A. Kaidalov, and Yu. Simonov, Phys. Lett. B **323**, 41 (1994); Yad. Fiz. **56** (12), 213 (1993) [Phys. At. Nucl. **56**, 1745 (1993)].
29. Yu. A. Simonov, Nucl. Phys. B **307**, 512 (1988); Yad. Fiz. **54**, 192 (1991) [Sov. J. Nucl. Phys. **54**, 115 (1991)].
30. Yu. A. Simonov, hep-ph/0210309.
31. E. A. Kuraev, L. N. Lipatov, and V. S. Fadin, Zh. Éksp. Teor. Fiz. **71**, 825 (1976) [Sov. Phys. JETP **44**, 443 (1976)]; **72**, 377 (1977) [**45**, 199 (1977)]; Ya. Ya. Balitsky and L. N. Lipatov, Yad. Fiz. **28**, 1597 (1978) [Sov. J. Nucl. Phys. **28**, 822 (1978)].
32. V. S. Fadin and L. N. Lipatov, Phys. Lett. B **429**, 127 (1998); G. Camici and M. Ciafaloni, Phys. Lett. B **430**, 349 (1998).
33. S. J. Brodsky *et al.*, Pis'ma Zh. Éksp. Teor. Fiz. **70**, 161 (1999) [JETP Lett. **70**, 155 (1999)].
34. Yu. A. Simonov, Phys. Lett. B **249**, 514 (1990).
35. A. B. Kaidalov and Yu. A. Simonov, Phys. Lett. B **477**, 163 (2000); Yad. Fiz. **63**, 1507 (2000) [Phys. At. Nucl. **63**, 1428 (2000)].
36. V. N. Gribov, Zh. Éksp. Teor. Fiz. **53**, 654 (1967).
37. A. Mueller, Phys. Rev. D **2**, 2963 (1970).
38. O. V. Kancheli, Pis'ma Zh. Éksp. Teor. Fiz. **11**, 397 (1970) [JETP Lett. **11**, 267 (1970)].
39. A. I. Veselov, O. I. Piskunova, and K. A. Ter-Martirosyan, Phys. Lett. B **158B**, 175 (1985).
40. V. A. Abramovskii, V. N. Gribov, and O. V. Kancheli, Yad. Fiz. **18**, 595 (1973).
41. K. A. Ter-Martirosyan, Phys. Lett. B **44B**, 377 (1973).
42. A. B. Kaidalov, K. A. Ter-Martirosyan, and Yu. M. Shabelskii, Yad. Fiz. **43**, 1282 (1986) [Sov. J. Nucl. Phys. **43**, 822 (1986)].
43. K. A. Ter-Martirosyan, Yad. Fiz. **44**, 1252 (1986) [Sov. J. Nucl. Phys. **44**, 817 (1986)].
44. A. B. Kaidalov, L. A. Ponomarev, and K. A. Ter-Martirosyan, Yad. Fiz. **44**, 722 (1986) [Sov. J. Nucl. Phys. **44**, 468 (1986)].
45. K. Kang and B. Nicolescu, Phys. Rev. D **11**, 2461 (1975); D. Joynson *et al.*, Nuovo Cimento A **30**, 345 (1975).
46. A. B. Kaidalov and O. I. Piskunova, Yad. Fiz. **43**, 1545 (1986) [Sov. J. Nucl. Phys. **43**, 994 (1986)].
47. O. I. Piskounova, Yad. Fiz. **56**, 176 (1993) [Phys. At. Nucl. **56**, 1094 (1993)].
48. G. H. Arakelyan, Yad. Fiz. **61**, 1682 (1998) [Phys. At. Nucl. **61**, 1570 (1998)].

49. N. S. Amelin *et al.*, Yad. Fiz. **51**, 512 (1990) [Sov. J. Nucl. Phys. **51**, 327 (1990)]; Yad. Fiz. **52**, 272 (1990) [Sov. J. Nucl. Phys. **52**, 172 (1990)].
50. A. B. Kaidalov and K. A. Ter-Martirosyan, Nucl. Phys. B **75**, 471 (1974).
51. A. B. Kaidalov, Phys. Rep. **50**, 157 (1979).
52. T. Ahmed *et al.* (H1 Collab.), Phys. Lett. B **299**, 374 (1993); C. Adloff *et al.* (H1 Collab.), Nucl. Phys. B **497**, 3 (1997).
53. M. Derrick *et al.* (ZEUS Collab.), Phys. Lett. B **293**, 465 (1992); J. Breitweg *et al.* (ZEUS Collab.), Phys. Lett. B **407**, 432 (1997).
54. M. Derrick *et al.* (ZEUS Collab.), Z. Phys. C **72**, 399 (1996).
55. C. Adloff *et al.* (H1 Collab.), Z. Phys. C **76**, 613 (1997).
56. L. V. Gribov, E. M. Levin, and M. G. Ryskin, Phys. Rep. **100**, 1 (1983); E. Laenen and E. Levin, Annu. Rev. Nucl. Part. Sci. **44**, 199 (1994); A. H. Mueller, hep-ph/9911289.
57. A. H. Mueller, Nucl. Phys. B **437**, 107 (1995); A. L. Ayala, M. B. Gay Ducati, and E. M. Levin, Phys. Lett. B **388**, 188 (1996); Nucl. Phys. B **493**, 305 (1997); E. Gotsman, E. Levin, and U. Maor, Nucl. Phys. B **493**, 354 (1997); Phys. Lett. B **425**, 369 (1998); **452**, 387 (1999); E. Gotsman, E. Levin, U. Maor, and E. Naftali, Nucl. Phys. B **539**, 535 (1999); M. MacDermott, L. L. Frankfurt, V. Guzey, and M. Strikman, Eur. Phys. J. C **16**, 641 (2000); K. Golec-Biernat and M. Wüsthoff, Phys. Rev. D **59**, 014017 (1999); **60**, 114023 (1999); A. H. Mueller, Eur. Phys. J. A **1**, 19 (1998).
58. L. McLerran and R. Venugopalan, Phys. Rev. D **49**, 2233 (1994); **50**, 2225 (1994); **53**, 458 (1996); J. Jalilian-Marian *et al.*, Phys. Rev. D **59**, 014014, 034007 (1999); A. Kovner, L. McLerran, and H. Weigert, Phys. Rev. D **52**, 3809, 6231 (1995); Yu. V. Kovchegov and A. H. Mueller, Nucl. Phys. B **529**, 451 (1998); Yu. V. Kovchegov, A. H. Mueller, and S. Wallon, Nucl. Phys. B **507**, 367 (1997); A. H. Mueller, Nucl. Phys. B **558**, 285 (1999).
59. A. Capella, A. Kaidalov, C. Merino, and J. Tran Thanh Van, Phys. Lett. B **337**, 358 (1994).
60. A. Kaidalov and C. Merino, Eur. Phys. J. C **10**, 153 (1999).
61. A. Kaidalov, C. Merino, and D. Pertermann, Eur. Phys. J. C **20**, 301 (2001).
62. A. Capella, E. Ferreiro, A. B. Kaidalov, and C. A. Salgado, Nucl. Phys. B **593**, 336 (2001); Phys. Rev. D **63**, 054010 (2001).
63. B. L. Ioffe, Phys. Lett. B **30B**, 123 (1969).
64. J. D. Bjorken and J. B. Kogut, Phys. Rev. D **8**, 1341 (1973).
65. L. L. Frankfurt and M. Strikman, Phys. Rep. **160**, 235 (1988).
66. N. N. Nikolaev and B. G. Zakharov, Z. Phys. C **49**, 607 (1990).
67. A. Capella, A. Kaidalov, C. Merino, and J. Tran Thanh Van, Phys. Lett. B **343**, 403 (1995); A. Capella, A. Kaidalov, C. Merino, *et al.*, Phys. Rev. D **53**, 2309 (1996).
68. R. J. Glauber, *Lectures in Theoretical Physics,* Ed. by W. E. Britten (Interscience Publ., New York, 1959), Vol. 1, p. 315.
69. V. N. Gribov, Zh. Éksp. Teor. Fiz. **56**, 892 (1969) [Sov. Phys. JETP **29**, 483 (1969)]; **57**, 1306 (1969) [**30**, 709 (1970)].
70. A. Schwimmer, Nucl. Phys. B **94**, 445 (1975).
71. A. Capella, A. Kaidalov, C. Merino, *et al.*, Eur. Phys. J. C **5**, 111 (1998).
72. M. Arneodo *et al.* (NMC Collab.), Nuovo Cimento A **107**, 2141 (1994); P. Amaudruz *et al.* (NMC Collab.), Nucl. Phys. B **441**, 3 (1995).
73. A. B. Kaidalov, Nucl. Phys. A **525**, 39c (1991).
74. I. V. Andreev and A. V. Chernov, Yad. Fiz. **28**, 477 (1978) [Sov. J. Nucl. Phys. **28**, 243 (1978)].
75. K. G. Boreskov and A. B. Kaidalov, Yad. Fiz. **48**, 575 (1988) [Sov. J. Nucl. Phys. **48**, 367 (1988)].
76. J. Formanek, Nucl. Phys. B **12**, 441 (1969).
77. W. Czyz and L. C. Maximon, Ann. Phys. (N.Y.) **52**, 59 (1969).
78. C. Pajares and A. V. Ramallo, Phys. Rev. D **31**, 2800 (1985).
79. K. G. Boreskov and A. B. Kaidalov, Acta Phys. Pol. B **20**, 397 (1989).
80. K. Werner, Phys. Rep. **232**, 87 (1993).
81. A. Capella, A. Kaidalov, and J. Tran Thanh Van, Heavy Ion Phys. **9**, 169 (1999).
82. B. B. Back *et al.* (PHOBOS Collab.), Phys. Rev. Lett. **87**, 102303 (2001).
83. A. Capella and D. Sousa, Phys. Lett. B **511**, 185 (2001).

Physics of Atomic Nuclei, Vol. 66, No. 11, 2003, pp. 2017–2032. From Yadernaya Fizika, Vol. 66, No. 11, 2003, pp. 2067–2082.

ELEMENTARY PARTICLES AND FIELDS
Theory

Multi-Reggeon Processes in QCD*

V. S. Fadin**

Budker Institute of Nuclear Physics, Siberian Division, Russian Academy of Sciences, pr. Akademika Lavrent'eva 11, Novosibirsk, 630090 Russia
Novosibirsk State University, ul. Pirogova 2, Novosibirsk, 630090 Russia

Received February 28, 2003

Abstract—We discuss the multi-Regge form of QCD amplitudes and outline a way how to prove this form. The key to the proof is given by the "bootstrap" requirement. This requirement leads to an infinite set of bootstrap relations for multiparticle production amplitudes. On the other hand, all these amplitudes are expressed in terms of the gluon trajectory and a finite number of Reggeon vertices. Therefore, it is extremely nontrivial to satisfy all these relations. However, it turns out that all of them can be fulfilled if the vertices and trajectory submit to several bootstrap conditions. Fulfillment of all these relations secures the Reggeized form of the radiative corrections order by order in perturbation theory. © *2003 MAIK "Nauka/Interperiodica".*

1. INTRODUCTION

Multiperipheral kinematics and multi-Reggeon processes were discovered by K.A. Ter-Martirosyan many years ago [1], long before the appearance of QCD, which is accepted now as a theory of strong interactions. The importance of multiperipheral kinematics recognized by Ter-Martirosyan became apparent in QCD very clearly, although not exactly in the same relation that was mainly discussed by Karen Avetovich. A marvelous property of QCD is the asymptotic freedom that makes it possible to apply perturbation theory to high-energy processes. A remarkable phenomenon exhibited by QCD perturbation theory is the Reggeization of elementary particles, quarks, and gluons [2–7]. Therefore, a primary Reggeon in QCD turns out to be the Reggeized gluon. The famous BFKL approach [4] to the description of high-energy processes is based on gluon Reggeization. The Pomeron, determining high-energy behavior of cross sections, and the Odderon, responsible for the difference of particle and antiparticle cross sections, emerge as compound states of two and three Reggeized gluons, respectively.

Dominant contributions to the total cross sections of QCD processes at high energy $\sqrt{s}$ come from multiperipheral, or, as it is now usually called, multi-Regge kinematics (MRK). In perturbation theory, amplitudes of such processes are given by gluon exchanges in channels with fixed (not increasing with s) transferred momenta. Despite a great number of contributing Feynman diagrams, it turns out that, in the MRK, amplitudes acquire a simple multiperipheral form. It is quite uncommon that radiative corrections to these amplitudes do not destroy this form, but give only simple Regge factors, which can be interpreted as a dependence of gluon spin on momentum transfer.

This wonderful phenomenon was proved in the leading logarithmic approximation (LLA), where only the leading terms $(\alpha_s \ln s)^n$ are resummed [8]. Owing to this, the BFKL approach was grounded in the LLA. Now, the approach is strongly developed in the NLA, where the terms $\alpha_s(\alpha_s \ln s)^n$ are also resummed. In this approximation, the gluon Reggeization still remains a hypothesis. Since it lies in the foundation of the BFKL approach, its proof is extremely desirable. It can be performed using the "bootstrap" relations, required by compatibility of the gluon Reggeization with the s-channel unitarity. It turns out that fulfillment of all these relations ensures the Reggeized form of the radiative corrections order by order in perturbation theory.

The bootstrap requirement leads to an infinite set of bootstrap relations for the multiparticle production amplitudes. On the other hand, all the amplitudes are expressed in terms of the gluon trajectory and a finite number of the Reggeon vertices. Therefore, it is extremely nontrivial to satisfy all these relations. Nevertheless, it turns out that all of them can be fulfilled if the vertices and trajectory submit to several bootstrap conditions.

Here, we discuss the Reggeized form of QCD amplitudes and outline a way of proof of this form in the NLA. The paper is organized in the following

*This article was submitted by the author in English.

** e-mail: fadin@inp.nsk.su

1063-7788/03/6611-2017$24.00

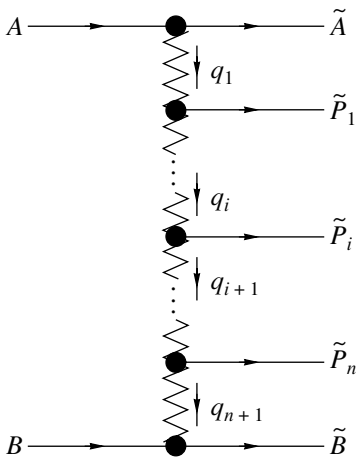

Schematic representation of the process $A + B \to \tilde{A} + \tilde{P}_1 + \ldots + \tilde{P}_n + \tilde{B}$ in the MRK. The zigzag lines represent Reggeized gluon exchange; the black circles denote the Reggeon vertices; q_i are the Reggeon momenta; and c_i are the color indices.

way. In the next section, all necessary definitions and notation are introduced and the multi-Regge form of QCD amplitudes is presented. In Section 3, the known results for the gluon Regge trajectory and the Reggeon vertices are reviewed. The bootstrap relations are derived in Section 4. The conditions imposed by these relations on the gluon Regge trajectory and the Reggeon vertices are presented in Section 5, where fulfillment of these conditions is briefly discussed. Section 6 summarizes the present status of gluon Reggeization.

2. QCD AMPLITUDES IN MULTI-REGGE KINEMATICS

We use the Sudakov decomposition of momenta, which proves to be very convenient for analysis of high-energy processes. For any momentum p, the decomposition is written as

$$p = \beta p_1 + \alpha p_2 + p_\perp, \quad (p_1 + p_2)^2 = 2p_1p_2 = s, \tag{1}$$
$$s\alpha\beta = p^2 - p_\perp^2 = p^2 + \mathbf{p}^2,$$

where p_1 and p_2 are light-cone momenta. Here and below, the vector sign is used for components of momenta transverse to the p_1–p_2 plane. These components are supposed to be limited (not growing with s). For high-energy process with initial particles A and B having momenta p_A and p_B, we can choose p_1 and p_2 in the p_A–p_B plane so that

$$p_A = p_1 + \left(m_A^2/s\right) p_2, \quad p_B = p_2 + \left(m_B^2/s\right) p_1, \tag{2}$$
$$(p_A + p_B)^2 \simeq s = 2p_1p_2.$$

The MRK means that, in the final state, we have space jets well separated in rapidity with limited invariant masses, which are supposed to be of the order of transverse momenta. Let us consider production of $n+1$ jets: $A + B \to \tilde{A} + \tilde{P}_1 + \ldots + \tilde{P}_n + \tilde{B}$ (see figure). If we denote momenta of the jets k_i, $0 \le i \le n+1$,

$$k_i = \beta_i p_1 + \alpha_i p_2 + k_{i\perp}, \tag{3}$$
$$s\alpha_i\beta_i = k_i^2 - k_{i\perp}^2 = k_i^2 + \mathbf{k}_i^2,$$

then we have

$$\alpha_0 \ll \alpha_1 \ll \cdots \ll \alpha_n \ll \alpha_{n+1}, \tag{4}$$
$$\beta_{n+1} \ll \beta_n \ll \cdots \ll \beta_1 \ll \beta_0.$$

Equations (3) and (4) ensure that the squared invariant masses of neighboring jets

$$s_i = (k_{i-1} + k_i)^2 \approx s\beta_{i-1}\alpha_i = \frac{\beta_{i-1}}{\beta_i}(k_i^2 + \mathbf{k}_i^2) \tag{5}$$

are large compared with the squared transverse momenta

$$s_i \gg \mathbf{k}_i^2 \sim |t_i| = |q_i^2|, \tag{6}$$

where

$$t_i = q_i^2 \approx q_{i\perp}^2 = -\mathbf{q}_i^2, \tag{7}$$

and their product is proportional to s:

$$\prod_{i=1}^{n+1} s_i = s\prod_{i=1}^{n}(k_i^2 + \mathbf{k}_i^2). \tag{8}$$

Multiparticle amplitudes have a complicated analytical structure. It is not simple even in the MRK (see, for instance, [9, 10]). Fortunately, only real parts of these amplitudes are used in the BFKL approach in the NLA as well as in the LLA. We restrict ourselves also to consideration of the real parts, although it is not explicitly indicated below. The real part of the production amplitude can be written as (see [11] and references therein)

$$\mathcal{A}_{AB}^{\tilde{A}\tilde{B}+n} = 4(p_Ap_B)\Gamma_{\tilde{A}A}^{c_1} \tag{9}$$
$$\times \left[\prod_{i=1}^{n}\frac{1}{t_i}\gamma_{c_ic_{i+1}}^{\tilde{P}_i}(q_i, q_{i+1})\left(\frac{s_i}{\sqrt{\mathbf{k}_{i-1}^2\mathbf{k}_i^2}}\right)^{\omega(t_i)}\right]$$
$$\times \frac{1}{t_{n+1}}\left(\frac{s_{n+1}}{\sqrt{\mathbf{k}_n^2\mathbf{k}_{n+1}^2}}\right)^{\omega(t_{n+1})}\Gamma_{\tilde{B}B}^{c_{n+1}},$$

where $\omega(t)$ is called a gluon Regge trajectory (although actually the trajectory is $j(t) = 1 + \omega(t)$); $\Gamma_{\tilde{A}A}^{a}$ and $\Gamma_{\tilde{B}B}^{b}$ are the particle–particle–Reggeon (PPR) vertices, i.e., the effective vertices for $A \to \tilde{A}$

and $B \to \tilde{B}$ transitions owing to interactions with the Reggeized gluons having color indices a and b, respectively; and $\gamma^{\tilde{P}_i}_{c_i c_{i+1}}(q_i, q_{i+1})$ are the Reggeon–Reggeon–particle (RRP) vertices, i.e., the effective vertices for production of jets $\tilde{P}_i$ with momenta $k_i = q_i - q_{i+1}$ in collisions of Reggeons with momenta q_i and $-q_{i+1}$ and color indices c_i and c_{i+1}. Actually, in the LLA, only one gluon can be produced in the RRP vertex; in the NLA, a jet can contain two gluons or a $q\bar{q}$ pair.

Note that, in the amplitude concerned, there are contributions of various color states and signatures in the t_i channels, so that, strictly speaking, we should indicate somehow on the left-hand side of (9) that only the contribution of a color octet with negative signature is retained. But since in this paper we are interested only in such contributions, here and below, we have omitted this indication in order not to entangle the notation; thus, a color octet and negative signature are always assumed, without explicit indication, in channels with gluon quantum numbers. Recall that, in each order of perturbation theory, amplitudes with a negative signature do dominate, owing to the cancellation of the leading logarithmic terms in amplitudes with a positive signature. The last amplitudes become pure imaginary in the LLA due to this cancellation.

In the following, we will use unitarity relations, which involve a variety of amplitudes and a variety of initial states, with momenta of initial particles not necessary lying in the p_1–p_2 plane. Therefore, it is important to realize that the multi-Regge form is valid in such cases also. Actually, for its applicability, it is sufficient to have small (compared with c.m.s. energy) transverse momenta and masses of all participating particles and strongly ordered longitudinal momenta of produced particles.

3. REGGEON VERTICES AND TRAJECTORY

3.1. Vertices and Trajectory for the LLA

In the leading order (LO), the Reggeon vertices and trajectory can be found without large efforts assuming the form (9). To find the vertex describing $A \to A'$ transition, it is sufficient to calculate the simplest elastic scattering amplitude with such transition in the Born approximation. Of course, other processes can be used to test whether form (9) is valid. In such a way, one can find that the vertex for $q(p) \to q(p')$ transition with momenta p and p' having predominant components along p_1 can be represented as

$$\Gamma^c_{Q'Q} = g\bar{u}(p')t^c \frac{\not{p}_2}{2pp_2} u(p), \tag{10}$$

where g is the QCD coupling constant and t^c are the color group generators in the fundamental representation; for antiquarks, correspondingly,

$$\Gamma^c_{\bar{Q}'\bar{Q}} = -g\bar{v}(p)t^c \frac{\not{p}_2}{2pp_2} v(p'). \tag{11}$$

The vertices for gluon transitions acquire a simple form in physical gauges. For gluons with predominant components of momenta along p_1, we will use physical polarization vectors $e(p)p_2 = 0$ in the light-cone gauge $e(p')p_2 = 0$, so that

$$e(p) = e(p)_\perp - \frac{(e(p)_\perp p_\perp)}{p_2 p} p_2, \tag{12}$$
$$e(p') = e(p')_\perp - \frac{(e(p')_\perp p'_\perp)}{p_2 p'} p_2,$$

and

$$\Gamma^c_{G'G} = -g(e^*(p')_\perp e(p)_\perp) T^c_{G'G}, \tag{13}$$

with the color generators in the adjoint representation. For momenta with predominant components along p_2, we have to replace in these formulas $p_2 \to p_1$ [evidently, this replacement in (12) means change of the gauge].

All these vertices have identical form in the helicity basis:

$$\Gamma^c_{P'P} = gT^c_{P'P}\delta_{\lambda_{P'}\lambda_P}, \tag{14}$$

where $T^c_{P'P}$ represent now the matrix elements of the color group generators in corresponding representations and λ_s are helicities of the partons. Here, the conservation of s-channel helicities is explicitly exhibited. Note that, for gluons and massive quarks, it is valid only in the leading order.

In the LLA, there is only one RRP vertex, namely, the RRG vertex, since only one gluon can be produced in Reggeon–Reggeon interactions. Knowledge of the vertices (10) and (13) makes it possible to extract the RRG vertex in the LO from Born amplitudes for one-gluon production in any collision: quark–quark, quark–gluon, and gluon–gluon. Evidently, vertices extracted from various processes must coincide, which gives a test of the multi-Regge form (9). The result [3] is

$$\gamma^G_{c_1c_2}(q_1, q_2) = gT^a_{c_1c_2} e^*_\mu(k) C^\mu(q_2, q_1), \tag{15}$$

where a, $k = q_1 - q_2$, and $e(k)$ are, respectively, the color index, momentum, and polarization vector of the gluon,

$$C^\mu(q_2, q_1) = -q_1^\mu - q_2^\mu \tag{16}$$
$$+ p_1^\mu \left(\frac{q_1^2}{kp_1} + 2\frac{kp_2}{p_1p_2} \right) - p_2^\mu \left(\frac{q_2^2}{kp_2} + 2\frac{kp_1}{p_1p_2} \right)$$
$$= -q_{1\perp}^\mu - q_{2\perp}^\mu - \frac{p_1^\mu}{2(kp_1)}(k_\perp^2 - 2q_{1\perp}^2)$$

$$+\frac{p_2^\mu}{2(kp_2)}(k_\perp^2-2q_{2\perp}^2).$$

In the light-cone gauge $e(k)p_2=0$, we have

$$e_\mu^*(k)C^\mu(q_2,q_1)=-2e_\perp^*(k)\left(q_{1\perp}-k_\perp\frac{q_{1\perp}^2}{k_\perp^2}\right). \quad (17)$$

To find the gluon Regge trajectory in the LO, it is sufficient to calculate one of the elastic-scattering amplitudes in the one-loop approximation with logarithmic accuracy. The result

$$\omega^{(1)}(t)=\frac{g^2N_ct}{2(2\pi)^{D-1}}\int\frac{d^{D-2}q_1}{\mathbf{q}_1^2(\mathbf{q}-\mathbf{q}_1)^2} \quad (18)$$
$$=-g^2\frac{N_c\Gamma(1-\epsilon)}{(4\pi)^{D/2}}\frac{\Gamma^2(\epsilon)}{\Gamma(2\epsilon)}(\mathbf{q}^2)^\epsilon$$

does not depend on the process used. Here and in the following, N_c is the number of colors, $D=4+2\epsilon$ is the spacetime dimension taken different from 4 to regularize infrared and ultraviolet divergencies, and $\Gamma(x)$ is the Euler function.

In the LLA, all QCD amplitudes in the MRK are expressed through these vertices and trajectory. In the NLA, the complication is twofold. The first is that the Reggeon vertices existing in the LLA and the gluon trajectory must be taken in the NLO. The second is the appearance of new vertices, since in the NLA one of the jets can contain two particles.

3.2. The LLA Vertices and Trajectory in the NLO

Of course, finding the NLO vertices and trajectory is not so easy. To find the PPR vertices, one has to calculate nonlogarithmic terms in one-loop elastic amplitudes; to discover the RRG vertex, it is necessary to compute with such accuracy a gluon production amplitude in the MRK. The vertices were found in [10, 12–14]. In the case of massless quarks, the QQR vertex can be represented as

$$\Gamma^a_{Q'Q}=\Gamma^{a(\mathrm{B})}_{Q'Q}\left(1+\frac{\omega^{(1)}(t)}{2}\left[\frac{1}{\epsilon}+\psi(1-\epsilon)\right.\right. \quad (19)$$
$$+\psi(1)-2\psi(1+\epsilon)+\frac{2+\epsilon}{2(1+2\epsilon)(3+2\epsilon)}$$
$$\left.\left.-\frac{1}{N_c^2}\left(\frac{1}{\epsilon}-\frac{(3-2\epsilon)}{2(1+2\epsilon)}\right)-\frac{n_f}{N_c}\frac{(1+\epsilon)}{(1+2\epsilon)(3+2\epsilon)}\right]\right),$$

where the superscripts (B) and (1) mean the Born and the one-loop approximations, $\psi(x)$ is the logarithmic derivative of the Euler Γ function, and n_f is the number of quark flavors. Evidently, helicity of massless quark is conserved, so that the one-loop vertex is proportional to the Born one. It is not so in the gluon case:

$$\Gamma^a_{G'G}=\Gamma^{a(\mathrm{B})}_{G'G} \quad (20)$$
$$\times\left\{1+\frac{\omega^{(1)}(t)}{2}\left[\frac{2}{\epsilon}+\psi(1)+\psi(1-\epsilon)\right.\right.$$
$$-2\psi(1+\epsilon)-\frac{9(1+\epsilon)^2+2}{2(1+\epsilon)(1+2\epsilon)(3+2\epsilon)}$$
$$\left.\left.+\frac{n_f}{N_c}\frac{(1+\epsilon)^3+\epsilon^2}{(1+\epsilon)^2(1+2\epsilon)(3+2\epsilon)}\right]\right\}$$
$$+gT^a_{G'G}e'^*_{\perp\mu}e_{\perp\nu}\left(g_\perp^{\mu\nu}-(D-2)\frac{q_\perp^\mu q_\perp^\nu}{q_\perp^2}\right)$$
$$\times\frac{\epsilon\omega^{(1)}(t)}{2(1+\epsilon)^2(1+2\epsilon)(3+2\epsilon)}\left(1+\epsilon-\frac{n_f}{N_c}\right).$$

The last term here exhibits violation of the helicity conservation.

The one-gluon production vertex $\gamma^G_{ab}(q_1,q_2)$ in the NLO was calculated in [10, 15–18]. The calculation has a long history. Note that the vertices (19) and (20) at once were calculated for arbitrary spacetime dimension D. It was not so in the case of the one-gluon production vertex. The quark part of the vertex also was found at once for arbitrary D [15]; instead, in the gluon part, which is much more complicated, firstly only the terms not vanishing at $\epsilon\to0$ were found [10]. But in the process of calculation of the NLO BFKL kernel, it was realized that, at small transverse momentum $\mathbf{k}$ of the produced gluon, the RRG vertex must be known for arbitrary D. After this, the vertex at small $\mathbf{k}$ was calculated [16] for arbitrary D. Later, the results of [10, 16] were obtained by another method in [17]. But then it became clear that, for verification of the bootstrap equation for the BFKL kernel, the vertex must be known for arbitrary D in a wider kinematical region. Finally, it was calculated for arbitrary D in [18]. Unfortunately, a complete expression for the vertex for arbitrary D is rather complicated. We present it here in the form where only terms singular at small $\mathbf{k}$ are given for arbitrary D, but others in the limit $\epsilon\to0$. The result is

$$\gamma^G_{c_1c_2}(q_1,q_2)=\gamma^{G(\mathrm{B})}_{c_1c_2}(q_1,q_2) \quad (21)$$
$$\times\left[1+\frac{2g^2N_c\Gamma(1-\epsilon)}{(4\pi)^{2+\epsilon}}(f_1+f_2)\right]$$
$$+gT^a_{c_1c_2}\frac{g^2N_c\Gamma(1-\epsilon)}{(4\pi)^{2+\epsilon}}[f_3-(2\mathbf{k}^2-\mathbf{q}_1^2-\mathbf{q}_2^2)f_2]$$
$$\times\left(\frac{p_A}{(kp_A)}-\frac{p_B}{(kp_B)}\right)_\mu e^*_\mu(k),$$

where $\gamma^{G(\mathrm{B})}_{ab}(q_1,q_2)$ is the Born vertex (15) and

$$2f_1=\left(\frac{11}{6}-\frac{n_f}{3N_c}\right)\frac{(\mathbf{q}_1^2+\mathbf{q}_2^2)}{(\mathbf{q}_1^2-\mathbf{q}_2^2)}\ln\left(\frac{\mathbf{q}_1^2}{\mathbf{q}_2^2}\right) \quad (22)$$

$$-\frac{1}{2}\ln^2\left(\frac{\mathbf{q}_1^2}{\mathbf{q}_2^2}\right)-\left(\mathbf{k}^2\right)^\epsilon\left(\frac{1}{\epsilon^2}-3\zeta(2)+2\epsilon\zeta(3)\right),$$

$$2f_2=\left(1-\frac{n_f}{N_c}\right)\frac{\mathbf{k}^2}{3(\mathbf{q}_1^2-\mathbf{q}_2^2)^2}\left[\mathbf{q}_1^2+\mathbf{q}_2^2-2\frac{\mathbf{q}_1^2\mathbf{q}_2^2}{\mathbf{q}_1^2-\mathbf{q}_2^2}\ln\left(\frac{\mathbf{q}_1^2}{\mathbf{q}_2^2}\right)\right],$$

$$f_3=\left(\frac{11}{3}-\frac{2n_f}{3N_c}\right)\frac{\mathbf{q}_1^2\mathbf{q}_2^2}{\mathbf{q}_1^2-\mathbf{q}_2^2}\ln\left(\frac{\mathbf{q}_1^2}{\mathbf{q}_2^2}\right)+\left(1-\frac{n_f}{N_c}\right)\frac{\mathbf{k}^2}{6},$$

where $\zeta(n)$ is the Riemann zeta function. Note that the vertex is presented in a form which is explicitly gauge-invariant. As compared with the Born vertex (15), it contains additional vector structure. The coefficient ahead of this structure is infrared-finite, as it should be.

The Reggeized gluon trajectory in the NLO was found at arbitrary D in terms of integrals over transverse momenta [19, 14]:

$$\omega(t)=\frac{g^2N_ct}{2(2\pi)^{D-1}}\int\frac{d^{D-2}q_1}{\mathbf{q}_1^2\left(\mathbf{q}_1-\mathbf{q}\right)^2}\times\left(1+f(\mathbf{q}_1,\mathbf{q})-2f(\mathbf{q}_1,\mathbf{q}_1)\right), \tag{23}$$

where

$$f(\mathbf{q}_1,\mathbf{q})=-\frac{g^2N_c\mathbf{q}^2}{2(2\pi)^{D-1}}\int\frac{d^{D-2)}q_2}{\mathbf{q}_2^2(\mathbf{q}_2-\mathbf{q})^2} \tag{24}$$

$$\times\left[\ln\left(\frac{\mathbf{q}^2}{(\mathbf{q}_1-\mathbf{q}_2)^2}\right)-2\psi(1+2\epsilon)-\psi(1-\epsilon)+2\psi(\epsilon)+\psi(1)+\frac{1}{1+2\epsilon}\left(\frac{1}{\epsilon}+\frac{1+\epsilon}{2(3+2\epsilon)}\right)\right]$$

$$+\frac{4g^2n_f\Gamma(2-D/2)\Gamma^2(D/2)}{(4\pi)^{D/2}\Gamma(D)}\left(\mathbf{q}^2\right)^{D/2-1}.$$

Let us stress that we systematically use the perturbative expansion in terms of the bare coupling g, so that everywhere before and below g is the bare coupling constant related to the renormalized coupling g_μ in the $\overline{MS}$ scheme by the relation

$$g=g_\mu\mu^{-\epsilon}\left[1+\left(\frac{11}{3}-\frac{2}{3}\frac{n_f}{N_c}\right)\frac{\bar g_\mu^2}{2\epsilon}\right], \tag{25}$$

$$\bar g_\mu^2=\frac{g_\mu^2N_c\Gamma(1-\epsilon)}{(4\pi)^{2+\epsilon}}.$$

The integrals can be expressed in terms of elementary functions only in the limit $\epsilon\to0$. They were calculated in this limit in [20]:

$$\omega(t)=\omega^{(1)}(t)\left\{1+\frac{\omega^{(1)}(t)}{4}\left(\mathbf{q}^2\right)^\epsilon\left[\frac{11}{3}+\left(\frac{\pi^2}{3}-\frac{67}{9}\right)\epsilon+\left(\frac{404}{27}-2\zeta(3)\right)\epsilon^2-\frac{2n_f}{3N_c}\left(1-\frac{5}{3}\epsilon+\frac{28}{9}\epsilon^2\right)\right]\right\}, \tag{26}$$

where $\omega^{(1)}(t)$ is the one-loop contribution (18). This result was confirmed in [21]. Recently, it was obtained quite independently by taking the high-energy limit of the two-loop amplitudes for parton–parton scattering [22].

Note that, as well as in the LO, since amplitudes of a variety of processes are expressed in terms of the same trajectory and vertices, some of the processes can be used to find the vertices and the trajectory and others to test the multi-Regge form (9).

3.3. The Reggeon Vertices for Two-Particle Production

The vertices and the trajectory presented above admit description in the NLA production of particles strongly ordered in the rapidity space, i.e., in the same kinematics that contributes in the LLA. To obtain production amplitudes in this kinematics in the NLA, it is sufficient to take one of the vertices or the trajectory in (9) in the NLO. But in the NLA, another kinematics also becomes important: one of the produced jets can contain two particles. It is called quasi-multi-Regge kinematics (QMRK). We will talk about it as about production of jets, one of which is a two-particle jet. Such a jet can be produced either in the regions of fragmentation of initial particles or in the central region, i.e., with rapidities far away from rapidities of colliding particles. Production amplitudes are given by (9), where the two-particle jet is in the first case either $\tilde A$ or $\tilde B$ and in the second one of $\tilde P_i$. Note that, because any two-particle jet in the unitarity relations leads to loss of a large logarithm, scales of energies in (9) are unimportant in the NLA; moreover, the trajectory and the vertices are needed there only in the LO. The trajectory and the RRG vertex in this order are given in Section 3.1; the Reggeon vertices for production of two-particle jets are presented below.

Production in the fragmentation region. Let us begin with vertices for production of two-particle jets in the fragmentation region. To be definite, we take the fragmentation region of the particle A. If the particle A is a quark, only a quark–gluon jet can be produced; but if it is a gluon, the jet can contain either two gluons or a $q\bar q$ pair. In all three cases, for generality, we take p_A as

$$p_A=k=\beta p_1+\frac{\mathbf{k}^2+m_A^2}{\beta s}p_2+k_\perp, \tag{27}$$

the momenta of produced particles as

$$k_1 = \beta_1 p_1 + \frac{\mathbf{k}_1^2 + m_1^2}{\beta_1 s} p_2 + k_{1\perp}, \qquad (28)$$
$$k_2 = \beta_2 p_1 + \frac{\mathbf{k}_1^2 + m^2}{\beta_2 s} p_2 + k_{2\perp},$$

and use the notation

$$\beta_1 = x_1\beta, \quad \beta_2 = x_2\beta, \quad x_1 + x_2 = 1. \qquad (29)$$

In all three cases, we take polarization vectors of participating gluons in the light-cone gauge (12).

In the case of quark–gluon production, let k_1 and k_2 be the momenta of final quark and gluon, respectively, so that $m_A = m_1 = m$, $m_2 = 0$. Then, from [23], one can obtain

$$\Gamma^c_{\{QG\}Q} = (t^a t^c)_{i_1 i_2} \left(\mathcal{A}((x_2 k_1 - x_1 k_2)_\perp)\right. \qquad (30)$$
$$\left. -\mathcal{A}((k_1 - x_1 k)_\perp)\right) - (t^c t^a)_{i_1 i_2}$$
$$\times \left(\mathcal{A}((-k_2 + x_2 k)_\perp) - \mathcal{A}((k_1 - x_1 k)_\perp)\right),$$

where i_1 and i_2 are the color indices of the outgoing and incoming quarks, a is the color index of the produced gluon G, and the amplitudes $\mathcal{A}$ have the form

$$\mathcal{A}(p_\perp) = -\frac{g^2}{p_\perp^2 - x_2^2 m^2} \bar{u}(k_1) \frac{\not{p}_2}{\beta s} \qquad (31)$$
$$\times \left(x_1 \not{e}^*_\perp \not{p}_\perp + \not{p}_\perp \not{e}^*_\perp + \not{e}^*_\perp x_2^2 m \right) u(k).$$

Here, e is the polarization vector of the produced gluon.

The Reggeon vertex for $q\bar{q}$ production can be found in [24]. It is written as

$$\Gamma^c_{\{Q\bar{Q}\}G} = (t^a t^c)_{i_1 i_2} \left(\mathcal{A}((k_1 - x_1 k)_\perp)\right. \qquad (32)$$
$$\left. -\mathcal{A}((x_2 k_1 - x_1 k_2)_\perp)\right) - (t^c t^a)_{i_1 i_2}$$
$$\times \left(\mathcal{A}((-k_2 + x_2 k)_\perp) - \mathcal{A}((x_2 k_1 - x_1 k_2)_\perp)\right),$$

where i_1 and i_2 are now the quark and antiquark color indices, and a is the color index of the incoming gluon G. The amplitudes $\mathcal{A}(p_\perp)$ in the light-cone gauge (12) are

$$\mathcal{A}(p_\perp) = \frac{g^2}{p_\perp^2 - m^2} \bar{u}(k_1) \frac{\not{p}_2}{\beta s} \qquad (33)$$
$$\times \left(x_1 \not{e}_\perp \not{p}_\perp - x_2 \not{p}_\perp \not{e}_\perp - \not{e}_\perp m \right) v(k_2).$$

Here, e is the gluon polarization vector, and $u(k_1)$ and $v(k_2)$ are the spin wave functions of the quark and antiquark, respectively.

The vertex $\Gamma^c_{\{G_1G_2\}G}$ for two-gluon production can be represented in the same form as (32), with the difference that k_1 and k_2 are now the momenta of the produced gluons and i_1 and i_2 are their color indices. Taking their polarization vectors e_1 and e_2 in the light-cone gauge (12), we have from [24]

$$\Gamma^c_{\{G_1G_2\}G} = (T^a T^c)_{i_1 i_2} \left(\mathcal{A}((k_1 - x_1 k)_\perp)\right. \qquad (34)$$
$$\left. -\mathcal{A}((x_2 k_1 - x_1 k_2)_\perp)\right) - (T^c T^a)_{i_1 i_2}$$
$$\times \left(\mathcal{A}((-k_2 + x_2 k)_\perp) - \mathcal{A}((x_2 k_1 - x_1 k_2)_\perp)\right),$$

where the amplitudes $\mathcal{A}(p_\perp)$ now have the form

$$\mathcal{A}(p_\perp) = \frac{2g^2}{p_\perp^2} \left[x_1 x_2 \left(e^*_{1\perp} e^*_{2\perp}\right)(e_\perp p_\perp) \right. \qquad (35)$$
$$\left. - x_1 \left(e^*_{1\perp} e_\perp\right)\left(e^*_{2\perp} p_\perp\right) - x_2 \left(e^*_{2\perp} e_\perp\right)\left(e^*_{1\perp} p_\perp\right) \right].$$

Production in the central region. In the central region, jets are produced by two Reggeons. Denoting Reggeon momenta q_1 and q_2, we can set

$$q_1 = \beta p_1 + q_{1\perp}, \qquad q_2 = -\alpha p_2 + q_{2\perp}, \qquad (36)$$
$$\beta = \beta_1 + \beta_2, \qquad \alpha = \alpha_1 + \alpha_2,$$

where β_i and α_i are the Sudakov parameters for the produced particles, $i = 1, 2$. The particles can be either $q\bar{q}$ or two gluons. For simplicity, we discuss below the case of massless quarks, although the massive case can be considered quite analogously. Then, for momenta of produced particles k_1 and k_2, we have

$$k = k_1 + k_2 = q_1 - q_2, \quad k_i = \beta_i p_1 + \alpha_i p_2 + k_{i\perp}, \qquad (37)$$
$$s\alpha_i\beta_i = -k_{i\perp}^2 = \mathbf{k}_i^2, \quad \beta_i = x_i\beta, \quad x_1 + x_2 = 1.$$

The Reggeon vertex for quark–antiquark production in Reggeon–Reggeon collisions was found in [25]. If k_1 and k_2 are the quark and antiquark momenta, respectively, the vertex has the form

$$\gamma^{Q\bar{Q}}_{c_1 c_2}(q_1, q_2) = \frac{1}{2} g^2 \bar{u}(k_1) \qquad (38)$$
$$\times \left[t^{c_1} t^{c_2} a(q_1; k_1, k_2) - t^{c_2} t^{c_1} \overline{a(q_1; k_2, k_1)} \right] v(k_2),$$

where $a(q_1; k_1, k_2)$ and $\overline{a(q_1; k_2, k_1)}$ can be written in the following way [26]:

$$a(q_1; k_1, k_2) = \frac{4\, \not{p}_1\, \not{Q}_1\, \not{p}_2}{s\tilde{t}_1} - \frac{1}{k^2}\, \not{\Gamma}, \qquad (39)$$
$$\overline{a(q_1; k_2, k_1)} = \frac{4\, \not{p}_2\, \not{Q}_2\, \not{p}_1}{s\tilde{t}_2} - \frac{1}{k^2}\, \not{\Gamma},$$

with

$$\tilde{t}_1 = (q_1 - k_1)^2, \qquad \tilde{t}_2 = (q_1 - k_2)^2, \qquad (40)$$
$$Q_1 = q_{1\perp} - k_{1\perp}, \qquad Q_2 = q_{1\perp} - k_{2\perp},$$
$$\Gamma = 2 \left[(q_1 + q_2)_\perp - \beta p_1 \left(1 - 2\frac{\mathbf{q}_1^2}{s\alpha\beta}\right) \right.$$
$$\left. + \alpha p_2 \left(1 - 2\frac{\mathbf{q}_2^2}{s\alpha\beta}\right) \right].$$

Using the notation $D(p,q)$ and $d(p,q)$,

$$D(p,q) = x_1 p_\perp^2 + x_2 q_\perp^2, \qquad (41)$$
$$d(p,q) = (x_1 p_\perp - x_2 q_\perp)^2,$$

for the denominators in the vertex and seeing that, for arbitrary $p_\perp$,

$$\bar{u}(k_1)\, \not{p}_\perp v(k_2) = \bar{u}(k_1)\frac{\not{p}_2}{s\beta} \qquad (42)$$
$$\times \left(\frac{\not{k}_{1\perp}\, \not{p}_\perp}{x_1} + \frac{\not{p}_\perp\, \not{k}_{2\perp}}{x_2} \right) v(k_2),$$

we can represent $a(q_1;k_1,k_2)$ and $\overline{a(q_1;k_2,k_1)}$ as

$$a(q_1;k_1,k_2) = \frac{4}{s\beta}\, \not{p}_2 b(q_1;k_1,k_2), \qquad (43)$$
$$\overline{a(q_1;k_2,k_1)} = \frac{4}{s\beta}\, \not{p}_2 \overline{b(q_1;k_2,k_1)},$$

where

$$b(q_1;k_1,k_2) = \frac{\not{k}_{1\perp}(\not{k}_{1\perp} - \not{q}_{1\perp})}{D(k_1-q_1,k_1)} \qquad (44)$$
$$- \frac{x_1x_2}{d(k_2,k_1)} \left(\frac{q_{1\perp}^2\, \not{k}_{1\perp}\, \not{k}_{2\perp}}{D(k_2,k_1)} - \frac{\not{k}_{1\perp}\, \not{q}_{1\perp}}{x_1} - \frac{\not{q}_{1\perp}\, \not{k}_{2\perp}}{x_2} \right.$$
$$\left. - q_{1\perp}^2 + 2(q_{1\perp}(k_1+k_2)_\perp) \right) - 1,$$
$$\overline{b(q_1;k_2,k_1)} = \frac{(\not{k}_{2\perp} - \not{q}_{1\perp})\, \not{k}_{2\perp}}{D(k_2,k_2-q_1)}$$
$$- \frac{x_1x_2}{d(k_2,k_1)} \left(\frac{q_{1\perp}^2\, \not{k}_{1\perp}\, \not{k}_{2\perp}}{D(k_2,k_1)} - \frac{\not{k}_{1\perp}\, \not{q}_{1\perp}}{x_1} - \frac{\not{q}_{1\perp}\, \not{k}_{2\perp}}{x_2} \right.$$
$$\left. - q_{1\perp}^2 + 2(q_{1\perp}(k_1+k_2)_\perp) \right) - 1.$$

The vertex for two-gluon production was obtained in [27] in a gauge-invariant form. In the light-cone gauge (12) for both gluons, the vertex takes the form [28]

$$\gamma_{ij}^{G_1G_2}(q_1,q_2) \qquad (45)$$
$$= 4g^2 (e_{1\perp}^*)_\alpha (e_{2\perp}^*)_\beta \left[\left(T^{i_1}T^{i_2}\right)_{ij} b^{\alpha\beta}(q_1;k_1,k_2) \right.$$
$$\left. + \left(T^{i_2}T^{i_1}\right)_{ij} b^{\beta\alpha}(q_1;k_2,k_1) \right],$$

where $e_{1,2}$ are the polarization vectors of the produced gluons, $i_{1,2}$ are their color indices, and

$$b^{\alpha\beta}(q_1;k_1,k_2) \qquad (46)$$
$$= \frac{1}{2} g_\perp^{\alpha\beta} \left[\frac{x_1x_2}{d(k_2,k_1)} \left(2q_{1\perp}(x_1k_2 - x_2k_1)_\perp \right.\right.$$
$$\left. + q_{1\perp}^2 \left(x_2 - \frac{x_1 k_{2\perp}^2}{D(k_2,k_1)} \right) \right)$$
$$- x_2 \left(1 - \frac{k_{1\perp}^2}{D(q_1-k_1,k_1)} \right) \Bigg]$$
$$- \frac{x_2 k_{1\perp}^\alpha q_{1\perp}^\beta - x_1 q_{1\perp}^\alpha (q_1-k_1)_\perp^\beta}{D(q_1-k_1,k_1)}$$
$$- \frac{x_1 q_{1\perp}^2 k_{1\perp}^\alpha (q_1-k_1)^\beta}{k_{1\perp}^2 D(q_1-k_1,k_1)}$$
$$- \frac{x_1 q_{1\perp}^\alpha (x_1k_2 - x_2k_1)_\perp^\beta + x_2 q_{1\perp}^\beta (x_1k_2 - x_2k_1)_\perp^\alpha}{d(k_2,k_1)}$$
$$+ \frac{x_1 q_{1\perp}^2 k_{1\perp}^\alpha k_{2\perp}^\beta}{k_{1\perp}^2 D(k_2,k_1)} + \frac{x_1x_2 q_{1\perp}^2}{d(k_2,k_1) D(k_2,k_1)}$$
$$\times \left((x_1k_2 - x_2k_1)_\perp^\alpha k_{2\perp}^\beta + k_{1\perp}^\alpha (x_1k_2 - x_2k_1)_\perp^\beta \right).$$

Here, we use the notation (41). Note that one can come to (46) starting from the vertex in the gauge $e(k_1)p_1 = 0, e(k_2)p_2 = 0$ [29]. Our $b^{\alpha\beta}(q_1;k_1,k_2)$ can be obtained from $c^{\alpha\beta}(k_1,k_2)$ defined in [29] by the gauge transformation

$$b^{\alpha\beta}(q_1;k_1,k_2) = \left(g_\perp^{\alpha\gamma} - 2\frac{k_{1\perp}^\alpha k_{1\perp}^\gamma}{k_{1\perp}^2} \right) c_\gamma^\beta(k_1,k_2). \qquad (47)$$

4. BOOTSTRAP RELATIONS

To derive the bootstrap relation for elastic scattering amplitudes in the NLA, it is sufficient to note that, with this accuracy,

$$\frac{1}{-2\pi i} \mathrm{disc}_s (\ln^n(-s) + \ln^n s) \qquad (48)$$
$$= \frac{1}{2} \frac{\partial}{\partial \ln s} \Re \left[\ln^n(-s) + \ln^n s \right],$$

where disc_s denotes the s-channel discontinuity and $\Re$ denotes the real part. Therefore, we have

$$\frac{1}{-2\pi i s} \mathrm{disc}_s \mathcal{A}_{AB}^{A'B'} = \frac{1}{2} \frac{\partial}{\partial \ln s} \Re \left[\frac{1}{s} \mathcal{A}_{AB}^{A'B'} \right]. \qquad (49)$$

Using the Reggeized form (9) of the elastic amplitude the on the right-hand side, we arrive at the bootstrap relation

$$\frac{1}{-2\pi i s} \mathrm{disc}_s \mathcal{A}_{AB}^{A'B'} = \frac{1}{2} \omega(t) \Re \left[\frac{1}{s} \mathcal{A}_{AB}^{A'B'} \right]. \qquad (50)$$

Note that it is not an exact relation; we can not demand it in approximations higher than the NLA.

The important point is that the left-hand side of (50) can be calculated using the amplitudes (9) in the unitarity condition. Since the amplitudes are expressed through the gluon Regge trajectory and the vertices of Reggeon interactions, relation (50) imposes strong restrictions on the trajectory and the vertices. The restrictions can be formulated as the

bootstrap conditions for the color octet impact factors and the BFKL kernel in the NLO [11]. Although these conditions are very strict, their fulfillment cannot be considered as proof of the Reggeization. Evidently, there are bootstrap relations for the production amplitudes, and one can expect that restrictions which they give are stronger. To derive these relations, we need to use analytical properties of the production amplitudes. Unfortunately, we do not know much about them. But, fortunately, in the NLA, we do not need much.

Let us consider the one-particle production amplitude $A + B \to A' + B' + G$ in the MRK. The discontinuities concerned with large logarithms are s_1-, s_2-, and s-channel ones. Here, we face two complications in comparison with the elastic case. Firstly, the discontinuities are not pure imaginary (e.g., the discontinuity in s can have, in turn, discontinuities in s_1 and s_2). The second is that, due to the relation

$$\frac{s_1 s_2}{s} = \mathbf{k}_1^2, \tag{51}$$

the amplitude [without the common factor s, see (9)] can depend on s_1, s_2, and s not only through powers of (large) logarithms of these variables. These complications can be overcome if only imaginary parts of the discontinuities are considered and appropriate combinations of them are taken [30].

Recall that we consider only negative signatures in both t_i channels, i.e., the part of the amplitude which is antisymmetric with respect to any of the substitutions $s_1 \to -s_1$ and $s_2 \to -s_2$. Due to relation (51), which holds in all physical channels, this part is also antisymmetric with respect to $s \to -s$.

An important observation is that a discontinuity of a product fg is expressed through discontinuities of f and g:

$$f_+ g_+ - f_- g_- = \frac{1}{2}(f_+ - f_-)(g_+ + g_-) + \frac{1}{2}(f_+ + f_-)(g_+ - g_-).$$

The second important observation is that the sum of discontinuities of $F(\mathbf{k}_1^2)$ on s_1 and s is zero. From these two observations, it follows that, for such a sum, instead of analytical functions of $\mathbf{k}_1^2$, we can take their real parts. The same is true for the sum of the discontinuities on s_2 and s and for the difference of the discontinuities on s_1 and s_2.

Now, if the variables s_1, s_2, and s enter into the amplitude not as the combination $s_1 s_2/s = \mathbf{k}_1^2$, they can enter only as $\hat{\mathcal{S}} \ln^{n_1}(-s_1) \ln^{n_2}(-s_2) \ln^{n_3}(\pm s)$, with $n_1 + n_2 + n_3 = n$, where n is less than or equal to the order of perturbation theory and $\hat{\mathcal{S}}$ is the operator of symmetrization with respect to exchanges $s_1 \leftrightarrow -s_1$, $s \leftrightarrow -s$ and $s_2 \leftrightarrow -s_2, s \leftrightarrow -s$. Note that the terms containing products of $\ln(-s_i)\ln(s_i)$, where s_i can be s_1, s_2, or s, are forbidden, on the same grounds as the terms containing $\ln(-s)\ln(s)$ are forbidden in the elastic amplitudes. Since in the NLO we need to keep only the first two leading powers of n, calculating the imaginary part of the discontinuity in any one of the variables s_1, s_2, or s, we can take only the real parts of logarithms of other variables. It means that, with our accuracy,

$$\Re\left[\frac{1}{-2\pi i}\mathrm{disc}_{s_i}\left(\hat{\mathcal{S}} \ln^{n_1}(-s_1) \ln^{n_2}(-s_2) \ln^{n_3}(\pm s)\right)\right] = \frac{1}{2}\frac{\partial}{\partial \ln s_i}\Re\left[\hat{\mathcal{S}} \ln^{n_1}(-s_1) \ln^{n_2}(-s_2) \ln^{n_3}(\pm s)\right], \tag{52}$$

where s_i can be s_1, s_2, or s and the partial derivative is taken at fixed $s_j \neq s_i$. Therefore, we have, for example,

$$\Re\left[\frac{1}{-2\pi i s}\left(\mathrm{disc}_{s_1} + \mathrm{disc}_s\right)\mathcal{A}_{AB}^{A'GB'}\right] = \frac{1}{2}\left(\frac{\partial}{\partial \ln s_1} + \frac{\partial}{\partial \ln s}\right)\Re\left[\frac{1}{s}\mathcal{A}_{AB}^{A'GB'}\right], \tag{53}$$

where in the right part the first derivative is taken at fixed s_2 and s and the second at fixed s_1 and s_2. Using the fact that

$$\left(\frac{\partial}{\partial \ln s_1} + \frac{\partial}{\partial \ln s}\right) f(s_1, s_2, s) = \frac{\partial}{\partial \ln s_1} f\left(s_1, s_2, \frac{s_1 s_2}{\mathbf{k}_1^2}\right), \tag{54}$$

we arrive at

$$\Re\left[\frac{1}{-2\pi i s}\left(\mathrm{disc}_{s_1} + \mathrm{disc}_s\right)\mathcal{A}_{AB}^{A'GB'}\right] = \frac{1}{2}\frac{\partial}{\partial \ln s_1}\Re\left[\frac{1}{s}\mathcal{A}_{AB}^{A'GB'}\right], \tag{55}$$

where in the right part the amplitude is considered as a function of s_1, s_2, and $\mathbf{k}_1^2$. The requirement of the Reggeized form (9) of the amplitude on the right-hand side gives us the bootstrap relation

$$\Re\left[\frac{1}{-2\pi i}\left(\mathrm{disc}_{s_1} + \mathrm{disc}_s\right)\mathcal{A}_{AB}^{A'GB'}\right] = \frac{1}{2}\omega(t_1)\Re\mathcal{A}_{AB}^{A'GB'}. \tag{56}$$

In the same way, we obtain

$$\Re\left[\frac{1}{-2\pi i}\left(\mathrm{disc}_{s_2} + \mathrm{disc}_s\right)\mathcal{A}_{AB}^{A'GB'}\right] = \frac{1}{2}\omega(t_2)\Re\mathcal{A}_{AB}^{A'GB'}. \tag{57}$$

The bootstrap relations for the amplitudes of multiparticle production in the MRK can be derived in the same way. Denoting $\mathcal{A}_{AB}^{A'B'+n}$ as the amplitude for the process $A+B\to A'+G_1+\ldots+G_n+B'$, we have for any k from 0 to $n+1$

$$\Re\left[\frac{1}{-2\pi i s}\left(\sum_{l=k+1}^{n+1}\mathrm{disc}_{s_{k,l}}-\sum_{l=0}^{k-1}\mathrm{disc}_{s_{l,k}}\right)\mathcal{A}_{AB}^{A'B'+n}\right] \tag{58}$$

$$=\frac{1}{2}\left(\frac{\partial}{\partial\log s_{k,k+1}}-\frac{\partial}{\partial\log s_{k-1,k}}\right)\times\Re\left[\frac{1}{s}\mathcal{A}_{AB}^{A'B'+n}(s_{i,i+1})\right],$$

where

$$s_{i,j}=(k_i+k_j)^2,\quad 0\le i,j=0\le n+1, \tag{59}$$
$$k_0=p_{A'},\quad k_1=p_{G_1},\ldots,\quad k_n=p_{G_n},\quad k_{n+1}=p_{B'}.$$

Note that since $s_{0,n+1}\simeq s$, $\mathrm{disc}_{s_{0,n+1}}$ in (58) includes the s-channel discontinuity. On the right-hand side of (58), the amplitude is expressed in terms of $s_{i,i+1}$, which are considered as independent variables, and transverse momenta.

If the amplitudes have the Reggeized form (9), we obtain [30]

$$\Re\left[\frac{1}{-2\pi i}\left(\sum_{l=k+1}^{n+1}\mathrm{disc}_{s_{k,l}}-\sum_{l=0}^{k-1}\mathrm{disc}_{s_{l,k}}\right)\mathcal{A}_{AB}^{A'B'+n}\right] \tag{60}$$

$$=\frac{1}{2}\left(\omega(t_{k+1})-\omega(t_k)\right)\Re\mathcal{A}_{AB}^{A'B'+n}.$$

This equation gives a general form of the bootstrap relations. Equations (50), (56), and (57) appear as particular cases of (60) for $n=0$ and $n=1$.

Until now, we have considered production of single particles in the MRK. As was already discussed, in the NLA, a two-particle jet can be produced instead of a solitary particle. Therefore, one can expect that, to make the set (60) complete, we have to add the bootstrap relations for the case of production of such jets. But actually, (60) covers this case also, if we allow one of the final particles with momentum k_m to be replaced by a jet consisting of two particles with momenta l_{m1} and l_{m2}, $l_{m1}+l_{m2}=k_m$. Then $\mathrm{disc}_{s_{i,m}}$ means the sum of discontinuities in the channels $(k_i+l_{m1})^2$, $(k_i+l_{m2})^2$, and $(k_i+k_m)^2$.

Evidently, (60) imposes much stronger restrictions on the Reggeon vertices and trajectory than (50). Their fulfillment proves the Reggeization hypothesis in the NLA, since the energy dependence of the amplitudes can be calculated order by order in perturbation theory using Eqs. (58). Indeed, the discontinuities entering into the left-hand side of these equations in some order in the coupling constant g can be expressed with the help of the unitarity relations through the multiparticle amplitudes in lower orders in g. Fulfillment of the bootstrap relations means that the energy dependence has the Regge form.

5. BOOTSTRAP CONDITIONS FOR THE REGGEON VERTICES

To obtain conditions imposed by the bootstrap relations (60) on the gluon Regge trajectory and the Reggeon vertices, we need to calculate the discontinuities on the left-hand side of (60). It can be done with the help of the unitarity condition, where the amplitudes (9) must be used. The calculation is rather complicated and intricate, and even representation of the results is rather tedious. To simplify this, it is convenient to introduce operators in the transverse momentum representation. From the t-channel point of view, we have to consider two interacting Reggeized gluons with "coordinates" $\mathbf{r}$ and $\mathbf{q}-\mathbf{r}$ in the transverse momentum space, where $\mathbf{q}$ is the total transverse momentum in the t channel. Let us introduce $\hat{\mathbf{r}}$ as the coordinate operator of one of the Reggeized gluons in the transverse momentum space: $\hat{\mathbf{r}}|\mathbf{r}_i\rangle=\mathbf{r}_i|\mathbf{r}_i\rangle$. The total transverse momentum $\mathbf{q}$ is considered as the c number. With the normalization $\langle\mathbf{q}_1|\mathbf{q}_2\rangle=\mathbf{q}_1^2(\mathbf{q}_1-\mathbf{q})^2\delta^{D-2}(\mathbf{q}_1-\mathbf{q}_2)$, we have

$$\langle\Psi_2|\Psi_1\rangle=\langle\Psi_2|\mathbf{r}\rangle\langle\mathbf{r}|\Psi_1\rangle \tag{61}$$
$$=\int\frac{d^{D-2}r}{\mathbf{r}^2(\mathbf{q}-\mathbf{r})^2}\left(\Psi_2(\mathbf{r})\right)^*\Psi_1(\mathbf{r}).$$

For the elastic amplitude $\mathcal{A}_{AB}^{A'B'}$, the calculation of the discontinuity in the NLA was presented in detail in [31]. The result is expressed in terms of the impact factors $\Phi_{A'A}$ and $\Phi_{B'B}$, which describe the transitions $A\to A'$ and $B\to B'$ caused by the interaction with Reggeized gluons, and the octet kernel $\mathcal{K}$ of the nonforward BFKL equation. Both the kernel and the impact factors are unambiguously defined in terms of the gluon Regge trajectory and the Reggeon vertices [11]. In the operator formalism, the s-channel discontinuity is written as

$$\frac{\mathrm{disc}_s\mathcal{A}_{AB}^{A'B'}}{-2\pi i}=\frac{2sN_c}{(2\pi)^{D-1}}\langle A'A|\left(\frac{s}{-t}\right)^{\hat{\mathcal{K}}}|BB'\rangle. \tag{62}$$

The impact factors appear as the wave functions of the t-channel states:

$$\langle A'A|\mathbf{r}\rangle=\Phi_{A'A}(\mathbf{r},\mathbf{q}-\mathbf{r}), \tag{63}$$
$$\langle\mathbf{r}|BB'\rangle=\left(\langle BB'|\mathbf{r}\rangle\right)^*=\Phi_{B'B}(\mathbf{r}-\mathbf{q},-\mathbf{r}),$$

where $q = p_A - p_{A'} = p_{B'} - p_B$; and the kernel as the operator $\hat{\mathcal{K}}$ with the matrix elements

$$\langle \mathbf{r}_1 | \hat{\mathcal{K}} | \mathbf{r}_2 \rangle = \mathcal{K}(\mathbf{r}_1, \mathbf{r}_2; \mathbf{q}). \tag{64}$$

The last relation in (63) follows from the definition of the impact factors given below [see Eqs. (72) and (73)]. Note that we have changed here normalization of the impact factors with respect to [11]. Recall that a color octet is always assumed in the t channel, so that the impact factors have a color index. We omit this index here and will omit it (as well as color indices of Reggeon vertices) everywhere if it does not lead to uncertainties.

The kernel is given by the sum of the "virtual" part, determined by the gluon trajectory, and the "real" part $\mathcal{K}_r$, related to the real particle production in Reggeon–Reggeon collisions:

$$\mathcal{K}(\mathbf{q}_1, \mathbf{q}_2; \mathbf{q}) = \left[\omega\left(-\mathbf{q}_1^2\right) + \omega\left(-\mathbf{q}_1'^{\,2}\right)\right] \times \mathbf{q}_1^2 \mathbf{q}_1'^{\,2} \delta^{D-2}(\mathbf{q}_1 - \mathbf{q}_2) + \mathcal{K}_r(\mathbf{q}_1, \mathbf{q}_2; \mathbf{q}), \tag{65}$$

where $q_i' = q - q_i$. The real part of the kernel can be represented as [11]

$$\mathcal{K}_r(\mathbf{q}_1, \mathbf{q}_2; \mathbf{q}) = \mathcal{K}_r^{\Lambda}(\mathbf{q}_1, \mathbf{q}_2; \mathbf{q}) - \frac{1}{2}\int \frac{d^{D-2}r}{\mathbf{r}^2(\mathbf{q}-\mathbf{r})^2} \mathcal{K}_r^{(\mathrm{B})}(\mathbf{q}_1, \mathbf{r}; \mathbf{q}) \times \mathcal{K}_r^{(\mathrm{B})}(\mathbf{r}, \mathbf{q}_2; \mathbf{q}) \ln\left(\frac{s_\Lambda^2}{(\mathbf{q}_1 - \mathbf{r})^2 (\mathbf{q}_2 - \mathbf{r})^2}\right), \tag{66}$$

where the "nonsubtracted" kernel $\mathcal{K}_r^{\Lambda}$ is

$$\mathcal{K}_r^{\Lambda}(\mathbf{q}_1, \mathbf{q}_2; \mathbf{q}) = \frac{f_{c_1 c_1' c} f_{c_2 c_2' c}}{N_c(N_c^2 - 1)} \sum_J \int \gamma^J_{c_1 c_2}(q_1, q_2) \times \left(\gamma^J_{c_1' c_2'}(-q_1', -q_2')\right)^* \frac{d\phi_J}{2(2\pi)^{D-1}}. \tag{67}$$

In (67), the sum is over all contributing jets J and their quantum numbers; $d\phi_J$ is the phase-space element for a jet J consisting of particles with momenta l_i, with total momentum k_J:

$$d\phi_J = \frac{dk_J^2}{2\pi} \theta(s_\Lambda - k_J^2)(2\pi)^D \times \delta^D\left(k_J - \sum_i l_i\right) \prod_i \frac{d^{D-1} l_i}{(2\pi)^{D-1} 2\epsilon_i}. \tag{68}$$

The intermediate parameter s_Λ in (66) must be taken tending to infinity. The second term on the right-hand side of (66) appears only in the NLO and serves for subtraction of the contribution of the large k_J^2 region, in order to avoid double counting of this region. In the LO, only one-gluon production contributes, so that $k_J^2 = 0$, equation (67) does not depend on s_Λ and gives the kernel in the leading (Born) order

$$\mathcal{K}_r^{(\mathrm{B})}(\mathbf{q}_1, \mathbf{q}_2; \mathbf{q}) = \frac{g^2 N_c}{2(2\pi)^{D-1}} \left(\frac{\mathbf{q}_1^2 \mathbf{q}_2'^{\,2} + \mathbf{q}_2^2 \mathbf{q}_1'^{\,2}}{(\mathbf{q}_1 - \mathbf{q}_2)^2} - \mathbf{q}^2\right). \tag{69}$$

In the NLO, the jets J in (67) can also contain a two-gluon or a quark–antiquark pair. At large k_J^2, only the contribution of the two-gluon jet survives, so that the dependence on s_Λ in (66) disappears due to the factorization property of the two-gluon production vertex [11].

The remarkable properties of the kernel are

$$\mathcal{K}_r(0, \mathbf{q}_2; \mathbf{q}) = \mathcal{K}_r(\mathbf{q}_1, 0; \mathbf{q}) = \mathcal{K}_r(\mathbf{q}, \mathbf{q}_2; \mathbf{q}) = \mathcal{K}_r(\mathbf{q}_1, \mathbf{q}; \mathbf{q}) = 0 \tag{70}$$

and

$$\mathcal{K}_r(\mathbf{q}_1, \mathbf{q}_2; \mathbf{q}) = \mathcal{K}_r(\mathbf{q}_1', \mathbf{q}_2'; \mathbf{q}) = \mathcal{K}_r(-\mathbf{q}_2, -\mathbf{q}_1; -\mathbf{q}). \tag{71}$$

The properties (70) mean that the kernel goes to zero at zero transverse momenta of the Reggeons and appears as a consequence of the gauge invariance; Eq. (71) follows from symmetries of the right-hand sides of Eqs. (65) and (67).

Representation of the impact factors is similar to (66):

$$\Phi^i_{A'A}(\mathbf{q}_1, \mathbf{q}_1') = \Phi^{i(\Lambda)}_{A'A}(\mathbf{q}_1, \mathbf{q}_1') - \frac{1}{2}\int \frac{d^{D-2}r}{\mathbf{r}^2 \mathbf{r}'^2} \Phi^{i(\mathrm{B})}_{A'A}(\mathbf{r}, \mathbf{r}') \mathcal{K}_r^{(\mathrm{B})}(\mathbf{r}, \mathbf{q}_1; \mathbf{q}) \times \ln\left(\frac{s_\Lambda^2}{(\mathbf{q}_1 - \mathbf{r})^2 \mathbf{q}^2}\right), \tag{72}$$

where $r' = q - r$, $q = p_A - p_{A'}$,

$$\Phi^{i(\Lambda)}_{A'A}(\mathbf{q}_1, \mathbf{q}_1') = i\frac{f^{icc'}}{N_c} \times \sum_{\tilde{A}} \int \Gamma^c_{\tilde{A}A} \Gamma^{c'}_{A'\tilde{A}} \left(\frac{\mathbf{q}^2}{\mathbf{q}_1^2}\right)^{\omega(q_1^2)/2} \left(\frac{\mathbf{q}^2}{\mathbf{q}_1'^{\,2}}\right)^{\omega(q_1'^{\,2})/2} d\phi_{\tilde{A}}. \tag{73}$$

Here, we have written explicitly the color index i of the impact factor; the sum is over jets $\tilde{A}$ in the fragmentation region of the particle A, $q_1 = p_A - p_{\tilde{A}}$, $q_1' = p_{\tilde{A}} - p_{A'}$, $q_1^2 \simeq q_{1\perp}^2$, $q_1'^{\,2} \simeq q_{1\perp}'^2$. We have used the property of the vertices $\Gamma^c_{A\tilde{A}} = (\Gamma^c_{A\tilde{A}})^*$, so that the definitions (72), (73) differ only by the factor $i/\sqrt{N_c}$ from that given in [11]. It is worthwhile to say that the impact factors are supposed to be symmetric with respect to the substitution $\mathbf{q}_1 \leftrightarrow \mathbf{q}_1'$. For the quark [23] and gluon [24] impact factors, this property is fulfilled automatically. It is not so in more complicated cases;

therefore, in the general case, symmetrization with respect to the substitution $\mathbf{q}_1 \leftrightarrow \mathbf{q}_1'$ is assumed on the right-hand side of Eq. (73).

We have to warn that, although sometimes to present formulas in a more convenient way we do not perform explicitly an expansion in the coupling g^2, actually the expansion is assumed and only the NLA accuracy is warranted.

Comparing (50) and (62), we obtain

$$\frac{2sN_c}{(2\pi)^{D-1}}\langle A'A|\left(\frac{s}{-t}\right)^{\hat{\mathcal{K}}}|BB'\rangle \tag{74}$$
$$= \frac{\omega(t)}{2}\frac{2s}{t}\Gamma_{A'A}\left(\frac{s}{-t}\right)^{\omega(t)}\Gamma_{B'B}.$$

If this equation were exact, then it should be [32]

$$|AA'\rangle_i = \frac{g}{2}\Gamma^i_{A'A}|R_\omega\rangle, \quad (\hat{\mathcal{K}}-\omega(t))|R_\omega\rangle = 0, \tag{75}$$
$$\frac{g^2N_c}{2(2\pi)^{D-1}}\langle R_\omega|R_\omega\rangle = \frac{\omega(t)}{t},$$

with a universal (process-independent) eigenfunction $|R_\omega\rangle$ of the kernel with the eigenvalue $\omega(t)$. These equations are called the strong bootstrap conditions [33, 34]. In the LO, they were known long ago. Fulfillment of the first of them in this order is easily seen from Eqs. (73) and (14). Moreover, it follows from these equations that

$$\langle \mathbf{r}|R^{(\mathrm{B})}_\omega\rangle = 1. \tag{76}$$

After that, fulfillment of the second and third equations follows immediately from Eqs. (65), (69), and (18).

An important point is that, in the NLO, the conditions (75) cannot be derived from (50). Performing respondent to the NLA expansions and using fulfillment of (75) in the LO, one can see that, to satisfy (74), it is sufficient [11] to require

$$\langle R^{(\mathrm{B})}_\omega|(\hat{\mathcal{K}}-\omega(t))|R^{(\mathrm{B})}_\omega\rangle = 0, \tag{77}$$
$$\frac{2gN_ct}{(2\pi)^{D-1}}\langle R^{(\mathrm{B})}_\omega|AA'\rangle_i = (2\omega^{(1)}(t)+\omega^{(2)}(t))\Gamma^i_{A'A}.$$

Fulfillment of the first of these conditions was shown in [35] and [36] for the quark and gluon contributions to the kernel, respectively. The quark contribution to $\mathcal{K}_r$ was calculated in [35]. It has a very simple form:

$$\mathcal{K}^Q_r(\mathbf{q}_1,\mathbf{q}_2;\mathbf{q}) = \frac{g^4n_fN_c}{(2\pi)^{D-1}} \tag{78}$$
$$\times\frac{\Gamma(1-\epsilon)}{\epsilon(4\pi)^{2+\epsilon}}\frac{\Gamma^2(2+\epsilon)}{\Gamma(4+2\epsilon)}\Bigg\{\frac{(\mathbf{k}^2)^\epsilon}{\mathbf{k}^2}(\mathbf{q}_1^2\mathbf{q}_2'^2+\mathbf{q}_2^2\mathbf{q}_1'^2)$$
$$+\mathbf{q}^2\left((\mathbf{q}^2)^\epsilon-(\mathbf{q}_1^2)^\epsilon-(\mathbf{q}_2^2)^\epsilon\right)-\frac{\mathbf{q}_1^2\mathbf{q}_2'^2-\mathbf{q}_2^2\mathbf{q}_1'^2}{\mathbf{k}^2}$$
$$\times\left((\mathbf{q}_1^2)^\epsilon-(\mathbf{q}_2^2)^\epsilon\right)+(\mathbf{q}_1\leftrightarrow\mathbf{q}_1',\mathbf{q}_2\leftrightarrow\mathbf{q}_2')\Bigg\},$$

where $\mathbf{k}=\mathbf{q}_1-\mathbf{q}_2=\mathbf{q}_2'-\mathbf{q}_1'$. Showing that it satisfies (77) is a simple task. The properties (70), (71) for this contribution are evident.

The gluon piece of $\mathcal{K}_r$ includes contributions of one-gluon and two-gluon production. The one-gluon contribution is determined by the RRG vertex, which is known now for arbitrary D [18]. The two-gluon contribution was found in [37] also for arbitrary D. Unfortunately, the gluon piece of $\mathcal{K}_r$ has a rather complicated form for arbitrary D, so that we present it here only in the limit $\epsilon\to 0$ [37]:

$$\mathcal{K}^G_r(\mathbf{q}_1,\mathbf{q}_2;\mathbf{q}) = \frac{g^2N_c}{2(2\pi)^{D-1}} \tag{79}$$
$$\times\Bigg\{\left(\frac{\mathbf{q}_1^2\mathbf{q}_2'^2+\mathbf{q}_1'^2\mathbf{q}_2^2}{\mathbf{k}^2}-\mathbf{q}^2\right)$$
$$\times\left(\frac{1}{2}+\frac{g^2N_c\Gamma(1-\epsilon)(\mathbf{k}^2)^\epsilon}{(4\pi)^{2+\epsilon}}\left(-\frac{11}{6\epsilon}+\frac{67}{18}-\zeta(2)\right.\right.$$
$$\left.\left.+\epsilon\left(-\frac{202}{27}+7\zeta(3)+\frac{11}{6}\zeta(2)\right)\right)\right)$$
$$+\frac{g^2N_c\Gamma(1-\epsilon)}{(4\pi)^{2+\epsilon}}\Bigg[\mathbf{q}^2\left(\frac{11}{6}\ln\left(\frac{\mathbf{q}_1^2\mathbf{q}_2^2}{\mathbf{q}^2\mathbf{k}^2}\right)\right.$$
$$\left.+\frac{1}{4}\ln\left(\frac{\mathbf{q}_1^2}{\mathbf{q}^2}\right)\ln\left(\frac{\mathbf{q}_1'^2}{\mathbf{q}^2}\right)+\frac{1}{4}\ln\left(\frac{\mathbf{q}_2^2}{\mathbf{q}^2}\right)\ln\left(\frac{\mathbf{q}_2'^2}{\mathbf{q}^2}\right)\right)$$
$$+\frac{1}{4}\ln^2\left(\frac{\mathbf{q}_1^2}{\mathbf{q}_2^2}\right)-\frac{\mathbf{q}_1^2\mathbf{q}_2'^2+\mathbf{q}_2^2\mathbf{q}_1'^2}{2\mathbf{k}^2}\ln^2\left(\frac{\mathbf{q}_1^2}{\mathbf{q}_2^2}\right)$$
$$+\frac{\mathbf{q}_1^2\mathbf{q}_2'^2-\mathbf{q}_2^2\mathbf{q}_1'^2}{\mathbf{k}^2}\ln\left(\frac{\mathbf{q}_1^2}{\mathbf{q}_2^2}\right)$$
$$\times\left(\frac{11}{6}-\frac{1}{4}\ln\left(\frac{\mathbf{q}_1^2\mathbf{q}_2^2}{\mathbf{k}^4}\right)\right)+\frac{1}{2}\Bigg[\mathbf{q}^2(\mathbf{k}^2-\mathbf{q}_1^2-\mathbf{q}_2^2)$$
$$+2\mathbf{q}_1^2\mathbf{q}_2^2-\mathbf{q}_1^2\mathbf{q}_2'^2-\mathbf{q}_2^2\mathbf{q}_1'^2+\frac{\mathbf{q}_1^2\mathbf{q}_2'^2-\mathbf{q}_2^2\mathbf{q}_1'^2}{\mathbf{k}^2}$$
$$\times(\mathbf{q}_1^2-\mathbf{q}_2^2)\Bigg]\int_0^1\frac{dx}{(\mathbf{q}_1(1-x)+\mathbf{q}_2x)^2}$$
$$\times\ln\left(\frac{\mathbf{q}_1^2(1-x)+\mathbf{q}_2^2x}{\mathbf{k}^2x(1-x)}\right)\Bigg]\Bigg\}+\frac{g^2N_c}{2(2\pi)^{D-1}}$$
$$\times\{\mathbf{q}_i\longleftrightarrow\mathbf{q}_i'\}.$$

Note that the one-gluon and two-gluon contributions separately have singularities $\sim 1/\epsilon^2$. Due to their cancellation, the leading singularity of the kernel is $1/\epsilon$. It turns again into $\sim 1/\epsilon^2$ after subsequent integrations of the kernel because of the singular behavior of the kernel at $\mathbf{k}^2=0$. The additional singularity arises from the region of small $\mathbf{k}^2$, where $\epsilon|\ln\mathbf{k}^2|\sim 1$.

Therefore, we have not expanded the term $\left(\mathbf{k}^2\right)^\epsilon$ in ϵ. The terms $\sim\epsilon$ are taken into account in the coefficient of the expression divergent at $\mathbf{k}^2=0$ in order to conserve all contributions nonvanishing after the integrations in the limit $\epsilon\to 0$.

The symmetries (71) of the kernel are easily seen. The first of them is explicit in (79). To notice the second, it is sufficient to change $x\leftrightarrow(1-x)$ in the integral in (79). In order to check that the kernel (79) goes to zero at zero transverse momenta of the Reggeons, one has to know the behavior of the integral in (79). A representation suitable for this purpose is

$$\int\limits_0^1 \frac{dx}{(\mathbf{q}_1(1-x)+\mathbf{q}_2 x)^2}\ln\left(\frac{\mathbf{q}_1^2(1-x)+\mathbf{q}_2^2 x}{\mathbf{k}^2 x(1-x)}\right) \tag{80}$$

$$=\int\limits_0^\infty \frac{dz}{z+\mathbf{k}^2}\frac{1}{\sqrt{(\mathbf{q}_1^2+\mathbf{q}_2^2+z)^2-4\mathbf{q}_1^2\mathbf{q}_2^2}}$$

$$\times\ln\left(\frac{\mathbf{q}_1^2+\mathbf{q}_2^2+z+\sqrt{(\mathbf{q}_1^2+\mathbf{q}_2^2+z)^2-4\mathbf{q}_1^2\mathbf{q}_2^2}}{\mathbf{q}_1^2+\mathbf{q}_2^2+z-\sqrt{(\mathbf{q}_1^2+\mathbf{q}_2^2+z)^2-4\mathbf{q}_1^2\mathbf{q}_2^2}}\right).$$

From this representation, one can see that singularities of the integral at zero transverse momenta of the Reggeons are not more than logarithmic. After this, no problems remain to verify (70).

In [23] and [24], the second condition (77) was checked and proved to be satisfied for quarks and gluons, respectively. The strong bootstrap conditions (75) were also verified, although they are not necessary for fulfillment of (74), and were proved to be satisfied. For the impact factors it was done in [32], where the eigenfunction R_ω in the NLO was found:

$$\langle\mathbf{r}|R_\omega\rangle=1+\frac{\omega^{(1)}(t)}{2}\left[\tilde{K}_1+\left(\left(\frac{\mathbf{r}^2}{\mathbf{q}^2}\right)^\epsilon\right.\right. \tag{81}$$

$$\left.+\left(\frac{\mathbf{r}'^2}{\mathbf{q}^2}\right)^\epsilon-1\right)\left\{\frac{1}{2\epsilon}+\psi(1+2\epsilon)-\psi(1+\epsilon)\right.$$

$$\left.+\frac{11+7\epsilon}{2(1+2\epsilon)(3+2\epsilon)}-\frac{n_f}{N_c}\frac{(1+\epsilon)}{(1+2\epsilon)(3+2\epsilon)}\right\}$$

$$\left.-\frac{1}{2\epsilon}+\psi(1)+\psi(1+\epsilon)-\psi(1-\epsilon)-\psi(1+2\epsilon)\right],$$

where $\mathbf{r}'=\mathbf{q}-\mathbf{r}$, $t=-\mathbf{q}^2$,

$$\tilde{K}_1=\frac{(4\pi)^{2+\epsilon}\Gamma(1+2\epsilon)\epsilon\left(\mathbf{q}^2\right)^{-\epsilon}}{4\Gamma(1-\epsilon)\Gamma^2(1+\epsilon)} \tag{82}$$

$$\times\int\frac{d^{D-2}k}{(2\pi)^{D-1}}\ln\left(\frac{\mathbf{q}^2}{\mathbf{k}^2}\right)\frac{\mathbf{q}^2}{(\mathbf{k}-\mathbf{r})^2(\mathbf{k}+\mathbf{r}')^2}.$$

The result of integration in (82), in the form of an expansion in ϵ, can be found in [23].

Check of the strong bootstrap condition (75) for the quark contribution to the kernel was performed in [35, 34, 38]. For the gluon contribution, verification requires much more efforts, but recently it was also done [39].

Equation (74) also remains valid in the case when A' represents a two-particle jet in the region of fragmentation of the particle A. It leads to the bootstrap conditions for the Reggeon vertices $\Gamma^i_{\{P_1P_2\}A}$ describing productions of two-particle jets. Recall that, in this case, the scale of energy in (74) is not important and the trajectory and the vertices have to be taken in the LO. Taking into account fulfillment of (75) in the LO, the conditions can be written as

$$\frac{gN_c}{(2\pi)^{D-1}}\langle\{P_1P_2\}A|R_\omega^{(\mathrm{B})}\rangle_i=\frac{\omega(t)}{t}\Gamma^i_{\{P_1P_2\}A}, \tag{83}$$

where the impact factor $\langle\{P_1P_2\}A|R_\omega^{(\mathrm{B})}\rangle$ is given by (73) in the LO with the substitution $A'\to\{P_1P_2\}$. It gives

$$\frac{igf^{cab}}{(2\pi)^{D-1}}\int\frac{d^{D-2}r}{\mathbf{r}^2\mathbf{r}'^2}\sum_{\tilde{A}}\Gamma^a_{\tilde{A}A}\Gamma^b_{\{P_1P_2\}\tilde{A}} \tag{84}$$

$$=\frac{\omega(t)}{t}\Gamma^c_{\{P_1P_2\}A},$$

where $r_\perp=(p_A-p_{\tilde{A}})_\perp$, $r'_\perp=q_\perp-r_\perp$, $q=p_A-k_J$, and k_J is the jet momentum. In [28], it is shown that this equation is fulfilled.

Fulfillment of the strong bootstrap conditions (75) would be a miracle if there were not reasons for them. But it occurs [39] that they must be satisfied for realization of the bootstrap relations for inelastic amplitudes. Let us consider the amplitude $A+B\to A'+G+B'$ for production of the gluon G with momentum $k=\beta p_1+[\mathbf{k}^2/(\beta s)]p_2+k_\perp$, polarization e, and color index a in the MRK. The unitarity condition in the s_2 channel gives [30]

$$\frac{\mathrm{disc}_{s_2}\mathcal{A}_{AB}^{A'GB'}}{-2\pi i}=\frac{2sN_c}{(2\pi)^{D-1}}\Gamma_{A'A} \tag{85}$$

$$\times\frac{1}{t_1}\left(\frac{s_1}{\sqrt{\mathbf{q}_1^2\mathbf{k}^2}}\right)^{\omega(t_1)}\langle GR|\left(\frac{s_2}{\sqrt{\mathbf{k}^2\mathbf{q}_2^2}}\right)^{\hat{\mathcal{K}}}|BB'\rangle,$$

where $q_1=p_A-p_{A'}$, $q_2=p_{B'}-p_B$, and $q_1-q_2=k$; we can set $q_1=\beta p_1+q_{1\perp}$ and $q_2=-[\mathbf{k}^2/(\beta s)]p_2+q_{2\perp}$; $\langle GR|$ is the t_2-channel state of the produced gluon G and the t_1-channel Reggeized gluon R. The wave function of this state (it is the generalization of the impact factor for the case when the on-mass-shell gluon is replaced by the Reggeized gluon) is

expressed in terms of the Reggeon vertices. In the LO,

$$\langle GR|r_\perp\rangle_{ij}^{(\mathrm{B})} = i\frac{f^{jcc'}}{N_c}\sum_{G'}\gamma_{ic}^{G'}(q_1,r)\Gamma_{GG'}^{c'}, \qquad (86)$$

where i and j are the color indices in the t_1 and t_2 channel, respectively, and the sum is over discrete quantum numbers of the gluon G' with momentum $k' = \beta p_1 + [(\mathbf{q}_1-\mathbf{r})^2/(\beta s)]p_2 + q_{1\perp} - r_\perp$. Again, the symmetrization with respect to $\mathbf{r} \leftrightarrow \mathbf{r}'$ is assumed, as well as for the impact factors; the difference is that now two Reggeized gluons are in the t_2 channel, so that $\mathbf{r}' = \mathbf{q}_2 - \mathbf{r}$. Using (15) and (13), one obtains in the light-cone gauge (12)

$$\langle GR|r_\perp\rangle_{ij}^{(\mathrm{B})} = -\frac{g^2}{2}T_{ij}^a e_\perp^* \qquad (87)$$
$$\times\left(2q_{1\perp} - q_{1\perp}^2\left(\frac{k_\perp + r_\perp}{(k_\perp+r_\perp)^2} + \frac{k_\perp + r'_\perp}{(k_\perp+r'_\perp)^2}\right)\right).$$

With the NLO accuracy,

$$\langle GR|r_\perp\rangle_{ij} = i\frac{f^{jcc'}}{N_c}\sum_J\int\gamma_{ic}^J(q_1,r)\Gamma_{GJ}^{c'} \qquad (88)$$
$$\times\left(\frac{k_\perp^2}{(q_1-r)_\perp^2}\right)^{(\omega(q_1^2)+\omega(r_\perp^2))/2}$$
$$\times\left(\frac{k_\perp^2}{(q_2-r)_\perp^2}\right)^{\omega((q_2-r)_\perp^2)/2} d\phi_J$$
$$-\frac{1}{2}\int\frac{d^{D-2}r_{1\perp}}{r_{1\perp}^2(q_2-r_1)_\perp^2}\mathcal{K}_r^{(\mathrm{B})}(r_{1\perp},r_\perp;q_{2\perp})$$
$$\times\langle GR|r_{1\perp}\rangle_{ij}^{(\mathrm{B})}\ln\left(\frac{s_\Lambda^2}{k_\perp^2(r-r_1)_\perp^2}\right).$$

The symmetrization with respect to $\mathbf{r} \leftrightarrow \mathbf{q}_2 - \mathbf{r}$ is assumed.

The s-channel discontinuity can be represented as [30]

$$\frac{\mathrm{disc}_s\mathcal{A}_{AB}^{A'GB'}}{-2\pi i} = \frac{2sN_c}{(2\pi)^{D-1}} \qquad (89)$$
$$\times\langle A'A|\left(\frac{s_1}{\sqrt{\mathbf{q}_1^2\mathbf{k}^2}}\right)^{\hat{\mathcal{K}}}\hat{\mathcal{G}}\left(\frac{s_2}{\sqrt{\mathbf{k}^2\mathbf{q}_2^2}}\right)^{\hat{\mathcal{K}}}|BB'\rangle,$$

where $\hat{\mathcal{G}}$ is the operator of the gluon production with change of total two-Reggeon state momentum from q_1 to q_2. In the LO,

$$\langle r_{1\perp}|\hat{\mathcal{G}}(q_1,q_2)|r_{2\perp}\rangle_{ij}^{(\mathrm{B})} = 2\frac{f^{iaa'}f^{jbb'}}{N_c}\delta_{ab}r_{1\perp}^2 \qquad (90)$$
$$\times\gamma_{a'b'}^{G(\mathrm{B})}(q_1-r_{1\perp},q_2-r_{2\perp})\delta^{D-2}(r_{1\perp}-r_{2\perp}).$$

These matrix elements are assumed to be symmetrized with respect to $r_{1\perp} \leftrightarrow (q_1-r_1)_\perp$ and $r_{2\perp} \leftrightarrow (q_2-r_2)_\perp$. In the NLO,

$$\langle r_{1\perp}|\hat{\mathcal{G}}(q_1,q_2)|r_{2\perp}\rangle_{ij} = \frac{f^{iaa'}f^{jbb'}}{N_c} \qquad (91)$$
$$\times\Bigg[2\gamma_{a'b'}^G(q_1-r_{1\perp},q_2-r_{2\perp})r_{1\perp}^2\delta_{ab}$$
$$\times\delta^{D-2}(r_{1\perp}-r_{2\perp}) + \int\limits_{\mathbf{k}'^2/s_\Lambda}^{1-\mathbf{k}^2/s_\Lambda}\frac{dx'}{2x'(1-x')}$$
$$\times\sum_{G'}\gamma_{ab}^{\{G(k)G'(k')\}}(r_1,r_2)$$
$$\times\frac{\gamma_{a'b'}^{G'(-k')}(q_1-r_1,q_2-r_2)}{(2\pi)^{D-1}} + \int\limits_{\tilde{\mathbf{k}}^2/s_\Lambda}^{1-\mathbf{k}^2/s_\Lambda}\frac{dx'}{2x'(1-x')}$$
$$\times\sum_{\tilde{G}}\frac{\gamma_{ab}^{\tilde{G}(\tilde{k})}(\tilde{r}_1,\tilde{r}_2)}{(2\pi)^{D-1}}$$
$$\times\gamma_{a'b'}^{\{G(k)\tilde{G}(-\tilde{k})\}}(q_1-\tilde{r}_1,q_2-\tilde{r}_2)\Bigg]$$
$$-\int\frac{d^{D-2}r_\perp\langle r_\perp|\hat{\mathcal{G}}(q_1,q_2)|r_{2\perp}\rangle_{ij}^{(\mathrm{B})}}{2r_\perp^2(r-q_1)_\perp^2}$$
$$\times\mathcal{K}_r^{(\mathrm{B})}(r_{1\perp},r_\perp;q_{1\perp})\ln\left(\frac{s_\Lambda^2}{(\mathbf{r}-\mathbf{r}_1)^2\mathbf{k}^2}\right)$$
$$-\int\frac{d^{D-2}r_\perp\langle r_{1\perp}|\hat{\mathcal{G}}(q_1,q_2)|r_\perp\rangle_{ij}^{(\mathrm{B})}}{2r_\perp^2(r-q_2)_\perp^2}$$
$$\times\mathcal{K}_r^{(\mathrm{B})}(r_\perp,r_{2\perp};q_{2\perp})\ln\left(\frac{s_\Lambda^2}{(\mathbf{r}-\mathbf{r}_2)^2\mathbf{k}^2}\right),$$

where $k' = \beta' p_1 - [k'^2_\perp/(\beta' s)]p_2 + k'_\perp$ and $\tilde{k} = \beta' p_1 - [\tilde{k}^2_\perp/(\beta' s)]p_2 + \tilde{k}_\perp$ are the momenta of the intermediate gluon G' and $\tilde{G}$, $k'_\perp = r_{1\perp} - r_{2\perp} - k_\perp$, $\tilde{k}_\perp = \tilde{r}_{1\perp} - \tilde{r}_{2\perp}$, $x' = \beta'/(\beta+\beta')$,

$$r_1 = (\beta+\beta')p_1 + r_{1\perp}, \qquad (92)$$
$$r_2 = \left(\frac{k'^2_\perp}{\beta' s} + \frac{k_\perp^2}{\beta s}\right)p_2 + r_{2\perp},$$
$$\tilde{r}_1 = \beta' p_1 + r_{1\perp}, \quad \tilde{r}_2 = \frac{\tilde{k}^2_\perp}{\beta' s}p_2 + r_{2\perp}.$$

With account of (85) and (89), the bootstrap rela-

tion (57) takes the form

$$\frac{2sN_c}{(2\pi)^{D-1}}\left[\langle A'A|\left(\frac{s_1}{\sqrt{\mathbf{q}_1^2\mathbf{k}^2}}\right)^{\hat{\mathcal{K}}}\hat{\mathcal{G}}\right. \tag{93}$$
$$\left.+\,\Gamma_{A'A}\frac{1}{t_1}\left(\frac{s_1}{\sqrt{\mathbf{q}_1^2\mathbf{k}^2}}\right)^{\omega(t_1)}\langle GR|\right]\left(\frac{s_2}{\sqrt{\mathbf{k}^2\mathbf{q}_2^2}}\right)^{\hat{\mathcal{K}}}$$
$$\times|BB'\rangle=\frac{\omega(t_2)}{2}\cdot 2s\Gamma^i_{A'A}\frac{1}{t_1}\left(\frac{s_1}{\sqrt{\mathbf{q}_1^2\mathbf{k}^2}}\right)^{\omega(t_1)}$$
$$\times\,\gamma^G_{ij}(q_1,q_2)\left(\frac{s_2}{\sqrt{\mathbf{k}^2\mathbf{q}_2^2}}\right)^{\omega(t_2)}\frac{1}{t_2}\Gamma^j_{B'B}.$$

Relation (93) can be satisfied only if Eqs. (75) are fulfilled. Therefore, implementation of the strong bootstrap conditions is an indispensable term of the gluon Reggeization.

Besides (75), relation (93) imposes a restriction on the state $\langle GR|$ and the operator $\hat{\mathcal{G}}$. In the strong form, it is written as

$$\frac{gt_1}{2}\langle R_\omega|\hat{\mathcal{G}}_{ij}+\langle GR|_{ij}=\gamma^G_{ij}(q_1,q_2)\frac{g}{2}\langle R_\omega|. \tag{94}$$

Actually, (75) requires a weaker form of this condition, not for vectors of states, but only for their projections on $|R_\omega\rangle$, similarly to (77). But if we go further [40] and consider production of two gluons in the MRK, then we come to the strong form (94).

The bootstrap relation for production in the central region of a jet J containing a couple of particles P_1 and P_2 (it can be two gluons or a $q\bar{q}$ pair) with momenta

$$k_i=\beta_i p_1+\frac{m_i^2-k_{i\perp}^2}{\beta_i s}p_2+k_{i\perp},\quad i=1,2, \tag{95}$$
$$k_1+k_2=k,\quad \beta_1+\beta_2=\beta,$$

is obtained by the replacement $G\to J$ from (93) with arbitrary energy scales and the Reggeon trajectory and vertices taken in the LO. In this order, one has [28]

$$\langle\{P_1P_2\}R|r_\perp\rangle_{c_1c_2} \tag{96}$$
$$=i\frac{f^{ijc_2}}{N_c}\left[\sum_G\gamma^G_{c_1i}(q_1,q_1-k')\Gamma^j_{\{P_1P_2\}G}\right.$$
$$+\sum_{\tilde{P}_1}\gamma^{\tilde{P}_1P_2}_{c_1i}(q_1,q_1-k_1'-k_2)\Gamma^j_{P_1\tilde{P}_1}$$
$$\left.+\sum_{\tilde{P}_2}\gamma^{P_1\tilde{P}_2}_{c_1i}(q_1,q_1-k_1-k_2')\Gamma^j_{P_2\tilde{P}_2}\right],$$

where

$$k'=\beta p_1-\frac{(q_1-r)_\perp^2}{\beta s}p_2+(q_1-r)_\perp, \tag{97}$$
$$k_1'=\beta_1p_1+\frac{m_1^2-(q_1-k_2-r)_\perp^2}{\beta_1 s}p_2$$
$$+(q_1-k_2-r)_\perp,$$
$$k_2'=\beta_2p_1+\frac{m_2^2-(q_1-k_1-r)_\perp^2}{\beta_2 s}p_2$$
$$+(q_1-k_1-r)_\perp$$

are the momenta of the intermediate particles G, $\tilde{P}_1$, and $\tilde{P}_2$, respectively;

$$\langle R_\omega|\hat{\mathcal{J}}\{P_1P_2\}|r_\perp\rangle_{c_1c_2}=2\frac{f^{ijc_1}f^{i'j'c_2}}{N_c} \tag{98}$$
$$\times\left[\frac{1}{(q_1-r)_\perp^2}\gamma^{P_1P_2}_{jj'}(q_1-r_\perp,q_2-r_\perp)\delta_{ii'}\right.$$
$$+\frac{1}{\tilde{q}_{1\perp}^2(q_1-\tilde{q}_1)_\perp^2}\gamma^{P_2}_{ii'}(q_1-\tilde{q}_1,q_1-\tilde{q}_1-k_2)$$
$$\left.\times\,\gamma^{P_1}_{jj'}(\tilde{q}_1,\tilde{q}_1-k_1)\right],$$

where $\tilde{q}_1=\beta_1p_1+(k_1+q_2-r)_\perp$. The last term here appears only in the case of two-gluon production. As usual, symmetrization with respect to $r_\perp\leftrightarrow(q_2-r)_\perp$ is assumed. The bootstrap condition

$$\frac{g}{2}t_1\langle R_\omega|\hat{\mathcal{J}}\{P_1P_2\}_{ij}+\langle\{P_1P_2\}R|_{ij} \tag{99}$$
$$=\gamma^{\{P_1P_2\}}_{ij}(q_1,q_2)\frac{g}{2}\langle R_\omega|$$

is satisfied [28]. Note that, actually, the bootstrap condition which was checked in [28] is weaker: it is given by projection of (99) on $|R_\omega\rangle$. But from the proof given in [28], it is easy to see that the condition is fulfilled in the strong form (99).

Analogously, although for the impact factors $\langle\{P_1P_2\}A|$ only condition (83) was proven in [28], it is easy to see from the proof given there that the stronger condition

$$\frac{g}{2}\langle\{P_1P_2\}A|_i=\Gamma^i_{\{P_1P_2\}A}\langle R_\omega| \tag{100}$$

is fulfilled in the LO.

Fulfillment of the bootstrap conditions (75), (100), (99), and (94) ensures fulfillment of the bootstrap relations for all MRK amplitudes, which is quite nontrivial and crucial for proof of the gluon Reggeization. Only the last of these conditions has not been checked yet.

6. SUMMARY

Multiperipheral kinematics plays an outstanding role in QCD. It is extremely important since it gives a dominant contribution to the total cross sections of high-energy QCD processes. A remarkable phenomenon is that QCD amplitudes in this kinematics have a simple multi-Regge form and are expressed in terms of the gluon Regge trajectory and a few vertices of Reggeon interactions. The trajectory and the vertices are known now in the next-to-leading order.[1)]

The multi-Regge form was proven in the leading logarithmic approximation, but in the next-to-leading approximation, it still remains a hypothesis, which is not yet proven, although it stands a number of tests. The tests are related to its compatibility with the s-channel unitarity. The requirement of the compatibility leads to an infinite set of bootstrap relations for the multiparticle production amplitudes. It turns out that all these relations can be fulfilled if the vertices and trajectory submit to several bootstrap conditions. This circumstance is extremely nontrivial since an infinite set of demands is satisfied by a few functions.

The bootstrap conditions are extraordinary significant, since they ensure fulfillment of the bootstrap relations, which, being satisfied, guarantee the multi-Regge form of QCD amplitudes in the MRK. Therefore, fulfillment of all bootstrap conditions opens a way for the proof of the gluon Reggeization in the NLA. Now, all these conditions are derived and fulfillment of only one of them is not yet proven.

ACKNOWLEDGMENTS

I thank the Alexander von Humboldt Foundation for the research award and the Universität Hamburg and DESY for their warm hospitality while a part of this work was done.

This work was supported in part by INTAS (grant nos. INTAS-00-00366, INTAS-00-00679) and by the Russian Foundation for Basic Research (project no. 01-02-16042).

[1)]In this paper, we have considered Reggeon vertices and impact factors only for quarks and gluons. For phenomenological applications, the most interesting are impact factors of a highly virtual photon (see, for instance, [41] and references therein). However, this is a separate large topic which cannot be covered here.

REFERENCES

1. K. A. Ter-Martirosyan, Nucl. Phys. **68**, 591 (1965).
2. M. T. Grisaru, H. J. Schnitzer, and H.-S. Tsao, Phys. Rev. Lett. **30**, 811 (1973); Phys. Rev. D **8**, 4498 (1973).
3. L. N. Lipatov, Yad. Fiz. **23**, 642 (1976) [Sov. J. Nucl. Phys. **23**, 338 (1976)].
4. V. S. Fadin, E. A. Kuraev, and L. N. Lipatov, Phys. Lett. B **60B**, 50 (1975); E. A. Kuraev, L. N. Lipatov, and V. S. Fadin, Zh. Éksp. Teor. Fiz. **71**, 840 (1976) [Sov. Phys. JETP **44**, 443 (1976)]; Zh. Éksp. Teor. Fiz. **72**, 377 (1977) [Sov. Phys. JETP **45**, 199 (1977)]; Ya. Ya. Balitskii and L. N. Lipatov, Yad. Fiz. **28**, 1597 (1978) [Sov. J. Nucl. Phys. **28**, 822 (1978)].
5. V. S. Fadin and V. E. Sherman, Pis'ma Zh. Éksp. Teor. Fiz. **23**, 599 (1976) [JETP Lett. **23**, 548 (1976)]; Zh. Éksp. Teor. Fiz. **72**, 1640 (1977) [Sov. Phys. JETP **45**, 861 (1977)]; V. S. Fadin and R. Fiore, Phys. Rev. D **64**, 114012 (2001); hep-ph/0107010.
6. A. V. Bogdan, V. Del Duca, V. S. Fadin, and E. W. Glover, J. High Energy Phys. **0203**, 032 (2002); hep-ph/0201240.
7. M. I. Kotsky, L. N. Lipatov, A. Principe, and M. I. Vyazovsky, Nucl. Phys. B **648**, 277 (2003); hep-ph/0207169.
8. Ya. Ya. Balitskii, L. N. Lipatov, and V. S. Fadin, in *Proceedings of IV Winter School of LNPI, Leningrad, 1979,* p. 109.
9. J. Bartels, Nucl. Phys. B **175**, 365 (1980).
10. V. S. Fadin and L. N. Lipatov, Nucl. Phys. B **406**, 259 (1993).
11. V. S. Fadin and R. Fiore, Phys. Lett. B **440**, 359 (1998).
12. V. S. Fadin and R. Fiore, Phys. Lett. B **294**, 286 (1992).
13. V. S. Fadin, R. Fiore, and A. Quartarolo, Phys. Rev. D **50**, 2265 (1994).
14. V. S. Fadin, M. I. Kotsky, and R. Fiore, Phys. Lett. B **359**, 181 (1995).
15. V. S. Fadin, R. Fiore, and A. Quartarolo, Phys. Rev. D **50**, 5893 (1994).
16. V. S. Fadin, R. Fiore, and M. I. Kotsky, Phys. Lett. B **389**, 737 (1996).
17. V. Del Duca and C. R. Schmidt, Phys. Rev. D **59**, 074004 (1999).
18. V. S. Fadin, R. Fiore, and A. Papa, Phys. Rev. D **63**, 034001 (2001); hep-ph/0008006.
19. V. S. Fadin, Pis'ma Zh. Éksp. Teor. Fiz. **61**, 342 (1995) [JETP Lett. **61**, 346 (1995)]; V. S. Fadin, R. Fiore, and A. Quartarolo, Phys. Rev. D **53**, 2729 (1996); M. I. Kotsky and V. S. Fadin, Yad. Fiz. **59**, 1080 (1996) [Phys. At. Nucl. **59**, 1035 (1996)].
20. V. S. Fadin, R. Fiore, and M. I. Kotsky, Phys. Lett. B **387**, 593 (1996).
21. J. Blumlein, V. Ravindran, and W. L. van Neerven, Phys. Rev. D **58**, 091502 (1998).
22. V. Del Duca and E. W. N. Glover, J. High Energy Phys. **0110**, 035 (2001); hep-ph/0109028.

23. V. S. Fadin, R. Fiore, M. I. Kotsky, and A. Papa, Phys. Rev. D **61**, 094006 (2000).
24. V. S. Fadin, R. Fiore, M. I. Kotsky, and A. Papa, Phys. Rev. D **61**, 094005 (2000).
25. V. S. Fadin and L. N. Lipatov, Nucl. Phys. B **477**, 767 (1996).
26. V. S. Fadin, R. Fiore, A. Flachi, and M. I. Kotsky, Phys. Lett. B **422**, 287 (1998); hep-ph/9711427; V. S. Fadin, R. Fiore, A. Flachi, and M. I. Kotsky, Yad. Fiz. **62**, 1066 (1999) [Phys. At. Nucl. **62**, 999 (1999)].
27. L. N. Lipatov and V. S. Fadin, Pis'ma Zh. Éksp. Teor. Fiz. **49**, 311 (1989) [JETP Lett. **49**, 352 (1989)]; Yad. Fiz. **50**, 1141 (1989) [Sov. J. Nucl. Phys. **50**, 712 (1989)].
28. V. S. Fadin, M. G. Kozlov, and A. V. Reznichenko, hep-ph/0302224.
29. V. S. Fadin, M. I. Kotsky, and L. N. Lipatov, Phys. Lett. B **415**, 97 (1997); M. I. Kotsky, L. N. Lipatov, and V. S. Fadin, Yad. Fiz. **61**, 716 (1998) [Phys. At. Nucl. **61**, 641 (1998)].
30. V. S. Fadin, *Talk given at the NATO Advanced Research Workshop "Diffraction 2002," Aug. 31—Sept. 6, 2002, Alushta, Crimea, Ukraine* in *Diffraction 2002*, Ed. by R. Fiore *et al.*, NATO Science Series, Vol. 101, p. 235.
31. V. S. Fadin, in *High Energy Physics* (Rio de Janeiro, 1998), p. 742; hep-ph/9807528.
32. V. S. Fadin, R. Fiore, M. I. Kotsky, and A. Papa, Phys. Lett. B **495**, 329 (2000); hep-ph/0008057.
33. M. Braun, hep-ph/9901447.
34. M. Braun and G. P. Vacca, Phys. Lett. B **447**, 156 (2000).
35. V. S. Fadin, R. Fiore, and A. Papa, Phys. Rev. D **60**, 074025 (1999).
36. V. S. Fadin, R. Fiore, and M. I. Kotsky, Phys. Lett. B **494**, 100 (2000); hep-ph/0007312.
37. V. S. Fadin and D. A. Gorbachev, Pis'ma Zh. Éksp. Teor. Fiz. **71**, 322 (2000) [JETP Lett. **71**, 222 (2000)]; Yad. Fiz. **63**, 2253 (2000) [Phys. At. Nucl. **63**, 2157 (2000)].
38. M. Braun and G. P. Vacca, Phys. Lett. B **454**, 319 (1999).
39. V. S. Fadin and A. Papa, Nucl. Phys. B **640**, 309 (2002); hep-ph/0206079.
40. J. Bartels, V. S. Fadin, and R. Fiore, hep-ph/0307076.
41. V. S. Fadin, D. Y. Ivanov, and M. I. Kotsky, Nucl. Phys. B **658**, 156 (2003); hep-ph/0210406.

Physics of Atomic Nuclei, Vol. 66, No. 11, 2003, pp. 2033–2037. From Yadernaya Fizika, Vol. 66, No. 11, 2003, pp. 2083–2087.

ELEMENTARY PARTICLES AND FIELDS
Theory

From Three Nucleons to Three Quarks*

Yu. A. Simonov**

Institute of Theoretical and Experimental Physics,
Bol'shaya Cheremushkinskaya ul. 25, Moscow, 117259 Russia

Received December 23, 2002

Abstract—Some short history of three-body methods originated from the famous Skornyakov–Ter-Martirosyan equation is given, including the latest development of Faddeev formalism and Efimov states. The $3q$ system is shown to require an alternative, which is provided by the hyperspherical method (K harmonics), highly successful for baryons. © *2003 MAIK "Nauka/Interperiodica".*

1. INTRODUCTION

The Skornyakov and Ter-Martirosyan paper [1], which appeared in 1956, marked the beginning of a new era in few-body physics, when a somewhat neglected part of nuclear physics was promoted to the successful domain of theoretical physics. As a result, the few-body science has become a field accumulating fast-developing methods: Faddeev generalized the Skornyakov–Ter-Martirosyan equation (STME) [2] and has given a rigorous mathematical foundation for the theory of three particles [3], and many numerical methods have been introduced; for a review and references, see [4]. As an immediate consequence of the STME, a new effect was found in 1970, called the Efimov effect [5], which has been studied until now with respect to possible experimental consequences [6].

The STME and Faddeev technique is most useful when particles are nearly on-shell, so that, e.g., three-body results do not depend much on the potential shape, but rather are described by the on-shell two-body t matrix as it is for the quartet n–d scattering. The bound states of tritium and ^{3}He provide another example where the interaction at small distances (far off-shell) is important. To treat such systems, an alternative method, the hyperspherical formalism (HF) (or K-harmonics method), was developed and the system of the Schrödinger-like equations was written [7]. The development of the method was marked with many successful applications in both nuclear and atomic physics (see, e.g., [8, 9]). Recently, it was understood that the HF is probably the best suitable for systems with confinement, such as three quarks, where the interaction is a three-body one and confining, so that the t-matrix formalism cannot be applied. The accuracy of the HF as applied to the $3q$ system was found to be remarkably good [10, 11], allowing for a 1% bias in the baryon mass [12].

This paper is intended to demonstrate the physics of the three-body system and a qualitative analysis of two alternative approaches discussed above.

2. THE STME AND FADDEEV APPROACH

In the system of three equal-mass particles with arbitrary numeration, one can introduce the total kinetic energy E and the momentum $\mathbf{k}$ in the pair $(2, 3)$ and the relative momentum $\mathbf{p}$ of particle 1, namely,

$$\mathbf{p} = \frac{\mathbf{k}_2 + \mathbf{k}_3}{3} - \frac{2}{3}\mathbf{k}_1, \quad \mathbf{k} = \frac{\mathbf{k}_2 - \mathbf{k}_3}{2}.$$

The symmetric function of the ground state Ψ_{symm} is expressed through partial w.f.:

$$\Psi_{\text{symm}} = \psi(\mathbf{k}_{23}, \mathbf{p}_1) + \psi(\mathbf{k}_{31}, \mathbf{p}_2) + \psi(\mathbf{k}_{12}, \mathbf{p}_3) \quad (1)$$

with the normalization condition

$$\int |\Psi_{\text{symm}}|^2 d\mathbf{k} d\mathbf{p} = 1. \quad (2)$$

*This article was submitted by the author in English.
**e-mail: simonov@heron.itep.ru

1063-7788/03/6611-2033$24.00

It is convenient to extract the free three-body Green's function, introducing

$$\psi(\mathbf{k},\mathbf{p}) = \frac{\chi(\mathbf{k},\mathbf{p})}{\mathbf{k}^2 + 3\mathbf{p}^2/4 - mE}, \quad (3)$$

and the three-body rescattering equation, equivalent to summing the "bridge" Feynman diagrams (nonrelativistic), is [2]

$$\chi(\mathbf{k},\mathbf{p}) = \chi_0(\mathbf{k},\mathbf{p}) - 2\int m\frac{t(k,|\mathbf{p}/2+\mathbf{p}'|,E-3p^2/(4m))\chi(|\mathbf{p}+\mathbf{p}'/2|,p')d\mathbf{p}'}{\mathbf{p}'^2+\mathbf{p}\cdot\mathbf{p}'+\mathbf{p}^2-mE}. \quad (4)$$

Here, $t(k,k',\varepsilon)$ is the two-body t matrix, representing the "knot" in a bridge diagram, and

$$\chi_0(\mathbf{k},\mathbf{p}) = -2m \times \frac{t(k,\mathbf{p}/2+\mathbf{p}_0,E-3p^2/(4m))\varphi_\alpha(\mathbf{p}+\mathbf{p}_0/2)}{\mathbf{p}^2+\mathbf{p}_0^2+\mathbf{p}\cdot\mathbf{p}_0-mE}, \quad (5)$$

where φ_α is the two-body bound state, while $\mathbf{p}_0$ is the momentum of incident particle.

Near the bound-state pole, the t matrix can be written as

$$t(k,k',\varepsilon) = \frac{g(k,\varepsilon)g(k',\varepsilon)}{(2\pi)^2 m(\alpha+i\sqrt{2m\varepsilon})} + O(r_0), \quad (6)$$

where $\alpha = 1/a$, a being the scattering length; r_0 is the effective radius; and $g(k,\varepsilon)$ is the form factor; $g(0,0) = 1$ and $g(k,\varepsilon)$ decreases fast when $k \sim 1/r_0$ and $\varepsilon \sim 1/(mr_0^2)$.

Let us assume now that the range of integration in (4) is small, $p, p' \ll 1/r_0$. Then, one can insert (6) into (4) with $g \cong 1$, and one gets for the three-body bound-state w.f.

$$\left(\alpha - \sqrt{\frac{3}{4}\mathbf{p}^2 - E}\right)\chi(\mathbf{k},\mathbf{p}) + 8\pi\int\frac{d\mathbf{p}'}{(2\pi)^3} \times \frac{\chi(|\mathbf{p}+\mathbf{p}'/2|,p')}{\mathbf{p}'^2+\mathbf{p}\cdot\mathbf{p}'+\mathbf{p}^2-mE} = 0. \quad (7)$$

This is the STME for a three-body bound state. The off-shell generalization of the STME is the Faddeev Eq. (4). As was correctly stated in [1], the bound-state Eq. (7) cannot be used for tritium and ^{3}He, since it has no lower bound for energy due to the Thomas theorem [13]. This can be easily understood rewriting (7) in the form $\chi = \int K\chi d\mathbf{p}'$ and calculating the norm of K, $||K|| = \int d\mathbf{p}d\mathbf{p}'(K(\mathbf{p},\mathbf{p}'))^2$, which diverges logarithmically at large momenta, implying that there are formally infinitely many bound states. The physical situation corresponds to the cutoff form factors $g(k,\varepsilon)$ present in K, which lead to the finite result for the norm $||K||$.

A specific situation occurs when the two-body scattering length a is large, $a \gg r_0$. Then, the number of bound states lying between $-1/(ma^2)$ and $-1/(mr_0^2)$ is approximately equal to

$$N \sim \frac{1}{\pi}\ln\frac{|a|}{r_0}, \quad (8)$$

and when $|a|$ is increasing, $|a| \to \infty$, there appears an accumulation point of bound states (the Efimov effect [5]). For three nucleons, however, $N < 1$ and the effect is absent, but for three ^{4}He atoms, $a = 104$ Å, $r_0 \cong 7$ Å, and the effect is theoretically possible [6].

Since the Efimov states are almost on-shell, it is convenient to calculate them using the three-body unitarity and the N/D method [14]. Numerical results obtained (see Fig. 7 of [14]) support the estimate (8) and yield the explicit position of levels near the energy threshold.

To conclude with the bound-state Eq. (7), it is interesting to study the properties of the bound wave function, e.g., the size of the bound system. Here, one encounters an important difference between two- and three-body systems [15]. Namely, the two-body loosely bound system with a small binding energy ε, $m\varepsilon r_0^2 \ll 1$, has a radius of the order of $r_2 = 1/\sqrt{m\varepsilon}$, $r_2 \gg r_0$. For the three-body system, the situation may be twofold. In the case where a bound two-body system exists as a subsystem and the three-body bound state is close to the $2+1$ threshold, one has a quasi-two-body situation, whereas, when two-body bound subsystems are absent, the size of the three-body bound state is always r_0, however small the binding energy is [16]. Modern calculations of three-body bound states in the framework of the STME and its development—Faddeev equations—are done for ^{3}H and ^{3}He using systems of about 30 equations and exploiting realistic potentials describing NN scattering and bound states in a large energy interval (0–350 MeV) (see, e.g., the review in [17]). Unfortunately, the results of calculations yield significant underbinding of around 10–15%, maybe due to three-body forces, which are not known exactly; hence, the final results are model dependent (see [18] for an example and references).

We go now to dN scattering, which was also a topic of the primary paper [1]. The corresponding equations look like

$$\frac{(\sqrt{3k^2/4 - mE} - \alpha_t)}{k^2 - k_0^2}a_{3/2}(\mathbf{k},\mathbf{k}_0) \quad (9)$$

$$= \frac{-1}{k_0^2 + k^2 + \mathbf{k}\cdot\mathbf{k}_0 - mE}$$
$$- \int \frac{4\pi a_{3/2}(\mathbf{k}', \mathbf{k}_0)}{(k^2 + k'^2 + \mathbf{k}\cdot\mathbf{k}' - mE)(k^2 - k_0^2)} \frac{d\mathbf{k}'}{(2\pi)^3},$$
$$\frac{(\sqrt{3k^2/4 - mE} - \alpha_t)}{k^2 - k_0^2} a_{1/2}(\mathbf{k}, \mathbf{k}_0)$$
$$= \frac{1/2}{k_0^2 + k^2 + \mathbf{k}\cdot\mathbf{k}_0 - mE}$$
$$+ \int \frac{4\pi\{(a_{1/2}/2)(\mathbf{k}', \mathbf{k}_0) + (3b_{1/2}/2)(\mathbf{k}', \mathbf{k}_0)\}}{(k^2 + k'^2 + \mathbf{k}\cdot\mathbf{k}' - mE)(k^2 - k_0^2)} \times \frac{d\mathbf{k}'}{(2\pi)^3},$$
$$\frac{(\sqrt{3k^2/4 - mE} - \alpha_t)}{k^2 - k_0^2} b_{1/2}(\mathbf{k}, \mathbf{k}_0)$$
$$= \frac{3/2}{k_0^2 + k^2 + \mathbf{k}\cdot\mathbf{k}_0 - mE}$$
$$+ \int \frac{4\pi\{(3a_{1/2}/2)(\mathbf{k}', \mathbf{k}_0) + (b_{1/2}/2)(\mathbf{k}', \mathbf{k}_0)\}}{(k^2 + k'^2 + \mathbf{k}\cdot\mathbf{k}' - mE)(k^2 - k_0^2)} \times \frac{d\mathbf{k}'}{(2\pi)^3}.$$

Here, α_t^{-1} is the triplet scattering length of NN; $a_{3/2}$ is the Nd quartet ($S = 3/2$) scattering amplitude, and $b_{1/2}$ and $a_{1/2}$ are doublet ($S = 1/2$) amplitudes corresponding to the singlet and triplet last NN interaction, respectively. It is seen that the kernel for $S = 3/2$ is mostly negative and allows for a faster convergence, in contrast to the doublet ($S = 1/2$) case. The numerical result for quartet scattering length $a_{3/2} = 5.1$ fm obtained in [1] is not far from the experimental value [19], whereas doublet scattering requires a full off-shell calculation [4].

3. HYPERSPHERICAL METHOD

Heretofore, the basic dynamics was assumed to be quasi-two-body (however, the Faddeev technique allows for the full off-shell description), in the sense that the typical distance R between an interacting pair and a third spectator particle is large, $R \gg r_0$. However, this situation is an exception, and not the rule, which can be understood from the representation of the w.f. through the three-body Green's function ($\boldsymbol{\xi}, \boldsymbol{\eta}$ are Jacobi coordinates)

$$\psi(\boldsymbol{\xi}, \boldsymbol{\eta}) = \int G(\boldsymbol{\xi} - \boldsymbol{\xi}', \boldsymbol{\eta} - \boldsymbol{\eta}') V_3(\boldsymbol{\xi}', \boldsymbol{\eta}') \times \psi(\boldsymbol{\xi}', \boldsymbol{\eta}') d\boldsymbol{\xi}' d\boldsymbol{\eta}'. \quad (10)$$

Here, $G(\boldsymbol{\xi}, \boldsymbol{\eta}) = K_2(\kappa\rho)/\rho^2$, $\kappa = \sqrt{2m|E|}$, $\rho = \sqrt{\boldsymbol{\xi}^2 + \boldsymbol{\eta}^2}$, and V_3 includes all interaction terms. The asymptotics of ψ is given by G and is equal to

$$\psi(\boldsymbol{\xi}, \boldsymbol{\eta}) \sim 1/\rho^4, \quad \rho \to \infty. \quad (11)$$

Hence, the three-body kinematics tends to concentrate all three-body w.f. inside the interaction region of all three particles, which generates a small radius of w.f. even for barely bound three-body states. (This is also true for N-body systems $N \geq 3$.) In this situation, any pair angular momentum l_{ij} contributes to the total energy of the system an amount $\Delta E \sim l_{ij}(l_{ij} + 1)/(2mr_0^2)$, which, for the three-nucleon system with $r_0 \sim 1$ fm and for $l_{ij} = 1$, is of the order of $\Delta E \sim 50$ MeV, while, for the $3q$ system with $m = m_q \sim 0.3$ GeV and $r_0 \sim 0.5$ fm, $\Delta E_q \sim 600$ MeV.

Therefore, it is advantageous to have a wave function with the minimal number of nonzero pair angular momenta for the given total momentum L. The basis for that is provided by hyperspherical functions (K harmonics) due to the following properties:

(i) The solution of the condition $\hat{l}_{ij}\Psi = 0, i \neq j = 1, \ldots, N$, is given by the representation $\Psi_{K=0} = \Psi_0(\rho)$,

$$\rho^2 = \frac{1}{N} \sum_{i<j=1}^{N} (\mathbf{r}_i - \mathbf{r}_j)^2, \quad (12)$$

where all particles are assumed to have the same mass.

(ii) The function $\Psi_K(\mathbf{r}_1, \ldots, \mathbf{r}_N) = u_K(\Omega)\chi_K(\rho)$, where $u_K(\Omega) = \mathcal{P}_K(\mathbf{r}_1, \ldots, \mathbf{r}_N)/\rho^K$ and $\mathcal{P}_K$ is a harmonic polynomial, contains excited angular momenta in Jacobi coordinates $l_1, \ldots, l_{N-1}$, the arithmetic sum of which is equal to K.

Therefore the basis Ψ_K corresponds to the minimal excitation of angular momenta and is advantageous for compact N-body systems. Since, as was explained, the majority of such systems are compact, the hyperspherical expansion approach (HEA) [7] formulated as a system of coupled integral or differential equations has proved to be very successful both for few-nucleon systems [7, 8], where short-range correlations can be taken into account in the hyperspherical correlated basis (last reference in [18]), and in atomic physics [9]. It was understood afterwards [10, 11] that the HEA works even better for $3q$ systems, since interaction there contains no repulsive core and confinement excludes two-body channels.

Therefore, already the lowest approximation with $K = 0$ yields a 1% accuracy for the baryon energy [10–12].

In the general case, the baryon state is characterized by the grand angular momentum K and radial

Baryon masses (in GeV) averaged over hyperfine spin splitting for $\sigma = 0.15$ GeV^2, $\alpha_s = 0.4$, $m_i = 0$

State	$M_{Kn} + \langle \Delta H_{\rm self} \rangle$	$\langle \Delta H_{\rm C} \rangle$	$M^{\rm tot}_{Kn}$	$M^{\rm tot}$(exp)
$K = 0, n = 0$	1.36	−0.274	1.08	1.08
$K = 0, n = 1$	2.19	−0.274	1.91	?
$K = 0, n = 2$	2.9	−0.274	2.62	?
$K = L = 1, n = 0$	1.85	−0.217	1.63	1.6
$K = 2, n = 0$	2.23	−0.186	2.04	?

quantum number $n = 0, 1, 2$, which counts the number of zeros of the w.f. in the ρ space. A typical calculation was done in [12], and the result depends on only two input parameters, string tension $\sigma = 0.15$ GeV^2 and $\alpha_s = 0.4$, while current masses of light quarks have been set to zero. The spin-averaged masses $(M_N + M_\Delta)/2$ have been computed to eliminate the effect of hyperfine splitting.

To illustrate the simplicity of the method, let us quote the equation for the dominant hyperspherical harmonics $\psi_K(\rho) = \chi_K(\rho)/\sqrt{\rho}$,

$$-\frac{1}{2\mu}\frac{d^2\psi_K}{d\rho^2} + W_{KK}(\rho)\psi_K(\rho) = E_K\psi_K(\rho), \quad (13)$$

where $W_{KK}(\rho)$ is the sum of kinetic (angular) and potential energies, and μ is a constituent quark mass to be found below dynamically. The nonrelativistic appearance of this equation nevertheless contains the full relativistic dynamics, since μ is the einbein field needed to get rid of square roots in the relativistic quark action.

The explicit expression for W_{KK} is

$$W_{KK}(\rho) = \frac{d}{2\mu\rho^2} + V_{KK}(\rho), \quad (14)$$
$$d = (K + 3/2)(K + 5/2),$$

while $V_{KK}(\rho) = (u^+_K(\Omega)\hat{V}u_K(\Omega))$ is the total potential $\hat{V}$, including two-body and three-body parts, averaged over hyperspherical harmonics, which is done analytically. For example, for the Y-type $3q$ confining potential, one has $V_{KK}(\rho) = 1.58\sigma\rho$. It is remarkable that, to find the eigenvalues E_K with 1% accuracy, one does not need to solve Eq. (13), but instead can approximate $W_{KK}(\rho)$ near the minimum point ρ_0 by the oscillator well:

$$W_{KK}(\rho) = W_{KK}(\rho_0) + \frac{1}{2}(\rho - \rho_0)^2 W''_{KK}(\rho_0), \quad (15)$$
$$\left.\frac{dW_{KK}}{d\rho}\right|_{\rho=\rho_0} = 0.$$

The resulting eigenvalues are found immediately:

$$E_{Kn} \cong W_{KK}(\rho_0) + \omega(n + 1/2), \quad (16)$$
$$\omega^2 = W''_{KK}/\mu.$$

The total baryon mass is calculated as $M_{Kn}(\mu) = 3\mu/2 + E_{Kn}(\mu)$, and finally $\mu = \mu_0$ is to be found from the stationary point condition

$$\left.\frac{\partial M_{Kn}(\mu)}{\partial\mu}\right|_{\mu=\mu_0} = 0.$$

This gives the constituent quark mass $\mu_0 = 0.957\sqrt{\sigma} = 0.37$ GeV, and, finally, the baryon mass is $M_{Kn}(\mu_0)$. The masses $(M_n + M_\Delta)/2$ computed in this way are shown in table, taken from [12], where also definitions of all terms are given.

As is seen from table, the calculated spin-averaged mass $(M_N + M_\Delta)/2$ agrees well with the experimental average; the same is also true for lowest negative parity states with $K = L = 1$, which should be compared with the $1/2^-$, $3/2^-$ states of N and Δ, respectively.

We also notice that breathing modes ($n > 0$) have excitation energy around 0.8 GeV, while orbital excitations $K = L = 1$ have an energy interval around 0.5 GeV.

One important advantage of the HEA is that, in the lowest approximation, there is no need for numerical computations—as demonstrated above, the result for the mass can be obtained analytically with 1% accuracy, as can be checked by comparison with exact calculations (see [10–12]).

In conclusion, the on-shell approach of the STME (and its Faddeev generalization) and the HEA are two alternatives that describe opposite physical situations. Their coexistence has played a very important stimulating role for the development of few-body physics in the last four decades.

ACKNOWLEDGMENTS

I am greatly indebted to L.N. Bogdanova for the help and useful discussions.

This work was supported by the Russian Foundation for Basic Research (project nos. 00-02-17836 and 00-15-96736) and INTAS (grant nos. 00-110 and 00-366).

REFERENCES

1. G. V. Skornyakov and K. A. Ter-Martirosian, Zh. Éksp. Teor. Fiz. **31**, 775 (1956).
2. L. D. Faddeev, Zh. Éksp. Teor. Fiz. **39**, 1459 (1960).
3. L. D. Faddeev, Tr. Mat. Inst. Steklova **LXIX**, 3 (1963).
4. *Model and Methods in Few-Body Physics,* Lectures Notes in Phys. **283** (1987).
5. V. N. Efimov, Phys. Lett. B **33B**, 563 (1970); Yad. Fiz. **12**, 1080 (1970); Nucl. Phys. A **210**, 157 (1973).
6. E. Braaten, H.-W. Hammer, and M. Kusunoki, cond-mat/0201281; cond-mat/0206232.
7. Yu. A. Simonov, Yad. Fiz. **3**, 630 (1966); A. M. Badalian and Yu. A. Simonov, Yad. Fiz. **3**, 1032 (1966); F. Calogero and Yu. A. Simonov, Phys. Rev. **169**, 789 (1968); M. Fabre de la Ripelle, Rev. Roum. Phys. **14**, 1215 (1969).
8. G. Erens, J. L. Visschers, and R. van Wageningen, Ann. Phys. (N.Y.) **67**, 461 (1971); J. L. Ballot and M. Fabre de la Ripelle, Ann. Phys. (N.Y.) **127**, 62 (1980); A. Kievsky, S. Rosati, and M. Viviani, Nucl. Phys. A **501**, 974 (1989).
9. J. M. Macek, J. Phys. B **1**, 831 (1968); V. B. Mandelzweig, Few-Body Syst., Suppl. **7**, 371 (1994).
10. B. O. Kerbikov, M. I. Polikarpov, and L. V. Shevchenko, Nucl. Phys. B **331**, 19 (1990); M. Fabre de la Ripelle and Yu. A. Simonov, Ann. Phys. (N.Y.) **212**, 235 (1991); Yu. S. Kalashnikova, I. M. Narodetskii, and Yu. A. Simonov, Yad. Fiz. **46**, 1181 (1987) [Sov. J. Nucl. Phys. **46**, 689 (1987)].
11. P. Hasenfratz *et al.*, Phys. Lett. B **94B**, 401 (1980); J.-M. Richard *et al.*, Phys. Lett. B **95B**, 299 (1980); J. Kuti, Nucl. Phys. B (Proc. Suppl.) **73**, 72 (1999).
12. B. O. Kerbikov and Yu. A. Simonov, Phys. Rev. D **62**, 093016 (2000); Yu. A. Simonov, hep-ph/0205334; I. M. Narodetskii and M. A. Trusov, Yad. Fiz. **65**, 949 (2002) [Phys. At. Nucl. **65**, 917 (2002)].
13. L. Thomas, Phys. Rev. **47**, 903 (1935).
14. Yu. A. Simonov, I. L. Grach, and M. Zh. Shmatikov, Nucl. Phys. A **334**, 80 (1980).
15. Yu. A. Simonov, in *Proc. of the Problem Symposium on Nuclear Physics, Tbilisi, 1967,* p. 7.
16. F. Calogero and Yu. A. Simonov, Phys. Rev. Lett. **33**, 436 (1974).
17. R. Machleidt, Nucl. Phys. A **689**, 11c (2001).
18. B. F. Gibson, Few-Body Syst., Suppl. **7**, 80 (1994); M. T. Peña, H. Henning, and P. V. Sauer, Phys. Rev. C **42**, 855 (1990); H. Haberzettl and W. C. Parke, Few-Body Syst., Suppl. **7**, 274 (1994).
19. C. Lachanoine-Leluc *et al.*, J. Phys. (Paris) **48**, 985 (1987); Rev. Mod. Phys. **65**, 47 (1993); D. V. Bugg, Annu. Rev. Nucl. Part. Sci. **35**, 295 (1985).

Physics of Atomic Nuclei, Vol. 66, No. 11, 2003, pp. 2038–2044. From Yadernaya Fizika, Vol. 66, No. 11, 2003, pp. 2088–2094.

ELEMENTARY PARTICLES AND FIELDS
Theory

Spectrum and Regge Trajectories in QCD*

Yu. A. Simonov**

Institute of Theoretical and Experimental Physics,
Bol'shaya Cheremushkinskaya ul. 25, Moscow, 117259 Russia

Received December 23, 2002

Abstract—Starting in the 1960s, an active group of physicists under the guidance of Prof. K.A. Ter-Martirosyan began creating the theory of high-energy processes in QCD. From the beginning, the key element of this theory is the notion of Regge trajectories and, in particular, of the Pomeron trajectory, which have been introduced phenomenologically. In this talk, I review the problem of the spectrum and Regge trajectories as it can be derived from nonperturbative QCD dynamics. © *2003 MAIK "Nauka/Interperiodica".*

1. INTRODUCTION

The problem of the QCD spectrum is the central issue in nonperturbative QCD and is intimately connected to problems of confinement and mass generation in QCD. These latter issues make QCD so much different from QED and unusual; in addition, an explicit form of nonperturbative interaction (NPI) was not known for a long time. Recently, with the introduction of the field correlator method (FCM) [1, 2], the situation has changed favorably, since NPI is defined there in a gauge-invariant way and the simple field correlators, which are sufficient for all dynamical calculations, are known from lattice data [3, 4] and analytic results [5].

In view of all this, one can put the problem of the QCD spectrum in the most general framework, as the many-channel problem of bound states of quarks, antiquarks, and valence gluons with all possible mixings, the states being stable in the limit $N_c \to \infty$, and acquiring decay widths when $N_c = 3$. It is the purpose of this talk to describe the QCD spectrum in the Hamiltonian language, using the FCM and the $N_c \to \infty$ limit. In addition, the FCM provides another convenient limit—the gluon correlation length T_g tends to zero, while the string tension σ is kept constant. As a result, the universal Hamiltonian becomes local and has a transparent structure for any number of constituents. As will be seen, it contains only two fixed input parameters, σ and α_s (or $\Lambda_{\rm QCD}$), in addition to current quark masses and is able to predict any meson, baryon, hybrid, and glueball states and their mixings (for a review, see [6]).

In doing so, one solves the following puzzles: (i) constituent mass of quarks and gluons; (ii) meson Regge trajectories with a correct slope and intercept; (iii) the explicit notion of the valence gluon; (iv) hybrid spectra and Regge trajectories.

Remarkably, all calculated spectra are in very good agreement with lattice data and experiment, which gives an additional justification for the FCM. However, the immediate consequences of the whole approach are far more reaching. They include a new formulation of perturbation theory, the so-called background perturbation theory (BPTh) [7] with α_s saturating at small Euclidean momenta instead of diverging near the Landau ghost pole. The whole structure of QCD becomes interconnected with the spectrum via the quark–hadron duality, and hybrids and glueballs play a very important role in scattering and decay.

2. HAMILTONIAN

There are two possible approaches to incorporating nonperturbative field correlators in the quark–antiquark (or $3q$) dynamics. The first has to deal with the effective nonlocal quark Lagrangian containing field correlators [8]. From this, one obtains first-order Dirac-type integro-differential equations for heavy–light mesons [8, 9], light mesons [10], and baryons [10, 11]. These equations contain the effect of chiral symmetry breaking [8], which is directly connected to confinement.

The second approach is based on the effective Hamiltonian for any gauge-invariant quark–gluon system. In the limit $T_g \to 0$, this Hamiltonian is simple and local, and in most cases where spin interaction can be considered as a perturbation, one obtains

*This article was submitted by the author in English.

** e-mail: simonov@heron.itep.ru

1063-7788/03/6611-2038$24.00

results for the spectra in an analytic form, which is transparent.

For this reason, we choose below the second, Hamiltonian, approach [12, 13]. We start with the exact Fock–Feynman–Schwinger representation for the $q\bar{q}$ Green's function (for a review, see [14]), taking for simplicity the nonzero flavor case

$$G_{q\bar{q}}^{(x,y)} = \int_0^\infty ds_1 \int_0^\infty ds_2 (Dz)_{xy} (D\bar{z})_{xy} r^{-K_1-K_2} \quad (1)$$
$$\times \langle \mathrm{tr}(\Gamma_{\mathrm{in}}(m_1 - \hat{D}_1) W_\sigma(C) \Gamma_{\mathrm{out}}(m_2 - \hat{D}_2)) \rangle_A,$$

where

$$K_i = \int_0^{s_1} d\tau_i \left(m_i + \frac{1}{4} (\dot{z}_\mu^{(i)})^2 \right),$$

s_i, τ_i, m_i, $\hat{D}_i$ are proper times, current mass, and covariant derivative for particle i; $\Gamma_{\mathrm{in,out}} = 1, \gamma_5, \ldots$ are meson vertices; and $W_\sigma(C)$ is the Wilson loop with spin insertions, taken along the contour C formed by paths $(Dz)_{xy}$ and $(D\bar{z})_{xy}$,

$$W_\sigma(C) = P_F P_A \exp\left(ig \int_C A_\mu dz_\mu \right) \quad (2)$$
$$\times \exp\left(g \int_0^{s_1} \sigma_{\mu\nu}^{(1)} F_{\mu\nu} d\tau_1 - g \int_0^{s_2} \sigma_{\mu\nu}^{(2)} F_{\mu\nu} d\tau_2 \right).$$

Here, P_A and P_F are ordering operators for the first and second exponent, respectively. The last factor in (2) defines the spin interaction of quark and antiquark. The average $\langle W_\sigma \rangle_A$ in (1) is taken over gluonic vacuum with standard action and can be computed exactly through field correlators $\langle F(1)...F(n) \rangle_A$; keeping only the lowest one, $\langle F(1)F(2) \rangle$, which yields according to lattice calculation [15] accuracy around 1% [16], one obtains

$$\langle W_\sigma(C) \rangle_A \quad (3)$$
$$\simeq \exp\left(-\frac{1}{2} \left[\int_{S_{\min}} ds_{\mu\nu}(1) \int_{S_{\min}} ds_{\lambda\sigma}(2) \right.\right.$$
$$\left.\left. + \sum_{i,j=1}^{2} \int_0^{s_i} \sigma_{\mu\nu}^{(i)} d\tau_i \int_0^{s_j} \sigma_{\lambda\sigma}^{(j)} d\tau_j \right] \langle F_{\mu\nu}(1) F_{\lambda\sigma}(2) \rangle \right).$$

Here, $S_{\min}$ is the surface of minimal area for the contour C. The Gaussian correlator $\langle F_{\mu\nu}(1) F_{\lambda\sigma}(2) \rangle \equiv D_{\mu\nu,\lambda\sigma}(1,2)$ can be rewritten identically in terms of two scalar functions $D(x)$ and $D_1(x)$ [2], which have been computed on the lattice [3] to have the exponential form $D(x)D_1(x) \sim \exp(-|x|/T_g)$ with the gluon correlation length $T_g \approx 0.2$ fm.

Thus, the first term in the exponent (3) yields the area law $\langle W_\sigma \rangle \cong \exp(-\sigma S_{\min})$, with the string tension σ [2]

$$\sigma = \frac{1}{2} \int D(x) d^2 x. \quad (4)$$

We concentrate now on this confining term in (3) and quote the result for the spin-dependent term at the end of this section.

The important point to be discussed now is the character of dynamics that one gets from (3), (4). To this end, one should compare two characteristic lengths (times) T_g and T_q [17], where T_q is the typical period of quark motion, e.g., the classical period of motion along the Coulomb orbit (for heavy quarks) or along the orbit in the linear potential (for light quarks). In all cases, one gets $T_q \gtrsim 1$ fm and, hence, $T_q \gg T_g$. Thus, one has a local dynamics, however, relativistic for light quarks, but in any case the excitation of gluonic vacuum degrees of freedom can be neglected in the first approximation, so that the dynamics is of the potential type.

As the next step, one introduces the einbein variables μ_i and ν, the first one to transform the proper times s_i, τ_i into the actual (Euclidean) times $t_i \equiv z_4^{(i)}$. One has [13]

$$2\mu_i(t_i) = \frac{dt_i}{d\tau_i}, \quad \int_0^\infty ds_i (D^4 z^{(i)})_{xy} \quad (5)$$
$$= \mathrm{const} \cdot \int D\mu_i(t_i) (D^3 z^{(i)})_{xy}.$$

The variable ν enters in the Gaussian representation of the Nambu–Goto form for $S_{\min}$ and its stationary value $\nu_{(0)}$ has the physical meaning of the energy density along the string. In the case of several strings, as in the baryon case or the hybrid case, each piece of string has its own parameter $\nu_{(i)}$.

To get rid of the path integration in (1), one can go over to the effective Hamiltonian using the identity

$$G_{q\bar{q}}(x,y) = \langle x | \exp(-HT) | y \rangle, \quad (6)$$

where T is the evolution parameter corresponding to the hypersurface chosen for the Hamiltonian: it is the hyperplane $z_4 = \mathrm{const}$ in the c.m. case [13] and $z_+ = \mathrm{const}$ in the light-cone case [18, 19].

The final form of the c.m. Hamiltonian (apart from the spin and perturbative terms to be discussed later) for the $q\bar{q}$ case is [13, 20]

$$H_0 = \sum_{i=1}^{2} \left(\frac{m_i^2 + \mathbf{p}_i^2}{2\mu_i} + \frac{\mu_i}{2} \right) \quad (7)$$

$$+\frac{\hat{L}^2/r^2}{2[\mu_1(1-\zeta)^2+\mu_2\zeta^2+\int\limits_0^1 d\beta(\beta-\zeta)^2\nu(\beta)]}$$
$$+\frac{\sigma^2 r^2}{2}\int\limits_0^1\frac{d\beta}{\nu(\beta)}+\int\limits_0^1\frac{\nu(\beta)}{2}d\beta.$$

Here, $\hat{L}^2\equiv L(l+1)$, where L is the angular momentum;

$$\zeta=\left(\mu_1+\int\limits_0^1\beta\nu d\beta\right)\Big/\left(\mu_1+\mu_2+\int\limits_0^1\beta\nu d\beta\right);$$

and μ_i and $\nu(\beta)$ are to be found from the stationary point of the Hamiltonian

$$\left.\frac{\partial H_0}{\partial\mu_i}\right|_{\mu_i=\mu_i^{(0)}}=0,\quad \left.\frac{\partial H_0}{\partial\nu}\right|_{\nu=\nu_{(0)}}=0. \tag{8}$$

Note that H_0 contains as input only m_1, m_2, and σ, where m_i are current masses defined at the scale 1 GeV. The further analysis is simplified by the observation that, for $L=0$, one finds $\nu_{(0)}=\sigma r$ from (8) and $\mu_i^{(0)}=\sqrt{m^2+\mathbf{p}^2}$; hence, H_0 becomes the usual relativistic quark model (RQM) Hamiltonian [21]

$$H_0(L=0)=\sum_{i=1}^{2}\sqrt{m_i^2+\mathbf{p}^2}+\sigma r. \tag{9}$$

For large L, however, one can neglect μ_i as compared to ν and one gets

$$H_0^2\approx 2\pi\sigma\sqrt{L(L+1)}, \tag{10}$$
$$\nu_{(0)}(\beta)=\sqrt{\frac{8\sigma L}{\pi}}\frac{1}{\sqrt{1-4(\beta-1/2)^2}}.$$

From (9), (10), one can see that $\nu_{(0)}(\beta)$ is indeed the energy density along the string and $\mu^{(0)}$ is the c.m. energy of the quark, which plays the role of constituent quark mass, as will be seen below.

To proceed, one can use two approximations. First, replace H_0 in (8) by its eigenvalue M_0, which is accurate within 5% [22]. Second, approximate the L-dependent term in (7), introducing the correction $\Delta H_{\rm str}$, namely,

$$H_0\approx H_R+\Delta H_{\rm str}, \tag{11}$$
$$H_R=\sum_{i=1}^{2}\left(\frac{\mathbf{p}^2+m_i^2}{2\mu_i}+\frac{\mu_i}{2}\right)+\sigma r,$$

and the mass correction due to $\Delta H_{\rm str}$ for the equal mass case is [13]

$$\Delta_{\rm str}(L)=\langle\Delta H_{\rm str}\rangle=-\frac{16}{3}\frac{\sigma^2 L(L+1)}{M_0^3}, \tag{12}$$

where M_0 is the eigenvalue of H_R; a more accurate approximation is given by [23]

$$\Delta_{\rm str}(L)=-\frac{2\sigma L(L+1)\langle 1/r\rangle}{M_0^2}. \tag{13}$$

But H_0 is not the whole story; one should take into account three additional terms: spin terms in (3) which produce two types of contributions: self-energy correction [24]

$$H_{\rm self}=\sum_{i=1}^{2}\frac{\Delta m_q^2(i)}{2\mu_i},\quad \Delta m_q^2(i)=-\frac{4\sigma}{\pi}\eta(m_i), \tag{14}$$
$$\eta(0)\cong 1{-}0.9,$$

where $\eta(m_i)$ is a calculable function of m_i [24], and spin-dependent interaction between quark and antiquark $H_{\rm spin}$ [6, 25], which is entirely described by the field correlators $D(x), D_1(x)$, including also the one-gluon exchange part present in $D_1(x)$.

Finally, one should take into account gluon exchange contributions [7, 11], which can be divided into the Coulomb part $H_{\rm Coul}=-(4/3)(\alpha_s(r)/r)$ and $H_{\rm rad}$ including spacelike gluon exchanges and perturbative self-energy corrections (we shall systematically omit these corrections since they are small for light quarks to be discussed below). In addition, there are gluon contributions that are nondiagonal in number of gluons n_g and quarks (until now, only the sector $n_g=0$ was considered) and, therefore, mixing meson states with hybrids and glueballs [26]. We call these terms $H_{\rm mix}$ and refer the reader to [26] and the references cited there for more discussion. Assembling all terms together, one has the following total Hamiltonian in the limit of large N_c and small T_g:

$$H=H_0+H_{\rm self}+H_{\rm spin}+H_{\rm Coul}+H_{\rm rad}+H_{\rm mix}. \tag{15}$$

We start with $H_0=H_R+\triangle H_{\rm str}$. The eigenvalues M_0 of H_R can be given with 1% accuracy by [27]

$$M_0^2\approx 8\sigma L+4\pi\sigma(n+3/4), \tag{16}$$

where n is the radial quantum number, $n=0,1,2,\ldots$. Remarkably, $M_0\approx 4\mu_0$, and for $L=n=0$, one has $\mu_0(0,0)=0.35$ GeV for $\sigma=0.18$ GeV^2, and μ_0 increases fast with growing n and L. This fact explains that spin interactions become unimportant beyond $L=0,1,2$ since they are proportional to $d\tau_1 d\tau_2\sim(1/4\mu_1\mu_2)dt_1dt_2$ {see (3) and [25]}. Thus, constituent mass (which is actually "constituent energy") μ_0 is "running." The validity of μ_0 as a socially accepted "constituent mass" is confirmed by its numerical value given above, by the spin splittings of light [28] and heavy–light mesons [29], and by baryon magnetic moments expressed directly through μ_0 and being in agreement with experimental values [30].

3. REGGE TRAJECTORIES

The next topic is Regge trajectories in QCD. As is clear from (10), one has the correct asymptotic Regge slope coinciding with the string picture, while for small L, $L \leq 4$, the approximation (11), (12) holds [23] with almost the same slope. The Regge intercept depends strongly on the term $H_{\rm self}$ [24], since (16) yields too large a value for M_0; e.g., $M_0(0,0) \approx$ 1.4 GeV is almost twice the ρ mass. However, the self-energy term (14) defined unambiguously through σ [24] has a negative sign and a magnitude that brings the mass back near the experimental value. Thus, one can understand the origin of the large negative phenomenological constant, which is usually introduced in the RQM, but it is also rewarding that it is not actually constant, but depends on n, L via $\mu_0(n,L)$, so that the linear Regge behavior is preserved.

To compare with the experiment and disentangle the contribution of spin interaction, we shall consider the center-of-gravity (c.o.g.) masses for each meson multiplet as in [23]. Then, the masses of all orbital excitations ($n = 0$) can be nicely described by the linear Regge trajectory, which we call the Regge L trajectory with experimental parameters [23]

$$\bar{M}^2(L) = (1.23 \pm 0.02)L + 0.37 \pm 0.02 \ (\mathrm{GeV}^2) \tag{17}$$

or

$$L = 0.81\bar{M}^2(L) - 0.30. \tag{18}$$

This is different from the leading ρ trajectory $\alpha_J(M^2)$

$$J = \alpha'_J M^2(J) + 0.48, \quad \alpha'_J = 0.88 \ \mathrm{GeV}^2, \quad \alpha_J(0) = 0.48, \tag{19}$$

since its parameters depend on spin interactions. Now, using (11)–(16), one obtains [23]

$$L = 0.80\bar{M}^2(L) - 0.34, \tag{20}$$

which agrees with experiment (18) within 10%, the accuracy being in accordance with the estimates of the neglected terms from (15), namely, $H_{\rm rad}$ and $H_{\rm mix}$, while $H_{\rm Coul}$ is accounted for. In this way, one solves the problem of Regge trajectories for orbital excitations in QCD, thus supporting the foundations of the wide and fruitful activity undertaken by Prof. K.A. Ter-Martirosyan and his group to describe the high-energy scattering and production processes in the framework of the Regge theory. This important contribution was reviewed in [31].

We now come to the gluon-containing systems, hybrids and glueballs. Referring the reader to the original papers [32–34], one can recapitulate the main results for the spectrum. In both cases, the total Hamiltonian has the same form as in (15); however, the contribution of corrections differs.

For glueballs, it was argued in [34] that H_0 (11) has the same form, but with $m_i = 0$ and $\sigma \to \sigma_{\rm adj} = (9/4)\sigma$, while $H_{\rm self} = 0$ due to gauge invariance and $H_{\rm coul}$ is small due to strong cancellation between tree graphs and loop corrections [35]. Thus, glueball masses are expressed through only $\sigma = 0.18$ GeV^2 (fixed by meson Regge trajectories) for the center of gravity and, in addition, through α_s for the spin splittings. One can see in Table 1 of the first paper in [34] the theoretical c.o.g. mass values computed in [34] in comparison with lattice data. The agreement is striking, especially if one takes into account that, in theoretical calculations, there are no parameters at all, σ was fixed beforehand at the same value as in the lattice, and α_s was neglected altogether for the reason stated above.

We now come to the delicate and very important topic of glueball trajectories and especially of the Pomeron trajectory. Since the glueball Hamiltonian is basically the same as for mesons, one expects that the asymptotic slope of all Regge trajectories would be

$$\alpha'_G(M^2 \to \infty) \approx \frac{1}{2\pi\sigma_{\rm adj}} = \frac{4}{9}\alpha'_M, \tag{21}$$

where the subscripts G and M refer to glueball and meson trajectories, respectively. One expects that the Pomeron trajectory passes through the states 2^{++} (2.29 GeV for $\sigma = 0.18$ GeV^2) and 4^{++} (around 3.2 GeV), in which case the Pomeron intercept appears too low, $\alpha_{\rm P}(0) < 1$. A possible way out was suggested in [34], where the intersection of the two lowest meson trajectories with the Pomeron trajectory was introduced yielding the correct intercept $\alpha_{\rm P}(0) = 1.1$–1.2 for reasonable parameters of trajectory interactions. However, this topic is far from clear, and the BFKL perturbative results for $\alpha_{\rm P}(0)$ seem to be unstable with respect to inclusion of higher orders and/or nonperturbative effects. It seems that the Pomeron trajectory depends on both perturbative and nonperturbative contributions and their possible interference, and the problem was never considered in that fullness.

Now, we come to the final topic of this talk—hybrids and their role in hadron dynamics. We start with the hybrid Hamiltonian and spectrum. This topic in the framework of FCM was considered in [32, 33]. The Hamiltonian H_0 for a hybrid looks like [6]

$$H_0^{(\rm hyb)} = \frac{m_1^2}{2\mu_1} + \frac{m_2^2}{2\mu_2} + \frac{\mu_1 + \mu_2 + \mu_g}{2} + \frac{\mathbf{p}_\xi^2 + \mathbf{p}_\eta^2}{2\mu} + \sigma \sum_{i=1}^{2} |\mathbf{r}_g - \mathbf{r}_i| + \Delta H_{\rm str}, \tag{22}$$

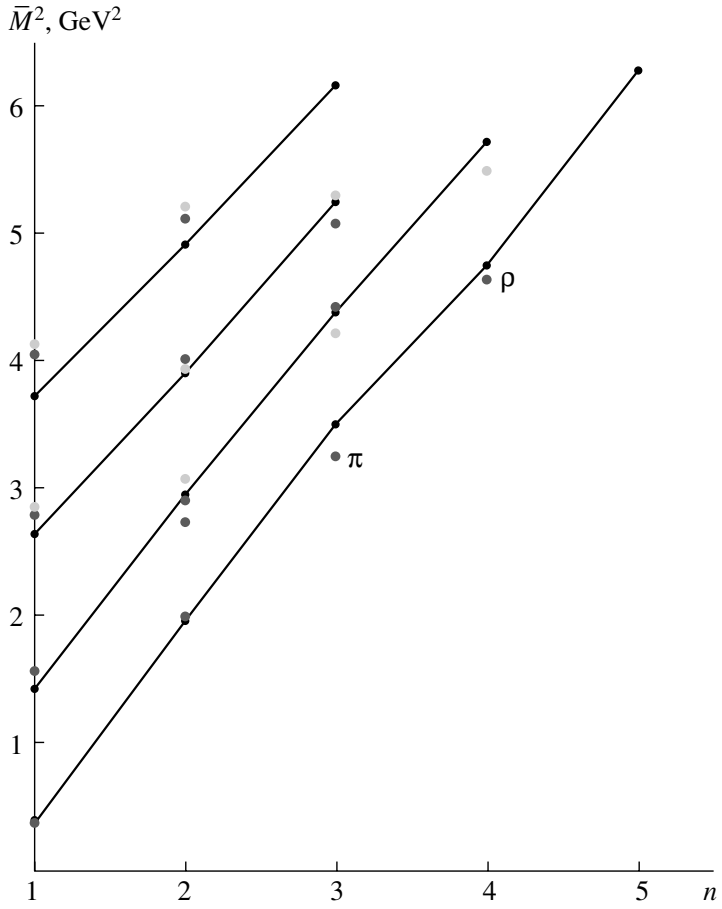

The spin-averaged meson mass squared $\bar{M}^2(L, n_r)$ vs. $n = n_r + 1$. Theoretically calculated masses [39] are depicted by small black dots and are connected by straight lines. Other points are experimental candidates. The lines from bottom up correspond to $L = 0, 1, 2, 3$, respectively.

where μ_g is the einbein variable for the gluon; $\mathbf{r}_g$ is its coordinate; and $\mathbf{p}_\xi, \mathbf{p}_\eta$ are Jacobi momenta of the three-body system. H_{self} is the same as for a meson, while H_{spin} and H_{Coul} have different structure [33].

The main feature of the present approach based on the BPTh is that the valence gluon in the hybrid is situated at some point on the string connecting the quark and antiquark, and the gluon creates a kink on the string, so that two pieces of the string move independently (however, connected at the point of the gluon). This differs strongly from the flux-tube model, where the hybrid is associated with the string excitation as a whole.

The difference between the two approaches is especially pronounced in the case of the hybrid with static quarks separated by the distance R [33], where the flux-tube model predicts for large R the terms $E_n(R) \sim \pi n/R$, while in the FCM there is another branch corresponding to the longitudinal d.o.f. of the gluon $E(R) \sim \text{const}/R^{1/3}$ [6, 33], and the lattice results certainly prefer the latter and contradict the flux-tube asymptotics. Also, at intermediate interquark distances R, the spectrum of the FCM approach is in much better agreement with lattice data than any other model (see [33] for details and discussion).

Results for light and heavy exotic 1^{-+} hybrids are also given in [6] and are in agreement with lattice calculations. Typically, an additional gluon in the exotic ($L = 1$) state "weights" 1.2–1.5 GeV for light to heavy quarks, while a nonexotic gluon ($L = 0$) brings about 1 GeV to the mass of the total $q\bar{q}g$ system.

It is understandable now that hybrids play a very special role in QCD; namely, they describe the excitation of the film (the string world sheet), which is between q and $\bar{q}$ and, in particular, covers the gluon and quark loops appearing in the α_s renormalization. The "additional gluon" mass $M_g \approx 1$ GeV cited above enters as a screening mass in the one-loop running α_s (see [7–36] for details and derivations),

$$\alpha_s(Q) = 4\pi \left[b_0 \ln \left(\frac{Q^2 + M_g^2}{\Lambda^2_{\text{QCD}}} \right) \right]^{-1}, \qquad (23)$$

and this form (in r space) is in a perfect agreement with a recent calculation of α_s on the lattice [37].

Thus, one can say that the perturbative QCD in the IR region is defined by the hybrid physics. A similar conclusion can be drawn with respect to the DIS diagrams at small to moderate Q^2, $Q^2 \lesssim 1$ GeV^2, where familiar ladder diagrams with gluon exchanges are replaced by (multi)hybrid Green's functions, and to the hadron–hadron scattering, where, e.g., a sequence of BFKL ladders is replaced by multihybrid diagrams. Progress in this direction is highly desirable.

All discussion above refers to the leading large-N_c limit, which has a remarkable accuracy, as was recently demonstrated on the lattice [38] and by comparison of calculated and experimental masses in [23, 29, 33, 34]. We now turn to the $1/N_c$ effects, which, as shown in [39], strongly modify the masses of radially excited mesons. Typically, these mesons have radii larger than 1.5 fm, and, as was argued in [39], at the interquark distances $R \geq 1.4$ fm, there appear sea-quark holes in the confining film connecting q and $\bar{q}$ trajectories. It was assumed in [39] that the film with virtual holes establishes a quasi-stationary state, which can be called the "predecay state." It is clear that the effective string tension decreases due to holes and the confining potential is partly screened at $R \geq 1.4$ fm. The masses of radially excited mesons for $L = 0, 1, 2, 3$ and $n_r = 0, 1, 2, 3, 4$ have been calculated in [39] with the help of this potential and are shown in figure. One can see a remarkable agreement of theoretical masses (black dots) with experimental candidates. Another remarkable feature is the almost exact linearity of trajectories $\bar{M}^2(L, n_r)$ vs. n_r. The effect of mass decrease due to the sea-quark holes is significant (for high n_r, it is around 0.5 GeV).

Concluding the paper, I would like to stress the simplicity of the method (FCM), which solves at least four important problems in the QCD spectrum: (i) Regge slope; (ii) Regge intercept; (iii) the problem of constituent masses; (iv) problem of radial Regge trajectories.

ACKNOWLEDGMENTS

I am indebted to A.B. Kaidalov and Yu.S. Kalashnikova for useful discussions. During all the years of the development of the present method, I had the constant interest and helpful attention and support from K.A. Ter-Martirosyan, which are very gratefully acknowledged.

This work was partially supported by the Russian Foundation for Basic Research (project nos. 00-02-17836 and 00-15-96786) and by INTAS (grant nos. 00-110 and 00-00366).

REFERENCES

1. H. G. Dosch, Phys. Lett. B **190**, 177 (1987); Yu. A. Simonov, Nucl. Phys. B **307**, 512 (1988); A. Di Giacomo, H. G. Dosch, V. I. Shevchenko, and Yu. A. Simonov, Phys. Rep. **372**, 319 (2002); hep-ph/0007223.
2. H. G. Dosch and Yu. A. Simonov, Phys. Lett. B **205**, 339 (1988).
3. A. Di Giacomo and H. Panagopoulos, Phys. Lett. B **285**, 133 (1992); A. Di Giacomo, E. Meggiolaro, and H. Panagopoulos, Nucl. Phys. B **483**, 371 (1997); A. Di Giacomo and E. Meggiolaro, hep-lat/0203012; G. S. Bali, N. Brambilla, and A. Vairo, Phys. Lett. B **421**, 265 (1998).
4. M. Foster and C. Michael, Phys. Rev. D **59**, 094509 (1999).
5. Yu. A. Simonov, Nucl. Phys. B **592**, 350 (2001); M. Eidemueller, H. G. Dosch, and M. Jamin, Nucl. Phys. B (Proc. Suppl.) **86**, 421 (2000).
6. Yu. A. Simonov, in *QCD: Perturbative or Nonperturbative,* Ed. by L. Ferreira, P. Nogueira, and J. I. Silva-Marcos (World Sci., Singapore, 2001); hep-ph/9911237.
7. Yu. A. Simonov, Yad. Fiz. **58**, 113 (1995) [Phys. At. Nucl. **58**, 107 (1995)]; Pis'ma Zh. Éksp. Teor. Fiz. **57**, 513 (1993) [JETP Lett. **57**, 525 (1993)]; Lect. Notes Phys. **479**, 139 (1996).
8. Yu. A. Simonov, Phys. At. Nucl. **60**, 2069 (1997); hep-ph/9704301; Yu. A. Simonov and J. A. Tjon, Phys. Rev. D **62**, 014501, 194511 (2000).
9. Yu. A. Simonov, Phys. At. Nucl. **63**, 94 (2000).
10. Yu. A. Simonov, Yad. Fiz. **62**, 2087 (1999) [Phys. At. Nucl. **62**, 1932 (1999)]; hep-ph/9912383.
11. Yu. A. Simonov, J. A. Tjon, and J. Weda, Phys. Rev. D **65**, 094013 (2002).
12. Yu. A. Simonov, Phys. Lett. B **226**, 151 (1989); **228**, 413 (1989).
13. A. Yu. Dubin, A. B. Kaidalov, and Yu. A. Simonov, Phys. Lett. B **323**, 41 (1994); Yad. Fiz. **56** (12), 213 (1993) [Phys. At. Nucl. **56**, 1745 (1993)].
14. Yu. A. Simonov and J. A. Tjon, Ann. Phys. (N.Y.) **300**, 54 (2002).
15. G. S. Bali, Phys. Rev. D **62**, 114503 (2000); S. Deldar, Phys. Rev. D **62**, 034509 (2000).
16. Yu. A. Simonov, JETP Lett. **71**, 127 (2000); V. I. Shevchenko and Yu. A. Simonov, Phys. Rev. Lett. **85**, 1811 (2000).
17. D. Gromes, Phys. Lett. B **115B**, 482 (1982); V. Marquard and H. G. Dosch, Phys. Rev. D **35**, 2238 (1987); A. Krämer, H. G. Dosch, and R. A. Bertlmann, Phys. Lett. B **223**, 105 (1989); Yu. A. Simonov, Yad. Fiz. **54**, 192 (1991) [Sov. J. Nucl. Phys. **54**, 115 (1991)].
18. A. Yu. Dubin, A. B. Kaidalov, and Yu. A. Simonov, Yad. Fiz. **58**, 348 (1995) [Phys. At. Nucl. **58**, 300 (1995)].
19. V. L. Morgunov, V. I. Shevchenko, and Yu. A. Simonov, Yad. Fiz. **61**, 739 (1998) [Phys. At. Nucl. **61**, 664 (1998)]; Phys. Lett. B **416**, 433 (1998); hep-ph/9704282.

20. E. L. Gubankova and A. Yu. Dubin, Phys. Lett. B **334**, 180 (1994).
21. D. P. Stanley and D. Robson, Phys. Rev. D **21**, 3180 (1980); J. Carlson, J. Kogut, and V. R. Pandharipande, Phys. Rev. D **27**, 233 (1983); J. L. Basdevant and S. Boukraa, Z. Phys. C **28**, 413 (1985); J. M. Richard and P. Taxil, Phys. Lett. B **128B**, 453 (1983); Ann. Phys. (N.Y.) **150**, 267 (1983); S. Godfrey and N. Isgur, Phys. Rev. D **32**, 189 (1985).
22. V. L. Morgunov, A. V. Nefediev, and Yu. A. Simonov, Phys. Lett. B **464**, 265 (1999); hep-ph/9906318.
23. A. M. Badalian and B. L. G. Bakker, Phys. Rev. D **66**, 034025 (2002).
24. Yu. A. Simonov, Phys. Lett. B **515**, 137 (2001).
25. Yu. A. Simonov, Nucl. Phys. B **324**, 67 (1989); A. M. Badalian and Yu. A. Simonov, Yad. Fiz. **59**, 2247 (1996) [Phys. At. Nucl. **59**, 2164 (1996)].
26. Yu. A. Simonov, Yad. Fiz. **64**, 1959 (2001) [Phys. At. Nucl. **64**, 1876 (2001)].
27. T. J. Allen, G. Goebel, M. G. Olsson, and S. Veseli, Phys. Rev. D **64**, 094011 (2001).
28. A. M. Badalian, B. L. G. Bakker, and V. L. Morgunov, Phys. At. Nucl. **63**, 1635 (2000); A. M. Badalian and B. L. G. Bakker, Phys. Rev. D **64**, 114010 (2001).
29. Yu. S. Kalashnikova, A. V. Nefediev, and Yu. A. Simonov, Phys. Rev. D **64**, 014037 (2001).
30. B. O. Kerbikov and Yu. A. Simonov, Phys. Rev. D **62**, 093016 (2000).
31. V. Yu. Glebov, A. B. Kaidalov, S. T. Sukhorukov, and K. A. Ter-Martirosyan, Yad. Fiz. **10**, 1065 (1969); A. B. Kaidalov and K. A. Ter-Martirosyan, Nucl. Phys. B **75**, 471 (1974); A. B. Kaidalov, Phys. Rep. **50**, 157 (1979); M. Baker and K. A. Ter-Martirosyan, Phys. Rep. **28C**, 1 (1976).
32. Yu. A. Simonov, in *Proc. of the Workshop on Physics and Detectors for DAΦNE, Frascatti, 1991*; Yu. A. Simonov, Nucl. Phys. B (Proc. Suppl.) **23**, 283 (1991); in *Hadron-93*, Ed. by T. Bressani, A. Felicielo, G. Preparata, and P. G. Ratcliffe, Nuovo Cimento A **107**, 2629 (1994); Yu. S. Kalashnikova and Yu. B. Yufryakov, Phys. Lett. B **359**, 175 (1995); Yu. B. Yufryakov, hep-ph/9510358.
33. Yu. S. Kalashnikova and D. S. Kuzmenko, hep-ph/0203128.
34. A. B. Kaidalov and Yu. A. Simonov, Phys. Lett. B **477**, 163 (2000); Phys. At. Nucl. **63**, 1428 (2000).
35. V. S. Fadin and L. N. Lipatov, Phys. Lett. B **429**, 127 (1998); M. Ciafaloni and G. Camici, Phys. Lett. B **430**, 349 (1998).
36. Yu. A. Simonov, Yad. Fiz. **65**, 140 (2002) [Phys. At. Nucl. **65**, 135 (2002)]; hep-ph/0109159.
37. A. M. Badalian and D. S. Kuzmenko, Phys. Rev. D **65**, 016004 (2002).
38. M. Teper, hep-ph/0203203.
39. A. M. Badalian, B. L. G. Bakker, and Yu. A. Simonov, Phys. Rev. D **66**, 034026 (2002).

Physics of Atomic Nuclei, Vol. 66, No. 11, 2003, pp. 2045–2050. From Yadernaya Fizika, Vol. 66, No. 11, 2003, pp. 2095–2100.

ELEMENTARY PARTICLES AND FIELDS
Theory

Nonperturbative Mechanisms of Strong Decays in QCD*

Yu. A. Simonov**

Institute of Theoretical and Experimental Physics,
Bol'shaya Cheremushkinskaya ul. 25, Moscow, 117259 Russia

Received February 17, 2003

Abstract—Three strong decay mechanisms are derived systematically from the QCD Lagrangian using the field correlator method. The resulting operators contain no arbitrary parameters and depend only on characteristics of field correlators known from lattice and analytic calculations. When compared to existing phenomenological models, parameters are in good agreement with the corresponding fitted values.

1. INTRODUCTION

An enormous amount of experimental data on strong decays of mesons and baryons is partly used by theoreticians for comparison in the framework of the $^3P_0$ model [1] and its flux-tube modifications [2]. The analysis done in [3] confirmed the general validity of the model, whereas in [4] results of other forms of decay operators have also been investigated in meson decays, and in [5] in baryon decays. On the whole, the phenomenological picture seems to be satisfactory for the $^3P_0$ model with some exclusions discussed in [3] and [6]. The recent extensive study of strong decays of strange quarkonia based on the $^3P_0$ model was done in [7].

The key element that is missing in this situation is the systematic derivation of all terms in the decay Hamiltonian from the basic principles, i.e., from the QCD Lagrangian. It is the purpose of the present paper to make some progress in this direction using the field correlator method (FCM) [8] and background perturbation theory [9] to treat nonperturbative (NP) QCD contributions together with perturbative ones.

In doing so, one should take into account the special role of pions in the hadron decays and, therefore, accurately perform the chiral bosonization of the effective quark Lagrangian obtained from the basic QCD Lagrangian. This will give the first term in the decay Hamiltonian, and the corresponding decay mechanism will be referred to as a chiral decay mechanism (CDM). At the same time, one should take into account the string degrees of freedom in the original meson and the possibility of string breaking due to the $q\bar{q}$-pair creation. The corresponding term in the decay Hamiltonian will be derived below without free parameters and this second mechanism will be called the string-breaking mechanism (SBM). As will be seen, the dominant term of the SBM has a structure that can be compared quantitatively with the phenomenological fits of the $^3P_0$ model in [3, 4].

Finally, the QCD perturbation theory in the perturbative background developed in [9] allows one to derive two additional terms in the decay Hamiltonian: one for the OZI-allowed decays, which has the Lorentz form of the $^3S_1$ type but proceeds through the intermediate hybrid state, and another for the OZI-forbidden decays, which proceeds through the intermediate glueball state and only at very small distances reduces to the two-gluon or three-gluon $q\bar{q}$-pair creation. We shall call these mechanisms the hybrid mediated decay (HMD) and the glueball mediated decay (GMD), respectively.

2. THE CHIRAL BOSONIZATION AND THE CHIRAL DECAY MECHANISM

One starts with the QCD Lagrangian in Euclidean spacetime and averages over the gluonic fields writing the general form of the gauge-invariant correlator (known from lattice or analytic calculations—see references in [8]) which contains the confining part $D(x)$, namely,

$$\frac{g^2}{N_c}\left\langle \mathrm{tr}\big(F_{\mu\nu}(x)\Phi(x,y)F_{\lambda\sigma}(y)\Phi(y,x)\big)\right\rangle = (\delta_{\mu\lambda}\delta_{\nu\sigma}-\delta_{\mu\sigma}\delta_{\nu\lambda})D(x-y)+O(D_1), \quad (1)$$

where $O(D_1)$ contains a relatively small nonconfining part $D_1(x)$ and $\Phi(x,y)=P\exp(ig\int_y^x A_\mu dz_\mu)$ is the parallel transporter.

*This article was submitted by the author in English.

**e-mail: simonov@heron.itep.ru

Assuming also that all higher correlators can be neglected (as is supported by lattice data—see [10]), one obtains the effective quark Lagrangian (EQL) [11]

$$L^{(2)}_{\rm EQL} = \frac{1}{2N_c}\int d^4x \int d^4y\, {}^f\psi^+_{a\alpha}(x) \times {}^f\psi_{b\beta}(x)\, {}^g\psi^+_{b\gamma}(y)\, {}^g\psi_{a\varepsilon}(y) \times \left[\gamma^{(4)}_{\alpha\beta}\gamma^{(4)}_{\gamma\varepsilon} J_E(x,y) + \gamma^{(i)}_{\alpha\beta}\gamma^{(i)}_{\gamma\varepsilon} J_M(x,y)\right], \quad (2)$$

where the kernel $J(x,y)$ is expressed through $D(x)$; ${}^f\psi_{a\alpha}$ is the quark operator with flavor index f, color a, and spinor α; $\gamma^{(\mu)}_{\alpha\beta}$ is the Euclidean Dirac matrix,

$$J_{E(M)}(x,y) = \int\limits_Y^x du_i \int\limits_Y^y dv_i K^{(E(M))}_{xy}(u,v) D(u-v), \quad i=1,2,3; \quad (3)$$

and $D(x)$ is connected to the string tension σ in the usual way, $\sigma = \frac{1}{2}\int d^2x D(x)$. Here, the string kernel $J_{E(M)}$ contains color electric (magnetic) fields and the former is dominant at large distances, and therefore the magnetic part will be omitted for simplicity. At this point, one should specify the choice of integration contours, the kernel K, and the point Y in (3). As is known, the full result of the integration over gluon fields does not depend on the gauge and shape of the contours (when all correlators are taken into account); however, to write the contribution of bilocal correlator (1) in the gauge-invariant form, one has to use one of the variants of the contour gauge, e.g., [12], where $K^{(E)}_{xy} \equiv 1$, and to choose the contour corresponding to the minimal string that minimizes the contribution of higher correlators. In this section, we consider the following geometry: the quarks at the points x, y in (2) are at one end of the string (they are dynamically close [11]), while the point Y is at the position of the heavy antiquark, as was introduced in [11]. In the next section, we shall consider a more general geometry where two points Y in (3) are different and integration over du_i and dv_i runs over two different pieces of the broken string. For the results of the present section, the exact definition of the point Y is inessential since the pion is emitted from the end of the string under consideration, while another end of string is a spectator.

As the next step, the bosonization of the Lagrangian (2) can be done in the usual way, however, with nonlocal mesonic fields with the result [13]

$$\Delta L = i\int d^4x d^4y \psi^+(x)\hat{M}(x,y)\psi(y), \quad (4)$$

where the kernel $\hat{M}(x,y)$ can be written as a nonlinear form for pseudoscalar (PS) meson fields ϕ_A:

$$\hat{M}(x,y) = M_S(x,y)\exp(i\gamma_5\hat{\phi}(x,y)) + \ldots, \quad \hat{\phi} = \frac{\phi_A\lambda^A}{F_\pi}, \quad F_\pi = 93\ \text{MeV}. \quad (5)$$

Here, $M_S(x,y) = \frac{1}{4}{\rm tr}(\hat{\partial} + \hat{M})^{-1} J_E(x,y)$, and the ellipsis implies all other omitted terms, including those containing isovector scalars, vectors, and pseudovectors.

One should note that, in our case, where confinement is present, the constant condensate of scalar–isoscalar field always enters multiplied by $J(x,y)$ and thus produces the scalar confining potential of the string in $M_S(x,y)$ [13]. Namely, for long enough a string, i.e., for $|\mathbf{x}-\mathbf{Y}| \gg T_g$, where T_g is the gluonic correlation length in $D(x)$, one has approximately [11]

$$M_S(x,y) \approx \sigma|\mathbf{x}|\delta^{(4)}(x-y). \quad (6)$$

This is different from the instanton, or the NJL model, where the scalar–isoscalar field acquires a nonzero condensate, which is constant in all spacetime.

Inserting (6) into (5), one obtains a localized form of the quark–meson Lagrangian, describing interaction on one end of the string; to the lowest order in PS field

$$\Delta L^{(1)} = \int \overline{\psi}(x)\sigma|\mathbf{x}-\mathbf{Y}|\gamma_5\frac{\phi_A\lambda^A}{F_\pi}\psi(x)dtd^3x. \quad (7)$$

One can visualize in (7) the simultaneous presence of quark fields $\psi, \bar{\psi}$, together with the string $\sigma|\mathbf{x}-\mathbf{Y}|$ and Nambu–Goldstone (NG) fields ϕ_A, $A = 1, \ldots, n_f^2 - 1$.

Using the Dirac equation for the quark field $\psi(x)$, one arrives, as in [13], at the familiar Weinberg Lagrangian [14]

$$\Delta L^{\rm W} = g^q_A {\rm tr}(\overline{\psi}\gamma_\mu\gamma_5\omega_\mu\psi), \quad \omega_\mu = \frac{i}{2}(u\partial_\mu u^+ - u^+\partial_\mu u), \quad (8)$$

where $u(x) = \exp\left(\frac{i}{2}\gamma_5\hat{\phi}(x,x)\right)$. In our derivation, g^q_A is uniquely defined in the local limit,

$$g^q_A \equiv 1, \quad (9)$$

which agrees with the large-N_c limit, discussed in [14].

Note that both Lagrangians (7), (8) are local limits of nonlocal expression (4), and for not a very long string with the length $L \sim T_g \sim 0.2$ fm, the nonlocality is essential. Although a string is apparently not

present in (8), both quark operators there are solutions of the Dirac equation with the string entering as a scalar potential. It is clear that the Lagrangian (8) describes the pion field emission both from the quark at one end of the string and from the antiquark at the other end of the string. In case of baryons, one should sum up in (8) over all three quarks.

The form (8) was used in [15] for the calculation of pionic transitions in the heavy–light mesons with g_A^q playing role of a fitting parameter, which turned out to be around 0.7. This difference from (9) can be considered as an indication of a possible role of nonlocality.

3. THE STRING-BREAKING MECHANISM

This mechanism was considered in some detail in [16] (see also references therein). In the present section, we shall consider the pair-creation vertex due to the nonperturbative QCD configurations. In the $^3P_0$ model [1], this vertex was modeled by an adjustable constant and in [16] by some function F. It is our purpose here to derive this vertex from the basic $4q$ effective Lagrangian (2).

To describe the creation of the $q\bar{q}$ pair in the presence of the string that connects quark Q and antiquark $\bar{Q}$, one can, as in [11], take the large-N_c limit of the same $4q$ Lagrangian (2), which is obtained by replacing ${}^f\psi_{b\beta}(x){}^g\psi^+_{b\gamma}(y) \to \delta_{fg}N_c S_{\beta\gamma}(x,y)$, $S = i(\hat{\partial} + M)^{-1}$.

The resulting Lagrangian describes the creation of the quark and antiquark at the points x and y, respectively. Physically, it is clear that x and y should lie on the (deformed) string connecting quark Q at the point X and antiquark $\bar{Q}$ at the point $\bar{X}$. Since the final two strings connect X and x, and $\bar{X}$ and y, we can also choose the contours of integration along the strings: e.g., $A_4(x) = \int_x^X du_1 E_1(u_1)$, $A_4(y) = \int_{\bar{X}}^y dv_1 E_1(v_1)$, and the string is along axis 1. [This change of contours from (3) can be traced to the effect of cancellation in the sum of contours from the quark Q to the point Y and with opposite sign, from the antiquark $\bar{q}$ to the point Y, which results in the contour integral between positions $Q(X)$ and $\bar{q}(x)$.] As a result, the kernel J_E is

$$J_E(\mathbf{x}, x_4; \mathbf{y}, y_4) = \int_x^X du_1 \int_{\bar{X}}^y dv_1 D(u_1 - v_1) \quad (10)$$
$$\cong \frac{\sigma}{\pi} \exp\left(-\frac{(x_4 - y_4)^2}{4T_g^2}\right),$$

where for $D(x)$ the Gaussian form was used (cf. [11]). As in (4), one can find the effective mass operator (due to color electric fields) $M(x,y)$, using the definition [12]

$$M(x,y) = -i\gamma_4 S(x,y)\gamma_4 J(x,y), \quad (11)$$

and the estimate of the quark Green's function $S(x,y)$ for a long string, $L \gg T_g$, done in [11, 13], gives $S(x,y) \sim i\delta^{(3)}(\mathbf{x} - \mathbf{y})$.

As a result, one obtains for the effective Lagrangian the same form as in (4), but with another, string-breaking, mass operator $M^{(\mathrm{br})}$:

$$\Delta L^{(\mathrm{SBM})} = i \int d^4x d^4y \psi_a^+(x) M^{(\mathrm{br})}(x,y)\psi_a(y), \quad (12)$$

where

$$M^{(\mathrm{br})}(x,y) = \frac{\sigma}{\pi}\delta^{(3)}(\mathbf{x} - \mathbf{y}) \exp\left[\frac{(x_4 - y_4)^2}{4T_g^2}\right]. \quad (13)$$

Integrating over $d(x_4 - y_4)$, one gets in the Minkowskian spacetime

$$\Delta L^{(\mathrm{SBM})} = \frac{2T_g\sigma}{\sqrt{\pi}} \int d^4x \bar{\psi}(x)\psi(x). \quad (14)$$

The string-breaking Hamiltonian can be written as

$$H_I^{(\mathrm{SBM})} = g \int d^3x \bar{\psi}(x)\psi(x), \quad (15)$$
$$g = 2T_g\sigma/\sqrt{\pi}, \quad \gamma \equiv \frac{T_g\sigma}{\sqrt{\pi}\mu} = \frac{g}{2\mu},$$

where μ is the constituent quark mass computed through σ [17]. Taking $T_g \sim (0.2\text{–}0.3)$ fm, $\sigma \approx 0.2$ GeV^2, and $\mu \approx 0.35$ GeV, one obtains $\gamma \sim 0.3\text{–}0.5$, i.e., the values in the same ballpark as in the phenomenological analysis [3, 4]. Several remarks are now in order. Firstly, above, the simplified Gaussian form of $D(x)$ was used in (10), which requires the redefinition of T_g; secondly, the contribution of magnetic correlators and the term D_1 in (1) has been neglected. These additional contributions will be considered elsewhere.

4. "PERTURBATIVE" PAIR CREATION VIA THE HYBRID OR GLUEBALL FORMATION

Two decay mechanisms discussed in previous sections are of purely nonperturbative origin. Now, we turn to the mechanisms that contain as a limit a purely perturbative $q\bar{q}$-pair creation by a gluon. At large distances, one has to know how this process is modified by the presence of nonperturbative confining fields and to this end we shall use the background perturbation theory (BPTh) developed in [10], where the

total gluonic field A_μ is separated into valence gluon field a_μ and background B_μ, $A_\mu = B_\mu + a_\mu$. The field B_μ saturates correlator $D(x)$ and therefore contains its own mass scale, while perturbation theory is done in powers of ga_μ. The main physical outcome of the analysis of [10] is that the valence gluons propagate inside the film of the string world sheet, so that all Feynman diagrams in the coordinate space can be considered as filled inside by this film on the minimal surface with boundaries specified by quark and gluon trajectories.

At this point, it is clear that one should use the path integral representation for the quark and gluon Green's function, namely, the Fock–Feynman–Schwinger (FFS) formalism [18]. The FFS method has proved useful in conjunction with the BPTh to study meson, hybrid, and glueball Green's functions (see [17] for a review). In [19], this method has been exploited to calculate mixing between meson, hybrid, and glueball states, and in what follows we shall pursue the same way to study matrix elements of decays proceeding via hybrid and glueball intermediate states.

We start with the OZI-allowed planar pair creation mechanism by a gluon, propagating inside the film in a hybrid state $\varphi^{(H)}$, and therefore the matrix element for the meson decay via the hybrid states can be written as

$$W^{(H)} = \sum_n \lambda_n^{(\mathrm{MH})} W_n^{(H)}, \qquad (16)$$

where $\lambda_n^{(\mathrm{MH})}$ is the dimensionless mixing coefficient of the nth hybrid state in the given initial meson, which according to [19] can be written as

$$\lambda_n^{(\mathrm{MH})} = \frac{V_{\mathrm{on}}^{(\mu)}}{\sqrt{2\mu_g(n)}|M_H^{(n)} - M_M|}. \qquad (17)$$

Here, $M_H^{(n)}$ and M_M are hybrid and meson masses, respectively, and $\mu_g(n)$ is the constituent gluon mass in the nth hybrid state, computed through the string tension as in [17, 19].

The matrix element $V_{\mathrm{on}}^{(\mu)}$, introduced in [19], is that of the pair-creation operator H_1,

$$H_1 = g \int \bar{q}(\mathbf{x}, 0)\hat{a}(\mathbf{x}, 0)q(\mathbf{x}, 0)d^3x, \qquad (18)$$

between the meson state $\Phi_{\alpha\beta}^{(M)}(\mathbf{r})$ and the hybrid state $\Phi_{\mu,\gamma\delta}^{(H)}(\mathbf{r}_1, \mathbf{r}_2)$, where we have specified quark Dirac indices $\alpha\beta, \gamma\delta$ and gluon component index μ (this is the 4×4 representation typical for the Bethe–Salpeter wave functions which is used to build up $2j + 1$ components of meson and hybrid wave functions—for discussion and references see [19]).

In a simplified form, V_{on} can be written as [19]

$$V_{\mathrm{on}}^{(\mu)} = g \int d\mathbf{r}\phi^{*(H)}(0, \mathbf{r})\Gamma\phi^{(M)}(\mathbf{r}) + \mathrm{perm.}, \qquad (19)$$

where "perm." implies another term with gluon emitted by antiquark, and $\Gamma = \gamma_\mu$.

The term $W_n^{(H)}$ in (16) is the decay amplitude of the nth hybrid state into two mesons, which can be written as

$$W_n^{(H)} = \frac{V_{n,12}}{\sqrt{2\mu_g(n)V}}, \qquad (20)$$

$$V_{n,12} \equiv \int \Phi^{*(M_1)}(\mathbf{r}_1)\Phi^{*(M_2)}(\mathbf{r}_2) \times \Gamma^{(H)}(\mathbf{r}_1, \mathbf{r}_2)d\mathbf{r}_1 d\mathbf{r}_2,$$

where $\Gamma^{(H)}(\mathbf{r}_1, \mathbf{r}_2)$ is the vertex operator for the hybrid decay. Normalization of wave functions is (summation over repeating Dirac indices, which are omitted, is implied)

$$\int |\Phi^{(H)}|^2 d\mathbf{r}_1 d\mathbf{r}_2 = 1, \quad \int |\Phi^{(M_i)}|^2 d\mathbf{r} = 1. \qquad (21)$$

Finally, the two-body decay probability of the hybrid with mass M into two mesons with energies E_1 and E_2 is

$$dw = 2\pi |W_n^{(H)}|^2 \delta(E_1 - E_2 - M)\frac{V d\mathbf{k}}{(2\pi)^3}. \qquad (22)$$

As it is seen from (16) and (17), the decay probability is strongly enhanced when the decaying meson mass is in the vicinity of some hybrid level. One should stress that this situation is standard in the mass range above 1.4 GeV, where the density of hybrid ground and excited states is fast growing with mass.

We now turn to the OZI-forbidden, i.e., nonplanar, $q\bar{q}$-pair creation via valence gluons. The essential step in this mechanism is the creation of the new flavor quark–antiquark pair with the new string between them; hence, the creation operator contains at least a two-gluon exchange. In the confining background, trajectories of these two gluons are connected by the adjoint string (or, equivalently, at large N_c by a double fundamental string), and therefore a new meson is created by the two- or more-gluon glueball, which is emitted virtually from the original meson. The amplitude for this process can be written as

$$W^{(G)} = \sum_n \frac{V_n^{(MM_2)} V_n^{(GM_1)}}{M - E_n^{(G)} - E(M_2)}, \qquad (23)$$

where notation

$$V_n^{(MM_2)} = \langle \phi^{(M_2)} | \Lambda_n^{(G)} | \phi^{(M)} \rangle, \qquad (24)$$

$$V_n^{(GM_1)} = (\phi^{(M_1)*}\bar{\Lambda}_n^{(G)})$$

is used, and the two-gluon glueball vertex is

$$\Lambda^{(G)}_{n,\alpha\beta}(x_1,x_2) \quad (25)$$
$$= \Psi^{*(G)}_{n,\nu_1\nu_2}(x_1,x_2)(\gamma_{\nu_1}S^{(f)}(x_1,x_2)\gamma_{\nu_2})_{\alpha\beta},$$
$$\bar{\Lambda}^{(G)}_{n,\alpha\beta}(y_1,y_2)$$
$$= (\gamma_{\mu_1}S^{(g)}(y_1,y_2)\gamma_{\mu_2})_{\alpha\beta}\Psi^{(G)}_{n,\mu_1\mu_2}(y_1,y_2).$$

Here, $\Psi^{(G)}$ is the glueball wave function, and $S^{(g,f)}$ is the Green's function of quarks with flavor g, f.

When all distances $|y_i - x_k|$, $|x_1 - x_2|$, $|y_1 - y_2|$ are small as compared to T_g, the two-gluon Green's function reduces to the two-gluon exchange of free gluons. This limiting perturbative mechanism has been known for a long time [20]. In the opposite limit, only the lowest-mass term survives in the sum (23).

The most interesting case occurs when the denominator in (23) becomes small, which is possible when the mass of some glueball state is close to the mass of the emitted meson M_1. This amplification may thus occur in the 0^{++} channel for M_1 around 1.5 GeV or in other channels for $M_1 \gtrsim 2$ GeV [21]. A similar mechanism may take place in hadron–hadron scattering with creation of the $c\bar{c}$ states in the mass range 3–4 GeV, where also glueball states are predicted in lattice and in analytic calculations [21].

5. CONCLUSION

In the present paper, the first qualitative step was done aimed at the systematic derivation of strong decay amplitudes from the QCD Lagrangian. We have considered three decay mechanisms, where the nonperturbative contribution is very important.

The first one, the CDM, was already successfully checked in heavy–light meson decays [15]. The next step would be to apply the CDM to the pionic and kaonic decays of light–light mesons and investigate double- and more-pion decays, which are given by the nonlinear Lagrangian (8). The second mechanism, the SBM, turns out to be mostly $^3P_0$ (additional terms due to the smaller nonscalar component in the quark Green's function S considered in [11] have been neglected above) and its amplitude is close to the phenomenological fits [4]. The third type of mechanism with a hybrid or a glueball in the intermediate state is the nonperturbative background generalization of the original purely perturbative mechanisms of the $^3S_1$ type [22] and of two-gluon exchange [20], respectively. It is argued that a strong enhancement of decay amplitudes is possible when the corresponding levels of a hybrid or a glueball are close to the mass of the original or final meson, respectively. The paper does not contain quantitative predictions, which are planned for the future, but is rather concentrated on the general discussion of possible decay mechanisms as they emerge from the basic QCD Lagrangian.

One of the immediate extensions of the present result is the inclusion of the baryon decays, where all three mechanisms discussed above are present in the same form with only the replacement of the simple mesonic string by the Y-shaped baryonic string.

Finally, one should have in mind that all three mechanisms discussed above enter the decay amplitude additively, and therefore one can expect, in general, some interference effects, which make the analysis of data more complicated and perhaps more interesting.

ACKNOWLEDGMENTS

Numerous discussions and the stimulating interest of Prof. K.A. Ter-Martirosian have been crucial for my activity in this field and are gratefully acknowledged.

I am grateful to Yu.S. Kalashnikova and V.I. Shevchenko for valuable discussions.

The financial support of INTAS (grant nos. 00-110 and 00-366) and the Russian Foundation for Basic Research (project nos. 00-02-17836 and 00-15-96786) is gratefully acknowledged.

REFERENCES

1. L. Micu, Nucl. Phys. B **10**, 521 (1969); A. Le Yaouanc, L. Olivier, O. Pene, and J. Raynal, Phys. Rev. D **8**, 2223 (1973); **9**, 1415 (1974); **11**, 1272 (1975); **21**, 182 (1980).
2. R. Kokoski and N. Isgur, Phys. Rev. D **35**, 907 (1987).
3. H. Blundell and S. Goldfrey, Phys. Rev. D **53**, 3700 (1996); T. Barnes, F. E. Close, P. R. Page, and E. S. Swanson, Phys. Rev. D **55**, 4157 (1997).
4. P. Geiger and E. Swanson, Phys. Rev. D **50**, 6855 (1994); E. S. Ackleh, T. Barnes, and E. S. Swanson, Phys. Rev. D **54**, 6811 (1996).
5. R. Koniuk and N. Isgur, Phys. Rev. D **21**, 1868 (1980); S. Capstick and W. Roberts, Phys. Rev. D **47**, 1994 (1993).
6. T. Barnes, hep-ph/0202157; A. Donnachie and Yu. S. Kalashnikova, Phys. Rev. D **60**, 114011 (1999).
7. T. Barnes, N. Blank, and P. R. Page, nucl-th/0208072.
8. H. G. Dosch, Phys. Lett. B **190**, 177 (1987); H. G. Dosch and Yu. A. Simonov, Phys. Lett. B **205**, 339 (1988); Yu. A. Simonov, Nucl. Phys. B **307**, 512 (1988); A. Di Giacomo, H. G. Dosch, V. I. Shevchenko, and Yu. A. Simonov, Phys. Rep. **372**, 319 (2002); hep-ph/0007223.
9. Yu. A. Simonov, Yad. Fiz. **58**, 113 (1995) [Phys. At. Nucl. **58**, 107 (1995)]; Lect. Notes Phys. **479**, 139 (1996).

10. V. I. Shevchenko and Yu. A. Simonov, Phys. Rev. Lett. **85**, 1811 (2000).
11. Yu. A. Simonov, Yad. Fiz. **60**, 2252 (1997) [Phys. At. Nucl. **60**, 2069 (1997)]; hep-ph/9704301; Yad. Fiz. **63**, 106 (2000) [Phys. At. Nucl. **63**, 94 (2000)]; Yu. A. Simonov and J. A. Tjon, Phys. Rev. D **62**, 014501 (2000); hep-ph/0001075; Phys. Rev. D **62**, 094511 (2000); hep-ph/0006237.
12. I. I. Balitsky, Nucl. Phys. B **254**, 166 (1985).
13. Yu. A. Simonov, Phys. Rev. D **65**, 094018 (2002); hep-ph/0201170.
14. S. Weinberg, Phys. Rev. Lett. **67**, 3473 (1991).
15. J. L. Goity and W. Roberts, Phys. Rev. D **60**, 034001 (1999); hep-ph/9809302.
16. H. G. Dosch and D. Gromes, Phys. Rev. D **33**, 1378 (1986).
17. Yu. A. Simonov, in *QCD: Perturbative or Non-perturbative,* Ed. by L. Ferreira, P. Nogueira, and J. I. Silva-Marcos (World Sci., Singapore, 2001); hep-ph/9911237.
18. Yu. A. Simonov and J. A. Tjon, Ann. Phys. (N.Y.) **228**, 1 (1993); **300**, 54 (2002).
19. Yu. A. Simonov, Yad. Fiz. **64**, 1959 (2001) [Phys. At. Nucl. **64**, 1876 (2001)]; hep-ph/0110033.
20. R. Barbieri, R. Gatto, and E. Remiddi, Phys. Lett. B **61B**, 465 (1976).
21. C. Morningstar and M. Peardon, Nucl. Phys. B (Proc. Suppl.) **63**, 22 (1998); Phys. Rev. D **60**, 034509 (1999); A. B. Kaidalov and Yu. A. Simonov, Phys. Lett. B **477**, 167 (2000); hep-ph/9912434; Phys. At. Nucl. **63**, 1428 (2000); hep-ph/9911291.
22. E. Eichten, K. Gottfried, K. D. Lane, and T. M. Yan, Phys. Rev. Lett. **37**, 477 (1976); Phys. Rev. D **17**, 3090 (1978); **21**, 203 (1980); J. W. Alcock, M. J. Burfitt, and W. N. Cottingham, Z. Phys. C **25**, 161 (1984); S. Kumano and V. R. Pandharipande, Phys. Rev. D **38**, 146 (1988).

Physics of Atomic Nuclei, Vol. 66, No. 11, 2003, pp. 2051–2061. Translated from Yadernaya Fizika, Vol. 66, No. 11, 2003, pp. 2101–2110.

ELEMENTARY PARTICLES AND FIELDS
Theory

Is the Number of Light Flavors in QCD Great?

I. T. Dyatlov*

Petersburg Nuclear Physics Institute, Russian Academy of Sciences, Gatchina, 188350 Russia

Received December 24, 2002; in final form, May 22, 2003

Abstract—At a qualitative level, it is well known that QCD featuring a large number of quark flavors must differ drastically from actual QCD. However, it is possible to consider the large-N_f limit (where N_f is the number of light flavors in QCD) such that the basic dynamics of the system remains unchanged. This is the region of chiral perturbation theory, where the limit $N_f \to \infty$ is simultaneously the limit of a large number of colors, N_c. Features are indicated that make it possible, in such a situation, to compare analytically the same quantity in a simplified model of actual QCD and in the large-N_f limit, and methods are proposed for calculating these features. Calculations in the limit $N_f \to \infty$ are of no use in assessing quantities of the theory at small N_f. © *2003 MAIK "Nauka/Interperiodica".*

1. INTRODUCTION

Investigation of models involving a large number N of components of multiplets of physical fields (colors, N_c; light flavors, N_f; replicas) has been widespread in theoretical physics since the proposal of 't Hooft [1] to consider QCD where the number of colors tends to infinity, $N_c \to \infty$. The objectives of such investigations are quite diverse: some are aimed at exploring possible nonperturbative phenomena [2] or at deducing information that could be of use in evaluating perturbative contributions [3], while others are devoted to assessing the properties of actual systems [4].[1)]

There arise the question of whether such estimates may faithfully reproduce the situation in observed physical processes and the question of whether the features calculated in this way are close to those that are observed if one substitutes $N_c = 3$ or $N_f = 3$. The next question to be answered is that of whether it is advisable to refine such estimates by calculating higher order approximations in N^{-1}.

It is quite clear that the change in N_c and especially in N_f affects the dynamical structure of QCD significantly. In what is concerned with N_f, this is well known: at large N_f, the asymptotic-freedom regime is replaced by the zero-charge regime and a chiral condensate is not formed. At the same time, the asymptotic-freedom regime persists at arbitrarily large values of N_c; therefore, one assumes that the properties of QCD, including confinement, remain unchanged for $N_c \to \infty$. On the other hand, investigation of supersymmetric gauge models reveals [5] that dynamics greatly depends on the ratio of N_c and N_f.

For QCD, it would be desirable to perform a direct comparison of the results of exact calculations in the limit $N \to \infty$ and calculations at the observed value of N for the same physical quantity. Of course, such calculations must be performed in a situation where, in both versions, the theory in question has the same dynamical structure—that is, features that are preserved there include confinement, the presence of a chiral condensate, and the presence of a multiplet of pseudoscalar bosons arising as Goldstone particles that are associated with the violation of chiral symmetry in the theory of massless quarks.

A direct comparison for the number of colors, $N = N_c$, would be of greatest interest here, but explicit calculations cannot be presently performed for this case. However, an indirect way to $N_c \to \infty$ through the limit $N_f \to \infty$ for the number of light quarks is quite feasible, and we will follow it in the present study. Let us clarify this statement.

The point is that, in the region of low energies, QCD can be formulated in terms of only a light flavor without recourse to color degrees of freedom. This occurs in so-called chiral perturbation theory (ChPT) [6, 7]. Within this approach, the limit $N_f \to \infty$ is straightforwardly implementable; it is admissible to calculate it without changing the dynamical structure inherent in actual QCD, the observable properties of this theory being preserved. This is obvious in any calculations within chiral chromodynamics and will be explicitly expounded in the present study. But from the point of view of the quark formulation of

*e-mail: dyatlov@thd.pnpi.spb.ru

1)The literature on these subjects is enormous. We will restrict ourselves to examining a few typical examples.

QCD, the possibility of preserving dynamical properties under any changes in N_f implies that N_c also changes, adjusting itself in an appropriate way. For example, the dynamics of the simplest beta function in QCD undergoes no qualitative changes if, simultaneously with going over to the limit $N_f \to \infty$, one increases N_c at a greater rate, $N_f/N_c < 11/2$.

Within chiral perturbation theory, low-energy physics is controlled by the leptonic-pion-decay constants f_π and the condensate density for one flavor, $\langle \bar{q}_R q_L \rangle$. These quantities could be considered, by definition, to be independent of N_f, if the invariability of dynamical properties in QCD upon going over to the limit $N_f \to \infty$ did not require that N_c also change. For this limit to be precisely QCD at large N_f inclusive, it is necessary to consider the dependence of parameters on N_c as well.[2)] For a given ratio $N_f/N_c = \rho$ and at large values of N_c, the parameter f_π^2 can be represented in the form

$$f_\pi^2 = N_c Q(\rho) = \frac{N_f Q(\rho)}{\rho}\,; \qquad (1)$$

that is, f_π^2 grows in direct proportion to N_c or N_f everywhere, with the exception of small vicinities of the zeros of the function $Q(\rho)$.

Formula (1) arises if, at large values of N_c and N_f, one sums only planar diagrams [1] featuring various numbers of internal irreducible quark loops (that is, loops beyond the QCD beta function). The function $Q(\rho)$ has the form of an alternating series and can have real-valued zeros. The derivation of formula (1) and its corollaries are discussed in the Appendix. The expectation value $\langle \bar{q}_R q_L \rangle$ possesses similar properties.

The asymptotic procedure considered here will be briefly referred to as the transition to the large-N_f limit. This procedure is of particular interest owing to the fact that it additionally involves large values of N_c.

In the present study, it is shown that features of actual QCD, where $N_f = 3$, differ significantly from those that are obtained by substituting $N_f = 3$ into the results of the calculations at large values of N_f. Any numerical consistency between the two results in question may only be coincidental. At large values of N_f, both versions—(i) $f_\pi^2 \sim N_f$ and (ii) f_π^2 is a constant or grows more slowly than N_f—lead to results that, upon the substitution of $N_f = 3$, will differ from those that are calculated in actual QCD, since they are determined by different parts of the same expressions and different properties.

First of all, it is necessary to choose a physical object such that an analysis of this object would make it possible to draw a comparison between the cases of $N_f \to \infty$ and $N_f = 3$. For this purpose, it is convenient to consider, within the simple model of chiral QCD (where the quark mass is $m_q = 0$), the second-order corrections in the quark masses to the vacuum energy and to the masses of particles belonging to the pseudoscalar multiplet. Because of the complexity of the problem, a complete calculation up to a final result cannot be performed even for this modest, approximate, fragment of QCD. However, we can select such physically significant quantities calculable at any value of N_f that the results of the $N_f \to \infty$ and $N_f = 3$ procedures are obviously different for them.

The fragment chosen here belongs completely to the low-energy region, where QCD is described by chiral perturbation theory, whose basic objects are [7] unitary matrices that implement a nonlinear realization of the $SU_L(3) \times SU_R(3)$ flavor group; that is,

$$U(x) = \exp\left\{ i\sqrt{2}\frac{\pi_A(x) t^A}{f_\pi} \right\}, \qquad (2)$$

where t^A is the flavor matrix, $\pi_A(x)$ are the operators of the pseudoscalar multiplet of bosons arising as Goldstone states of QCD in the limit of zero quark masses ($m_q = 0$), and f_π is the known leptonic-pion-decay constant ($f_\pi = 93.4$ MeV).

The representation of low-energy QCD in (2) is similar to the bosonized representation of two-dimensional fermion models [8, 9]. Therefore, the procedure for isolating the sought correction to the energies of states, as well as its physical properties, can be clarified by calculating the corresponding quantity in an appropriate exactly solvable two-dimensional model.

In the present study, we will restrict ourselves to a detailed analysis of the simplest problem—that of calculating corrections to the vacuum state. A more sophisticated analysis of corrections to the masses of pseudoscalar particles can also be performed, but the results of such an analysis will be similar. When required, we mention these results to confirm our conclusions.

The ensuing exposition is organized as follows. The procedure for isolating that part of m_q corrections to the energies of states in chiral QCD which receive the main contribution from long distances is outlined in Section 2. This procedure is clarified via the corresponding calculation within the two-dimensional Schwinger model [9]. We follow here the bosonization technique developed in [10]. In Sections 3 and 4, the quantity in which we are interested is reduced to a form that is convenient for calculating the limit $N_f \to \infty$, which is explored in Section 5. Mathematically, the QCD problem requires disentangling the product of two non-Abelian exponentials. In Sections 4 and 5,

[2)] It was V.Yu. Petrov who called my attention to this point.

we investigate the properties of such a procedure that are necessary for our purposes. The consequences of the formulas derived in the present study are discussed in Section 6. The derivation of formula (1) is clarified in the Appendix.

2. STRUCTURE OF THE SECOND PERTURBATIVE CORRECTION IN THE QUARK MASSES

In the QCD of massless quarks, the octet of pseudoscalar bosons is the Goldstone multiplet of $SU_L(3) \times SU_R(3)$ flavor symmetry broken by a quark condensate whose density is

$$\langle \bar{q}q \rangle = \langle \bar{q}_R q_L \rangle + \langle \bar{q}_L q_R \rangle, \tag{3}$$

where $q_{R,L}(x)$ are the operators of right- and left-handed chiral quarks.

The quark masses m_q^f lead to a direct breakdown of chiral and flavor symmetries via the mass term in the QCD Lagrangian,

$$H'(x) = \sum_f m_q^f \bar{q}^f(x) q^f(x) \tag{4}$$
$$= \sum_f m_q^f \left[\bar{q}_R^f(x) q_L^f(x) + \bar{q}_L^f(x) q_R^f(x) \right]$$
$$= h(x) + h^+(x),$$
$$f = u, d, s.$$

Nonzero masses of pseudoscalar mesons are thought to be an observable manifestation of $H'(x)$. To the first order in the interaction in (4)—that is, in the quark masses, the pseudoscalar-particle masses are given by the well-known expressions [6]

$$m_\pi^2 = -\frac{\langle \bar{q}q \rangle}{f_\pi^2}(m_u + m_d), \tag{5}$$
$$m_{K^+}^2 = -\frac{\langle \bar{q}q \rangle}{f_\pi^2}(m_s + m_u),$$
$$m_{K^0}^2 = -\frac{\langle \bar{q}q \rangle}{f_\pi^2}(m_s + m_d),$$
$$m_\eta^2 = -\frac{1}{3}\frac{\langle \bar{q}q \rangle}{f_\pi^2}(m_u + m_d + 4m_s).$$

Similar contributions arise for other states and other quantities in QCD. Such contributions are taken into account within chiral perturbation theory [7].

The standard formula for the second-order correction to the energy of the nth level is straightforwardly reduced to the relativistic form

$$\delta E_n^{(2)} = \frac{1}{2i} \int d^4x \langle n | T\{H'(x), H'(0)\} | \rangle n. \tag{6}$$

The matrix element of the time-ordered product in (6) receives contributions only from connected diagrams that are irreducible with respect to the state $|n\rangle$. For $n \neq 0$, the quantity $\delta E_n^{(2)}$ is then a correction that is reckoned from the vacuum energy, which, in turn, is also calculated to second-order terms in $H'(x)$ inclusive.

The two operator terms on the right-hand side of (4) change the helicity of a state by 1 and -1, respectively. In view of this, the product

$$H'(x)H'(0) = h(x)h(0) + h^+(x)h^+(0) \tag{7}$$
$$+ h^+(x)h(0) + h(x)h^+(0) = R_{\pm 2}(x) + R_0(x)$$

is broken down into the term $R_{\pm 2}$, which changes the helicity by ± 2, and the helicity-conserving term R_0. The matrix elements of these two terms have sharply different properties.

1. The matrix elements (6) of the nonzero-helicity operators $R_{\pm 2}(x)$ do not vanish only because of nonperturbative terms, owing to the presence of condensate (3). The contribution to this component from the correction in (6) comes predominantly from the low-momentum region—that is, the region of long distances in the integral in (6). There, QCD is represented by the effective Lagrangian of chiral theory [7] and is expressed in terms of the operator in (2), which takes into account the lightest pseudoscalar bosons. The contribution from that part of (7) is finite for $x \to 0$. The four-dimensional integral of $R_{\pm 2}(x)$ with respect to x over the region of small x is determined by the size of the region.

2. The chirality-conserving part of (7), $R_0(x)$, grows fast for low x. It is the term $R_0(x)$ that involves the perturbative component—the corresponding part of the time-ordered product at low x (in the asymptotic-freedom region) is a loop of free massless R and L quarks that involves the propagators G_R and G_L; that is,

$$\mathrm{tr}\, G_R(x) G_L(-x) = \mathrm{tr}\left(\frac{\hat{x}}{x^4} \frac{-\hat{x}}{x^4} \right) \sim O\left(\frac{1}{x^6} \right). \tag{8}$$

Therefore, the correction to the vacuum-state energy from $R_0(x)$ diverges; as for corrections to the masses of pseudoscalar particles, it can be shown that they are finite, but no reliable estimates can be obtained for them at present.

For our purposes, it is convenient to use that part of the correction which originates from $R_{\pm 2}(x)$. The part that is associated with $R_0(x)$ could not be estimated within QCD.

As is well known from chiral perturbation theory, there exists, for the matrix $M_{ff'} = \bar{q}_R^{(f)} q_L^{(f')}$ in the region of low energies, the representation that was introduced in [7] and which is based on the use of the flavor matrix (2). For $M_{ff'}$, we adopt here a somewhat

different, but equivalent form, representing (2) as a normal-ordered product; that is,

$$M_{ff'} = \bar{q}_R^f(x) q_L^{f'}(x) \tag{9}$$
$$= N\left\{\exp\left[i\sqrt{2}\frac{\pi_A(x)t^A}{f_\pi}\right]\langle\bar{q}_R q_L\rangle\right\}_{ff'},$$

where the condensate density is

$$\langle\bar{q}_R q_L\rangle = \frac{1}{2}\langle\bar{n}n\rangle = \frac{1}{2}\langle\bar{d}d\rangle = \frac{1}{2}\langle\bar{s}s\rangle \tag{10}$$

and the operators $\pi_A t^A$ are defined in terms of the matrix of physical (massless!) pseudoscalar bosons as

$$\pi_A t^A = \begin{vmatrix} \frac{\pi^0}{\sqrt{2}} + \frac{\eta_8}{\sqrt{6}} & \pi^+ & K^+ \\ \pi^- & -\frac{\pi^0}{\sqrt{2}} + \frac{\eta_8}{\sqrt{6}} & K_0 \\ K^- & \bar{K}^0 & -\frac{2\eta_8}{\sqrt{6}} \end{vmatrix}. \tag{11}$$

In (9), only the creation operators $\pi_A^+(x)$ and the annihilation operators $\pi_A^-(x)$ are disposed according to the normal-order prescription, while the matrices t^A remain disentangled.

Usually, $M_{ff'}$ is written without recourse to a normal-ordered product, but the representation in (9) is more convenient for specific calculations. With the aid of formula (11), it can straightforwardly be verified that all of the first-order results in the interaction in (4) are reproduced by (9) in a form that is identical to that which is obtained on the basis of the standard technique of chiral perturbation theory—namely, the mass formulas (5), the definition of f_π in terms of the flavor current $\bar{d}i\gamma_\mu\gamma_5 u$, and the mixing of π^0 and η [6, 7].

Our model will consist in calculating quantities in QCD with the aid of the representation in (9) with the free operators $\pi_A(x)$, but at all values of N_f (that is, at N_c as well).

The procedure for isolating two parts of the mass correction to the energy of a state will be clarified by considering the example where this correction is calculated within the massive Schwinger model.

The point is that the operator $U(x)$ of chiral perturbation theory has a form that is similar to the boson form of the operator of a massless two-dimensional fermion (see [8, 10]). From this form, we obtain, for the products $\bar{\psi}_R\psi_L$ and $\bar{\psi}_L\psi_R$ of two-dimensional operators, a representation that has the form of a normal-ordered product and which is similar to (9); that is,

$$\bar{\psi}_R(x)\psi_L(x) = N\left\{\exp\left[i\left(\sqrt{4\pi}\phi(x) + \theta\right)\right]\langle\bar{\psi}_R\psi_L\rangle\right\}, \tag{12}$$

where θ is a constant parameter (ang1e θ) peculiar to two-dimensional electrodynamics (that is, the Schwinger model [9]);

$$\phi(x) = \frac{1}{\sqrt{V}}\sum_{\mathbf{p}}\left(A(\mathbf{p})\frac{e^{ipx}}{\sqrt{2\omega_p}} + A^+(\mathbf{p})\frac{e^{-ipx}}{\sqrt{2\omega_p}}\right) \tag{13}$$

is the operator of a massive boson whose mass is

$$m^2 = g^2/\pi, \qquad \omega_p = \sqrt{m^2 + \mathbf{p}^2}; \tag{14}$$

g is the coupling constant; and $A(\mathbf{p})$ and $A^+(\mathbf{p})$ are, respectively, the boson-annihilation and the boson-creation operator. The wave functions in (13) are normalized to a finite volume V. The condensate density here is given by [10]

$$\langle\bar{\psi}_R\psi_L\rangle = me^C/(4\pi), \tag{15}$$

where C is the Euler constant. The role of the factor e^C in the Schwinger model is identical to that of the nonperturbative factor $\exp(1/g^2)$ in QCD. Since the charge is a dimensional quantity in two dimensions, this factor can only have the form $\exp\left(am^2/g^2\right)$, which features no dependence on the coupling constant [this is because $m^2 \sim g^2$ (14)].

Using (12) и (13) and dividing (6) by the volume V, we find the correction to the energy density in the QED_2 vacuum state. The result is

$$E_0^{(2)} = \frac{m_q^2}{4i}\int d^2x\left(\frac{me^C}{2\pi}\right)^2 \tag{16}$$
$$\times\left[\left(e^{-2K_0(x)} - 1\right)\cos 2\theta + \left(e^{2K_0(x)} - 1\right)\right],$$

where $K_0(x) \equiv K_0(m(-x^2 + i\varepsilon)^{1/2})$ is a Bessel function and $x^2 = t^2 - \mathbf{x}^2$. For $z \to 0$,

$$K_0(z) \to -\frac{1}{2}\ln\frac{z^2}{4} - C; \tag{17}$$

in this region, we therefore have

$$\exp 2K_0(x) \Rightarrow \frac{e^{-2C}}{2\pi^2(-x^2 + i\varepsilon)}, \tag{18}$$
$$\exp[-2K_0(x)] \Rightarrow e^{2C}(-x^2).$$

It can be seen that, for $|x| \to \infty$, the relevant integrals are well convergent and that the integration contours can be shifted to the Euclidean region. The first term in the bracketed expression on the right-hand side of (16) corresponds to the contribution of $R_{\pm 2}$. In this part of the integral, the contribution from low values of x possesses no special features and is small in relation to the contribution from the dominant region around $x \sim m^{-1}$. For the R_0 part of the integral (second term), the integrand is singular—it is proportional to x^{-2} [see (18)]—and the integral

diverges. This singularity is described by the product of two-dimensional fermion propagators belonging to the type in (8). The coefficient of the singularity does not depend on the nonperturbative factor e^C or on the parameter θ. It coincides with the contribution of the two-dimensional fermion loop.

The question of whether the singularity noticed here—that of the type in (8)—which is a direct corollary of asymptotic freedom, may be an impediment to calculating quantities in QCD [$(x^2)^{-3}$! singularity] by the methods of chiral perturbation theory (that is, by means of an expansion in powers of the quark masses) is of secondary importance for our purposes, but, to conclude this section, we will discuss it for the sake of completeness. The Schwinger model demonstrates that only in an "unobservable" correction to the vacuum state does there arise a singularity. In the hadron mass (14), the correction calculated within the model ($p^2 = m^2$) no longer involves a divergence:

$$\delta m^2 = -\frac{2\pi m_q^2}{i}\int d^2x\Big(\frac{me^C}{2\pi}\Big)^2 \qquad (19)$$
$$\times\Big\{\cos^2\frac{px}{2}\Big[e^{-2K_0(x)} - 1 + 2K_0(x)\Big]\cos 2\theta$$
$$+ 2\sin^2\frac{px}{2}\Big[e^{2K_0(x)} - 1 - 2K_0(x)\Big]\Big\}.$$

Here, $K_0(x)$ is the same function as in (16), $px = p_0x_0 - \mathbf{p}\cdot\mathbf{x}$, and $p^2 = m^2$. The singularity at low values of x is compensated by a factor that represents the hadron "wave function."

A similar situation may exist in QCD as well: a compensating factor proportional to x^2 will emerge from the cancellation of various contributions generated by the external factors of the nth state; it can then be shown that the remaining $(x^2)^{-2}$ singularity is canceled by logarithmic corrections to the quark loop.

3. CORRECTIONS TO THE ENERGY OF THE QCD VACUUM: HELICITY-CHANGING CONTRIBUTION

Let us now consider that part of the QCD correction (6) which is associated with the nonperturbative operator $R_{\pm2}(x)$ in (7). Since the region of low x does not play a significant role here, the quantity being studied can be calculated on the basis of the representation in (9), which corresponds to the properties of QCD at rather large distances ($x^2 \gtrsim f_\pi^{-2}$).

For the correction to the vacuum state, we have

$$\delta E_0^{(2)} = \frac{1}{i}\int d^4x\langle\bar q_R q_L\rangle^2 \qquad (20)$$
$$\times\langle 0|T\Big\{\mathrm{tr}\Big[N\Big(M\exp\Big(i\sqrt{2}\frac{\pi_A(x)t^A}{f_\pi}\Big)\Big)\Big]$$
$$\times\mathrm{tr}\Big[N\Big(M\exp\Big(i\sqrt{2}\frac{\pi_A(0)t^A}{f_\pi}\Big)\Big)\Big]\Big\}|0\rangle,$$

where the matrix M is given by (9) and (11). The contribution from large distances $|x^2| \gg f_\pi^{-2}$, which is the only quantity calculable at any value of N_f, is obtained in the following way. In (20), we have considered that R_{+2} and R_{-2} make identical contributions. For the vacuum time-ordered product, we obtain

$$\sum_{n,n'}\Big(\frac{i\sqrt{2}}{f_\pi}\Big)^{n+n'}\frac{1}{n!n'!}\mathrm{tr}(Mt^{i_1}t^{i_2}\dots t^{i_n}) \qquad (21)$$
$$\times\,\mathrm{tr}(Mt^{j_1}t^{j_2}\dots t^{j_{n'}})\delta_{nn'}\Delta^n(x)$$
$$\times I(i_1,i_2,\dots,i_n;j_1,j_2,\dots,j_{n'}),$$

where i_l and $j_{l'}$ number the flavor indices A in (20); the propagator of a massless Goldstone boson has the form

$$\Delta(x)\delta_{AA'} = \frac{1}{4\pi^2}\frac{1}{-x^2+i\varepsilon}\delta_{AA'} \qquad (22)$$

(of course, it is diagonal in flavor); and the operator I represents a sum over all permutations of the indices $j_1\dots j_{n'}$,

$$I_{nn'} = \sum_P \delta_{i_1j_1}\delta_{i_2j_2}\dots\delta_{i_nj_n}\delta_{nn'}. \qquad (23)$$

The series to be calculated can be reduced to the form

$$\sum_n(-1)^n\Big(\frac{2\Delta(x)}{f_\pi^2}\Big)^n\frac{1}{(n!)^2}\mathrm{tr}(Mt^{i_1}t^{i_2}\dots t^{i_n}) \qquad (24)$$
$$\times\sum_P\mathrm{tr}(Mt^{i_1}t^{i_2}\dots t^{i_n}).$$

The sum over the permutations P implies that the matrices $t^{i_1}\dots t^{i_n}$ in the second trace must be taken in all possible orders of the indices $i_1\dots i_n$. The total number of such terms is obviously equal to $n!$.

If all of these terms made identical contributions, as is the case in Abelian theories, the result would be similar to that in (16). It would involve (in Euclidean space) the exponential function

$$\exp\Big(-\frac{1}{4\pi^2f_\pi^2x^2}\Big), \qquad (25)$$

which is convergent for $x^2 \to 0$. It can easily be verified that, for the R_0 contribution, the sign in the exponent would be different, which corresponds to a nonintegrable growth. In the non-Abelian case, the sum over the flavors $i = 1, 2, \dots, N_f$ is

$$t^i_{k\ell}t^i_{mn} = \frac{1}{2}\Big(\delta_{kn}\delta_{\ell m} - \frac{1}{N_f}\delta_{k\ell}\delta_{mn}\Big). \qquad (26)$$

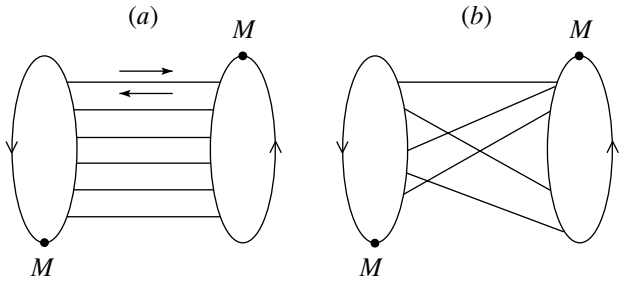

Fig. 1. Notation for terms in the sum of the products of traces in (24).

The problem consists in determining the coefficients in the series in (24) and their dependence on n and N_f. Obviously, we can consider any values of N_f.

First of all, we will show that all terms involving $(1/N_f)\delta_{k\ell}\delta_{mn}$ in (26) can be summed. As a result, the problem reduces to taking into account only the first term in this formula. The point is that terms involving $\delta_{k\ell}\delta_{mn}$ merely eliminate two matrices t from the product of the traces. In (24), we will now consider any term where the first terms from (26) are taken in the n products $t^i t^i$ and where the second terms are taken in the k products of respective matrices. The problem of performing summation over k then reduces to a combinatorial analysis:

$$\sum_k (-1)^{n+k} \left(\frac{\Delta(x)}{f_\pi^2}\right)^{n+k} \left(\frac{-1}{N_f}\right)^k \qquad (27)$$
$$\times \frac{1}{[(n+k)!]^2} \left[\frac{(n+k)!}{n!k!}\right]^2 k! = \frac{1}{(n!)^2}$$
$$\times \left(\frac{-\Delta(x)}{f_\pi^2}\right)^n \exp\frac{\Delta(x)}{N_f f_\pi^2}.$$

Thus, we obtain an exponential function that grows for $x^2 \to 0$. However, it is not hazardous, since an exact calculation of (24) with allowance for all factors must lead to convergence, as occurred in the Abelian case. We will observe this property in the following. We note that $\exp(\Delta(x)/(N_f f_\pi^2))$ begins to grow in the region $x^2 \lesssim 1/(N_f f_\pi^2)$—that is, beyond the region of applicability of chiral perturbation theory. Since the main contribution to the integral with respect to x in (20) comes from the chiral-perturbation-theory region $x^2 \gtrsim 1/f_\pi^2$, we can discard the exponential function (27).

It follows that the integrand in the correction considered here [see expression (20)] has the form

$$\sum_n \left(\frac{-\Delta(x)}{f_\pi^2}\right)^n \frac{C(n,N_f)}{(n!)^2}\{\mathrm{tr}\, M^2, (\mathrm{tr}M)^2\}. \qquad (28)$$

In (28), it is considered that any term in the total sum over permutations reduces either to $\mathrm{tr}M^2$ or to $(\mathrm{tr}M)^2$.

It should be borne in mind that, with allowance for the factor in (27), summation in the sum over n actually begins from $n = 2$, since $n = 0$ corresponds to disconnected diagrams and since the total sum in (24) does not involve $n = 1$ because of the absence of transitions from the vacuum to a pseudoscalar state. This is of importance since the $n = 0$ and $n = 1$ contributions are those that decrease most slowly for $x^2 \to \infty$. The absence of the $n = 0, 1$ contributions results in that the large-x behavior of the integral in (20) features a logarithmic divergence, which is a natural infrared singularity of chiral perturbation theory, where this singularity generates, as is well known (see [6]), terms that are not analytic in the quark masses.

4. CALCULATION OF THE COEFFICIENTS $C(n, N_f)$

We will now proceed to analyze the dependence of the coefficients $C(n, N_f)$ and of the sum in (28) on N_f, leaving aside variations in f_π^2 for the time being. Our manipulations will eventually enable us to visualize any possible version of the behavior of f_π^2.

Let us represent the traces in (24) in the form of closed ovals on which we specify points associated with the matrices M and the matrices t_i, the latter corresponding to the points at which the ovals intersect straight-line segments connecting them (see Fig. 1). It is convenient to arrange, in opposite directions, the numbering of points associated with different traces. Arrows indicate the direction of summation of indices. The term $\delta_{kn}\delta_{\ell m}$ in (26) corresponds to the transition of summation over matrix indices from one trace to another, a line that connects the ovals representing this in the figures. Such a transition proceeds on one side of the line for the indices kn and on the other side for the indices ℓm. Figure 2 shows the simplest connections: two lines forming a closed contour and lines that split two matrices M [contribution to $(\mathrm{tr}M)^2$].

Any closed contour that bypasses M yields the factor N_f. At a given value of n, the maximum possible number of contours not involving M is $n-1$ (see Fig. 1*a*). Each such contour includes only two connecting lines. There can exist closed contours containing a greater number of lines: $4, 6, \ldots$ (see Fig. 3). Therefore, the dependence of the coefficients $C(n, N_f)$ on N_f can be represented as the series

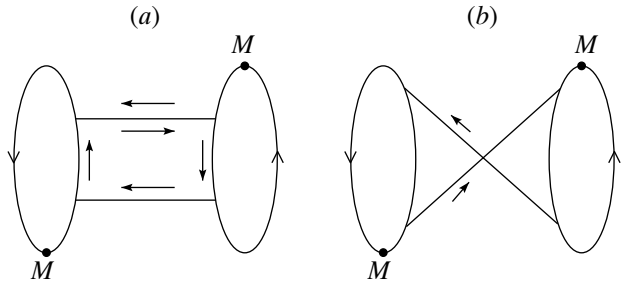

Fig. 2. Simplest contributions to the coefficients $C(n, N_f)$ of $(a)\,\mathrm{tr}M^2$ and $(b)\,(\mathrm{tr}M)^2$.

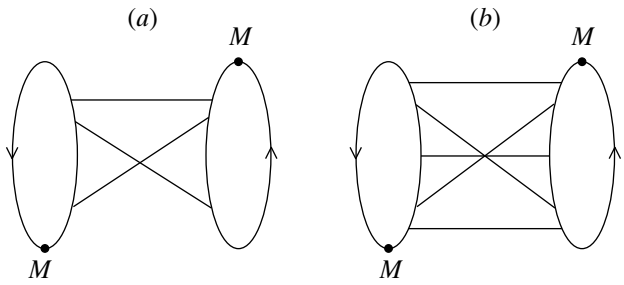

Fig. 3. Simplest diagrams determining the coefficients $c_{k'+1}(k)$.

[here, we restrict ourselves to considering the contribution to $\mathrm{tr}M^2$—the situation around the contribution to $(\mathrm{tr}M)^2$ is similar]

$$C(n,N_f) = N_f^{n-1} + a_2(n)N_f^{n-3} + \ldots + a_{2\left[\frac{n-1}{2}\right]}(n)N_f^{n-1-2\left[\frac{n-1}{2}\right]}, \quad (29)$$

where $\left[\dfrac{n-1}{2}\right]$ is the integral part of $\dfrac{n-1}{2}$. The quantity $\kappa = n-1-2\left[\dfrac{n-1}{2}\right]$ is equal to zero for odd and to unity for even n.

The coefficients $a_{2k}(n)$ are equal to the number of diagrams (formed by n connecting lines) where the power of $(N_f)^{2k}$ is less by unity than that which is the maximum possible one for diagrams involving n lines, N_f^{n-1}. Since all calculations deal exclusively with lines connecting two traces in (24), we imply only such lines in the following and omit the modifier "connecting."

The dependence on n in $a_{2k}(n)$ can be separated from the dependence on k. This can be done in the following way.

Diagrams that contain the simplest contours involving two lines will be referred to as reducible diagrams: these two lines are reduced to one line without changing the structure of the remaining trace (only N_f is lost). After such a reduction, there remain only irreducible diagrams, which may contain loops, but these loops feature a greater number of lines, $4, 6, \ldots$ (see Fig. 3*b*).[3)] We denote by $c_{k'+1}(k)$ the number of irreducible diagrams that involve $k'+1$ lines (the appearance of "1" is associated with the choice of the contribution $\mathrm{tr}M^2$) and in which $2k$ powers of N_f are lost in relation to its maximum possible power, that in $N_f^{k'}$. The number k' is obviously not less than $2k$, since the diagram in which each line leads to the loss of N_f (for example, the diagram in Fig. 3*a* and its multiple repetitions) is minimal. At the same time, there exists the greatest number of $k' = 4k$, which arises because $c_{k'+1}(k)$ contains only irreducible closed contours involving not less than four lines (more precisely, four sides of these lines). Diagrams featuring the maximum number of lines arise in the case where the addition of four lines increases the number of closed contours by the maximum number of 2 (recall that both sides of the lines are involved). The loss of N_f is then given by N_f^2. These are diagrams belonging to the type of repetitions of the diagram in Fig. 3*b* (and more complicated ones).

Therefore, we have

$$2k \le k' \le 4k. \quad (30)$$

The dependence of n is determined by the distribution of the remaining $n-(k'+1)$ lines between reducible loops that are formed by combining, in all possible ways, all lines of irreducible diagrams. There arises the series

$$a_{2k}(n) = \frac{(n-1)(n-2)\ldots(n-4k)}{(4k)!}c_{4k+1} + \frac{(n-1)(n-2)\ldots(n-4k+1)}{(4k-1)!}c_{4k} + \ldots + \frac{(n-1)(n-2)\ldots(n-2k)}{(2k)!}c_{2k+1} = \sum_{k'=2k}^{4k}\frac{\Gamma(n)}{\Gamma(n-k')}\frac{c_{k'+1}(k)}{\Gamma(k'+1)}. \quad (31)$$

It is very difficult to calculate the coefficients $c_{k'+1}(k)$, especially as all diagrams must be distributed between two possibilities, $\mathrm{tr}M^2$ versus $(\mathrm{tr}M)^2$.[4)] Let us

[3)] One can continue such an analysis in order to calculate the coefficients c_{k+1} in (31), but this is not necessary for the purposes of the present study.

[4)] In calculating similar corrections to the masses of the Goldstone pseudoscalar bosons π^A, the number of combinations of traces belonging to the $\mathrm{tr}(M\pi^A M\pi^A)$ type is as large as nine.

present the values of $c_{k'+1}$ for small k:

$$k=0:\ a_0(n)=1; \qquad (32)$$
$$k=1:\ c_5=1,\quad c_4=3,\quad c_3=3;$$
$$k=2:\ c_9=13,\quad c_8=71,\quad c_7=150,$$
$$c_6=124,\quad c_5=40.$$

At the same time, the series in (28) are well convergent—all coefficients in $C(n,N_f)$ cannot grow with n faster than the total number $n!$ of diagrams. The quantities $a_{2k}(n)$, which are associated with $\mathrm{tr}M^2$, grow much more slowly. The closer k' to $4k$, the lower the rate of growth of the coefficients $c_{k'+1}(k)$ with k' (that is, with k) in relation to the number $(k'+1)!$ of possible diagrams involving $k'+1$ lines, those of them that grow at the greatest rate satisfying the condition $c_{2k+1}\lesssim(2k+1)!$. In order to calculate the sum in (28) at large N_f, it is necessary to know, as we will see below, the values of the quantities $a_{2k}(n)$ at large n and $k\ll n$.

5. COMPARISON OF SMALL AND LARGE N_f

Formulas (21)–(31) provide an exact expression for the integrand in the correction specified by (20) and studied here. Two large parameters, $|N_f\Delta(x)/f_\pi^2|\gg1$ and $|\Delta(x)/f_\pi^2|\gg1$, are possible for constant or slowly growing f_π^2 in the sum in (28). The first is large not only for $N_f\to\infty$ but also, together with the second, for $x^2\to0$ as well. The common type of behavior of this parameter at large N_f and small x is an impediment to drawing pure distinctions for different values of N_f. It is necessary to perform summation and integration over all values of x with exact QCD expressions, but this is impossible. Moreover, the region $|\Delta(x)/f_\pi^2|\gg1$ is beyond the boundaries of applicability of chiral perturbation theory and has no bearing on QCD in calculations on the basis of chiral perturbation theory.

However, this region cannot be of great importance. The point is that the series in (28) are well convergent at large n for any N_f, since the coefficients $a_{2k}(n)$ in (29) grow more slowly than $n!$. To demonstrate this, we note that, at a given value of n, the total number of permutations in (24) (the number of diagrams belonging to the type in Fig. 1) is $n!$. Therefore, the number of diagrams contributing to $\mathrm{tr}M^2$ or to $(\mathrm{tr}M)^2$ is

$$\sum_{k=0}^{\left[\frac{n-1}{2}\right]}a_{2k}(n)<n!. \qquad (33)$$

Owing to the fact that the series in (28) are alternating, there arises, in either case, a function that is integrable for $x^2\to0$. (This is precisely the circumstance that was taken into consideration in choosing the helicity-changing correction as an object of analysis.) In view of this, the contribution to the integral in (20) from the region of small x^2—that is, from the region $|\Delta(x)/f_\pi^2|>1$—is rather modest.

This means that, for our purposes, an examination of the main region of chiral perturbation theory, $|\Delta(x)/f_\pi^2|\lesssim1$, is quite sufficient, which simplifies and clarifies a comparison at different values of N_f. The parameter $|N_f\Delta(x)/f_\pi^2|\gg1$ will be the only possible large parameter of the scheme. After that, it will not be difficult to trace the version of linear growth, $f_\pi^2\sim N_f$.

At small values of N_f, it is possible to recast (28) into the form of a series in powers of N_f, this series beginning from the last terms in the series in (29) for $C(n,N_f)$. The higher the power of N_f, the smaller the coefficient of the corresponding term, since it originates from terms corresponding to large n and contains the large factors $[\Gamma(n+1)]^2$ in the denominators. At the same time, the series in n for specific powers of N_f are well convergent and can be summed. At actual values of N_f, we will thereby obtain a series in powers of N_f, and it is sufficient to retain, in actual practice, only a few first terms in this series.

Let us compare it with the calculation for $N_f\gg1$ under the same conditions. For this purpose, we rewrite expression (28) by changing the variable of summation as

$$N=n-2k \qquad (34)$$

in order to collect all terms at powers of N_f. For the part associated with $\mathrm{tr}M^2$, we have

$$\frac{1}{N_f}\sum_{N,k}\left(\frac{-\Delta(x)N_f}{f_\pi^2}\right)^N\frac{1}{[\Gamma(N+2k+1)]^2} \qquad (35)$$
$$\times\left(\frac{\Delta(x)}{f_\pi^2}\right)^{2k}\sum_{k'=2k}^{4k}\frac{\Gamma(N+2k)}{\Gamma(N+2k-k')}\frac{c_{k'+1}(k)}{\Gamma(k'+1)}.$$

Here, $n>2k+1$; therefore, we have $N\geq1$.

At large N_f, large N are operative, the sums over k being convergent for any power of N^{-1} even upon the expansion in terms of N. Using (31), we do indeed find, upon the expansion in N, that

$$\frac{1}{N_f}\sum_{N}\left(\frac{-\Delta(x)N_f}{f_\pi^2}\right)^N\frac{1}{N^{2N}} \qquad (36)$$

$$\times \sum_k \left[\frac{c_{4k+1}}{\Gamma(4k+1)} + \frac{1}{N}\frac{c_{4k}}{\Gamma(4k)} + \ldots \right.$$
$$\left. + \frac{1}{N^{2k}}\frac{c_{2k+1}}{\Gamma(2k+1)} \right] \left(\frac{\Delta(x)}{f_\pi^2}\right)^{2k}.$$

It should be recalled that the coefficient $c_{k'+1}(k)$, for example, is the number of irreducible diagrams where $k'-2k$ closed loops involving four or more lines are formed from $k'+1$ lines ($k' \le 4k$). With increasing k' (and k), the coefficients in question grow more slowly than the number of diagrams from $k'+1$ lines—that is, than $(k'+1)!$. Taking into account only the factorial factors (this means that we discard exponential factors), which are the most important for convergence, we obtain the following relationships at large k.

The coefficient corresponding to the smallest number $(2k+1)$ (at given k) of lines is restricted only by the number of permutations of these lines, ($c_{2k+1} < (2k+1)!$)—that is, by the maximum possible value. For $2k < k' < 4k$, the coefficients $c_{k'+1}$ grow in accordance with the interpolation formula $c_{k'+1} \sim (4k-k'+1)!(k'-2k)!$. The coefficient corresponding to the maximum number $(4k+1)$ of lines is subjected to the most stringent constraint with respect to the number of permutations, $c_{4k+1} \lesssim (2k)!$.

We further outline the proof of the last statement, which is of greatest importance for our analysis.

In terms of the diagrams introduced in Section 4, the change in the number c_{4k+1} in response to the shift $k \to k+1$ proceeds in the following two ways:

(i) Each of the $4k+1$ lines is replaced by the set of lines in Fig. 3*b* (four lines and two closed irreducible loops are added). Thus, the number of diagrams is a linear function of k, while the total number of diagrams grows in proportion to $(4k+1)[4(k-1)+1]\ldots \sim k!$. This is not, however, the main way.

(ii) Each intersecting pair of lines is replaced by two intersecting plates whose end faces are again connected by lines. There are three types of such connections. The number of lines again increases by four, and there additionally arise two loops, as this must occur for the inclusion in c_{4k+1} to be implemented. The number of intersections grows in proportion to the square of the number of lines—that is, in proportion to $(4k+1)2k$. But not all of the lines intersect in all c_{4k+1} diagrams; therefore, the actual growth is slower by a numerical factor. To a factorial precision, the total number of diagrams grows in proportion to $(k!)^2 \lesssim (2k)!$.

At any fixed exponent in N^{-m}, the series in k that involve the coefficients $c_{4k-m+1}/\Gamma(4k-m+1)$ converge. In the sum over k in (36), we therefore arrive at an asymptotic series in powers of N^{-1}, the contribution to (36) from the first term in this series being

$$\frac{1}{N_f}\sum_N \left(\frac{-\Delta(x)N_f}{f_\pi^2}\right)^N \times \frac{1}{N^{2N}}\sum_k \frac{c_{4k+1}}{\Gamma(4k+1)}\left(\frac{\Delta(x)}{f_\pi^2}\right)^{2k}. \quad (37)$$

The quantity in (37) can be represented as the product of the asymptotic expression for the Bessel function $J_0\left(2\sqrt{\Delta(x)N_f/f_\pi^2}\right)$ and some special function $K(z)$ depending on the argument $z = \Delta(x)/f_\pi^2$ and having good properties in the region $z \lesssim 1$. At $z=0$, we have $K(0)=1$. The values of N that are of importance in the sum over n are

$$N \sim \sqrt{\frac{\Delta(x)N_f}{f_\pi^2}}. \quad (38)$$

They are great for $N_f \to \infty$ and constant or slowly growing f_π. The contributions from the sequence of terms in the bracketed expression on the right-hand side of (36) decrease in proportion to powers of N_f; that is, we have an asymptotic series in N_f^{-1}.

A direct substitution of (37) into the four-dimensional integral with respect to x in (20) would lead to a divergence at large x, but the quantity $|\Delta(x)N_f/f_\pi^2|$ will become less than unity in this region, so that expression (37) is inapplicable there. As was mentioned above, it is necessary to take into account, in this region, the subtraction of the first two terms in the series over n, whereupon there remains only a logarithmic infrared singularity, which is typically observed in chiral perturbation theory [6].

In the region of its applicability, formula (37) solves the problem being considered. Obviously, expression (37) has no bearing on the first terms of the series in (28), which reproduce the physical situation.

Let us now consider linearly growing $f_\pi^2 \sim N_f$. The region of N values as large as those in (38) then disappears. Over the entire region of applicability of chiral perturbation theory, the quantity $|\Delta(x)N_f/f_\pi^2|$ is less than or on the order of unity. The situation becomes similar to that which was described at the beginning of this section for small values of N_f: only a few first terms in the fast convergent series (28) are operative at small values of the arguments. For the coefficient of $\mathrm{tr}M^2$, these are (we recall that $n \ge 2$ for the vacuum contribution)

$$\left(\frac{\Delta(x)}{f_\pi^2}\right)^2 \frac{N_f}{(2!)^2} - \left(\frac{\Delta(x)}{f_\pi^2}\right)^3 \frac{N_f^2+3}{(3!)^2} \quad (39)$$

$$+\left(\frac{\Delta(x)}{f_\pi^2}\right)^4 \frac{N_f^3+12N_f}{(4!)^2}+\ldots,$$

where $(\Delta(x)N_f/f_\pi^2)\sim 1$ for $N_f\to\infty$ and where only lower order quantities in powers of N_f in the numerators of the terms in the series in (39) are disregarded in the asymptotic calculations. If the coefficients decrease fast, the role of these lower order quantities is insignificant [the sum of all coefficients of all powers of N_f in the nth term of the series and in all combinations involving $\mathrm{tr}M^2$ and $(trM)^2$ is $n!$]. If, in addition, we assume that, upon the substitution of N_f and $N_c=3$, the asymptotic value of f_π from planar diagrams becomes equal to the physical value, the expressions obtained by calculating (39) for $N_f=3$ and $N_f\to\infty$ will be close to each other.

However, even this proximity is purely coincidental. Under the same conditions, we will calculate the contribution to the mass of the pseudoscalar Goldstone boson. It can be proven that the contributions from $R_{\pm 2}$ (7) to the square of the mass and to the coefficients of the factors $\mathrm{tr}(M\phi_\pi M\phi_\pi)$, $\mathrm{tr}(M\phi_\pi\phi_\pi M)$, $(\mathrm{tr}M\phi_\pi)^2,\ldots$ can be represented as the series in (28) with different $C(n,N_f)$ (here, ϕ_π are matrices corresponding to the multiplet particles). The sum of all coefficients of all powers of N_f and of the combinations $\mathrm{tr}(M\phi_\pi M\phi_\pi)\ldots$ now grows in proportion to $(n+1)^2n!$. As before, the series converges fast; for a pseudoscalar boson, it begins at $n=3$ since there are no $\pi\to 2\pi$ transitions. We have [for $\mathrm{tr}(M\phi_\pi M\phi_\pi)$]

$$-\left(\frac{\Delta(x)}{f_\pi^2}\right)^3 \frac{2N_f^2+20}{(3!)^2}+\left(\frac{\Delta(x)}{f_\pi^2}\right)^4 \frac{2N_f^3+70N_f}{(4!)^2} \tag{40}$$

$$-\left(\frac{\Delta(x)}{f_\pi^2}\right)^5 \frac{2N_f^4+162N_f^2+560}{(5!)^2}+\ldots.$$

Even in the first term, the factor 20 exceeds (at $N_f=3$) the contribution that is reproduced in calculating the asymptotic behavior in N_f by 100%. From the coefficients of the series, it can be seen how fast the number of nonplanar contributions belonging to the type in Fig. 1*b* grows in relation to planar contributions, which are taken into account in the asymptotic regime. In calculating higher order terms of the expansion in N_f^{-2}, it is therefore necessary to include ever farther terms of the series, and the result at $N_f=3$ in each order in N_f will again be inaccurate by 100%.

6. CONCLUSION

At large values of N_f, the result in (37) arises only from terms in the series in (28) that correspond to large n. At small N_f, these terms are virtually immaterial since the main contribution comes from the first terms of the series in n. At large N_f, the contribution from expression (37) is small since, for $N_f\to\infty$, the quantity in (37) decreases in proportion to $N_f^{-(1+1/4)}$. However, its continuation to actual values of N_f would considerably affect the result obtained there. It should be emphasized once again that formula (37) and expressions that correspond to small values of N_f emerge from different fragments on the series in n. In the two case in question, that of small N_f and that of $N_f\to\infty$, terms from the opposite ends of the series in (29) for $C(n,N_f)$ are used in the calculations.

If, at large N_f, we have $f_\pi^2\to N_fQ(\rho)/\rho$ [at $\rho=N_f/N_c=\mathrm{const}$], the situation undergoes virtually no changes. First, it would be natural to assume that, in the low-energy series for f_π^2 and $\langle\bar q_Rq_L\rangle$, the parameters that are determined from an asymptotic calculation, but which are taken at $N_f=N_c=3$, will be different from physical QCD values. Second, it can be conjectured that, even if this is not so, the emergence of close results from calculations at small N_f and $N_f\to\infty$ is accidental.

Under such conditions, it would be inadequate to estimate the result of actual QCD on the basis of the asymptotic behavior for $N_f\to\infty$.

ACKNOWLEDGMENTS

I am grateful to V.Yu. Petrov for stimulating discussions and enlightening comments.

It is a great pleasure for me to congratulate heartily K.A. Ter-Martirosyan on the occasion of his birthday and to acknowledge gratefully the great role that he has played in my scientific activities.

This work was supported by the Russian Foundation for Basic Research (project no. 01-02-17126).

APPENDIX

The derivation of formula (1) is based on the following properties of QCD at large N_c:

1. At large N_c, it is necessary to sum only the contributions of planar diagrams [1], but, owing to the fact that N_f takes simultaneously large values, one must include all possible quark loops. The invariant charge is in inverse proportion to N_c {for the one-loop contribution to the beta function, we have $\alpha_s\sim[N_c(11-2\rho)]^{-1}$}. Diagrams that determine f_π (diagrams for $\langle\pi|J_\mu^{(5)}(0)|0\rangle$) are then proportional to N_c or $N_f=\rho N_c$.

2. The dependence on ρ in the function $Q(\rho)$ stems from two sources. First, there is a dependence

through the invariant charge—that is, the dependence that emerges from quark loops within gluon propagators (we refer to such loops as reducible loops). Second, there are contributions from diagrams involving irreducible quark loops. Each loop yields a minus sign and the factor $N_f = \rho N_c$. The series in the loop contributions is alternating. In view of this, the occurrence of real-valued zeros is highly probable for the function $Q(\rho)$. Of course, QCD dynamics must be retained—that is, the possible values of ρ are constrained ($\rho < 11/2$ for the one-loop beta function).

3. The wave function $\langle\pi|$ of the hadron entering into the diagrams for f_π introduces the factor $N_c^{-1/2}$.

4. It is assumed that these diagrammatic statements can be extended to the nonperturbative regions of QCD as well.

We also note that the quantity $N_f Q(\rho)$ emerges exclusively from planar diagrams, whence it follows that, at $N_f = 3$ and $\rho = 1$, it must not generally coincide with the physical constant f_π^2, which receives contributions not only from planar but also from nonplanar diagrams, the number of the latter being, in each order, greater than the number of the former by a factorial factor. The quark-condensate density must also change. All this may also affect the numerical values of the calculated quantities.

REFERENCES

1. G. 't Hooft, Nucl. Phys. B **72**, 461 (1974).
2. E. Witten, Nucl. Phys. B **149**, 285 (1979); D. I. Diakonov, V. Yu. Petrov, and P. V. Pobylitsa, Nucl. Phys. B **306**, 809 (1988).
3. J. A. Gracey, Nucl. Instrum. Methods Phys. Res. A **389**, 361 (1997); hep-ph/9509276.
4. L. N. Lipatov, Zh. Éksp. Teor. Fiz. **90**, 536 (1986) [Sov. Phys. JETP **63**, 904 (1986)].
5. K. A. Intriligator and N. Seiberg, Nucl. Phys. B **431**, 551 (1994); N. Seiberg, Nucl. Phys. B **435**, 129 (1995).
6. J. Gasser and H. Leutwyler, Phys. Rep. **87**, 79 (1982).
7. G. Colangelo and G. Isidory, hep-ph/0101264.
8. S. Coleman, Phys. Rev. D **11**, 2088 (1975).
9. J. Schwinger, Phys. Rev. **128**, 2425 (1962); J. Kogut and L. Susskind, Phys. Rev. D **11**, 3594 (1975).
10. G. S. Danilov, I. T. Dyatlov, and V. Yu. Petrov, Zh. Éksp. Teor. Fiz. **79**, 2017 (1980); Phys. Lett. B **99B**, 240 (1981).

Translated by A. Isaakyan

Physics of Atomic Nuclei, Vol. 66, No. 11, 2003, pp. 2062–2069. From Yadernaya Fizika, Vol. 66, No. 11, 2003, pp. 2111–2118.

ELEMENTARY PARTICLES AND FIELDS
Theory

Ghost–Matter Mixing and Feigenbaum Universality in String Theory*

I. Kogan†[1),2)] and D. Polyakov[3)]**

Received February 3, 2003

Abstract—Branelike vertex operators, defining backgrounds with ghost–matter mixing in Neveu–Schwarz–Ramond superstring theory, play an important role in a world-sheet formulation of D branes and M theory, being creation operators for extended objects in the second quantized formalism. We show that the dilaton beta function in ghost–matter mixing backgrounds becomes stochastic. The renormalization group (RG) equations in ghost–matter mixing backgrounds lead to non-Markovian Fokker–Planck equations whose solutions describe superstrings in curved spacetimes with branelike metrics. We show that the Feigenbaum universality constant $\delta = 4.669\ldots$, describing transitions from order to chaos in a huge variety of dynamical systems, appears analytically in these RG equations. We find that the appearance of this constant is related to the scaling of relative spacetime curvatures at fixed points of the RG flow. In this picture, the fixed points correspond to the period doubling of Feigenbaum iterational schemes.

1. INTRODUCTION

Superstring theory is our current hope to put gravity in a Prokrust bed of quantum mechanics. In spite of all the spectacular progress in the last quarter of the century [1], the full structure and underlying symmetries of the theory have yet to be unveiled. One of the most striking features of string theory is a deep relation between renormalization group (RG) flows on a world sheet and an evolution in a target space. Critical points of these RG flows, described by 2D conformal field theories (CFT), determine equations of motion in a target space. The structure of these equations is determined by the world-sheet correlation functions of the appropriate vertex operators in respective CFT [2]. Thus, in the standard string perturbation theory, the beta-function equations describe the behavior of small fluctuations around flat backgrounds. The CFT description of strings in curved backgrounds, such as of strings in the presence of branes, as well as the underlying CFT of strongly coupled strings, is much harder a problem to tackle, in particular, because adequate knowledge of quantum degrees of freedom of M theory and nonperturbative strings is still lacking. Some time ago, we proposed the formalism [3–6] that describes the nonperturbative dynamics of solitons in string and M theory in terms of a special class of vertex operators, called branelike states. The crucial distinction of these vertex operators from a usual one (such as a photon or a graviton) is that they exist at nonzero ghost pictures only. The simplest example of these vertices in the closed-string case is given by

$$V_5^{(-3)}(q) = \int d^2z e^{-3\phi-\bar{\phi}}\psi_{t_1}\ldots\psi_{t_5}\bar{\psi}_{t_6}e^{iq_aX_a}(z,\bar{z}), \tag{1}$$

$$V_5^{(-2)}(q) = \int d^2z c\partial\chi e^{\chi-3\phi-\bar{\phi}}\psi_{t_1}\ldots\psi_{t_5}\bar{\psi}_{t_6} \times e^{iq_aX_a}(z,\bar{z}),$$

$$V_5^{(+1)}(q) = \int d^2z e^{\phi-\bar{\phi}}\psi_{t_1}\ldots\psi_{t_5}\bar{\psi}_{t_6}e^{iq_aX_a}(z,\bar{z}) + b-c\text{ ghosts};$$

$$a = 0,\ldots,3, \qquad t_i = 4,\ldots,9.$$

It is important that the BRST nontriviality and invariance conditions on this vertex confine its propagation to the four-dimensional subspace (labeled by the a index), transverse to its polarization defined by six t_i indices. This six-form vertex exists only at pictures below -2 or above $+1$, while there is no version of this operator at pictures 0 and -1.

This means that the discrete picture-changing gauge symmetry is broken for such operators and their superconformal ghost dependence cannot be removed by any picture-changing transformation. We shall refer to this property of the branelike vertices as ghost–matter mixing. The crucial property of these

*This article was submitted by the authors in English.
†Deceased.
[1)]Theoretical Physics, Department of Physics, Oxford University, UK.
[2)]ITEP, Moscow, Russia.
[3)]Department of Physical Sciences, University of Helsinki and Helsinki Institute of Physics, Helsinki, Finland.
**e-mail: Dimitri.Polyakov@helsinki.fi

special vertex operators is that they do not correspond to any perturbative string excitation but describe the nonperturbative dynamics of extended solitonic objects, such as D branes. It appears that the nonperturbative character of these vertices is closely related to their ghost–matter mixing properties on the world sheet, with the latter encoding crucial information about the brane dynamics. In [6], we have shown that the low-energy effective action of the sigma model with branelike states is given by the Dirac–Born–Infeld (DBI) action for D branes. From the world-sheet point of view, this means that the insertion of vertices with the ghost–matter mixing makes the deform CFT describing strings in flat spacetime and it flows to a new fixed point, corresponding to the CFT of strings in a curved background induced by D branes. In this paper, we shall further investigate RG flows in the ghost–matter mixing backgrounds. It appears that properties of these RG flows are stunningly different from the usual ones. We found that ghost–matter mixing adds to RG flow operator-valued stochastic terms. Even more intriguing is the emergence of a universal constant in the RG equations which with accuracy less than 0.5% is nothing but the logarithm of the famous Feigenbaum constant $\delta = 4.669$ [7]. This coincidence is not accidental but reflects remarkable and new relations between superstrings, chaos, gravity, and stochastic processes, which is the subject of this paper.

2. DILATON BETA FUNCTION IN GHOST–MATTER MIXING BACKGROUNDS

A crucial property of world sheet conformal beta functions (e.g., of a dilaton) in ghost–matter mixing backgrounds is the presence of stochastic terms in the RG equations. In usual perturbative backgrounds (e.g., of a graviton or an axion), such terms are absent and the beta-function equations are deterministic. Things, however, become different in backgrounds with ghost–matter mixing. One specific property of the branelike states, distinguishing them from usual perturbative vertex operators, is that their OPE algebra is picture-dependent. Below, we will show that this picture dependence leads to nondeterministic stochastic terms in the dilaton beta function. The stochasticity of the renormalization group, in turn, will be shown to be closely related to the nonperturbative nature of the branelike states and their relevance to the nonperturbative description of branes and strings in curved backgrounds. Let us start with the Neveu–Schwarz–Ramond (NSR) sigma model in $D = 10$ perturbed by the dilaton and the ghost–matter mixing vertex (1). The generating functional for this model is given by

$$Z(\varphi,\lambda) = \int DXD\psi D[\text{ghosts}] : f(\Gamma) :: f(\bar{\Gamma}) : \tag{2}$$
$$\times \exp\left\{-S_{\text{NSR}} + \int d^4q\lambda(q)\int d^2z V_5^{(-3)}(z,\bar{z};q) + \int d^{10}p\varphi(p)\int d^2w V_\varphi^{(-2)}(w,\bar{w};p)\right\}.$$

Here, $V_5^{(-3)}$ is the ghost–matter mixing vertex (1), creating the $D3$-brane background; $V_\varphi^{(-2)}$ is the dilaton vertex operator taken at the ghost picture -2;

$$: f(\Gamma) : = : \frac{1}{1-\Gamma} : = 1 + : \Gamma : + : \Gamma^2 : + \ \ldots$$

is the measure function of picture-changing operator; $: \Gamma : = : e^{\phi} G :$ with $G = G_m + G_{\text{gh}}$ being the full matter plus ghost world-sheet supercurrent. This measure function is necessary to insure the correct ghost number balance in the correlation function; $: f(\bar{\Gamma}) :$ is defined similarly. In the perturbative case, the $: f(\Gamma) f(\bar{\Gamma}) :$ insertion simply insures that all the operator product expansions (OPE) of the vertex operators are equivalent at all the picture levels and all the structure correlation functions are picture-independent. The dilaton vertex operator can be taken at any negative picture. The negative value of the dilaton picture, along with the $: f(\Gamma) :$ in the measure, insures the correct overall ghost number in correlation functions involving the dilaton (which must be equal to -2 on the sphere); this vertex operator is picture-independent (meaning the picture independence of its matrix elements with other states) and the results of the dilaton beta function are independent of the V_φ picture as well. It is convenient to take V_φ at picture -2 (both left and right), as in this case the dilaton vertex operator is given by

$$V_\varphi(p) = \int d^2z e^{-2\phi-2\bar{\phi}}\partial X^m \times \partial X_n(\eta_{mn} - k_m\bar{k}_n - k_n\bar{k}_m).$$

In the absence of ghost–matter mixing, the functions $: f(\Gamma) :$ and $: f(\bar{\Gamma}) :$ simply insure that the beta-function equations for any closed-string spacetime fields are identical for any picture representation of corresponding closed-string vertex operators. In order to compute the dilaton beta function in the presence of the V_5 operator, one has to expand this generating functional in φ and λ. In the absence of ghost–matter mixing, the dilaton (or any other closed-string field's) beta function in any background is simply given by the appropriate three-point correlators, or

the structure constants. In the ghost–matter mixing case, however, the situation is different, since the structure constants are picture-dependent and, therefore, expressing the beta function in terms of three-point correlation functions is not well defined. Therefore, to determine the beta function, one has to point out the UV logarithmic divergences due to the OPE singularities (generally speaking, picture dependent) and to sum over all the pictures.

Expanding the generating functional (2) up to the third order of λ and the second order of φ, we obtain

$$Z(\varphi,\lambda)=\int DXD\psi D[\text{ghosts}]:f(\Gamma)::f(\bar\Gamma): \tag{3}$$
$$\times e^{-S_{\rm NSR}}\Big\{1+\int d^{10}p\varphi(p)\int d^2zV_\varphi^{(-2)}(z,\bar z;p)$$
$$+\int d^4q\lambda(q)\int d^2wV_5^{(-3)}(w,\bar w;q)$$
$$+\int d^{10}p\int d^4q\lambda(q)\varphi(p)\int d^2z\int d^2w$$
$$\times V_\varphi^{(-2)}(z,\bar z;p)V_5^{(-3)}(w,\bar w;q)$$
$$+\frac{1}{2}\int d^4q_1\lambda(q_1)\int d^4q_2\lambda(q_2)\int d^2w_1\int d^2w_2$$
$$\times V_5^{(-3)}(w_1,\bar w_1;q_1)V_5^{(-3)}(w_2,\bar w_2;q_2)$$
$$+\frac{1}{2}\int d^{10}p_1\varphi(p_1)\int d^{10}p_2\varphi(p_2)\int d^2z_1\int d^2z_2$$
$$\times V_\varphi^{(-2)}(z_1,\bar z_1;p_1)V_\varphi^{(-2)}(z_2,\bar z_2;p_2)$$
$$+\frac{1}{6}\int d^4q_1\int d^4q_2\int d^4q_3\lambda(q_1)\lambda(q_2)\lambda(q_3)$$
$$\times\int d^2w_1\int d^2w_2\int d^2w_3V_5^{(-3)}(w_1,\bar w_1;q_1)$$
$$\times V_5^{(-3)}(w_2,\bar w_2;q_2)V_5^{(-3)}(w_3,\bar w_3;q_3)+\dots\Big\},$$

where we dropped the higher order terms, as well as those irrelevant to our discussion (such as those of the order of $\lambda^2\varphi$ or $\varphi^2\lambda$). To determine the UV divergences in the partition function (2), (3), relevant to the dilaton beta function, one has to point out the relevant singular terms in the OPE algebra of the dilaton and V_5. In the on-shell limit, the relevant terms in the operator algebra are given by

$$V_5^{(-3)}(w_1,\bar w_1;q_1)V_5^{(-3)}(w_2,\bar w_2;q_2) \tag{4}$$
$$\sim\frac{C_{[-3|-3]}(q_1,q_2)V_\varphi^{(-6)}(q_1+q_2)}{|w_1-w_2|^2}+\dots,$$
$$V_5^{(-3)}(w_1,\bar w_1;q_1)V_5^{(+1)}(w_2,\bar w_2;q_2)$$
$$\sim\frac{C_{[-3|1]}(q_1,q_2)V_\varphi^{(-2)}(q_1+q_2)}{|w_1-w_2|^2}+\dots,$$
$$V_5^{(+1)}(w_1,\bar w_1;q_1)V_5^{(+1)}(w_2,\bar w_2;q_2)$$
$$\sim\frac{C_{[1|1]}(q_1,q_2)V_\varphi^{(+2)}(q_1+q_2)}{|w_1-w_2|^2}+\dots,$$

where

$$C_{[-3|-3]}(q_1,q_2)\sim(q_1q_2)(1+(q_1+q_2)^2), \tag{5}$$
$$C_{[-3|1]}(q_1,q_2)\sim(q_1q_2),$$
$$C_{[1|1]}(q_1,q_2)\sim(q_1q_2)(1-(q_1+q_2)^2).$$

Next, one has to point out the picture-changing rules for the left (holomorphic) part of the V_5 operator, in order to specify how it is acted on by $:f(\Gamma):$. The antiholomorphic part and its interaction with $:f(\bar\Gamma):$ do not interest us since it is the photon-like part existing at all pictures and all its picture changings are trivial. The picture-changing transformation rules for the V_5 operators (1) can be written in the form

$$:\Gamma:^n V_5^{(k)}(p)=\alpha_{[k|n+k]}V_5^{(N+k)}(p), \tag{6}$$
$$\alpha_{[i|j]}=\alpha_{[m|n]}=\alpha_{[s|t]}=1,$$
$$\alpha_{[a|j]}=\alpha_{[a|b]}=\alpha_{[s|a]}=0,$$
$$\alpha_{[i|m]}=\alpha_{[s|m]}=1+p^2;$$
$$s,t=-\infty,\dots,-4;\qquad i,j=-3,-2;$$
$$a,b=-1,0;\qquad m,n=1,2,\dots.$$

In the beta-function calculations, when the vertex operators are taken just slightly off-shell, the following identities are useful:

$$\alpha_{[i|m]}C_{[m|n]}=C_{[i|n]};\quad \alpha_{[i|m]}C_{[m|j]}=C_{[i|j]}. \tag{7}$$

Finally, using the fact that picture-changing operators form the polynomial ring

$$:\Gamma:^{m+n}=:\Gamma^m\Gamma^n:+[Q_{\rm BRST},\dots], \tag{8}$$

the action of the $:\Gamma^n:$ operator on the vertex operators inside the functional integral can be expressed as

$$\langle:\Gamma^n:(w)V_1(z_1)\dots V_N(z_N)\rangle=\sum_{k_1,\dots,k_{N-1}=0}^{k_1+\dots+k_{N-1}=n}N^{-n}\frac{n!}{k_1!\dots k_{N-1}!(n-k_1-\dots-k_{N-1})!} \tag{9}$$

$$\times \langle : \Gamma :^{k_1} V_1(z_1) \ldots : \Gamma :^{k_{N-1}} V_{N-1}(z_{N-1}) : \Gamma :^{n-k_1-\ldots-k_N} V_N(z_N)\rangle;$$

i.e., the correlator does not depend on w. The factor N^{-n} in (9) ensures the correct normalization of amplitudes in the picture-independent case. Using relations (6)–(9), we are finally in the position to start evaluating the beta function. The first contribution of interest to the beta function comes from the λ^2 term, bilinear in the V_5 operator. At any given picture level n, this term leads to the following divergence in the order of λ^2:

$$\frac{1}{2}\int d^2w_1 \int d^2w_2 \langle : \Gamma^{n+6} : V_5^{(-3)}(w_1,\bar{w_1}) \quad (10)$$
$$\times V_5^{(-3)}(w_2,\bar{w_2})\ldots\rangle = \log\Lambda \cdot 2^{-n-7}$$
$$\times \sum_{k=0}^{n+6} \frac{(n+6)!}{k!(n+6-k)!}\alpha_{[-3|k-3]}C_{[k-3|n+3-k]}$$
$$\times \alpha_{[-3|n+3-k]}\int d^2\xi \langle V_\varphi^{(n)}(\xi,\bar{\xi})\ldots\rangle,$$

where we introduced the coordinate change $\xi = 1/2(w_1+w_2), \eta = 1/2(w_1-w_2)$ and $\log\Lambda = \int_\Lambda d^2\eta/|\eta|^2$ is the log of the world-sheet UV cutoff, appearing as a result of the integration over η (note that the vertex operators on the right-hand side of the operator product (10) are η-independent). For the sake of brevity, we suppress the momentum dependence of fields, vertices, and structure constants here and below. This divergence is removed by renormalizing the dilaton field as

$$\varphi \to \varphi - \sum_{n=0}^{\infty} 2^{-n-7} \sum_{k=0}^{n+6} \frac{(n+6)!}{k!(n+6-k)!}\alpha_{[-3|k-3]} \quad (11)$$
$$\times C_{[k-3|n+3-k]}\alpha_{[-3|n+3-k]}\lambda^2\log\Lambda.$$

In the absence of picture dependence, the sum over k would have been reduced to $(1/2)C\lambda^2\log\Lambda$ for each picture, as it should be in the standard case when ghost–matter mixing is absent (where C are the structure constants with the picture indices suppressed).

As a result of the dilaton RG flow, the $\lambda\varphi$ cross-term is renormalized by λ^3 logarithmic divergence as

$$\lambda\varphi\int d^2w_1\int d^2w_2 \quad (12)$$
$$\times \langle : f(\Gamma) : V_5^{(-3)}V_\varphi^{(-2)}\ldots\rangle\lambda^3\log\Lambda\sum_{n=0}^{\infty}2^{-2n-12}$$
$$\times \sum_{k,l=0}^{k+l=n+5}\frac{(n+5)!(n+6)!}{k!l!(n+5-l)!(n+6-k)!}\alpha_{[-3|n+2-l]}$$
$$\times \alpha_{[-3|k-3]}\alpha_{[-3|n+3-k]}C_{[k-3|n+3-k]}\int d^2w_1$$
$$\times \int d^2w_2\langle V_\varphi^{(-6)}(w_1,\bar{w_1})V_5^{(n+6)}(w_2,\bar{w_2})\ldots\rangle,$$

where in our derivation we used the invariance of V_φ and transformation properties (6) of V_5 under the picture changing. In the absence of ghost–matter mixing when one always has $\alpha = 1$ and picture-independent C, it is easy to check that $\lambda\varphi$ would have been renormalized to

$$-\frac{1}{2}C\lambda^3\log\Lambda\int d^2w_1\int d^2w_2 V(w_1,\bar{w_1})V(w_2,\bar{w_2}) \quad (13)$$

at each picture level (again, we suppressed the relevant indices for the structure constants and vertex operators). In the case under consideration, however, using identities (7) relating α and C, we can recast the renormalization of the $\lambda\varphi$ term under the flow (11) as

$$A_{\lambda\varphi} \sim \lambda\varphi : f(\Gamma) : \lambda\varphi\int d^2w_1\int d^2w_2 V_5^{(-3)}V_\varphi^{(-2)} \quad (14)$$
$$\to -\lambda^3\log\Lambda C_{[-3|-3]}\alpha_{[-3|1]}\int d^2w_1\int d^2w_2 V_\varphi^{(-6)}(w_1,\bar{w_1})V_5^{(n+6)}(w_2,\bar{w_2})$$
$$\times \sum_{n=0}^{\infty}\sum_{k,l=0;\ k\neq 2,3,n+3,n+4;\ l\neq n+2,n+3}^{k=n+6;l=n+5}\frac{(n+5)!(n+6)!}{k!l!(n+5-l)!(n+6-k)!}.$$

This gives the renormalization of the $\lambda\varphi$ cross-term under the RG flow (11) of the dilaton field in the ghost–matter mixing case. This contribution to the world-sheet renormalization group has the order of λ^3. The other contribution of the same order of λ^3 to the dilaton beta function comes from the OPE

singularities inside the λ^3 term itself, appearing in the expansion (3) of the partition function. Using the OPE (4) and evaluating the singular world-sheet integrals as in (10), (11), we get

$$A_{\lambda^3} = \frac{1}{6}\lambda^3 \int d^2w_1 \int d^2w_2 \int d^2w_3 \qquad (15)$$
$$\times \langle V_5^{(-3)}(w_1,\bar{w}_1)V_5^{(-3)}(w_2,\bar{w}_2)$$
$$\times V_5^{(-3)}(w_3,\bar{w}_3)\dots\rangle \sim \frac{1}{2}\lambda^3 \log\Lambda \sum_{n=0}^{\infty} 3^{-n-10}$$
$$\times \sum_{k,l=0}^{k+l=n+9} \frac{(n+9)!}{k!l!(n+9-k-l)!} \int d^2w_1 \int d^2w_2$$
$$\times \langle V_\varphi^{(-6)}(w_1,\bar{w}_1)V_5^{(n+6)}(w_2,\bar{w}_2)\dots\rangle$$
$$\times \{C_{[k-3|l-3]}\alpha_{[-3|k-3]}\alpha_{[-3|n+6-k-l]}\alpha_{[-3|n+6]}$$
$$+ C_{[k-3|n+6-k-l]}\alpha_{[-3|k-3]}\alpha_{[-3|l-3]}\alpha_{[-3|n+6]}$$
$$+ C_{[k-3|n+6-k-l]}\alpha_{[-3|l-3]}\alpha_{[-3|n+6-k-l]}\alpha_{[-3|n+6]}\}.$$

Again, it is easy to see that, in the absence of ghost–matter mixing ($\alpha = 1$; all C are picture-independent), this contribution would sum up to

$$\frac{1}{2}C\lambda^3 \log\Lambda \int d^2w_1 \int d^2w_2 V(w_1,\bar{w}_1)V(w_2,\bar{w}_2), \qquad (16)$$

precisely canceling the divergence of the same λ^3 type originating from the renormalization of the $\lambda\varphi$ cross-term under the flow. In the picture-independent case, this ensures that the renormalization (11) of the dilaton field under the flow does not bring about any additional singularities from higher order terms, such as the cubic one and the $\lambda\varphi$ cross-term. In particular, this guarantees that terms of the type

$$\sim C\lambda^3 \log\Lambda \int_\Lambda d^2w V_5(w,\bar{w}) \qquad (17)$$

($\int_\Lambda$ denotes the world-sheet integral cut at the Λ scale) never appear in the dilaton or other perturbative close-string field beta functions in the picture-independent case. This ensures, in turn, that, in the absence of ghost–matter mixing, the world-sheet beta function is always deterministic (just as it is well known to be the case in the standard string perturbation theory). On the contrary, should terms of this type appear in the beta function, that would imply that the RG equations become stochastic, since, from the point of view of the spacetime fields, world-sheet operator $\int_\Lambda d^2w V_5(w,\bar{w})$ is a stochastic random variable, with the cutoff parameter Λ playing the role of the stochastic time. In this case, the RG equations have the form of non-Markovian Langevin equations, where the memory of the noise is determined by the world-sheet correlation of the V_5 operators. This exactly is what happens in the ghost–matter mixing backgrounds, when the OPE of vertex operators are picture-dependent. As a result of the picture dependence, the flows of the $\lambda\varphi$ and λ^3 terms under the RG do not cancel each other and, as a result, the beta function of the dilaton gets the stochastic terms, as $A_{\lambda^3} + A_{\lambda\varphi} \neq 0$. Indeed, using identities (7), we can write (15) in the form

$$\frac{1}{2}C_{[-3|-3]}\alpha_{[-3|1]}\lambda^3 \log\Lambda \sum_{n=0}^{\infty} 3^{-n-9} \sum_{k,l=0;k\neq 2,3;l\neq 2,3;k+l\neq n+5,n+6}^{k+l=n+9} \frac{(n+9)!}{k!l!(n+9-k-l)!} \qquad (18)$$
$$\times \int d^2w_1 \int d^2w_2 \langle V_\varphi^{(-6)}(w_1,\bar{w}_1)V_5^{(n+6)}(w_2,\bar{w}_2)\dots\rangle,$$

giving the contribution of the A_{λ^3} term to the flow. Now, to get the total flow on the λ^3 level, one has to subtract the flow (14) from this expression. The difference would give the overall coefficient before the stochastic term of the type (17) in the beta function of the dilaton. Comparing (14) and (18) and performing the summations, we find that the additional renormalization of the dilaton field necessary to remove the extra singularities from the λ^3 and $\lambda\varphi$ terms, arising due to the OPE picture dependence in ghost–matter mixing backgrounds, is given by

$$\varphi \to \varphi - C_{[-3|-3]}\alpha_{[-3|1]}\lambda^3 \log\Lambda \qquad (19)$$

$$\times \int d^2w V_5^{(-3)}(w,\bar{w})\Big\{ -1 + \sum_{n=0}^{\infty} \big[(n+4)^2$$
$$\times (n+5)^3(n+6)\cdot 2^{-2n-12} + \frac{1}{96}(n+8)(n+9)$$
$$\times (n+13)(2/3)^{n+9} - ((n+4)^2(n+5)$$
$$+ (1/2)(n+5)^2(n+6))\cdot 2^{-n-6}\big]\Big\}.$$

The summation over n converges to

$$-\sigma = -1 + \sum_{n=0}^{\infty} \Big[(n+4)^2(n+5)^3 \qquad (20)$$

$$\times (n+6)\cdot 2^{-2n-12} + \frac{1}{96}(n+8)(n+9)$$
$$\times (n+13)(2/3)^{n+9} - ((n+4)^2(n+5)$$
$$+ (1/2)(n+5)^2(n+6))\cdot 2^{-n-6}\Big] = -1.534.$$

Therefore, the resulting beta-function equations for the dilaton in the ghost–matter mixing background give

$$\frac{d\varphi}{d\log\Lambda} = -\frac{\delta S_\varphi}{\delta\varphi} + \sigma C_{[-3|-3]}\alpha_{[-3|1]} \times \int\limits_\Lambda d^2 w V_5^{(-3)}(w,\bar{w}), \quad (21)$$

where $S_\varphi \sim \int dx \partial_m\varphi\partial^m\varphi$ is the low-energy effective action for the dilaton in the absence of the V_5 background.

With the restored momentum dependence, this equation can be written as

$$\frac{d\varphi(p)}{d\log\Lambda} = -\frac{\delta S_\varphi}{\delta\varphi(p)} + \sigma C(p)\int d^4 q\lambda(q) \times \int\limits_\Lambda d^2 w V_5^{(-3)}(w,q), \quad (22)$$

$$C(p) = \int d^4 k C_{[-3|-3]}(p,k)\lambda\left(\frac{k+p}{2}\right)\lambda\left(\frac{k-p}{2}\right),$$

with $\sigma = 1.534\ldots$. Thus far, we have considered only one particular example of the ghost–matter mixing—the branelike vertex operator $V_5^{(-6)}$ and its incarnations in higher pictures. There are other examples of vertex operators with ghost–matter mixing, and they also lead to stochastic terms in the beta function of the dilaton. In particular, we have also considered the dilaton field in the background of closed-string operators of higher ghost cohomologies:

$$W_5 \sim \int d^2 z e^{-4\phi-\bar{\phi}}\partial X_{(m_1}\ldots\partial X_{m_3)}\bar{\psi}_{m_6} \times e^{ik^\perp X}G_{m_1\ldots m_5,m_6}, \quad (23)$$

where the G tensor is symmetric and traceless in $m_1,\ldots,m_5$ (round brackets imply the symmetrization in spacetime indices) and $k^\perp$ is transverse to $m_1,\ldots,m_6$ directions, and

$$U_5 \sim \int d^2 z e^{-4\phi-\bar{\phi}}\partial X_{(m_1}\ldots\partial X_{m_4)}\psi_{m_5} \times \psi_{m_6}\bar{\psi}_{m_7}e^{ik^\perp X}G_{m_1\ldots,m_7}. \quad (24)$$

We have found that, even though the OPE details are quite different in each case, nevertheless, in the end one always gets the beta-function equations in the form (22). The crucial point is that the σ factor, reflecting the stochasticity of the beta function, appears to be universal and its value is independent of details of the ghost–matter mixing. Namely, we have found [8] $\sigma = 1.541\ldots$ for the W_5 insertion and $\sigma = 1.538\ldots$ for the U_5 case. In other words, the form of these equations is determined by the corresponding coefficient of the OPE of two operators before the dilaton and the numerical factor of σ. What is quite remarkable, the coefficient $\sigma = 1.534\ldots$ before the stochastic term is always the same and seems to be invariant to details of the ghost–matter mixing (in the absence of ghost–matter mixing, of course, $\sigma = 0$). What is even more remarkable, we can easily check that, in fact,

$$\sigma = \ln\delta, \quad (25)$$

where $\delta = 4.669\ldots$ is the famous Feigenbaum universality constant describing the universal scaling of the iteration parameter in a huge variety of dynamical systems under bifurcations and transitions from order to chaos [7]. Usually, this constant can be obtained numerically for the dynamical systems under the bifurcations. In our approach, however, the log of the Feigenbaum constant has emerged analytically, as the limit of convergent series (20) in the stochastic term in the beta function for various ghost–matter mixing backgrounds. In the next section, we will show that the appearance of the Feigenbaum constant in the beta function for the dilaton in ghost–matter mixing backgrounds is not at all occasional, but is deeply related to the peculiarities of the non-Markovian stochastic processes, associated with the Langevin equations and their implications for the spacetime geometry.

3. FEIGENBAUM UNIVERSALITY AND FIXED POINTS OF STOCHASTIC RG EQUATIONS

To understand the physical meaning behind the appearance of the Feigenbaum constant in (20), it is necessary to analyze the non-Markovian Fokker–Planck (FP) equation describing the stochastic process which can be straightforwardly derived from the Langevin Eq. (22). We shall present here the FP equation for scaling functions $\lambda(q) = \lambda_0/q^4$:

$$\frac{\partial P_{\rm FP}(\varphi,\tau)}{\partial\tau} = -\int d^4 p\int d^4 q\frac{\delta}{\delta\varphi(p,\tau)}\left(\frac{\delta S_\varphi}{\delta\varphi(q,\tau)}P_{\rm FP}(\varphi,\tau)\right) + \sigma^2\lambda_0^6\int d^4 k_1\int d^4 k_2\int\frac{d^4 p}{p^4}\int\frac{d^4 q}{q^4}\int d\xi\alpha_{[-3|1]} \times C_{[-3|-3]}\left(\frac{k_1+p}{2}\right)\alpha_{[-3|1]}C_{[-3|-3]} \quad (26)$$

$$\times\left(\frac{k_2+q}{2}\right)\frac{\delta}{\delta\varphi(p,\tau)}G_5(\xi,\tau)\frac{\delta}{\delta\varphi(q,\xi)}P_{\rm FP}(\varphi,\tau),$$

where $\tau=\log\Lambda$ now plays the role of the stochastic time variable. The Green's function $G_5(\xi,\tau,p,q)$ is defined by the cutoff dependence of the two-point correlator of the V_5 vertices:

$$G_5(\xi,\tau)=\int\limits_{\Lambda_1}d^2z\int\limits_{\Lambda_2}d^2w|z-w|^{-4} \qquad (27)$$

$$\times\,\delta(p+q)=\left(\frac{1+e^{\xi-\tau}}{1-e^{\xi-\tau}}\right)^2\delta(p+q),$$

$$\xi=\log\Lambda_1,\qquad \tau=\log\Lambda_2.$$

We shall look for the ansatz solving this equation in the form (for more details, see [3] and references therein)

$$P_{\rm FP}(\varphi,\tau)=\exp[-H_{\rm ADM}(\varphi,\tau)] \qquad (28)$$

$$=\exp\left[-\int d^4p\{g(\tau)(\partial_\tau\varphi)^2+f(\tau)p^2\varphi^2\}\right].$$

Substituting it into (26), we find that (28) solves the FP equation provided that the functions $f(\tau)$ and $g(\tau)$ satisfy the following differential equations:

$$g'(\tau)+4g(\tau)+\frac{\sigma^2\lambda_0^6}{2}=0, \qquad (29)$$

$$\frac{1}{4}f''+\left(1+\frac{1}{4\tau}\right)f'+\left(1+\frac{1}{4\tau}+\frac{1}{4\sigma^2\lambda_0^6}\right.$$

$$\left.\times\left(1-\frac{1}{\tau^2}\right)\right)f-\left(1-\frac{1}{\tau^2}\right)\left(e^{-2\tau}+\frac{1}{4\sigma^2\lambda_0^6}\right)=1.$$

The first equation is elementary, its solution being given by

$$g(\tau)=\frac{\sigma^2\lambda_0^6}{2}(e^{-4\tau}-1),\quad \tau<0. \qquad (30)$$

The second equation on $f(\tau)$ can be reduced to a Bessel-type equation by substituting

$$f(\tau)=\rho(\tau)e^{-2\tau}+\frac{1}{\sigma^2\lambda_0^6}.$$

The solution is given by

$$f(\tau)=1+\sigma^2\lambda_0^6e^{-2\tau}\left(1+J_{\frac{1}{\sigma\lambda_0^3}}\left(\frac{\tau}{\sigma\lambda_0^3}\right)\right), \qquad (31)$$

where $J_{\frac{1}{\sigma\lambda_0^3}}\left(\frac{\tau}{\sigma\lambda_0^3}\right)$ is a Bessel function. In terms of the τ coordinate, the stochastic process describing the RG flow in ghost–matter mixing backgrounds evolves in the direction of $\tau=-\infty$. Next, let us study the behavior of the FP distribution (28), (30), (31) in the conformal limit of $\tau\to-\infty$. In this limit, the exponents become very large and, moreover,

$$J_{\frac{1}{\sigma\lambda_0^3}}\left(\frac{\tau}{\sigma\lambda_0^3}\right)\sim O\left(\frac{1}{\sqrt{\tau}}\right)\ll 1, \qquad (32)$$

and after rescaling the distribution reduces to

$$H(\varphi,\tau)=R^2\int d^4p\{e^{-4\tau}(\partial_\tau\varphi)^2+p^2e^{-2\tau}\varphi^2\}, \qquad (33)$$

which is just the ADM Hamiltonian for the AdS_5 gravity in the temporal gauge [9]. It is easy to see that the λ_0^6 parameter has the meaning of the square of the radius R^2 of the metric.

Let us now analyze in more detail the solution (28), (30), (31) to the non-Markovian FP equation, leading to a new space geometry. Let us note first of all that the limit $\lambda_0\to 0$ is not the same as $\lambda_0=0$ (ghost–matter mixing absent). The RG flow described by the effective metric (30), (31) must be single-valued; since Bessel functions at zero argument are single-valued for integer orders only, this leads to the quantization condition

$$(\sigma\lambda_0^3)^{-1}=N. \qquad (34)$$

Moreover, since $J_\nu(\tau)\sim\tau^\nu$ as $\tau\to 0$, the absence of unphysical singularities at $\tau=0$ requires N to be positive. The quantization condition (32) implies that

$$((\lambda_0)_N)^{-3}=N\sigma,\quad e^{(\lambda_0)_N^{-3}}=\delta^N, \qquad (35)$$

implying the iteration law

$$\frac{e^{(\lambda_0)_{N+1}^{-3}}-e^{(\lambda_0)_N^{-3}}}{e^{(\lambda_0)_N^{-3}}-e^{(\lambda_0)_{N-1}^{-3}}}=\delta, \qquad (36)$$

with δ being the Feigenbaum number.

Therefore, the Feigenbaum iteration rule (36) determines the scaling of characteristic curvatures of geometries emerging at fixed points of the stochastic renormalization group. The role of the iteration parameter characterizing the bifurcations is played by $\sim\exp\left(-\frac{1}{R^2}\right)$, vanishing at $R=0$ and being finite at large R, as it should be the case for the scaling parameter of the Feigenbaum iteration scheme.

From the quantization condition (34), it is clear that the stochastic renormalization group (22) has fixed points for $0<\lambda_0<1$ (physically, these points correspond to large curvatures). Moreover, the period doublings that lead to the transition to chaos correspond to $N\to\infty$, i.e., $\lambda_0\to 0$, which is a singularity. Thus, we reached an amazing conclusion that, precisely near a singularity, our RG flow becomes chaotic. It is tempting to assume that this may be the mechanism which can solve the problem of singularities in string theory.

4. CONCLUSION

In this paper, we discussed how matter–ghost mixing can radically modify the nature of the world-sheet RG flows and lead to the emergence of chaos near curvature singularities. Here, we analyzed only dilaton evolution, but a similar picture can be obtained for other massless fields, for example, metric [8].

It is amusing that, recently, chaotic behavior of a metric was discussed in [10] (for earlier papers, see [11] and references therein), where the emergence of chaos in supergravity near a cosmological singularity was demonstrated in the presence of higher rank antisymmetric tensor fields, i.e., R–R fields. It will be extremely interesting to understand how chaos emerging during cosmological evolution in supergravity can be related to the chaotic nature of RG flows in underlying string theory in the presence of the sources of the background R–R fields.

It is tempting to assume that the resolution of the singularities problem is transition to chaos and emergence of smooth distributions of fields, not restricted on-shell. One can imagine that curvature R is some new Reynolds number in string theory, and for large R one has transition to chaotic behavior in a similar fashion as in hydrodynamics where there is a transition from a laminar to a turbulent flow. These ideas definitely need further investigation.

ACKNOWLEDGMENTS

I.K. is supported in part by PPARC rolling grant PPA/G/O/1998/00567 and EC TMR grants HPRN-CT-2000-00152 and HPRN-CT-2000-00148. D.P. acknowledges the support of the Academy of Finland under project no. 54023. Both I.K. and D.P. acknowledge interesting discussions with T. Damour and the hospitality of Institute des Hautes Etudes Scientifiques (IHES) in Bures-sur-Yvette, where part of this work has been done.

REFERENCES

1. A. M. Polyakov, *Gauge Fields and Strings* (Harwood, Chur, 1987); M. B. Green, J. H. Schwarz, and E. Witten, *Superstring Theory* (Cambridge Univ. Press, Cambridge, 1987), Vols. 1, 2; J. Polchinski, *String Theory* (Cambridge Univ. Press, Cambridge, 1998), Vol. 1, 2.
2. D. Fiedan, Phys. Rev. Lett. **45**, 1057 (1980); Ann. Phys. (N.Y.) **163**, 318 (1985); E. S. Fradkin and A. A. Tseytlin, Nucl. Phys. B **261**, 1 (1985); C. G. Callan, D. Friedan, E. J. Martinec, and M. J. Perry, Nucl. Phys. B **262**, 593 (1985); C. G. Callan and Z. Gan, Nucl. Phys. B **272**, 647 (1986); A. B. Zamolodchikov, Pis'ma Zh. Éksp. Teor. Fiz. **43**, 565 (1986) [JETP Lett. **43**, 730 (1986)]; Yad. Fiz. **46**, 1819 (1987) [Sov. J. Nucl. Phys. **46**, 1090 (1987)].
3. D. Polyakov, Class. Quantum Grav. **18**, 1979 (2001); hep-th/0005094.
4. I. I. Kogan and D. Polyakov, Int. J. Mod. Phys. A **16**, 2559 (2001); hep-th/0012128.
5. D. Polyakov, Phys. Rev. D **65**, 084041 (2002); hep-th/0111227.
6. I. I. Kogan and D. Polyakov, Int. J. Mod. Phys. A **18**, 1827 (2003); hep-th/0208036.
7. M. J. Feigenbaum, J. Stat. Phys. **19**, 25 (1978).
8. I. I. Kogan and D. Polyakov (in press).
9. J. de Boer, E. Verlinde, and H. Verlinde, J. High Energy Phys. **0008**, 003 (2000); hep-th/9912012.
10. T. Damour and M. Henneaux, Phys. Rev. Lett. **85**, 920 (2000); hep-th/0003139; Phys. Rev. Lett. **86**, 4749 (2001); hep-th/0012172; Gen. Relativ. Gravit. **32**, 2339 (2000); T. Damour, M. Henneaux, B. Julia, and H. Nicolai, Phys. Lett. B **509**, 323 (2001); hep-th/0103094; T. Damour, M. Henneaux, and H. Nicolai, Phys. Rev. Lett. **89**, 221601 (2002); hep-th/0207267; T. Damour, Int. J. Mod. Phys. A **17**, 2655 (2002).
11. V. D. Ivashchuk and V. N. Melnikov, J. Math. Phys. **41**, 6341 (2000); hep-th/9904077.

Physics of Atomic Nuclei, Vol. 66, No. 11, 2003, pp. 2070–2077. From Yadernaya Fizika, Vol. 66, No. 11, 2003, pp. 2119–2127.

ELEMENTARY PARTICLES AND FIELDS
Theory

Monopoles and Family-Replicated Unification*

L. V. Laperashvili[**], **H. B. Nielsen**[1)***], **and D. A. Ryzhikh**[****]

Institute of Theoretical and Experimental Physics,
Bol'shaya Cheremushkinskaya ul. 25, Moscow, 117259 Russia

Received December 26, 2002

Abstract—The present theory is based on the assumption that, at very small (Planck scale) distances our spacetime is discrete, and this discreteness influences the Planck scale physics. Considering our $(3+1)$-dimensional spacetime as a regular hypercubic lattice with a parameter $a = \lambda_{\rm Pl}$, where $\lambda_{\rm Pl}$ is the Planck length, we have investigated a role of lattice artifact monopoles, which is essential near the Planck scale if the family-replicated gauge group model (FRGGM) is an extension of the Standard Model (SM) at high energies. It was shown that monopoles have N times smaller magnetic charge in the FRGGM than in the SM (N is the number of families in the FRGGM). These monopoles can give an additional contribution to β functions of the renormalization-group equations for the running fine structure constants $\alpha_i(\mu)$ ($i = 1, 2, 3$ correspond to the $U(1)$, $SU(2)$, and $SU(3)$ gauge groups of the SM). We have used the Dirac relation for renormalized electric and magnetic charges. Also, we have estimated the enlargement of a number of fermions in the FRGGM leading to the suppression of the asymptotic freedom in the non-Abelian theory. The different role of monopoles in the vicinity of the Planck scale gives rise either to anti-GUT or to the new possibility of unification of gauge interactions (including gravity) at the scale $\mu_{\rm GUT} \approx 10^{18.4}$ GeV. We discussed the possibility of the $[SU(5)]^3$ SUSY or $[SO(10)]^3$ SUSY unifications.

1. INTRODUCTION

Trying to gain insight into nature and considering the physical processes at very small distances, physicists have made attempts to explain the well-known laws of low-energy physics as a consequence of the more fundamental laws of nature. The contemporary physics of electroweak and strong interactions is described by the Standard Model (SM), which unifies the Glashow–Salam–Weinberg electroweak theory with QCD theory of strong interactions.

The gauge group of symmetry in the SM is

$$\mathrm{SMG} = SU(3)_c \times SU(2)_L \times U(1)_Y, \qquad (1)$$

which describes the present elementary particle physics up to the scale ≈100 GeV.

Recently, it was shown in a number of papers [1] that the family-replicated gauge groups of the type

$$SU(n)^N \times SU(m)^N \qquad (2)$$

play an essential role in construction of renormalizable, asymptotically free, four-dimensional gauge theories that dynamically generate a fifth dimension (or fifth and sixth ones). This theory leads to natural electroweak symmetry breaking, relying neither on supersymmetry nor on strong dynamics at the TeV scale. The new TeV physics is perturbative, and radiative corrections to the Higgs mass are finite. The Higgs scalar is an extended object (pseudo-Nambu–Goldstone boson) and a novel Higgs potential emerges naturally requiring a second light $SU(2)$ doublet scalar.

We see that the family-replicated gauge groups provide a new way to stabilize the Higgs mass in the SM.

2. FAMILY-REPLICATED GAUGE GROUP

The extension of the SM with the family-replicated gauge group (FRGG)

$$G = (\mathrm{SMG})^N = [SU(3)_c]^N \times [SU(2)_L]^N \times [U(1)_Y]^N \qquad (3)$$

was first suggested by Froggatt and Nielsen [2].

In Eq. (3), N designates the number of quark and lepton families. If $N = 3$ (as experiment confirms), then the fundamental gauge group G is

$$G = (\mathrm{SMG})^3 = \mathrm{SMG}_{\text{1st fam}} \times \mathrm{SMG}_{\text{2nd fam}} \times \mathrm{SMG}_{\text{3rd fam}}. \qquad (4)$$

*This article was submitted by the authors in English.

[1)]Niels Bohr Institute, Copenhagen, Denmark.
[**]e-mail: laper@heron.itep.ru
[***]e-mail: hbech@alf.nbi.dk
[****]e-mail: ryzhikh@heron.itep.ru

The generalized fundamental group

$$G_f = (\mathrm{SMG})^3 \times U(1)_f \tag{5}$$

was suggested by the fitting of fermion masses of the SM [3].

Recently, a new generalization of FRGG model was suggested in [4], in which the fundamental group

$$\begin{aligned} G_{\mathrm{ext}} &= (\mathrm{SMG} \times U(1)_{B-L})^3 \\ &\equiv [SU(3)_c]^3 \times [SU(2)_L]^3 \\ &\times [U(1)_Y]^3 \times [U(1)_{(B-L)}]^3 \end{aligned} \tag{6}$$

takes into account the seesaw mechanism with right-handed neutrinos, describes all modern neutrino experiments, and gives a reasonable fitting of the SM fermion masses and mixing angles. The group $G = G_{\mathrm{ext}}$ contains $3 \times 8 = 24$ gluons, $3 \times 3 = 9$ W bosons, and $3 \times 1 + 3 \times 1 = 6$ Abelian gauge bosons.

The model is renormalizable: it has no anomalies, neither gauge nor mixed.

The gauge group G_{ext} undergoes spontaneous breakdown (at some orders of magnitude below the Planck scale) by seven different Higgs fields to the gauge group that is the diagonal subgroup of G_{ext}. Therefore, seven Higgs fields break the FRGG model to the SM. The field ϕ_{WS} corresponds to the Weinberg–Salam theory. Its VEV is known, $\langle \phi_{\mathrm{WS}} \rangle = 246$ GeV, so that we have only six free parameters (six VEVs) to fit the experiment in the framework of this model.

Froggatt, Nielsen, and Takanishi [4] have used them with aim to find the best fit to conventional experimental data for all fermion masses and mixing angles in the SM, and also to explain the experiments in the neutrino oscillations. The typical fit was encouraging in the crude approximation. Also, the neutrino masses were predicted.

Finally, we conclude that, in general, the theory with FRGG symmetry is successful in describing the SM experiment.

3. LATTICE-LIKE STRUCTURE OF OUR SPACETIME

Having an interest in the fundamental laws of physics, we can consider two possibilities:

(i) At very small (Planck length) distances, our spacetime is continuous and there exists a fundamental theory with a very high symmetry.

(ii) At very small distances, our spacetime is discrete, and this discreteness influences the Planck scale physics.

The second item is an initial (basic) point of view of the present theory, but not an approximation. It is a basis of the theory of physical processes proceeding at small distances on the order of the Planck scale $\lambda_{\mathrm{Pl}} = M_{\mathrm{Pl}}^{-1}$:

$$M_{\mathrm{Pl}} = 1.22 \times 10^{19} \ \mathrm{GeV}. \tag{7}$$

In the simplest case, we can imagine our $(3+1)$ spacetime as a regular hypercubic lattice with a parameter $a = \lambda_{\mathrm{Pl}}$. Then, the lattice artifact monopoles can play an essential role near the Planck scale. But, of course, it is necessary to comment that we do not know (at least on the level of our knowledge today) what lattice-like structure (random lattice, or foam, or string lattice, etc.) plays a role in the description of physical processes at very small distances [5].

The aim of the present paper is also to show that monopoles cannot be seen in the usual SM up to the Planck scale, because they have a huge magnetic charge and are completely confined. Supersymmetry does not help to see monopoles.

We suggest considering a possibility of the existence of monopoles in our world, extending the Standard Model group (SMG) to the family-replicated gauge group $((\mathrm{SMG})^N)$.

4. RENORMALIZATION-GROUP EQUATIONS FOR ELECTRIC AND MAGNETIC FINE STRUCTURE CONSTANTS

Schwinger [6] was first to investigate the problem of renormalization of the magnetic charge in quantum electromagnetodynamics (QEMD), i.e., in the Abelian quantum field theory of electrically and magnetically charged particles (with charges e and g, respectively).

Considering the "bare" charges e_0 and g_0 and renormalized (effective) charges e and g, Schwinger obtained

$$e/g = e_0/g_0, \tag{8}$$

which means the absence of the Dirac relation for the renormalized electric and magnetic charges.

But there exists another solution of this problem [7–9] which gives

$$eg = e_0 g_0 = 2\pi n, \quad n \in Z, \tag{9}$$

i.e., the existence of the Dirac relation (charge-quantization condition) for both, bare and renormalized, electric and magnetic charges. Here, we have $n = 1$ for the minimal (elementary) charges.

These two cases lead to the two possibilities for the renormalization-group equations (RGEs) describing the evolution of electric and magnetic fine-structure constants,

$$\alpha = \frac{e^2}{4\pi} \quad \text{and} \quad \widetilde{\alpha} = \frac{g^2}{4\pi}, \tag{10}$$

which obey the following RGEs containing the electric and magnetic β functions:

$$\frac{d(\log\alpha(\mu))}{dt} = \pm\frac{d(\log\widetilde{\alpha}(\mu))}{dt} = \beta^{(e)}(\alpha) \pm \beta^{(m)}(\widetilde{\alpha}). \tag{11}$$

In Eq. (11), we have

$$t = \log\left(\frac{\mu^2}{\mu_R^2}\right), \tag{12}$$

where μ is the energy scale and μ_R is the renormalization point.

The second possibility (with minuses) in Eq. (11) corresponds to the validity of the Dirac relation for the renormalized charges. We believe only in the case of the Dirac relation considered by the authors in [9], where we have used the Zwanziger formalism of QEMD [10].

In the present paper, excluding Schwinger's renormalization condition (8), we assume only the Dirac relation for running α and $\widetilde{\alpha}$:

$$\alpha\widetilde{\alpha} = 1/4. \tag{13}$$

It is necessary to comment that RGEs (11) are valid only for $\mu > \mu_{\text{threshold}} = m_{\text{mon}}$, where m_{mon} is the monopole mass.

If monopole charges, together with electric ones, are sufficiently small, then β functions can be considered perturbatively:

$$\beta(\alpha) = \beta_2(\alpha/4\pi) + \beta_4(\alpha/4\pi)^2 + \dots \tag{14}$$

and

$$\beta(\widetilde{\alpha}) = \beta_2(\widetilde{\alpha}/4\pi) + \beta_4(\widetilde{\alpha}/4\pi)^2 + \dots \tag{15}$$

with (see [18] and references therein)

$$\beta_2 = 1/3 \quad \text{and} \quad \beta_4 = 1 \quad \text{for scalar particles} \tag{16}$$

and

$$\beta_2 = 4/3 \quad \text{and} \quad \beta_4 \approx 4 \quad \text{for fermions.} \tag{17}$$

For scalar electric and magnetic charges, we have $\beta^{(e)} = \beta(\alpha)$ and $-\beta^{(m)} = \beta(\widetilde{\alpha})$; therefore,

$$\frac{d(\log\alpha(\mu))}{dt} = -\frac{d(\log\widetilde{\alpha}(\mu))}{dt} = \beta_2\frac{\alpha-\widetilde{\alpha}}{4\pi}\left(1 + 3\frac{\alpha+\widetilde{\alpha}}{4\pi} + \dots\right) \tag{18}$$

with $\beta_2 = 1/3$, and approximately the same result is valid for fermionic particles with $\beta_2 = 4/3$. Equation (18) shows that there exists a region where both fine structure constants are perturbative. Approximately, this region is given by the following inequalities:

$$0.2 \lesssim (\alpha, \widetilde{\alpha}) \leq 1. \tag{19}$$

Using the Dirac relation (13), we see from Eq. (18) that, in the region (19), the two-loop contribution is not larger than 30% of the one-loop contribution, and the perturbation theory can be realized in this case.

It is necessary to comment that the region (19) almost coincides with the region of phase-transition couplings obtained in the lattice compact QED [11].

5. EVOLUTION OF RUNNING FINE STRUCTURE CONSTANTS

The usual definition of the SM coupling constants is given in the modified minimal subtraction scheme ($\overline{MS}$):

$$\alpha_1 = \frac{5}{3}\alpha_Y, \quad \alpha_Y = \frac{\alpha}{\cos^2\theta_{\overline{MS}}}, \tag{20}$$
$$\alpha_2 = \frac{\alpha}{\sin^2\theta_{\overline{MS}}}, \quad \alpha_3 \equiv \alpha_s = \frac{g_s^2}{4\pi},$$

where α and α_s are the electromagnetic and $SU(3)$ fine-structure constants, respectively; Y is the hypercharge; and $\theta_{\overline{MS}}$ is the Weinberg weak angle in the $\overline{MS}$ scheme. Using RGEs with experimentally established parameters, it is possible to extrapolate the experimental values of three inverse running constants $\alpha_i^{-1}(\mu)$ (here, $i = 1, 2, 3$ correspond to $U(1)$, $SU(2)$, and $SU(3)$ groups of SM) from the electroweak scale to the Planck scale.

It is well known (see, for example, [12]) that (in the absence of monopoles) the one-loop approximation RGEs can be described by the following expressions:

$$\alpha_i^{-1}(\mu) = \alpha_i^{-1}(\mu_R) + \frac{b_i}{4\pi}t, \tag{21}$$

where slopes b_i are given by the following values:

$$b_i = (b_1, b_2, b_3) = \left(-\frac{4}{3}N_{\text{gen}} - \frac{1}{10}N_S, \right. \tag{22}$$
$$\left. \frac{22}{3}N_V - \frac{4}{3}N_{\text{gen}} - \frac{1}{6}N_S, \quad 11N_V - \frac{4}{3}N_{\text{gen}}\right).$$

The integers N_{gen}, N_S, and N_V are, respectively, the numbers of generations, Higgs bosons, and different vector gauge fields.

In the SM, we have

$$N_{\text{gen}} = 3, \quad N_S = N_V = 1, \tag{23}$$

and the corresponding slopes (22) describe the evolutions of $\alpha_i^{-1}(\mu)$.

The precision of the LEP data allows us to make the extrapolation of RGEs with small errors up to the Planck scale unless the new physics pops up, of course. Assuming that these RGEs for $\alpha_i^{-1}(\mu)$ contain only the contributions of the SM particles up to

$\mu = \mu_{\rm Pl} \equiv M_{\rm Pl}$ and doing the extrapolation with one Higgs doublet under the assumption of a "desert" and absence of monopoles, we have the following result obtained in [13]:

$$\alpha_1^{-1}(\mu_{\rm Pl}) \approx 33.3; \quad \alpha_2^{-1}(\mu_{\rm Pl}) \approx 49.5; \qquad (24)$$
$$\alpha_3^{-1}(\mu_{\rm Pl}) \approx 54.0.$$

The extrapolation of $\alpha^{-1}_{1,2,3}(\mu)$ up to the point $\mu = \mu_{\rm Pl}$ is shown in Fig. 1 as function of the variable $x = \log\mu$ (GeV). In this connection, it is very tempting to consider also the gravitational interaction.

The gravitational interaction between two particles of equal masses M is given by the usual classical Newtonian potential,

$$V_g = -G\frac{M^2}{r} = -\left(\frac{M}{M_{\rm Pl}}\right)^2 \frac{1}{r} = -\frac{\alpha_g(M)}{r}, \quad (25)$$

which always can be imagined as a tree-level approximation of quantum gravity.

Then, the quantity

$$\alpha_g = \left(\frac{\mu}{\mu_{\rm Pl}}\right)^2 \qquad (26)$$

plays a role of the running "gravitational fine-structure constant," and the evolution of its inverse quantity is also presented in Fig. 1 together with the evolutions of $\alpha_i^{-1}(\mu)$.

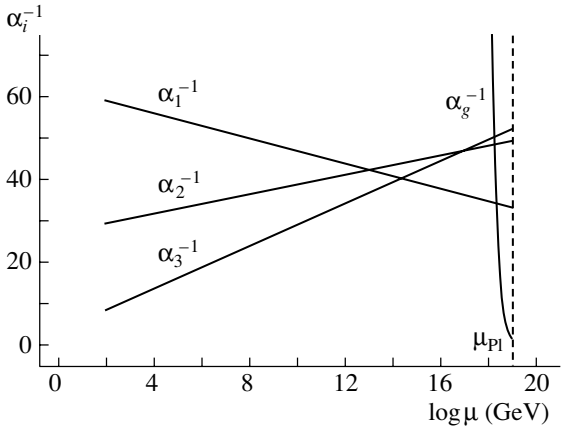

Fig. 1. The evolution of three inverse running constants $\alpha_i^{-1}(\mu)$, where $i = 1, 2, 3$ correspond to $U(1)$, $SU(2)$, and $SU(3)$ groups of the SM, respectively. The extrapolation of their experimental values from the electroweak scale to the Planck scale was obtained by using the renormalization group equations with one Higgs doublet under the assumption of a "desert." The precision of the LEP data allows us to make this extrapolation with small errors. The intersection of the inverse "gravitational fine structure constant" $\alpha_g^{-1}(\mu)$ with $\alpha_1^{-1}(\mu)$ occurs at the point (x_0, α_0^{-1}): $\alpha_0^{-1} \approx 34.4$, and $x_0 \approx 18.3$, where $x = \log\mu$ (GeV).

6. DROPPING OF THE MONOPOLE CHARGE IN THE FAMILY-REPLICATED GAUGE GROUP MODEL

In the simplest case, the scalar monopole β function in QEMD is (see [14] and [15])

$$\beta(\widetilde{\alpha}) = \frac{\widetilde{\alpha}}{12\pi} + \left(\frac{\widetilde{\alpha}}{4\pi}\right)^2 + \ldots \qquad (27)$$
$$= \frac{\widetilde{\alpha}}{12\pi}\left(1 + 3\frac{\widetilde{\alpha}}{4\pi} + \ldots\right).$$

From the last equation, it follows that the theory of monopoles cannot be considered perturbatively at least for

$$\widetilde{\alpha} > \frac{4\pi}{3} \approx 4. \qquad (28)$$

This limit is smaller for non-Abelian monopoles.

Using the Dirac relation, it is easy to estimate, in the simple SM, the Planck scale value $\widetilde{\alpha}(\mu_{\rm Pl})$ (minimal for $U(1)_Y$ gauge group):

$$\widetilde{\alpha}(\mu_{\rm Pl}) = \frac{5}{3}\alpha_1^{-1}(\mu_{\rm Pl})/4 \approx 55.5/4 \approx 14. \qquad (29)$$

This value is really very big compared with the estimate (28) and, of course, with the critical coupling $\widetilde{\alpha}_{\rm crit} \approx 1$, corresponding to the confinement–deconfinement phase transition in the lattice QED [11]. Clearly, we cannot do the perturbation approximation with such a strong coupling $\widetilde{\alpha}$.

It is hard for such monopoles not to be confined.

There is an interesting way out of this problem if one wants to have the existence of monopoles, namely, to extend the SM gauge group so cleverly that certain selected linear combinations of charges get bigger electric couplings than the corresponding SM couplings. That could create monopoles which for these certain charge linear combinations couple more weakly and thus have a better chance of being allowed "to exist." An example of such an extension of the SM that can impose the possibility of the allowance of monopoles is exactly the Family-Replicated Gauge Group Model (FRGGM). According to the FRGGM, at some point $\mu = \mu_G < \mu_{\rm Pl}$ (or really in a couple of steps), the fundamental group $G \equiv G_{\rm ext}$ undergoes spontaneous breakdown to its diagonal subgroup,

$$G \longrightarrow G_{\rm diag.subgr} = \{g, g, g || g \in {\rm SMG}\}, \qquad (30)$$

which is identified with the usual (low-energy) group SMG.

It should be said that, in the FRGGM, each family has its own gluons, own W, and own photons. The

breaking just makes a linear combination of a certain color combination of each family's gluons that exists in the SM below $\mu = \mu_G$ and down to low energies. We can say that the phenomenological gluon is a linear combination (with amplitude $1/\sqrt{3}$ for $N = 3$) for each of the FRGG gluons of the same color combination. Then, we have the following formula connecting the fine structure constants of the non-Abelian FRGG model and low-energy surviving diagonal subgroup $G_{\text{diag.subgr}} \subseteq (\text{SMG})^3$:

$$\alpha_{i,\text{diag}}^{-1} = \alpha_{i,\text{1st fam}}^{-1} + \alpha_{i,\text{2nd fam}}^{-1} + \alpha_{i,\text{3rd fam}}^{-1}. \quad (31)$$

Here, $i = 1, 2$ correspond to $SU(2)$, $SU(3)$, and $i = 3$ means that we talk about the gluon couplings.

Assuming that three FRGG couplings are equal to each other, we obtain

$$\alpha_{i,\text{diag}}^{-1} \approx 3\alpha_{i,\text{one fam}}^{-1} \equiv 3\alpha_{i,G}^{-1}. \quad (32)$$

In contrast to non-Abelian theories, in which the gauge invariance forbids the mixed (in families) terms in the Lagrangian of FRGG theory, the $U(1)$ sector of FRGG contains such mixed terms:

$$\frac{1}{g^2}\sum_{p,q} F_{\mu\nu,p}F_q^{\mu\nu} = \frac{1}{g_{11}^2}F_{\mu\nu,1}F_1^{\mu\nu} + \frac{1}{g_{12}^2}F_{\mu\nu,1}F_2^{\mu\nu} \quad (33)$$

$$+ \cdots + \frac{1}{g_{23}^2}F_{\mu\nu,2}F_3^{\mu\nu} + \frac{1}{g_{33}^2}F_{\mu\nu,3}F_3^{\mu\nu},$$

where $F_{\mu\nu,p}$ is the gauge field strength tensor and $p, q = 1, 2, 3$ are the indices of three families of the group $(\text{SMG})^3$. Now, it is easily seen that, if the specific electric charges of different families are equal (equal α_{pq}), then, taking the diagonal subgroup, we get [16]

$$\alpha_{\text{diag}}^{-1} \approx 6\alpha_G^{-1}, \quad (34)$$

which shows that we can increase electric α by a factor 6, replacing it with the electric $\alpha_{\text{one fam}} \equiv \alpha_G$.

Taking into account (34), we can get the monopole fine-structure constant $\widetilde{\alpha}_G = \alpha_G^{-1}/4$, which is smaller by a factor of 6 in comparison with $\widetilde{\alpha}$ in the SM. We can estimate at the Planck scale:

$$\widetilde{\alpha}_G(\mu_{\text{Pl}}) \approx 14/6 \approx 2.3. \quad (35)$$

But it seems (see below) that, in the FRGGM, we have at the Planck scale

$$\widetilde{\alpha}_G(\mu_{\text{Pl}}) \approx 1,$$

and the perturbation theory works for the β function of scalar monopoles near the Planck scale.

The conclusion: if one wants monopoles "to exist," it is necessary to drive in the direction of a model like FRGG.

7. THE POSSIBILITY OF GRAND UNIFICATION NEAR THE PLANCK SCALE

In the anti-GUT model by Froggatt and Nielsen [2–4], the FRGG breakdown was considered at $\mu_G \sim 10^{18}$ GeV.

But the aim of this investigation is to show that we can see quite different consequences of the extension of the SM to the FRGGM if the G group undergoes breakdown to its diagonal subgroup (i.e., SM) not at $\mu_G \sim 10^{18}$ GeV, but at $\mu_G \sim 10^{14}$ or 10^{15} GeV, i.e., before the intersection of $\alpha_2^{-1}(\mu)$ with $\alpha_3^{-1}(\mu)$ at $\mu \approx 10^{16}$ GeV.

Then, in the region $\mu_G < \mu < \mu_{\text{Pl}}$, we have three $\text{SMG} \times U(1)_{B-L}$ groups for three FRGG families. In this region, we have a lot of fermions, mass-protected or not mass-protected, belonging to usual families or to mirror ones. In the FRGGM, the additional six Higgs bosons, with their large VEVs, are responsible for the mass protection of many new fermions appearing in the region $\mu > \mu_G$. In this region, we designate the total number of fermions N_F, which is different from N.

Also, a role of artifact monopoles can be important in the vicinity of the Planck scale. Lattice monopoles are responsible for the confinement in lattice gauge theories, which is confirmed by many numerical and theoretical investigations (see review [17] and papers [18]). In the compact lattice gauge theory, the monopoles are not physical objects: they are lattice artifacts driven to infinite mass in the continuum limit.

In [19–22], we have developed the Higgs Monopole Model (HMM) approximating the lattice artifact monopoles as fundamental pointlike particles described by the Higgs scalar field. Indeed, the simplest effective dynamics describing the confinement mechanism in the pure gauge lattice $U(1)$ theory is the dual Abelian Higgs model of scalar monopoles [17, 18]. This model considers the following Lagrangian:

$$L = -\frac{1}{4g^2}F_{\mu\nu}^2(B) + \frac{1}{2}|(\partial_\mu - iB_\mu)\Phi|^2 - U(\Phi), \quad (36)$$

where

$$U(\Phi) = \frac{1}{2}\mu^2|\Phi|^2 + \frac{\lambda}{4}|\Phi|^4 \quad (37)$$

is the Higgs potential of scalar monopoles with magnetic charge g and B_μ is the dual gauge (photon) field interacting with the scalar monopole field Φ. In this model, λ is the self-interaction constant of scalar fields, and the mass parameter μ^2 is negative. Considering the renormalization-group improvement of the effective Coleman–Weinberg potential [14], written

in [19–22] for the dual sector of scalar electrodynamics in the two-loop approximation for β functions, we have calculated the $U(1)$ critical values of the magnetic fine-structure constant,

$$\tilde{\alpha}_{\rm crit} = g^2_{\rm crit}/4\pi \approx 1.20, \qquad (38)$$

and (by the Dirac relation) the electric fine-structure constant,

$$\alpha_{\rm crit} = \pi/g^2_{\rm crit} \approx 0.208. \qquad (39)$$

These values coincide with the lattice result [11].

Writing the following RGEs for $\alpha_i(\mu)$ containing β functions for the Higgs scalar monopoles,

$$\frac{d(\log \alpha_i(\mu))}{dt} = \beta(\alpha_i) - \beta^{(m)}(\widetilde{\alpha}_i), \;\; i = 1,2,3, \;\; (40)$$

we can use the one-loop approximation for $\beta(\alpha_i)$ because α_i are small and the two-loop approximation for dual β function $\beta^{(m)}(\widetilde{\alpha}_i)$ by the reason that $\widetilde{\alpha}_i$ are not very small near the Planck scale.

It was shown in a number of investigations (see, for example, [18] and references therein) that the confinement in the $SU(n)$ lattice gauge theory effectively comes to the same $U(1)$ formalism. The reason is the Abelian dominance in their monopole vacuum: monopoles of the Yang–Mills theory are the solutions of the $U(1)$ subgroups, arbitrarily embedded into the $SU(n)$ group. After a partial gauge fixing (Abelian projection by 't Hooft [23]), $SU(n)$ gauge theory is reduced to the Abelian $U(1)^{n-1}$ theory with $n-1$ different types of Abelian monopoles. With choice of the Abelian gauge for dual gluons, it is possible to describe the confinement in the lattice $SU(n)$ gauge theories by the analogous dual Abelian Higgs model of scalar monopoles.

Using the Abelian gauge by 't Hooft and taking into account that the directions in the Lie algebra of monopole fields are gauge-dependent, we have found in [21] an average over these directions and obtained the group-dependence relation between the phase-transition fine-structure constants for the groups $U(1)$ and $SU(n)/Z_n$:

$$\alpha^{-1}_{n,\rm crit} = \frac{n}{2}\sqrt{\frac{n+1}{n-1}}\alpha^{-1}_{U(1),\rm crit}. \qquad (41)$$

We have calculated this relation using only the one-loop approximation diagrams of non-Abelian theories.

According to Eq. (41), we have the following relations:

$$\alpha^{-1}_{U(1),\rm crit} : \alpha^{-1}_{2,\rm crit} : \alpha^{-1}_{3,\rm crit} = 1 : \sqrt{3} : 3/\sqrt{2}. \qquad (42)$$

Near the Planck scale, we are in the vicinity of the critical points [19–22].

Finally, taking into account that, in the non-Abelian sectors of the FRGG, we have the Abelian artifact monopoles, we obtain the following RGEs:

$$\frac{d(\alpha_i^{-1}(\mu))}{dt} = \frac{b_i}{4\pi} + \frac{N_M}{\alpha_i}\beta^{(m)}(\widetilde{\alpha}_{U(1)}), \qquad (43)$$

where b_i are given by the following values:

$$b_i = (b_1, b_2, b_3) = \left(-\frac{4}{3}N_F - \frac{1}{10}N_S, \qquad (44)\right.$$
$$\left.\frac{22}{3}N_V - \frac{4}{3}N_F - \frac{1}{6}N_S, \quad 11N_V - \frac{4}{3}N_F\right).$$

The integers N_F, N_S, N_V, and N_M are, respectively, the total numbers of fermions, Higgs bosons, vector gauge fields, and scalar monopoles in the FRGGM considered in our theory.

Approximating artifact monopoles by the Higgs scalar fields with a magnetic charge g, we have the following Abelian monopole β function in the two-loop approximation [21]:

$$\beta^{(m)}(\widetilde{\alpha}_{U(1)}) = \frac{\widetilde{\alpha}_{U(1)}}{12\pi}\Big(1 + 3\frac{\widetilde{\alpha}_{U(1)}}{4\pi}\Big). \qquad (45)$$

Using the Dirac relation $\alpha\widetilde{\alpha} = 1/4$, we have

$$\beta^{(m)} = \frac{\alpha^{-1}_{U(1)}}{48\pi}\Big(1 + 3\frac{\alpha^{-1}_{U(1)}}{16\pi}\Big), \qquad (46)$$

and the group dependence relation (41), which is approximately valid in the vicinity of the critical points on the Planck scale, gives

$$\beta^{(m)} = \frac{C_i {\alpha_i}^{-1}}{48\pi}\left(1 + 3\frac{C_i {\alpha_i}^{-1}}{16\pi}\right), \qquad (47)$$

where

$$C_i = (C_1, C_2, C_3) = \left(\frac{5}{3}, \frac{1}{\sqrt{3}}, \frac{\sqrt{2}}{3}\right). \qquad (48)$$

Finally, we have the following RGEs:

$$\frac{d(\alpha_i^{-1}(\mu))}{dt} = \frac{b_i}{4\pi} + N_M\frac{C_i {\alpha_i}^{-2}}{48\pi}\left(1 + 3\frac{C_i {\alpha_i}^{-1}}{16\pi}\right), \qquad (49)$$

where b_i and C_i are given by Eqs. (44) and (48), respectively.

In our FRGG model,

$$N_V = 3, \quad N_M = 6 \quad \text{for } i = 1, \qquad (50)$$
$$N_V = N_M = 3 \quad \text{for } i = 2,3,$$

because we have 3 times more gauge fields ($N = 3$) in comparison with usual SM and one Higgs scalar monopole in each family.

Assuming six scalar Higgs bosons ($N_S = 6$) breaking the FRGG to the SMG and the total

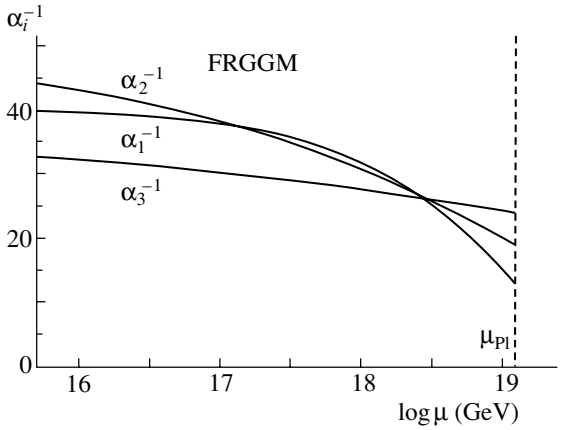

Fig. 2. The evolution of the inverse fine structure constants $\alpha_{1,2,3}^{-1}(\mu)$ beyond the SM in the FRGGM with influence of monopoles near the Planck scale.

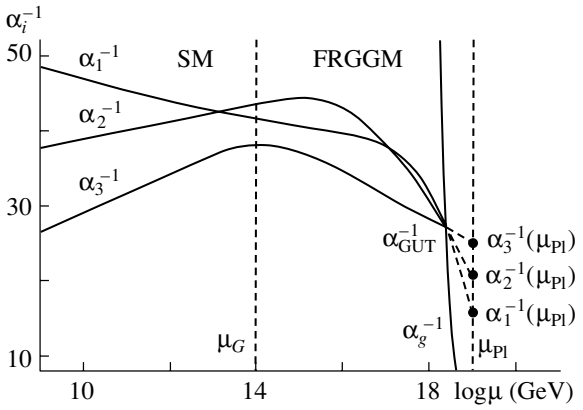

Fig. 3. The evolution of $\alpha_{1,2,3}^{-1}(\mu)$ in the SM and beyond it. The breakdown of FRGG occurs at $\mu_G \sim 10^{14}$ GeV. The possibility of the $[SU(5)]^3$ SUSY unification of all gauge interactions, including gravity, is shown at $\alpha_{\rm GUT}^{-1} \approx 27$ and $x_{\rm GUT} \approx 18.4$, where $x = \log \mu\,({\rm GeV})$.

number of fermions $N_F = 2N_{\rm tot}$ (usual and mirror families), $N_{\rm tot} = N \cdot N_{\rm gen} = 3 \times 3 = 9$ (three SMG groups with three generations in each group), we have obtained the evolutions of $\alpha_i^{-1}(\mu)$ near the Planck scale by numerical calculations for $N_F = 18$ and $\mu_G = 10^{14}$ GeV. Figure 2 shows the existence of the unification point. We see that, in the region $\mu > \mu_G$, many new fermions and a number of monopoles near the Planck scale change the one-loop approximation behavior of $\alpha_i^{-1}(\mu)$, which we had in the SM. In the vicinity of the Planck scale, these evolutions begin to decrease, when approaching the Planck scale $\mu = \mu_{\rm Pl}$, which means the suppression of the asymptotic freedom in the non-Abelian theories. Figure 3 demonstrates the unification of all gauge interactions, including gravity (the intersection of α_g^{-1} with α_i^{-1}), at

$$\alpha_{\rm GUT}^{-1} \approx 27 \quad \text{and} \quad x_{\rm GUT} \approx 18.4. \tag{51}$$

It is easy to calculate that, for one family, we have

$$\widetilde{\alpha}_{\rm GUT,\ one\ fam} = \frac{\alpha_{\rm GUT,\ one\ fam}^{-1}}{4} = \frac{\alpha_{\rm GUT}^{-1}}{4 \times 6} \approx \frac{27}{24} \approx 1.125, \tag{52}$$

and

$$\alpha_{\rm GUT,\ one\ fam} \approx 0.22, \tag{53}$$

which means that, at the GUT scale, electric and monopole charges are not large and can be considered perturbatively.

At this GUT scale, we can expect the existence of $[SU(5)]^3$ SUSY or $[SO(10)]^3$ SUSY unification with superparticles of masses

$$M \approx 10^{18.4}\ {\rm GeV}. \tag{54}$$

The scale $\mu_{\rm GUT} = M$, given by Eq. (54), can be considered as a SUSY-breaking scale.

The unification theory with $[SU(5)]^3$ symmetry was first suggested by Rajpoot [24].

Considering the predictions of such a theory for low-energy physics and cosmology, maybe in the future we shall be able to answer the question: "Does the unification of $[SU(5)]^3$ SUSY or $[SO(10)]^3$ SUSY really exist near the Planck scale?"

8. CONCLUSIONS

In the present paper, we have shown the following.

(i) The existence of monopoles in nature leads to the consideration of the FRGG of symmetry as an extension of the SM in the sense that, using monopoles corresponding to the family-replicated gauge fields, we can bring the monopole charge down from the unbelievably large value which it gets in the simple SM, according to the Dirac relation.

(ii) If our $(3+1)$-dimensional spacetime is discrete and has a lattice-like structure, then the lattice artifact monopoles play an essential role near the Planck scale if the FRGGM works there. We have approximated these artifact monopoles by the Higgs scalar fields.

(iii) The breakdown of FRGG at $\mu_G \sim 10^{14}$ GeV produces a lot of fermions in the region $\mu_G < \mu < \mu_{\rm Pl}$, which gives the suppression of asymptotic freedom near the Planck scale.

(iv) In contrast to the anti-GUT by Froggatt–Nielsen, predicting the absence of supersymmetry and unification up to the Planck scale, these fermions,

together with monopoles, lead to the possible existence of unification of all interactions (including gravity) at

$$\mu_{\mathrm{GUT}} = 10^{18.4}\ \mathrm{GeV}$$

and

$$\alpha_{\mathrm{GUT}}^{-1} = 27.$$

(v) The possibility of $[SU(5)]^3$ SUSY or $[SO(10)]^3$ SUSY unifications was discussed in the present investigation.

ACKNOWLEDGMENTS

We are deeply grateful to D. Bennett, C. Froggatt, R. Nevzorov, and Y. Takanishi for fruitful discussions and comments.

One of us (L.V.L.) thanks the Niels Bohr Institute for hospitality and financial support.

The ITEP researchers thank the Russian Foundation for Basic Research (project no. 02-02-17379) for financial support.

REFERENCES

1. N. Arkani-Hamed, A. G. Cohen, H. Georgi, *et al.*, hep-th/0104005; hep-ph/0105239; hep-ph/0206020; hep-ph/0206021.
2. H. B. Nielsen, in *Proc. of the XVII Scottish University Summer School in Physics, St. Andrews, 1976*, p. 528; C. D. Froggatt and H. B. Nielsen, *Origin of Symmetries* (World Sci., Singapore, 1991).
3. C. D. Froggatt, G. Lowe, and H. B. Nielsen, Phys. Lett. B **311**, 163 (1993); Nucl. Phys. B **414**, 579 (1994); **420**, 3 (1994); C. D. Froggatt, H. B. Nielsen, and D. J. Smith, Phys. Lett. B **385**, 150 (1996); C. D. Froggatt, M. Gibson, H. B. Nielsen, and D. J. Smith, Int. J. Mod. Phys. A **13**, 5037 (1998).
4. H. B. Nielsen and Y. Takanishi, Nucl. Phys. B **588**, 281 (2000); **604**, 405 (2001); Phys. Lett. B **507**, 241 (2001); hep-ph/0011168; hep-ph/0101181; hep-ph/0101307; C. D. Froggatt, H. B. Nielsen, and Y. Takanishi, Preprints DESY 02-006, GUPTA/01/12/01, NBI-HE-01-12; hep-ph/0201152.
5. L. V. Laperashvili and D. A. Ryzhikh, in *Festschrift for H. B. Nielsen* (Ljubljana, 2001); Preprint No. 24-01 (Inst. Theor. Exp. Phys., Moscow, 2001); hep-th/0110127.
6. J. Schwinger, Phys. Rev. **144**, 1087 (1966); **151**, 1048 (1966); **151**, 1055 (1966); **173**, 1536 (1968); Science **165**, 757 (1969); **166**, 690 (1969).
7. S. Coleman, in *The Unity of the Fundamental Interactions, Erice Lectures, 1982*, Ed. by A. Zichichi (Plenum, 1983), p. 21.
8. M. Blagojevic and P. Senjanovic, Phys. Rep. **157**, 234 (1988).
9. L. V. Laperashvili and H. B. Nielsen, Mod. Phys. Lett. A **14**, 2797 (1999).
10. D. Zwanziger, Phys. Rev. D **3**, 880 (1971); R. A. Brandt, F. Neri, and D. Zwanziger, Phys. Rev. D **19**, 1153 (1979).
11. J. Jersak, T. Neuhaus, and P. M. Zerwas, Phys. Lett. B **133B**, 103 (1983); Nucl. Phys. B **251**, 299 (1985); H. G. Everetz, J. Jersak, T. Neuhaus, and P. M. Zerwas, Nucl. Phys. B **251**, 279 (1985); J. Jersak, T. Neuhaus, and H. Pfeiffer, Phys. Rev. D **60**, 054502 (1999); Nucl. Phys. B (Proc. Suppl.) **83–84**, 491 (2000).
12. M. B. Voloshin and K. A. Ter-Martirosyan, *Theory of Gauge Interactions of Elementary Particles* (Énergoatomizdat, 1984).
13. P. Langacker and N. Polonsky, Phys. Rev. D **47**, 4028 (1993); **49**, 1454 (1994); **52**, 3081 (1995).
14. S. Coleman and E. Weinberg, Phys. Rev. D **7**, 1888 (1973).
15. D. R. T. Jones, Nucl. Phys. B **75**, 531 (1974); Phys. Rev. D **25**, 581 (1982).
16. D. L. Bennett and H. B. Nielsen, Int. J. Mod. Phys. A **9**, 5155 (1994); **14**, 3313 (1999).
17. T. Suzuki, Prog. Theor. Phys. Suppl. **131**, 633 (1998).
18. M. N. Chernodub and M. I. Polikarpov, in *Cambridge 1997, Confinement, Duality, and Nonperturbative Aspects of QCD*, Ed. by Pierre van Baal (Plenum Press, 1998), p. 357; hep-th/9710205; M. N. Chernodub, F. V. Gubarev, M. I. Polikarpov, and A. I. Veselov, Prog. Theor. Phys. Suppl. **131**, 309 (1998); hep-lat/9802036; M. N. Chernodub, F. V. Gubarev, M. I. Polikarpov, and V. I. Zakharov, Nucl. Phys. B **592**, 107 (2000); **600**, 163 (2001).
19. L. V. Laperashvili and H. B. Nielsen, in *Proc. of the Int. Workshop on What Comes Beyond the Standard Model, Bled, Slovenia, 1998* (Ljubljana, 1999), p. 15.
20. L. V. Laperashvili and H. B. Nielsen, Int. J. Mod. Phys. A **16**, 2365 (2001).
21. L. V. Laperashvili, H. B. Nielsen, and D. A. Ryzhikh, Int. J. Mod. Phys. A **16**, 3989 (2001).
22. L. V. Laperashvili, H. B. Nielsen, and D. A. Ryzhikh, Yad. Fiz. **65**, 377 (2002) [Phys. At. Nucl. **65**, 353 (2002)].
23. G. 't Hooft, Nucl. Phys. B **190**, 455 (1981).
24. S. Rajpoot, Nucl. Phys. B (Proc. Suppl.) **51A**, 50 (1996).

Physics of Atomic Nuclei, Vol. 66, No. 11, 2003, pp. 2078–2091. Translated from Yadernaya Fizika, Vol. 66, No. 11, 2003, pp. 2128–2140.

ELEMENTARY PARTICLES AND FIELDS
Theory

Gravitation Interactions at High Energies and Reggeon Scheme

O. V. Kancheli*

Institute of Theoretical and Experimental Physics,
Bol'shaya Cheremushkinskaya ul. 25, Moscow, 117259 Russia

Received January 22, 2003; in final form, May 26, 2003

Abstract—A parton–Reggeon model that, for basic partons, employs gravitons of virtuality on the order of the Planck scale is proposed to describe inelastic interactions at trans-Planckian energies. A graviton analog of the Pomeron with an intercept of $\alpha(0) = 3$ is introduced on the basis of the structure of the gravitational field of a fast particle. Its unitarization leads to inelastic cross sections growing in proportion to s and corresponds to the pattern of a collision between black disks of radius about $E_i^{1/2}$. The inclusive spectra of hard gravitions whose behavior is determined by the size of the region of overlap of colliding black disks at various impact parameters and various energies is found. The graviton system formed in this way proves to be unstable against the gravitational attraction of particles having close momenta. This leads to the emergence of a multiperipheral chain of black holes at the stage of divergence—the structure of such a chain depends greatly on the impact parameters of a collision. © *2003 MAIK "Nauka/Interperiodica".*

1. INTRODUCTION

Mechanisms that are responsible for the gravitational interaction of particles at trans-Planckian energies of $\sqrt{s} \gg m_p = G^{-1/2}$ have yet to be understood conclusively, although this issue has been explored for a long time [1–9]; some of the more recent studies are also worthy of note (see, for example [10–17]). Of course, the inability of modern particle theory to provide a decisive solution is due to the complexity of the problem itself and to the complete absence of experimental data. There are presently a few reasons for which a further study of this issue is of interest.

(i) Gravitational interaction becomes strong for $\sqrt{s} \gg m_p$. In view of this, its dynamics may have many features in common with the dynamics of hadron interactions, whose asymptotic behavior is controlled, to a considerable extent, by the set of nonlinear unitarity conditions. Therefore, an attempt at extending, to the case of gravitational interactions, basic methods that are successfully used to describe high-energy processes (such as the Reggeon approach and partons) would be quite reasonable.

(ii) At energies of $\sqrt{s} \gg m_p$, it is natural to expect the production of black holes that proceeds with large cross sections of about s/m_p^2. The pattern behind this, albeit a rather naive one, is the following. In a collision process, a high energy of about $\sqrt{s}$ is concentrated in a small spatial region. The static Schwarzschild radius corresponding to this mass is large, about $\sqrt{s}/m_p^2$. Therefore, it is possible that, in such a collision, there will arise a horizon of events that has transverse dimensions of about $\sqrt{s}/m_p^2$ and which will capture colliding particles and will transform into a long-lived black hole. Approaches in which a more precise picture were proposed in [1–9], but they also employ the classical general theory of relativity in configurations where curvatures are much greater than the Planck value.

(iii) In recent years, a number of models was proposed where the Planck scale $m_p \sim 10^{19}$ GeV falls effectively down to occur in the teraelectronvolt region [18]. If such a possibility is realized in nature, then gravitational interactions (and, hence, string interactions together with them) may become the subject of an experimental investigation at next-generation colliders.

A direct consideration of these issues within string theories is of course possible in principle and is the most consistent, but it so involved that only the first attempts have been undertaken along these lines. The situation here is similar to that in QCD, where a direct approach to describing soft processes characterized by large cross sections is yet impossible, although qualitative arguments inspired by QCD are of considerable use for obtaining deeper insight into the structure and magnitudes of quantities appearing in Reggeon phenomenology and the parton model.

In the approach employed in this study to tackle the above range of problems, we follow the Reggeon

*e-mail: kancheli@heron.itep.ru

1063-7788/03/6611-2078$24.00

scheme of strong interactions rather closely, taking into account the fact that gravitons are massless only through a correction. If gravity obeyed a massive theory (with the graviton mass satisfying the condition $\mu_g \ll m_p$) and if, at the same time, it were cut off at the Planck or the string scale, then the pattern of gravitational interactions would probably be similar to that in hadron collisions. But for $\mu_g \to 0$, there would appear new transverse long-wave effects; accordingly, the relevant cross sections would grow faster—the Froissart cross-section behavior $\sigma \sim (1/\mu_g^2)\ln^2 s$ would gradually give way to the power-law form $\sigma \sim (1/m_p^2)(s/m_p)^c$. However, no significant changes in the vicinity of the Planck scale is expected upon such a transition.

In the present study, we will also employ, to the maximum possible degree, the parton interpretation of the Reggeon scheme, since this interpretation absorbs all of the basic constraints that follow from the s-channel unitarity. For partons, we choose gravitons themselves and assume that, at the Planck scale, there is a short-wavelength cutoff following from the string approach.[1)]

The ensuing exposition is organized as follows. We begin by considering the gravitational field of a fast particle and expand it in terms of partons—this will yield the zero-order approximation to the parton wave function. We will then discuss changes that higher order corrections introduce in this parton distribution. As a result, we will arrive at a Reggeon whose intercept is $\alpha(0) = 3 + \Delta$ and which is an analog of the Pomeron for gravitational interactions. Further, we will estimate the effect of the fact that the graviton is massless on the contribution of this Reggeon. After that, we will discuss the unitarization of the problem being studied and consider some applications—specifically, we will calculate inclusive cross sections and estimate possible long-wave instabilities of the final state that lead to the formation of black holes.

2. GRAVITONS AS PARTONS: WW APPROXIMATION AND GRAVITON CASCADE

The simplest way to find the gravitational field of a fast particle whose mass is much less than the Planck mass, $m \ll m_p = G^{-1/2}$, is to boost the Schwarzschild solution in isotropic coordinates. For high energies of $E \gg m_p$, this yields a result that is nearly identical to that which corresponds to a boost of the Newtonian solution; that is,

$$g_{\mu\nu} - g^{(0)}_{\mu\nu} \simeq \frac{2GP_\mu P_\nu}{\sqrt{m^2x_\perp^2 + E^2(z-\beta t)^2}}, \qquad (1)$$

where $g^{(0)}_{\mu\nu}$ is the Minkowski metric, P_μ is the 4-momentum of the particle being considered, and $\beta = p/E$. Going over to the limit $\beta \to 1$ and performing a coordinate transformation that is singular in t and z, we can represent this metric in the standard Aichelburg–Sexl (AS) form [19]

$$ds^2 = dx^+dx^- + 4GE\ln x_\perp^2\,\delta(x^-)(dx^-)^2 - (dx_\perp)^2, \qquad (2)$$

where $x^+ = t + z$, $x^- = t - z$, and $x_\perp$ are the light-cone coordinates.

Let us now proceed to consider a parton representation of this metric. Of course, the choice of partons is not unambiguous. Possibly, some string coordinates (string bits [20]) would be the "best" partons, but the character of their interaction at high densities is unknown at present. For this reason, we will take transverse gravitons for partons and, for their spectra at $k_\perp \geq m_p$, use a prescription suggested by the string pattern (as a matter of fact, we merely cut them off at $k_\perp \sim m_p$).

Going over to the Fourier components of the metric,

$$\sum_\lambda a^\lambda(k)\epsilon^{(\lambda)}_{\mu\nu} = \omega\int d^3x e^{ikx}(g_{\mu\nu}(x) - g^{(0)}_{\mu\nu}(x)), \qquad (3)$$

where $\epsilon^{(\lambda)}_{\mu\nu}$ is the graviton polarization tensor and $\omega = \sqrt{k_z^2 + k_\perp^2}$, and substituting the AS metric from (2) or directly expression (1) into the expression on the right-hand side of (3), we obtain

$$\sum_\lambda a^\lambda(k)\epsilon^{(\lambda)}_{--} = \frac{E}{m_p}\omega\frac{1}{k_\perp^2}. \qquad (4)$$

It is convenient to use the gauge where $\epsilon^{(\lambda)}_{+\mu} = 0$. From the transverseness conditions $k^\mu\epsilon^{(\lambda)}_{\mu\nu} = 0$, we obtain the following relation between the longitudinal and the transverse projection of the polarization tensor:

$$\epsilon^{(\lambda)}_{--} = \epsilon^{(\lambda)}_{\perp\perp}\frac{(k^+)^2}{k_\perp^2}. \qquad (5)$$

If $a^\lambda(k)$ is normalized in accordance with (3), the total number of partons (transverse gravitons) in the field of a fast particle is given by

$$N = \int d^3k n^\perp(k) = \int\frac{d^3k}{\omega}\sum_\lambda a^\lambda(k)a^{+\lambda}(k). \qquad (6)$$

[1)] For the sake of simplicity, we will not take into account massless string degrees of freedom other than gravitons (such as the dilaton) or higher massive excitations. Moreover, we will not distinguish between the string scale and the Planck scale, since, within our consideration, this would probably lead only to additional coefficients.

Substituting (4) and (5) into (6), we obtain $n^{\perp}(k)$, which is the spectrum of gravitons in an AS disk; that is,

$$dn^{\perp}(E,\omega,k_{\perp}) \sim \frac{(a^{\lambda})^2}{\omega} d\omega d^2k_{\perp} \tag{7}$$
$$\sim \left(\frac{E}{m_p}\right)^2 \frac{\omega}{(k^+)^4} dk_z dk_{\perp}^2 \sim \left(\frac{E}{m_p}\right)^2 \frac{d\omega}{\omega^3} d^2k_{\perp}.$$

This spectrum differs significantly from "ordinary" QED spectra of vector partons[2)] both in the character of the dependence on ω and $k_{\perp}$ and in the general growth of the parton density in proportion to E^2.

Let us now discuss higher order corrections to these parton spectra. If gravitation is literally treated as a nonrenormalized theory, it is of course difficult to isolate the classes of dominant diagrams. But if one assumes that transverse momenta are cut off at some effective scale (about the Planck mass m_p), then ladder diagrams generating a "leading" Reggeon may become dominant, in just the same way as in superconvergent theories. As to further corrections, they can be obtained by systematically constructing various Reggeon diagrams from this Reggeon, whereby the complete unitarity of the approach is ensured.

In terms of partons, ladder diagrams can be associated with a parton cascade in which there arises an additional growth of the number of low-energy partons. The spectrum corresponding to such a parton cascade can be represented as a chain of $L-1$ successive convolutions of the primary spectra $n^{\perp}(\omega_i,\omega_{i+1},k_{\perp})$ belonging to the type in (7). As a result, we obtain

$$\int d\omega_1 d^2k_1 n^{\perp}(E,\omega_1,k_1) \tag{8}$$
$$\times \int d\omega_2 d^2k_2 n^{\perp}(\omega_1,\omega_2,k_2)\ldots$$
$$\times \int d\omega_{L-1} d^2k_{L-1} n^{\perp}(\omega_{L-1},\omega_L,k_L)$$
$$\sim \frac{\Delta^L}{(L-1)!}\left(\frac{E}{m_p}\right)^2 \frac{1}{\omega_L^3} \ln^{L-1}\left(\frac{E}{\omega_L}\right),$$

where

$$\Delta = m_p^{-2} \int d^2k_{\perp} \Gamma^2\left(\frac{k_{\perp}^2}{m_p^2}\right). \tag{9}$$

In order to take into account nonlocal (string) effects, which are responsible for the cutoff at high $k_{\perp}$, we also included in (8) the effective dimensionless graviton-emission vertices Γ; at low $k_{\perp} \ll m_p$, these vertices reduce to $\Gamma(k_{\perp}^2/m_p^2) = 1$. Performing summation over the number L of steps in the cascade, we obtain Reggeized parton–graviton spectra:

$$dn^{\perp}(E,\omega,k_{\perp}) = \left(\frac{E}{m_p}\right)^2 \left(\frac{E}{\omega}\right)^{\Delta} \frac{d\omega}{\omega^3} d^2k_{\perp}. \tag{10}$$

Such spectra are more strongly concentrated at low values of ω than the primary spectra in (7). However, the actual value of Δ may prove to be equal to zero, in which case the mean number of steps in a cascade does not grow asymptotically with energy, and we adduce arguments in favor of this below.

It should be noted that the parton spectra in (7) and (10) must be treated with caution since they violate the sum rules for the longitudinal momentum at $E \gg m_p$; the total momentum calculated with the aid of (10) grows in proportion to $E^{2+\Delta}$. We will correct this by introducing the saturation of partons (see below). It should also be noted that the quantity Δ is strictly positive only for symmetric (ladder) diagrams. Moreover, logarithmic corrections belonging to the $1/\ln^{2a}(E/\omega)$ type, where $a \sim 1$, and changing the character of the corresponding Regge singularity are possible for the most interesting case of $\Delta = 0$ in (10).

We will now consider, in a cascade (Reggeon), that the graviton is massless. Because of this, infrared contributions to the primary spectra $n^{\perp}$ appearing in (8) arise from the $k_{i\perp} \to 0$ regions. If some steps in the cascade in (8) involve small $k_{i\perp} \to 0$, then, in the space of impact parameters b, these steps (cells of the Reggeon ladder) correspond to large jumps $\delta b \sim k_{i\perp}^{-1}$. These jumps shift the hard cascade to a far region in b, with the result that the relevant expectation value becomes $\langle \delta b \rangle \sim m_p^{-1}$. This behavior of infrared cells leads to singularities of the $t\ln t$ type in t-channel amplitudes.

In order to take this phenomenon into account, we rewrite expressions for the parton cascade in (8) in terms of impact parameters; in $n^{\perp}(E,\omega,k_{\perp})$, this corresponds to a transition from $k_{\perp}$ to $x_{\perp}$. We start from one soft cell. Making a Fourier transformation in amplitudes, we can easily find the distribution of partons for $x_{\perp} \gg m_p^{-1}$. The result is

$$\frac{\partial^3 n}{\partial\omega\partial^2 x_{\perp}} \sim \left(\frac{E}{m_p}\right)^2 \frac{1}{\omega^3} \frac{1}{x_{\perp}^4}. \tag{11}$$

[2)] With the aid of the procedure usually used in textbooks on field theory, the spectra given by (7) can also be obtained from the Weizsäcker–Williams factorization of diagrams involving one-graviton exchange. Expression (7) can straightforwardly be generalized to the case of fields of arbitrary spin J. The result is $dn^{\perp} \sim g_J^2 \left(\frac{k_{\perp}E}{\omega}\right)^{2J} \left(\frac{\omega d\omega}{E^2}\right) \frac{d^2k_{\perp}}{k_{\perp}^4} = g_J^2 \frac{dx}{x^{2J-1}} \frac{d^2k_{\perp}}{k_{\perp}^{2(2-J)}}$, where $x = \omega/E$ is a scaling variable and g_J stands for the relevant coupling constants: $g_1 \leftrightarrow e_{\mathrm{QED}}$, $g_2 \leftrightarrow \sqrt{G}, \ldots$.

In (11), the mean transverse momenta of partons for $x_\perp \gg m_p^{-1}$ are about $\sim x_\perp^{-1}$; under such conditions, the spectra in (11) are actually determined by means of the substitution $\partial n/\partial x_\perp \sim \partial n/\partial k_\perp^{-1}$ in (7).

But if, in the cascade in (8), we insert two or more infrared chains, then we will obtain a smaller contribution at larger b. In order to demonstrate this, we note that, upon the convolution of two spectra belonging to the type in (11), there arise the integrals

$$\int\limits_{|x_\perp - b_i| > m_p^{-1}} d^2x_\perp/(b_1 - x_\perp)^4(x_\perp - b_2)^4 \sim m_p/(b_1 - b_2)^4,$$

in which, for $(b_1 - b_2)^2 \gg m_p^{-2}$, the main contribution comes from the regions near the boundaries of integration, in which case one of the cells is hard.

The spectra in (11) for $x_\perp \gg m_p^{-1}$ are associated with soft gravitons characterized by $\langle k_\perp \rangle \sim x_\perp^{-1}$, but their energies ω may be much greater than m_p. Therefore, such gravitons may in turn serve as a source for gravitons with $\langle k_\perp \rangle \sim m_p$ in subsequent hard steps of the cascade. Further, a simple generalization of (8) and (11) yields the Reggeized spectra

$$\frac{\partial^3 n}{\partial\omega\partial^2 x_\perp} \sim \left(\frac{E}{m_p}\right)^2 \left(\frac{E}{\omega}\right)^\Delta \frac{1}{\omega^3}\frac{1}{x_\perp^4}, \qquad (12)$$

$$\frac{\partial n}{\partial x_\perp^2} \sim \left(\frac{E}{m_p}\right)^{2+\Delta} \frac{m_p^2}{(m_p x_\perp)^4}$$

for hard partons characterized by $\langle k_\perp^2 \rangle \sim m_p^2$ and $x_\perp \gg m_p^{-1}$.

Let us now consider the interaction between a pointlike target and a fast particle whose partonic spectrum is given by (10). The growth of the total inelastic cross section with energy is described by the formula

$$\sigma_{\text{in}} = \int d\omega d^2k_\perp n(E, \omega, k_\perp)\hat{\sigma}(\omega, k_\perp) \sim s^{2+\Delta}, \qquad (13)$$

where $\hat{\sigma}$ is the cross section for parton scattering on a pointlike target.

3. GRAVITATIONAL ANALOG OF THE POMERON

Cross sections growing in accordance with (13) correspond to a Regge pole in the vacuum channel with the intercept

$$\alpha(0) = 3 + \Delta. \qquad (14)$$

This Reggeon can be treated as an analog of the Pomeron for gravitational interactions (for the sake of brevity, we will hereafter refer to this Reggeon as the $2G$ particle).[3] The cross section (13) can be rewritten in the space of impact parameters as

$$\sigma_{\text{in}}(s, b) \sim \left(\frac{s}{m_p^2}\right)^{2+\Delta} \frac{1}{(bm_p)^4}. \qquad (15)$$

The generalization of (15) to the case of an arbitrary number of (soft) infrared steps in a cascade (soft loops in the $2G$ Reggeon) has the form

$$\sigma_{\text{in}}(s, b) \sim \left(\frac{s}{m_p^2}\right)^{2+\Delta} \left(\frac{a_0}{\ln s}\exp\left(\frac{-b^2}{4\alpha' \ln s}\right) + \frac{a_1}{(bm_p)^4} + \frac{a_2 \ln b}{(bm_p)^6} + \ldots\right), \qquad (16)$$

where numerical coefficients have only been introduced to distinguish between contributions from different numbers of soft loops. In expression (16), the first term, which is proportional to a_0, corresponds to the contribution featuring no soft loops, $\alpha' \sim m_p^{-2}$, while the terms that follow correspond to loop contributions—the generic term proportional to a_n stems from the contribution involving n soft loops. The following structure of t-channel singularities in the elastic-scattering amplitude at $t \sim 0$ corresponds to this expression:

$$a_0 + a_1 t \ln t + a_2 (t \ln t)^2 + \cdots. \qquad (17)$$

From (16), it can be seen that, for $b \gg m_p^{-1}$, only one-soft-cell contributions, which lead to the term proportional to a_1, are significant. It follows that the terms in (17) that are singular in t can formally be included in the $(g_0(t) \to g_0(t) + g_1(t)\ln t + \ldots)$ vertices, which are associated with the exchange of a $2G$ Reggeon, although a wider rapidity interval may correspond to relevant cells.

It should be noted that, in contrast to what occurs in massive theories like QCD, only the first term, which involves a_0 and which decreases fast at large b [in proportion to $\exp(-b^2/(4\alpha' \ln s))$], is present in (16) if there are no massless particles in the spectrum. Upon unitarization, this leads to the Froissart behavior of cross sections ($\sim \ln^2 s$).

Let us now consider the unitarization of the gravitational cross sections (15). The cross sections

[3] States of the $2G$ type are not seen in "perturbative" sectors of string theories. Since the mean number of steps in a cascade is probably finite in view of the vanishing of Δ ($\Delta = 0$), it is more plausible that a $2G$ state must not be seen in principle—it may be masked by that contribution to the S matrix which corresponds to a unitarized black disk. Possibly, it is a composite state that manifests itself only in the case of strong coupling as some membrane-like object.

$\sigma_{\rm in}(s,b)$ grow fast with E and, at some E values dependent on b exceed the maximum possible value allowed by the unitarity condition, $\sigma_{\rm in}=1$, this upper limit corresponding to the absorption of the entire flux from the initial state at given b with a subsequent transition to other states.

The simplest way to remedy the situation without changing the parton wave function itself is to take into account parton shadowing during the interaction. Usually, this is done by means of one type of elastic eikonalization or another, in which case

$$\sigma_{\rm in}(s,b)\to F\big(\sigma_{\rm in}(s,b)\big), \tag{18}$$

where the function $F(v)$ is such that

$$F(v)\to 1 \text{ for } v\to\infty,$$

$$F(v)\simeq v \text{ for } v\ll 1.$$

The most popular form of eikonal unitarization is that for which $F(v)=1-\exp(-v)$. In terms of partons, it corresponds to the following: if a parton colliding with a dense target interacts, on average, with v particles and if these interactions are independent, then the probability $|S(s,b)|^2$ that this parton undergoes no interaction is given by the Poisson expression $\exp(-v)$, and this is the result that leads to the eikonal formula.

What is of importance is that, for any reasonable form of $F(v)$, the corresponding $S(s,b)$ matrix involves the contribution from a black disk, where the parton density $\partial n/dx_\perp^2$ in (12) exceeds the critical value of about m_p^2. The radius of this disk is determined from the condition $\sigma_{\rm in}(s\simeq 2mE,b)\sim 1$. The result is

$$R_\perp^2(E)\simeq m_p^{-2}\Big(\frac{E}{m_p}\Big)^{1+\Delta/2}. \tag{19}$$

Beyond this black disk, where $x_\perp>R_\perp(E)$, the density of gravitons playing the role of partons decreases as

$$\frac{\partial n}{\partial x_\perp^2}\sim m_p^2\Big(\frac{R_\perp(E)}{x_\perp}\Big)^4. \tag{20}$$

Unitarized expressions of the type in (18) for $\sigma_{\rm in}(s,b)$ take into account the mutual shadowing of partons in the process of their interaction with the target. But at the same time, the actual mean density of partons in a stationary state of a fast particle is given by the same expression (10), which grows with energy. It follows that, for $b<R_\perp(E)$, the two-dimensional density of partons having an energy $\omega\sim m_p$ considerably exceeds the Planck density; since such partons strongly interact with one another, their mean transverse momentum in such a state must be on the order of the inverse mean spacing between neighboring partons (more precisely, on the order of the mean inverse range in the parton medium of such density); that is, we generally have $\langle k_\perp\rangle\gg m_p$.

However, this is at odds with our basic assumption that the spectra of partons are cut off for $k_\perp\gg m_p$ (removed from the states being considered). Therefore, we also assume that the parton density is saturated[4)] at the scale on the order of the Planck scale m_p^2, ceasing to grow with energy in the internal part of the disk, where $x_\perp<R_\perp(E)$. In just the same way as this occurs in QCD, parton recombination may be the only mechanism responsible for this stabilization. The corresponding total S matrix

$$S(y,b)=\exp(i\delta_R(y,b)-\delta_I(y,b)) \tag{21}$$

involves the real part $\delta_R(y,b)$ of the phase shift; for large b, $b>R_\perp(E)$, this real part coincides with the "classical" phase shift

$$\delta_R(y,b)\sim\Big(\frac{s}{m_p^2}\Big)\ln\frac{B_0}{b}$$

and is responsible for elastic scattering. The imaginary part $\delta_I(y,b)$ of the phase shift decreases fast for $b>R_\perp(E)$: $\delta_I\simeq\sigma_{\rm in}^{(0)}(s,b)$. If partons are saturated within the black disk, the imaginary part of the phase shift is given there by $\delta_I(y,b)\simeq 1$ and is independent of b.

Such a black disk is similar to the parton black disk arising in the hadronic Froissart regime. The basic distinction consists in the energy dependence of the radius: $R\sim m^{-1}\ln(s/m^2)$ in the Froissart case for massive theories versus $R\sim m_p^{-2}\sqrt{s}$ in the case of massless gravity. Yet, it is difficult to estimate, for such a disk, its degree of blackness, which is given by $1-|S(y,b)|^2$, since it is governed by the

[4)] By the present time, many pieces of evidence have been accumulated that, in gravity and in string theory, the density of excited degrees of freedom can hardly exceed a maximum value that is determined by the Planck (string) scale (see, for example, the review article of Bousso [21]). The following pattern is popular at the moment: upon reaching (exceeding) this density, the system undergoes a transition to a different phase where it can adequately be represented only in terms of new degrees of freedom whose density is again less than the critical one. In this scenario, local fluctuations of the density that exceed the critical density are of course possible, but their contribution to the wave function is in all probability strongly suppressed. One cannot rule out the possibility that merely a faster recombination of extra degrees of freedom than their generation in the region of densities higher than the critical density always forms a basis for the corresponding microscopic mechanism.

details of dynamics at the Planck (string) scale.[5)] For the sake of simplicity, we assume below that, far from the boundaries, a saturated disk of Planck density is absolutely black, $|S|^2 = 0$. At a finite transparency that is independent of energy, additional coefficients of about unity arise in cross sections and spectra.

So far, we have considered only partons of energy $\omega \sim m_p$ since their contribution to the interaction is dominant. The above formulas can easily be generalized to partons of different energy ω; their spectrum at arbitrary ω and $x_\perp$ has the form

$$dn = F\big[\hat{n}(E,\omega,x_\perp)\big](m_p^2 d^2x_\perp)\frac{d\omega}{\omega}, \qquad (22)$$
$$\hat{n} = \Big(\frac{E}{\omega}\Big)^{2+\Delta}\frac{1}{(x_\perp m_p)^4},$$

where the density $\hat{n}$ is dimensionless and is invariant under boost transformations; as in (18), the operation $F[\ldots]$ corresponds to either unitarization or saturation. In terms of the logarithmic variables $Y = \ln(E/m_p)$, $y = \ln(\omega/m_p)$, and $\zeta = \ln(x_\perp m_p)^2$, the parton distribution (22) assumes a still simpler form; that is,

$$dn = F\big[e^{(2+\Delta)(Y-y)-\zeta}\big]dyd\zeta. \qquad (23)$$

From the condition $\hat{n} \sim 1$, we can obtain the radius of a black parton disk for various values of ω. The result is

$$R_\perp^2(E,\omega) = m_p^{-2}\Big(\frac{E}{\omega}\Big)^{1+\Delta/2}. \qquad (24)$$

It follows that, in the (ζ, y) space, the region that is filled with partons of saturated density is a cone whose boundary is given by $\zeta < (2+\Delta)(Y-y)$. In terms of the variables $x_\perp$ and ω, this corresponds to the region $x_\perp < R_\perp(E,\omega)$. The cone in question is surrounded by a diffuse cloud in which the parton distribution is given by the classic expression (23).

[5)] In QCD, we run into the analogous problem of the degree of transparency of a saturated Froissart disk. There, the two-dimensional density of partons (gluons) within the disk is not stabilized at a specific value of about $\Lambda_{\mathrm{QCD}}^{-2}$, but it continues indefinitely growing with energy; concurrently, the mean transverse momentum of partons in the disk grows. Therefore, the disk unboundedly blackens with increasing energy: $|S|^2 \to 0$. That the stabilization of the parton density is impossible in a theory featuring finite masses can be proven even on the basis of general arguments [22] by considering variations in the disk penetrability $|S|^2$ under longitudinal boosts. In gravitation, the picture is probably different, since a transverse long-range interaction, which was absent in the massive case, occurs here owing to zero mass of the graviton. In that case, a saturated disk may remain asymptotically gray, or it blackens because of some coherent mechanism associated with long-wave partons.

For soft partons of energy $\omega \ll m_p$, the density also seems to be saturated at values of $\hat{n} \sim 1$ up to $x_\perp \sim R_\perp(E,\omega)$, since we have assumed that, for partons with $k_\perp \sim m_p$, the density cannot exceed the Planck density m_p^{-2} and since these partons transform into soft partons under a longitudinal boost (see Section 5 below). On average, each such parton is localized (smeared) in the transverse plane within a region of dimension $\delta x_\perp(\omega) \sim 1/\omega$; therefore the density of partons is high on the natural quantum scale $(\delta x_\perp(\omega))^{-2}$, about $\hat{n}m_p^2(m_p\delta x_\perp)^2 \sim \hat{n}m_p^4/\omega^2$.

By comparing the size of the region of smearing, $\delta x_\perp(\omega)$, with the disk radius $R_\perp(E,\omega)$, we can find the critical values of $x_\perp$ and ω at which these two dimensions become commensurate:

$$x_\perp = \tilde{R}(E) \sim m_p^{-1}\Big(\frac{E}{m_p}\Big)^{1+2\Delta/(2-\Delta)},$$
$$\omega = \tilde{\omega} \sim 1/\tilde{R}(E).$$

For $x_\perp > \tilde{R}(E)$, the interaction of partons with the target is weak and basically reduces to classical elastic scattering and the classical emission of soft gravitational waves.

It can easily be proven that, on average, weakly interacting pointlike partons of energy ω are distributed over a longitudinal region having a dimension $l(\omega) \sim 1/\omega$ or a larger dimension—this yields the thickness of an ω disk. For basic partons forming a black disk, we have $l(\omega \sim m_p) \sim 1/m_p$. For partons of energy $\omega \gg m_p$, this leads to $l(\omega) \ll m_p^{-1}$, which looks suspicious and which probably requires an approach that directly employs string degrees of freedom. But for soft partons of energy $\omega \ll m_p$, the longitudinal dimensions of the localization region may become large and commensurate with the transverse dimensions, $l(\omega \sim \tilde{\omega}) \sim \tilde{R}(E)$.

To conclude this section, we note that, for the most interesting case of $\Delta = 0$, the expression for $R_\perp(E,\omega)$ may develop additional logarithmic corrections that change the form of (24), which would become

$$R_\perp^2(E,\omega) = \frac{E}{\omega m_p^2}\Big/\ln^a\Big(\frac{E}{\omega}\Big), \quad a \sim 1.$$

However, a more precise approach that is beyond the scope of the present study is required for refining this point.

4. INELASTIC GRAVITATIONAL PROCESSES

Let us now proceed to consider multiparticle-production processes in particle interactions at trans-Planckian energies. Such processes are predominantly determined by the excitation of partons in the

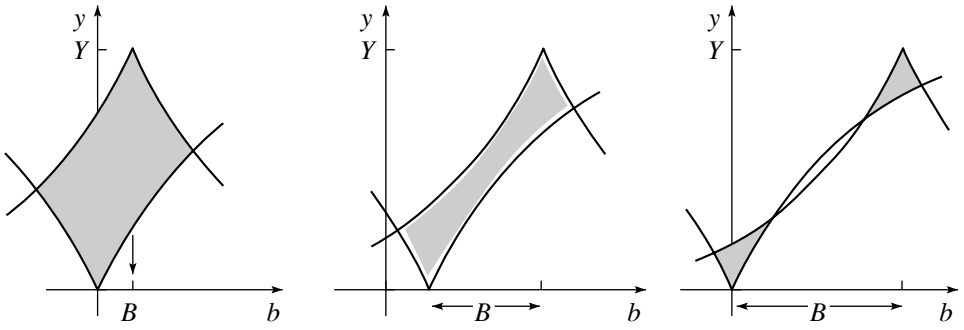

Fig. 1. Shapes of the overlapping regions (shaded regions) of colliding black disks in the (b, y) plane at various values of B. Only the projection $b_\perp$ is displayed. The width of the shaded region at a given value of y is approximately in direct proportion to the inclusive cross section at this value of y.

overlapping regions of colliding black disks. Since collisions of hard partons are local in $x_\perp$, it is natural to expect that the same degrees of freedom as those that were dominant in the initial state (these are gravitons with $k_\perp \sim m_p$) will be produced (released).

Here, we will make use of a rather general (albeit somewhat formal) approach where inclusive processes are constructed from cut Reggeons, the Reggeons themselves being such that they describe elastic scattering adequately and that they "correspond" to the partonic content of the fast particle involved. This approach, which is successfully applied to describing high-energy hadronic processes, is advantageous in that basic constraints following from t-channel unitarity prove to be automatically taken into account there. Also, we will simplify the situation considerably by taking, as a starting point, the unitarized S matrix (21), which corresponds to a saturated black disk (this matrix can be considered as an analog of the Froissaron in the case of QCD) rather than the $2G$ Reggeon.

As the main object intended for constructing Reggeon diagrams, we introduce the normalized Green's function defined in terms of the S matrix (21) as

$$D(y,b) = i(1 - S(y,b)) \qquad (25)$$
$$\sim i\,\theta\big(R_\perp^2(y) - b^2\big) + D^{\rm soft}(y,b),$$

where $D^{\rm soft}(y,b)$ is the soft component of D—it contains gravitons satisfying the conditions $\omega, k_\perp \ll m_p$.[6)] Further, the Green's function $D(y,b)$ can be used to calculate Reggeon diagrams for amplitudes and various inclusive cross sections. For example, the inelastic cross section for the production of gravitons characterized by $k_\perp \sim m_p$ is straightforwardly obtained by cutting $D(y,b)$:

$$\sigma_{\rm in}(Y) = \int d^2B\,{\rm Im}D(Y,B) \simeq \pi R_\perp^2(Y) + \sigma_{\rm in}^{\rm soft}(Y). \qquad (26)$$

The inclusive cross section corresponding to these processes and describing, at fixed values of the total energy $s = m_p^2 \exp(Y)$ and the impact parameter B, the production of a particle that has a specific transverse position b and a specific rapidity y is also readily expressed in terms of the contribution from a Reggeon diagram involving two cut D. The result is

$$\rho(y,b,Y,B) \simeq \gamma {\rm Im}D(y,b){\rm Im}D(Y-y,B-b) \qquad (27)$$
$$= V\theta\big(R_\perp^2(y) - b^2\big)\theta\big(R_\perp^2(Y-y) - (B-b)^2\big) + \rho^{\rm soft}(y,b,Y,B),$$

where γ is the inclusive vertex of the emission of gravitons characterized by $k_\perp \sim m_p$. This vertex depends, of course, on the details of dynamics at the Planck (string) scale and appears in (27) as a phenomenological parameter. Corrections from soft gravitions of energy $\omega \ll m_p$ and corrections from boundary effects were included in $\rho^{\rm soft}$.

By applying a similar procedure, one can easily construct two-particle correlation functions and other higher cross sections from $D(y,b)$.

Let us now consider the behavior of $\rho(y,b,Y,B)$ in greater detail. The region where the hard contribution to $\rho(y,b,Y,B)$ is not small is schematically shown in Fig. 1. Higher Reggeon diagrams for ρ, which involve additional loops of D, does not change ρ in the region where the black parts of D overlap. A similar mechanism of the cancellation of the contributions from loops involving the component $\theta\big(R_\perp(y) - b\big)$ of $D(y,b)$ was long ago indicated by Cardy [23] for the

[6)] Below, we assume everywhere (with the exception of Section 5) that $\Delta = 0$. This simplifies expressions appearing in the ensuing calculations and seems to correspond to a correct value.

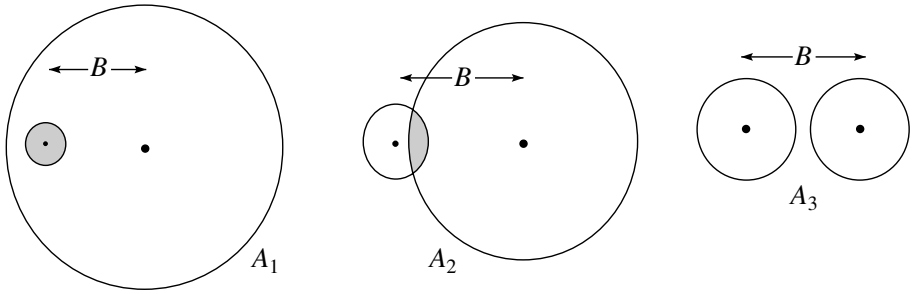

Fig. 2. Common configuration of colliding black disks at different rapidities and identical values of s and B. The pictures transform into one another under longitudinal boosts. Configuration A_1 is closer to the fragmentation region, while configuration A_3 refers to the c.m. frame; configuration A_2 is intermediate between them. There is a straightforward correspondence between these configurations and the inclusive spectra in Fig. 3.

Froissart case. At the same time, these contributions may be significant in the case where the edges of the disks touch each other. This is the region where there occur processes of diffractive generation and other peripheral processes.

At specific values of the rapidity y and the transverse coordinate $\mathbf{b}$, hard gravitons of transverse momentum $k_\perp \sim m_p$ can be formed only in collisions of those parts of the black disks that correspond to the same values of $\mathbf{b}$. This directly corresponds to the contribution of the overlap of two θ functions in (27). Therefore, the total inclusive spectrum of hard particles is proportional to the area of the region of overlap of two black disks at the preset value of the rapidity y.

For various values of B and y, there can arise three configurations of the overlap of these disks, as is shown in Fig. 2. For configurations of the A_1 and A_2 types, the disks overlap, and the area of the overlap region in Planck units, $A(B, R_\perp(E_1), R_\perp(E_2))$, determines the inclusive cross section at a given value of y. In configuration A_3, the black disks do not overlap at relevant values of B and y, so that the hard inclusive cross section is equal to zero.

If we disregard the smearing of the disk edges, then

$$\rho(B, y, Y) \simeq \gamma m_p^2 A(B, R_1, R_2), \qquad (28)$$

where $R_1 = R_\perp(E_1), R_2 = R_\perp(E_2), E_1 = m_p e^y$, and $E_2 = m_p e^{Y-y}$. The area $A(B, R_\perp(E_1), R_\perp(E_2))$ of the overlapping regions of the disks can be represented in the form

$$A \simeq \int d^2x_\perp \theta(R_1^2 - x_\perp^2)\theta(R_2^2 - |x_\perp - B|^2) \Rightarrow \begin{cases} A = \zeta_1 R_1^2 + \zeta_2 R_2^2 \ \text{ for } \ |R_1 - R_2| < B < R_1 + R_2 \\ A = \min(\pi R_1^2, \pi R_2^2) \ \text{ for } \ B < |R_1 - R_2|, \end{cases} \qquad (29)$$

where

$$\zeta_1 = \theta_1 - \frac{1}{2}\sin 2\theta_1, \quad \zeta_2 = \theta_2 - \frac{1}{2}\sin 2\theta_2,$$
$$\cos\theta_1 = \frac{B^2 + R_1^2 - R_2^2}{2BR_1}, \quad \cos\theta_2 = \frac{B^2 + R_2^2 - R_2^2}{2BR_2}.$$

The inclusive spectra corresponding to these expressions are schematically depicted in Fig. 3. The shape of the spectra depends greatly on the impact parameter, changing drastically from a structure having a sharp peak in y at the center for $B \sim 0$ to configurations featuring two small peaks near the edges of the spectrum at maximum values of $B \sim m_p^{-2}\sqrt{s}$. The region not filled with particles is formed around $y = Y/2$ in the central part of the inclusive spectrum for $B > B_{\rm cr}$, this occurring from $B = B_{\rm cr}$. This region corresponds to a configuration where only the edges of the two black disks touch each other, which determines $B_{\rm cr} = 2R_\perp(Y/2)$.

Obviously, the multiplicities of hard gravitons, $N(B, s) = \int \rho(B, y, Y)dy$, also strongly depend on B, and the character of this dependence changes sharply at $B \sim B_{cr} \sim m_p^{-1}(s/m_p^2)^{1/4}$. From (29), one can easily derive the approximate expression

$$N(B, s) = \theta\big(B_{\rm cr} - B\big)\frac{\sqrt{s}}{m_p} f\Big(\frac{B}{B_{\rm cr}(s)}\Big) + \gamma\frac{\theta\big(B - B_{\rm cr}\big)\theta\big(B_{\rm max} - B\big)}{(m_p B)^2}\frac{s}{m_p^2}, \qquad (30)$$

where the function

$$f(B/B_{\rm cr})$$

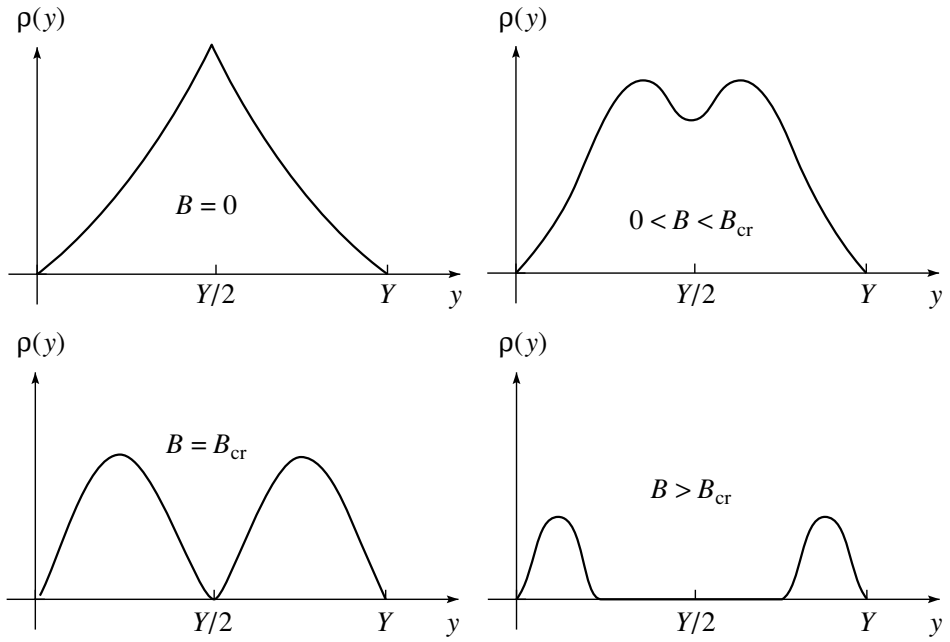

Fig. 3. Inclusive spectra of gravitons of transverse momenta $k_\perp \sim m_p$ for various values of the impact parameter B. Here, $B_{\rm cr}$ is the critical impact-parameter value at which the black parton disks of colliding particles begin to overlap in the c.m. frame.

$$= \frac{\gamma\, m_p}{\sqrt{s}} \int dy A\big(B, R_\perp(y), R_\perp(Y-y)\big) \sim 1$$

depends only slightly on the argument and $B_{\max} \sim m_p^{-3/2}\sqrt{s}$.

For $s \gg m_p^2$, the dimensions of the black disks are great, in which case possible local fluctuations of their density have virtually no effect on the mean number of product particles. Therefore, the multiplicity distribution of product hard particles is determined primarily by the geometric parameters of the collision—specifically, by fluctuations of B from one event to another. In this case, the distribution of the probability of formation of n hard gravitons can easily be estimated if the dependence $N(B,s)$ is known. This is done by inverting this dependence [$B = B(N,s)$]. The result is

$$w_n \simeq \frac{1}{n^2} + \left(\frac{m_p^2}{s}\right) f_1\left(n\frac{m_p}{\sqrt{s}}\right)\theta(n-n_{\rm cr}). \quad (31)$$

At small n, the term that decreases in proportion to $1/n^2$ and which receives contributions from collisions at large B, $B > B_{\rm cr}(s)$, is of importance in the distribution w_n. It corresponds to the second term on the right-hand side of (30) and to spectra featuring two maxima. The same region of n values makes a dominant contribution to the total inelastic cross section, that of order sm_p^{-4}. The term involving the function $f_1 \sim 1$, which is expressed in terms of f, is of importance only for $n > n_{\rm cr} \sim \sqrt{s}/m_p$ and arises from collisions at impact-parameter values in the region $B < B_{\rm cr}(s)$. In such processes, the multiplicity is large (about $\sqrt{s}$)—it is close to the maximum possible value; their cross sections grow only in proportion to $B_{\rm cr}^2(s) \sim m_p^{-2}\sqrt{s}/m_p$.

The mean multiplicity of hard gravitons that corresponds to (31) is small ($\langle n\rangle \sim 1$ for all s), but the variance of this distribution grows ($\langle n - \langle n\rangle\rangle^2 \sim \ln s$), albeit not sharply.

It is also noteworthy that, as follows from (28) and (29), the total inclusive spectra of hard gravitons,

$$\tilde\rho(y,Y) = \sigma_{\rm in}^{-1}(Y)\int d^2B\rho(B,y,Y) \quad (32)$$
$$\simeq \frac{\pi m_p^2 R_1^2 R_2^2}{R^2(s)} = \pi\frac{E_1E_2}{m_pE} \sim 1,$$

have a simple scaling form, as in the case of asymptotically constant total cross sections, although the corresponding multiplicity distribution (31) has nothing in common with the Poisson distribution. Also, the deviation from the Froissart regime is sizable here.

5. ON THE ROLE OF SOFT GRAVITONS TREATED AS PARTONS

For the inclusive production of hard particles at various values of y, we have considered above a simple partonic interpretation in terms of collisions of black disks filled with gravitons playing the role of partons and having the Planck density. However, an attempt

at developing a similar partonic interpretation of total inelastic cross sections runs into a difficulty.

The inelastic cross section corresponding to a collision of two black disks having energies E_1 and E_2,

$$\sigma_{\text{in}}(E_1, E_2) \simeq \pi\Big(R_\perp(E_1) + R_\perp(E_2)\Big)^2 \sim \Big(E_1^{(2+\Delta)/4} + E_2^{(2+\Delta)/4}\Big)^2,$$

depends on the choice of longitudinal coordinate frame. Under the longitudinal boost transformations

$$E_1 \to E_1\xi, \quad E_2 \to E_2/\xi, \tag{33}$$

the quantity $\sigma_{\text{in}}(E_1\xi, E_2\xi^{-1})$ is independent of ξ only at $\Delta = -2$, in which case the radii of the black disks exhibit no growth with energy. The quantity $\sigma_{\text{in}}(E_1, E_2)$ is maximal in the laboratory frame of one of the particles, where it coincides with the "invariant" expression (26). We then have the pattern of interaction between a large black disk and a slow (standing) target. In this coordinate frame, corrections from soft partons of energy $\omega \ll m_p$ are small. But in longitudinal coordinate frames, which are closer to the c.m. frame, the black disks do not overlap at the same large impact-parameter values of $B \sim \sqrt{s}/m_p^2$; however, the densities of soft partons are high, whence it follows that their interaction with the black disk of the other particles may lead to large cross sections.

The fact that, in the partonic description, the condition of the invariance of cross sections under boost transformations of the type in (33) may impose stringent constraints on dynamical quantities is interesting, but it is not surprising.[7)] A probable reason for this is that the condition requiring that all cross sections calculated in different longitudinal coordinate frames be invariant under boost transformations plays, for the partonic scheme, the role of the t-channel unitarity condition.

Before proceeding to estimate $\sigma_{\text{in}}(E_1, E_2)$ with allowance for soft partons, we will discuss the question of how particles of energy $\omega \ll m_p$ can interact with another black disk. For this, we will consider the interaction of a massless "test" particle of moderate energy E_2 with a trans-Planckian particle of energy E_1, assuming that $s \simeq 2E_1E_2 \gg m_p^2$. If we choose ξ (that is, the longitudinal coordinate frame) in such a way that $E_2 \sim m_p$, then, as was discussed above, the probability that the particle of energy E_2 is absorbed by the black part of the disk is equal to unity for all impact-parameter values satisfying the condition $x_\perp < x_{\perp 0} = R_\perp(E_1)$. This absorption initiates the excitation of the parton system of energy E_1 and subsequent particle production, as was described in the preceding section. The probability of such a process cannot depend on the choice of longitudinal coordinate frame. We now choose $\xi \gg 1$ in such a way that $E_2 \ll 1$, whereupon the interaction of the particle of energy E_2 for the same values of $x_\perp$ must not change—the particle in question must be absorbed by the black disk of energy E_1. But upon such a transition to a different coordinate frame, the radius of the black disk grows:

$$R_\perp(E_1) \to R_\perp(E_1\xi) = \xi^{1/2}R_\perp(E_1).$$

Therefore, the particle of energy E_2 must now be absorbed by the disk with a probability of unity at larger impact-parameter values of up to $x_\perp \sim \xi^{1/2}R_\perp(E_1)$. This probability must not depend on ξ either. Naturally, there arises the question of assessing values up to which one can increase ξ and, accordingly, maximum $x_\perp$ and simultaneously assume that the probability of soft-particle absorption remains equal to unity. For this, it is necessary, among other things, that the particle of energy E_2 be localized, to a fairly high degree of precision, within the black disk of energy E_1. It is clear that the dimension of the transverse region in which the particle is localized is not less than $1/E_2 \sim \xi$. This dimension grows with ξ faster than $R_\perp(E_1\xi) \sim \sqrt{\xi}$. Therefore, the condition of their equality, $1/E_2 \sim R_\perp(E_1)$, determines the minimum values $E_2 \ll m_p$ for which the probability of particle (parton) absorption by the black disk remains approximately equal to unity.

Let us now estimate maximum impact parameters B at which the probability of the capture of a soft parton from one disk by a part of the other black disk is equal to unity. Two conditions must be satisfied for this.

First, there is a geometric condition: the number of soft gravitons of energy $\omega \ll m_p$ that fall within the area of one of the colliding black disks and which belong to the tail of the distribution of partons with respect to b in the other black disk must not be less than unity:

$$\hat{n}(E_2, \omega, B)R_\perp^2(E_1, \omega_1 \sim m_p) \sim m_p^{-2}.$$

[7)] For massive theories like QCD, the asymptotic rate of growth of the partonic-black-disk radius $R_\perp(E)$ is determined, apart from a constant factor, from the condition of invariance of the inelastic cross section $\sigma_{\text{in}} = \pi(R_\perp(E_1\xi) + R_\perp(E_2/\xi))^2$ under variations of the boost-transformation parameter ξ. This condition yields only two solutions. These are $R_\perp(E) = \text{const}$ and $R_\perp(E) = c\ln E$, which lead to constant cross sections and the Froissart regime, respectively. Moreover, it can be proven, on the basis of invariance under boost transformations, that the blackness (nontransparency) of a Froissart disk becomes more pronounced with increasing energy [22].

Second, the dimension of the region of the transverse localization of a soft parton (on average, it is about $1/\omega$) must be much smaller than the radius of the other black disk; otherwise, a soft parton will predominantly undergo elastic scattering on the black disk instead of being captured by it. This yields a condition on minimal ω:

$$\omega R_\perp(E_1, m_p) \sim 1.$$

By employing these conditions and the explicit expressions (22) and (24) for, respectively, $\hat{n}$ and $R_\perp$ with an arbitrary intercept Δ, we can easily find $B = R_{\perp\max}$ and $\omega_{\min}$:

$$\omega_{\min} \sim m_p \Big(\frac{m_p}{E_1}\Big)^{(2+\Delta)/4},$$

$$(Bm_p)^2 \sim \Big(\frac{E_1}{m_p}\Big)^{1+3\Delta/4+\Delta^2/8} \Big(\frac{E_2}{m_p}\Big)^{1+\Delta/2}.$$

Therefore, the total inelastic cross section for the process being considered (in the chosen longitudinal coordinate frame) has the form

$$\begin{aligned}\sigma_{\text{in}}(E_1, E_2) &\sim \big(R_{\perp\max}(E_1, E_2)\big)^2 \\ &+ \big(R_{\perp\max}(E_2, E_1)\big)^2 \\ &\sim m_p^{-2}\Big(\frac{E_1}{m_p}\Big)^{1+3\Delta/4+\Delta^2/8} \\ &\times \Big(\frac{E_2}{m_p}\Big)^{1+\Delta/2} + \big(E_1 \leftrightarrow E_2\big).\end{aligned} \tag{34}$$

It can easily be verified that this cross section can be invariant under boost transformations (this corresponds to $\partial\sigma_{\text{in}}(E_1\xi, E_2\xi^{-1})/\partial\xi = 0$) only if the powers of E_1 and E_2 in (34) coincide. Only in this case is $\sigma_{\text{in}} \sim 2E_1E_2 \sim s$ independent of ξ, whence we obtain, for Δ, a condition that has two solutions,

$$\Delta = 0, \quad \Delta = -2.$$

The first solution corresponds to the cross section $\sigma_{\text{in}} \sim sm_p^{-4}$, which was considered in the preceding section, while the second solution is trivial and corresponds to constant $\omega_{\min} \sim m_p$ and $R_{\perp\max} \sim m_p^{-1}$.

6. FINAL-STATE INTERACTION: FORMATION OF A CHAIN OF BLACK HOLES

In the collision process, some partons are excited and are converted into free particles having inclusive spectra that are greatly dependent on B and E and which were described above. Within some time after a collision, product particles may continue interacting with their neighbors (until their three-dimensional density becomes small because of divergence), and this may additionally distort the spectra.

In the case of QCD, this final-state interaction is short-range; it follows that, although the spectra may undergo local changes because of resonance decays and some other low-energy reactions, the general structure of the spectra remains unchanged. In this case, the eventual spectra reproduce (apart from a factor of about unity) the spectra of product particles.

But in the case of gravity, we additionally have a long-wave interaction between product particles, and this may lead to the clustering of particles and to large distortions in the spectra of released partons.

The main instability is due to the attraction between particles of modest relative energy—that is, particles of the spectrum $\rho(y)$ that have close values of the rapidity y. Therefore, we can break down the spectrum $\rho(y)$, by convention, into rapidity layers of width $\delta \sim 1$ and choose δ in such a way that the relative energies of particles within the layers (these are predominantly gravitons characterized by $k_\perp \sim m_p$) are quite moderate. At the same time, δ must be such that particles from neighboring layers look like ultrarelativistic particles; that is, their mean longitudinal momenta must be much greater than their transverse counterparts.

It is of importance that immediately after a collision, the three-dimensional density of product particles is high—it is close to the critical density of about m_p^{-3}. Therefore, particles of close rapidity interact strongly with neighboring particles within a specific time interval, this taking place until the density of these particles becomes low. Owing to such a local interaction, the particles in question are thermalized to some extent and are delayed within a layer for some time. A much more comprehensive consideration, taking into account various details of string dynamics at Planck densities, is required for refining the value of δ, which is about unity. What is of importance for us here is that δ may be virtually independent of $s \gg m_p^2$ and B.

The following analogy is quite instructive. The longitudinal distribution with respect to the momenta of the system of particles produced in a collision of black disks (as well as in all multiperipheral reactions) is similar to that which would be observed in a one-dimensional expanding cosmological solution. In either case, particles are "injected" at the "initial instant," so that the distribution of particles logitudinally flying apart is identical in any longitudinally boosted coordinate frame. Moreover, the "injection" of particles (a transition of virtual partons to real particles) that occurs locally at $t = t_0 \sim m_p^{-1}$ takes place later by a time of about $t_0 \exp y$ in other longitudinally boosted systems (other layers) and, hence, at a longitudinal distance of about $t_0 \exp y$. In this analogy, the dimensions δ of the region are on the order of

distances to the horizon of events in the cosmological solution. In expanding cosmological solutions, the maximum dimensions of the regions in which the growth of density perturbations is possible are bounded by such a "horizon." For the same reasons, the formation of clusters larger than those that are contained in a region of dimension δ is improbable.

For the sake of simplicity, we have taken δ to be a constant equal to its mean value. Of course, the width of this region fluctuates; each time (and at each value of $x_\perp$ and y), it is determined by the density distribution of product (released) partons.

If we choose a longitudinal coordinate frame in such a way that a layer of given rapidity y_1 is at rest in it (this layer is indicated in Fig. 4), then particles from other lays fly apart fast in this coordinate frame. Moreover, these particles remain in a virtual (partonic) state for some time—only after a lapse of a time t of about $m_p \exp|y - y_1|$ do they become released (transform into free particles).

Therefore, we can consider a further evolution of this layer, disregarding the effect of other layers. Its mass is

$$M(y_1) \sim m_p^3 A(y_1, Y, B) \sim \rho(y_1, Y, B), \qquad (35)$$

where A is the transverse area of the layer corresponding to y_1. This mass of "thermalized" particles is concentrated in a spatial region of longitudinal dimension about $m_p^{-1} \exp(\delta)$, the transverse dimensions being about $\sqrt{A}$. These dimensions are much smaller than the dimensions of the horizon of a black hole having the same mass $M(y_1)$. At the same time, particles in the layer are not ultrarelativistic, the range being not longer than the longitudinal dimension of the layer (and the more so its transverse dimensions).

It follows that, within a time of about $\sqrt{A}$, the majority of the particles from the layer corresponding to y_1 will occur in a black hole having a mass $M(y_1)$ and a transverse position that is determined by the center of gravity of region A. Within the same time interval, the horizon "surrounding" the layer undergoes a transition from an oblate, pancakelike configuration to a sphere.[8)] It should be noted that this process may proceed through some stages of formation and subsequent fusion of smaller black holes corresponding to various $x_\perp$, since the transverse dimensions of a layer may be large.

The neighboring layers corresponding to $y_1 - \delta$ and $y_1 + \delta$ move fast with respect to the layer of rapidity y_1. They also undergo a transition to black holes having masses of $m_p\rho(y_1 - \delta)$ and $m_p\rho(y_1 + \delta)$, respectively, but this occurs much later, the velocities of these black holes with respect to the black hole of rapidity y_1 being about unity. In this way, a chain of black holes characterized by a multiperipheral rapidity distribution[9)] and masses determined by the quantity $\rho(y_1, Y, B)$ is formed from the layers.[10)]

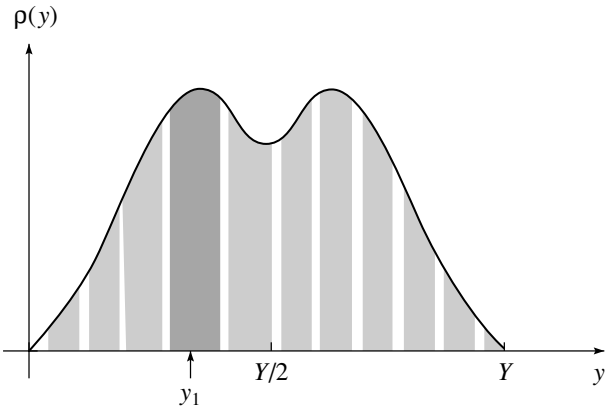

Fig. 4. Inclusive spectrum of product particles (gravitons) that is partitioned by convention into rapidity layers of width δ. The magnitude of δ is chosen in such a way as to correspond to the mean longitudinal dimension of the long-wave-instability region where the density grows. In the process of a further evolution, layers transform into black holes having the same values of the rapidity and mass, $\rho(y)$.

Since each such black hole is formed from a layer of partons having close longitudinal velocities, these black hole will not rotate. A slight rotation of a black hole may arise because of "thermal" fluctuations and boundary effects. But most of the angular momentum

[8)] The process of formation and growth of such horizons has so far been studied only for a classical evolution of the system. In terms of particles, the growth of the mutual coherence of product gravitons is likely to have some bearing on it.

[9)] It is possible that a uniform rapidity distribution of black holes is slightly distorted since the effective layer width δ can be weakly dependent on the layer mass (transverse dimensions).

[10)] Within this pattern of trans-Planckian interactions, black holes are formed because of final-state instability to long-wave attraction in a large cloud of product particles. In the evolution of the system, a long classical stage following the purely quantum stage of a collision between black partonic disks actually corresponds to this stage. In view of this, it is improbable that there exist simple operator constructions describing the production of black holes from the initial stage of colliding particles—in other words, it is hardly possible to find simple trajectories (instantons) in the relevant path integral that lead to the production of black holes. In this sense, a purely classical consideration of D'Eath [1], where, upon a collision of two AS disks, there can occur the focusing of their normals (partons), which is followed by the formation of gravitational singularities, is more consistent with our case; yet, one must then use, instead of the ordinary general theory of relativity, an effective classical theory that would include all higher order corrections to the action functional in curvature.

from the initial state (especially at large B) is converted into a relative motion in the chain of black holes and surrounding particles not captured into black holes.

The mass and rapidity distributions of black holes in individual events are determined primarily by the corresponding values of the impact parameter and by the behavior of the function $\rho(y, Y, B)$. For $B < B_{\rm cr} = m_p^{-1}(E/m_p)^{1/4}$, we have a multiperipheral chain of black holes that is continuous in y. For $B > B_{\rm cr}$, there arise two multiperipheral chains of black holes that are separated by a rapidity gap of width $\Delta y \simeq Y - 2\ln(Bm_p)$. For large Δy, in which case $B \sim \sqrt{s}/m_p^2$, such events look like a typical diffractive generation of black holes whose masses are about m_p.

Some product particles falling "in between" the layers and gravitons of low transverse momenta will not be captured into black holes. However, a qualitative investigation of this issue presents a separate problem, which is quite involved.

The question of whether a fragment of the black-hole chain (or even all terms of this chain) can merge into larger black holes during the process of divergence is also of interest. This can generally occur if the formation of horizons and their longitudinal growth proceed faster than the divergence of black holes, but it is necessary to perform a more accurate analysis in order to clarify this point.

To conclude this section, we will briefly discuss special features that the version considered above acquires in the limiting case where the layer width δ coincides with the entire continuous section of the inclusive spectrum in Fig. 4. In collisions at impact-parameter values in the region $B < B_{\rm cr}(s)$, all particles produced within a time interval of about $m_p^{-2}\sqrt{s}$ will then merge, in this regime, into a single black hole of mass about $\sqrt{s}$, while, in collisions at impact-parameter values of $B > B_{\rm cr}(s)$, two black holes will be produced that fly fast apart and which have masses of about $s/m^3B^2 \sim \sqrt{s}(B_{\rm cr}(s)/B)^2$.

This final state at small B is similar to that which is predicted by a naive classical pattern and that which is predicted in [1, 16] on the basis of an analysis of the formation of trap surfaces in a collision process within the classical theory of general relativity. This is quite surprising and, within the approach adopted in the present study, seems a mere coincidence since, in trans-Planckian collisions, curvatures at classical fronts corresponding to (2) are much greater than Planckian curvatures; therefore, corrections to the classical pattern may be large in general.

Also, it does not seem necessary, in this limiting case to introduce logarithmic corrections to the radii of black disks, and the sum rules for momenta can easily be satisfied. It may turn out that this case will stand out upon taking into account all string degrees of freedom.

7. CONCLUSION

For $E \gg m_p$, we have thus arrived at a pattern of gravitational interactions that is similar in many respects to the asymptotic pattern of hadronic reactions in the Froissart limit:

(i) A collision of trans-Planckian particles looks like a collision of black disks whose radii are dependent on their energies.

(ii) The production of secondaries having specific momenta occurs in the region of intersection of these disks in the longitudinal coordinate frame where the particles in question are slow.

The main distinctions between trans-Planckian interactions in QCD and those in gravity stem from the fact that the graviton is massless.

The radii of the black disks grow with energy much faster for gravitational interactions than for hadronic processes ($E^{1/2}$ versus $\ln E$).

Yet another important distinction between the hadronic and the gravitational case is that in the character of final-state interaction. In the case of QCD, this interaction is short-range; therefore, there occur no global changes in particle spectra in the process of hadronization and divergence of product particles. But in the case of gravitation, there also exists a long-range attraction, which leads to the growth of density perturbations collapsing, later on, into a chain of black holes.

ACKNOWLEDGMENTS

I am grateful to K.G. Boreskov, A.B. Kaidalov, and K.A. Ter-Martirosyan for stimulating discussions.

This work was supported by the Russian Foundation for Basic Research (project nos. 01-02-17383, 00-15-96786), INTAS (grant no. 00-00366), and NATO (grant no. PSTCLG 977275).

REFERENCES

1. P. D. D'Eath, Phys. Rev. D **18**, 990 (1978).
2. P. D. D'Eath and P. N. Payne, Phys. Rev. D **46**, 658 (1992).
3. L. N. Lipatov, Phys. Lett. B **116B**, 411 (1982).
4. L. N. Lipatov, Nucl. Phys. B **365**, 614 (1991).
5. I. J. Muzinich and M. Soldate, Phys. Rev. D **37**, 359 (1988).
6. D. Amati, M. Ciafaloni, and G. Veneziano, Phys. Lett. B **197**, 81 (1987).

7. D. Amati, M. Ciafaloni, and G. Veneziano, Phys. Lett. B **289**, 87 (1992).
8. D. Amati, M. Ciafaloni, and G. Veneziano, Nucl. Phys. B **347**, 550 (1990).
9. G. 't Hooft, Phys. Lett. B **198**, 61 (1987).
10. T. Banks and W. Fischler, hep-ph/9906038.
11. S. B. Giddings, hep-ph/0110127.
12. G. F. Giudice, R. Rattazzi, and J. D. Wells, hep-th/0112161.
13. S. Dimopoulos and G. Landsberg, hep-ph/0106295.
14. M. B. Voloshin, hep-ph/0107119; hep-ph/0111099.
15. S. B. Giddings and S. Thomas, hep-ph/0106219.
16. D. M. Eardley and S. B. Giddings, gr-qc/0201034.
17. M. Cavaglia, hep-ph/0210296.
18. N. Arkani-Hamed, S. Dimopoulos, and G. Dvali, Phys. Lett. B **429**, 263 (1998).
19. P. S. Aichelburg and R. U. Sexl, Gen. Relativ. Gravit. **2**, 303 (1971).
20. C. B. Thorn, hep-th/9405069; hep-ph/9607204.
21. R. Bousso, hep-th/0203101.
22. O. V. Kancheli, hep-ph/0008299.
23. J. L. Cardy, Nucl. Phys. B **75**, 413 (1974).

Translated by A. Isaakyan

Physics of Atomic Nuclei, Vol. 66, No. 11, 2003, pp. 2092–2102. From Yadernaya Fizika, Vol. 66, No. 11, 2003, pp. 2141–2151.

ELEMENTARY PARTICLES AND FIELDS
Theory

Quantum Gravity as Escher's Dragon*

A. V. Smilga[1)]

SUBATECH, Université de Nantes, Nantes, France

Received January 4, 2003

Abstract—The main obstacle in attempts to construct a consistent quantum gravity is the absence of independent flat time. This can in principle be cured by going out to higher dimensions. The modern paradigm assumes that the fundamental theory of everything is some form of string theory living in space of more than four dimensions. We advocate another possibility that the fundamental theory is a form of $D = 4$ higher derivative gravity. This class of theories has a nice feature of renormalizability, so that perturbative calculations are feasible. There are also finite $\mathcal{N} = 4$ supersymmetric conformal supergravity theories. This possibility is particularly attractive. Einstein's gravity is obtained in a natural way as an effective low-energy theory. The $\mathcal{N} = 1$ supersymmetric version of the theory has a natural higher dimensional interpretation due to V.I. Ogievetsky and E.S. Sokatchev, which involves embedding our curved Minkowski spacetime manifold into flat eight-dimensional space. Assuming that a variant of the finite $\mathcal{N} = 4$ theory also admits a similar interpretation, this may eventually allow one to construct consistent quantum theory of gravity. We argue, however, that, even though future gravity theory will probably use higher dimensions as construction scaffolds, its physical content and meaning should refer to four dimensions, where an observer lives. © *2003 MAIK "Nauka/Interperiodica".*

1. INTRODUCTION

Karen Avetovitch belongs to the first generation of the Landau school. A characteristic feature of Landau and his disciples was dislike of "philosophy." The latter was understood in the broad sense as any kind of discussion without explicit formulas or numbers. A scientific paper should involve a derivation of some new formula or new number—this was the main lesson that Landau taught to K.A. and which K.A. taught to his students including myself. In my own scientific activity, I mostly tried to follow this commandment, but human beings are weak and sinful, and cannot really be good all the time. Sometimes, when the task to derive things scientifically is too hard (as is the case for quantum gravity), it is very difficult to resist the temptation to think and, which is worse, to *talk* about these matters. When discussing the foundations of quantum gravity, one *has* to do a philosophical talk or no talk at all. Today, I have chosen the first option and can only hope that K.A. will not condemn me too much.

Actually, we do not understand what quantum gravity is. To understand why we do not understand this, let me briefly recall the things that we understand well.

(i) We understand well Newton's laws and, generically, the dynamics of any classical system, where equations of motion have Cauchy form: you set up the initial conditions at a given time moment and find out how the system will look at later times. The number of dynamic variables can be finite (this is called classical mechanics) or continuously infinite (this is called classical field theory). Such dynamic systems often enjoy extra symmetries. The symmetries might be global (with Nöther currents, etc.) or dynamical (involving the Hamiltonian). The important representative of the latter is Lorentz symmetry. There are also gauge symmetries, which *are* not symmetries but rather additional constraints imposed in phase space, which are respected during the time evolution of the system prescribed by its Hamiltonian.

(ii) We know how to construct quantum counterparts for all theories mentioned above. You introduce a Hilbert space and write the Schrödinger equation for wave functions (in the case where the number of degrees of freedom is finite) or wave functionals (in the case where the number of degrees of freedom is continuous). To tackle the continuous number of dynamic variables in field theories, one should first make it finite (introduce ultraviolet and infrared regularization) and then explore the limit when the corresponding cutoffs are lifted. In some cases (as for QED or for $\lambda\phi^4$ theory, or for any field theory with spacetime dimension 5 or greater), this leads to trouble: the

*This article was submitted by the author in English.

[1)]On leave of absence from ITEP, Moscow, Russia; e-mail: smilga@subatech.in2p3.fr

1063-7788/03/6611-2092$24.00

continuum limit does not exist. But in many physically important cases ($D = 4$ non-Abelian gauge theories), the continuous limit is well defined.

And this is all that we know *for sure*. The reader might be surprised why did I not mention classical gravity. A common believe is that, though quantum gravity is, indeed, not constructed and not understood yet, the *classical* theory, Einstein's gravity, is something which we know well and are sure about. Mostly, this is true, but not quite. The discussion of this nontrivial point is what I would like to begin with.

2. EINSTEIN'S GRAVITY

The action of the theory is

$$S = m_{\rm P}^2 \int R\sqrt{-g}\, d^4x + \int \mathcal{L}_{\rm matter}\sqrt{-g}\, d^4x. \quad (1)$$

The equations of motion are

$$R_{\mu\nu} - \frac{1}{2} g_{\mu\nu} R = \frac{1}{m_{\rm P}^2} T_{\mu\nu}, \quad (2)$$

where R is scalar curvature, $R_{\mu\nu}$ is Ricci's tensor, $m_{\rm P}$ is Planck mass, and $T_{\mu\nu}$ is the energy–momentum tensor of the matter fields.

The main problem of this theory is the *problem of time* (see, e.g., [1] for an extensive discussion). In "normal" systems, time is an independent variable, not a dynamical one. In gravity, time is just one of the coordinates on a $D = 4$ manifold and is intertwined with spatial coordinates, which are related to the dynamical variables. The dependence on time cannot be disentangled from other dependences. At the classical level, this means that the problem of solving Einstein's Eqs. (2) cannot always be reduced to a Cauchy problem.

We hasten to comment that, in all cases representing physical interest, it can. This can be done if the four-dimensional manifold can be represented as a set of three-dimensional slices of the same topology (the interval between any two points on such a slice is spacelike). In other words, the topology of spacetime should be $\Sigma \times R$. In the physically interesting case, Σ is topologically equivalent to R^3 and is asymptotically flat. Choosing *some* coordinate along the timelike factor R, we may call it time and rewrite Einstein's equations such that they would express evolution with respect to this time. This procedure is called the canonical Arnowitt–Deser–Misner (ADM) formalism [2].

Trouble strikes back in the following way. Suppose we pose some initial conditions at the spacelike slice Σ corresponding to the moment $t = 0$ and are interested in what happens at later times. For generic initial conditions, singularities will develop (black holes will be formed). The formation of black holes as such does not lead to inconsistencies. The point is that the singularity in the center of the hole is normally surrounded by an event horizon (as is the case for the Schwarzschild solution) and is thereby unreachable: if we place the observer far away from the holes, where the metric is nearly flat, he will not get signals from the regions close to singularities and, as far as this observer is concerned, the future evolution of the system *is* uniquely determined by the Cauchy data in the past.

The conjecture of Penrose [3] was that singularities are always surrounded by horizons and a "naked" singularity is never possible (the so-called *cosmic censorship principle*). It was found, however, that this conjecture is not true in its strong form: there *are* solutions to Einstein's equations involving naked singularities (see [4] for a recent review). A separate question is whether these solutions are physically realized. The answer to this is probably negative: all such solutions seem to be unstable, so that a small fluctuation of initial conditions destroys them. But *in principle*, naked singularities are not forbidden in general relativity.

The presence of a naked singularity means that a distant observer receives information from regions of arbitrarily large curvature, where classical theory does not apply. Still, he does not receive in this case information from the singularity proper, and Cauchy interpretation is not spoiled yet on this stage. But there are cases when it *is*. First of all, the symmetry of the equations with respect to time reversal tells one that, on top of black-hole solutions, there are white-hole solutions, for which the world lines, matter, and information flow out of the singularity through the horizon to infinity. Again, these solutions are not stable and are not physically realized (at least, at the macroscale), but, at the foundational level, they present trouble.

This conforms even more the wormhole solutions with closed time loops [5]. They have roughly the same status as the naked-singularity solutions and white-hole solutions. The topology of the corresponding 4-manifolds is more complicated than $\Sigma \times R$ (so that the ADM canonical formalism does not apply here) and involves a "handle" with two "mouths." The distance between the mouths in the usual space may be large, while the geodesic distance measured through the wormhole may be small. As a result, the particles traveling through the wormhole will effectively move faster than light from the viewpoint of an outer-space observer, and this means violation of causality, which *is* trouble. In particular, no Cauchy interpretation for the equations of motion is possible in this case [6].

In other words, general relativity describes well observable physical events at the macroscale level, but it has inherent problems at the foundational level. The same difficulty appears in any gravity theory including the general covariance principle. The basic reason for this is the absence of independent flat time.

3. QUANTIZATION

If the problems are there at the classical level, they are not going to disappear when we try to quantize the theory. Actually, they become much more severe. If in the classical case noncausality showed up only for rather special solutions, it is an inherent and unavoidable feature of quantum gravity.

I mean here in the first place Hawking's paradox [7] associated with black-hole formation. As was discussed above, in the classical theory, there are "benign" solutions that describe the formation of black holes prudently surrounded by a horizon. These solutions present no conceptual problems. But in quantum theory, black holes are not completely black; they radiate by a Hawking mechanism. This radiation is purely stochastic and does not carry any information on what particular kind of matter fell in the black hole. This information is lost completely. Therefore, our system, having presented a pure quantum state at $t = 0$, is *necessarily* transformed into mixed state after the black hole was formed and radiated a little bit. This means loss of unitarity.[2)] In a quantum system with a well-defined Hilbert space endowed by a norm invariant under time evolution, such a transformation of pure states into mixed states does not happen, and nobody knows how to formulate a quantum theory where the norm in Hilbert space is not conserved.

To be more precise, there were attempts to formulate non-Schrödinger quantum theories. In the framework of the ADM approach, one can naturally derive the so-called Wheeler–de Witt equation [8]. It says

$$\hat{H}\Psi = 0 \tag{3}$$

(no term $i\dot{\Psi}$ on the right side). One obtains zero on the right side, because the ADM Hamiltonian, the generator of time translations, represents here one of the gauge constraints: in gravity, the symmetry with respect to coordinate translations is local, not global. There are comparatively "kosher" quantum systems described by the wave equation of the Wheeler–de Witt type. One of them is a quantum relativistic particle. The Klein–Gordon equation $(\hat{p}^2 - m^2)\Psi = 0$ has exactly the form (3), and this is not accidental. The classical action

$$S = \frac{m}{2}\int \left(\frac{dx_\mu}{d\tau}\right)^2 d\tau \tag{4}$$

is invariant with respect to reparametrizations $\tau \to f(\tau)$ and is reminiscent of gravity in this respect. The Klein–Gordon operator plays exactly the role of the ADM Hamiltonian. However, this theory can also be formulated in a standard Schrödinger form if x_0 is chosen as time. The Schrödinger Hamiltonian is then $\hat{H}_{\text{Schröd}} = p_0 = \sqrt{\hat{\mathbf{p}}^2 + m^2}$. For systems where the wave function does not change too rapidly (so that the square root $\sqrt{-\partial_i^2 + m^2}\Psi$ is well defined), the equations $\hat{H}_{\text{ADM}}\Psi = 0$ and $\hat{H}_{\text{Schröd}}\Psi = i\dot{\Psi}$ are equivalent.

For gravity, one can in principle also use this trick, but:

Even for the simple system (4), there is still no complete equivalence of the Schrödinger equation and the Wheeler–de Witt one; the restriction for the wave functions not to change too rapidly should be imposed. Moreover, at least in the case when an external electromagnetic field is present, the Klein–Gordon equation (as well as the Dirac one) is known to be not internally self-consistent because it does not take into account the creation of particle–antiparticle pairs, which always occurs in strong fields.

In gravity (in contrast to the relativistic particle), we do not have a unique natural recipe how to choose time. As a result, the system (3) meets very serious, probably insurmountable, difficulties in interpretation [1].

4. STRING STORY

Besides the difficulties discussed above, a standard quantum gravity also has another problem: it is a theory with dimensional constant m_{P} and, as such, is nonrenormalizable. This refers to the quantum version of the standard Einstein's gravity and also to its supersymmetric versions (though some divergences cancel out in supergravity, even $\mathcal{N} = 8$ supersymmetry is not powerful enough to get rid of the infinite number of counterterms). To cure this problem, string theory was invented. The latter cures it for the simple reason that a finite size of a string serves as an ultraviolet regulator and the ultraviolet divergences are effectively cut off.

There are two points that I want to emphasize here.

[2)] In quantum theory, unitarity and causality are related notions, and breaking of unitarity usually leads to breaking of causality (see more detailed discussion at the end of Section 5). Causality in quantum gravity is broken also more directly via production of virtual wormholes.

(i) Even though perturbative string theory is, indeed, benign in ultraviolet, it is in some sense *not constructed* even now! We understand it well at the tree level: we can very well calculate tree string amplitudes described by the picture in Fig. 1*a* (2-sphere with sources) and also at the one-loop level (torus with sources). But already the calculation of the two-loop graph in Fig. 1*c* is a tremendously difficult task. It involves integration over moduli space for 2-manifolds of genus 2, and the latter has a very complicated structure. This moduli space (called Teichmüller space) involves certain singular points corresponding to the cases where the width of one of the handles in Fig. 1*c* shrinks to zero. The integral for string amplitudes becomes divergent at these singular points, and though these divergences are not ultraviolet, but rather infrared in nature, they are also nasty. Very recently, the solution of the problem for two-loop amplitudes was announced [9] (see also [10]), but we still do not know how to treat divergences and calculate string amplitudes in the general case.

(ii) Even if consistent string perturbation theory for an arbitrary number of loops is ever constructed, it will solve the problem of renormalizability, but will hardly solve *real* conceptual problems of quantum gravity discussed above: the absence of causality and unitarity.

Let us discuss this point in some more detail. String theory has one nice feature compared to simple-minded quantum gravity: if strings are embedded into *flat* multidimensional target space (usually called *bulk*), there *is* a natural definition of time. However, strings are nonlocal objects, and, in the full theory treated nonperturbatively, this should bring about noncausalities at the Planck scale (though perturbative string amplitudes are probably causal). Noncausalities in the bulk are bound to lead to noncausalities in effective four-dimensional theory.

The question whether string theory is unitary has different answers depending on whether we consider it in the bulk (then hopefully it is) or from the viewpoint of a four-dimensional observer. In the latter case, it is definitely not because the effective four-dimensional theory is still Einstein's (super) gravity and Hawking's paradox is still there.

My personal opinion (I will give more arguments in its favor later) is that string theory (at least the conventional string theory in the framework of mid-1980s paradigm) has little chance to prove to be the fundamental theory of quantum gravity and/or of Everything. Actually, nowadays, most string theorists also think that one should look *beyond* string theory to find a really fundamental one (*M theory*?).

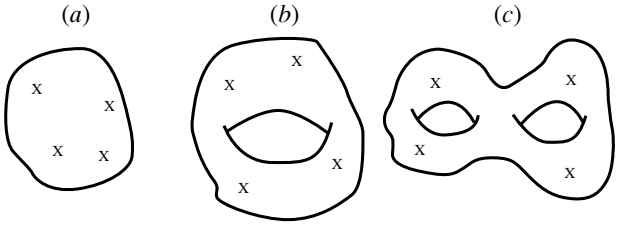

Fig. 1. String amplitudes: (*a*) tree level, (*b*) one loop, and (*c*) two loops. Crosses stand for sources.

My own suggestion, however, is that, instead of looking *beyond* strings, one can try to look in a different direction.

5. CONFORMAL GRAVITY

Going to strings instead of fields is a rather bold and radical step. The main conceptual problem is the impossibility of defining the Hilbert space and path integral in reasonably rigorous terms.

Of course, mathematicians maintain that the path integral is not defined even in field theory, but for a physicist, there is no problem there. The Euclidean path integral is defined constructively and has been calculated numerically by thousands of people in the last 20 years. We *believe* that the Minkowski path integral can also be calculated and the problem here is purely technical. But for strings, we have no idea how to do it. In field theory, we have an infinite number of dynamical variables marked by spatial points $\mathbf{x}$; in *string field theory*, dynamical variables are functionals on loop space; i.e., the argument for the string field variable is a particular embedding of the string in space $\{\mathbf{x}(\sigma)\}$. In quantum theory, the basic object would be a complex-valued "hyperfunctional" defined on the set of all such functionals. Many people tried to obtain some practical results in this direction, but to no avail. Two loops is the limit of our understanding now.

Bearing this in mind, it is reasonable to explore less revolutionary approaches. String theory makes gravity renormalizable, but is it not possible to make it renormalizable in a conservative field theory framework?

Yes, it is—is the answer. The quantum version of Einstein gravity is nonrenormalizable due to the presence of a dimensional constant. It is easy to write a generally covariant Lagrangian, where the coupling is dimensionless and the theory is renormalizable. The Einstein–Hilbert action (1) is linear in R. Renormalizable gravity is quadratic in R. There is a family of such theories with the actions

$$S = \alpha \int R_{\mu\nu} R^{\mu\nu} \sqrt{-g} d^4x + \beta \int R^2 \sqrt{-g} d^4x. \quad (5)$$

The structure $R_{\mu\nu\rho\sigma}R^{\mu\nu\rho\sigma}$ is reduced (at least, in perturbation theory) to the two structures in Eq. (5) due to the Gauss–Bonnet identity

$$R^2 - 4R_{\mu\nu}R^{\mu\nu} + R_{\mu\nu\rho\sigma}R^{\mu\nu\rho\sigma} = \text{total derivative}. \tag{6}$$

It has been known for a long time that the theories of the class (5) are renormalizable. Moreover, they are asymptotically free [11]! We will concentrate on one particular theory in the family (5) with the action

$$S = -\frac{1}{h}\int C_{\mu\nu\rho\sigma}C^{\mu\nu\rho\sigma}\sqrt{-g}d^4x, \tag{7}$$

where

$$C_{\mu\nu\rho\sigma} = R_{\mu\nu\rho\sigma} + \frac{1}{2}\left[g_{\mu\sigma}R_{\nu\rho} + g_{\nu\rho}R_{\mu\sigma} - g_{\mu\rho}R_{\nu\sigma} - g_{\nu\sigma}R_{\mu\rho}\right] + \frac{R}{6}\left[g_{\mu\rho}g_{\nu\sigma} - g_{\mu\sigma}g_{\nu\rho}\right] \tag{8}$$

is the Weyl tensor. A distinguishing feature of the theory (7) is its invariance under *local* scale transformations,

$$g_{\mu\nu}(x) \to \lambda(x)g_{\mu\nu}(x). \tag{9}$$

Bearing in mind the relation (6), the action (7) is perturbatively equivalent to (5) with $\beta = -\alpha/3 = 2/(3h)$.

An immediate objection against the idea that the theory (7) describes the real world could be that it does not have a Newtonian limit. The nonrelativistic potential corresponding to the action (7) is not Coulomb-like, but grows $\propto r$ (this follows from dimensional counting). The objection to this objection is that *effective* long-distance theory need not coincide with the fundamental one. In fact, it can well coincide with Einstein's gravity!

As was mentioned, conformal gravity is an asymptotically free theory. The explicit one-loop calculation gives [11]

$$\left.\frac{1}{h}\right|_\mu = \frac{1}{h_0} - \frac{199}{30}\frac{1}{16\pi^2}\ln\frac{\Lambda_{\rm UV}}{\mu}, \tag{10}$$

where $\Lambda_{\rm UV}$ is the ultraviolet cutoff. Asymptotic freedom makes the physics of conformal gravity rather similar to that of QCD. At large energies, perturbation theory works, but at some scale $\mu \sim \Lambda_{\text{conf. grav}}$, where the effective constant becomes large, nonperturbative effects come into play. The scale $\Lambda_{\text{conf. grav}}$ determines the mass of hadron-like states. This is the standard dimensional transmutation. It is natural to associate the scale $\Lambda_{\text{conf. grav}}$ with the Planck scale.

In QCD, there are distinguished states, the pions, which remain massless in the chiral limit. Thus, the effective theory for massless QCD is the chiral theory describing pion interactions. The form of the leading-order chiral effective Lagrangian

$$\mathcal{L}_{\rm chiral} = \frac{F_\pi^2}{4}{\rm Tr}\{\partial_\mu U\partial_\mu U^\dagger\} \tag{11}$$

is dictated by symmetry considerations.

The effective Lagrangian for conformal gravity is not invariant under local scale transformations (9), but general covariance should still be there. This dictates

$$S^{\rm eff} = \Lambda\int\sqrt{-g}d^4x + \kappa\int R\sqrt{-g}d^4x, \tag{12}$$

where Λ is now the cosmological constant. A priori, $\Lambda \sim m_{\rm P}^4$ and $\kappa \propto m_{\rm P}^2$. The estimate $\Lambda \sim m_{\rm P}^4$ is about 130 orders of magnitude larger that the experimental value of the cosmological constant. Thus, the theory (7) is not viable as a realistic fundamental theory of gravity. This refers actually to *any* nonsupersymmetric theory. But if we start with supersymmetric conformal gravity without the cosmological term, the induced cosmological constant vanishes.[3)] In other respects, the physics of conformal supergravity is similar to that of conformal gravity. In particular, conformal supergravity is asymptotically free and involves dimensional transmutation.

The second term in Eq. (12) is the induced Einstein's gravity. The idea by which the Einstein–Hilbert action is not present in the tree action, but is generated spontaneously due to loops of usual matter fields, was put forward a long time ago by Sakharov [12]. It was mentioned in [13] that this mechanism works also for conformal (super)gravity and the analogy with the dimensional transmutation mechanism in QCD was emphasized.

At the scale $p_{\rm char} \sim \Lambda_{\text{conf. grav}} \sim m_{\rm P}$, nonperturbative effects come into play. In QCD, the nonperturbative effects are not reduced to, but are well represented by, instantons, classical solutions to Euclidean field equations. In gravity, there are also such solutions; they are Ricci-flat four-dimensional manifolds called gravitational instantons. The simplest such solution is the Eguchi–Hanson (EH) solution [14] with the metric

$$ds^2 = \frac{dr^2}{1 - a^4/r^4} + r^2\left[\sigma_x^2 + \sigma_y^2 + \sigma_z^2\left(1 - \frac{a^4}{r^4}\right)\right], \tag{13}$$

where

$$\sigma_x = \frac{1}{2}\left(\sin\psi d\theta - \sin\theta\cos\psi d\phi\right), \tag{14}$$

[3)] In the real world, supersymmetry is broken and it is not clear, again, why the cosmological constant is so small. Nobody can yet answer this troublesome question.

$$\sigma_y = -\frac{1}{2}\left(\cos\psi d\theta + \sin\theta\sin\psi d\phi\right),$$
$$\sigma_z = \frac{1}{2}\left(d\psi + \cos\theta d\phi\right)$$

are Cartan–Mauer forms. The metric (13) is locally asymptotically flat. It satisfies the conditions $R_{\mu\nu} = 0$, which are equations of motion for Einstein's gravity without matter, but Ricci flatness also implies that the equations of motion for conformal gravity

$$g_{\mu\nu}(3C_{\alpha\beta\gamma\delta}C^{\alpha\beta\gamma\delta} + 2R^{;\alpha}_{;\alpha}) - 4(RR_{\mu\nu} - R_{;\mu;\nu}) \quad (15)$$
$$+ 12(2R^{\alpha}_{\mu}R_{\nu\alpha} - R^{;\alpha}_{\mu\nu\ ;\alpha} - R_{\mu\alpha\beta\gamma}R_{\nu}^{\alpha\beta\gamma}) = 0$$

are satisfied.

In contrast to Einstein's Euclidean action, which is not positive definite and the corresponding path integral is ill-defined, the Weyl action *is* positive definite. The Weyl action of the EH instanton is

$$S^{\text{inst}} = \frac{48\pi^2}{h}. \quad (16)$$

The contribution of the EH instanton to the path integral is nonanalytic in h, $\propto \exp\{-(48\pi^2)/h\}$, which is quite similar to what happens in Yang–Mills theory. The EH instanton is analogous to the BPST instanton also in other aspects: (i) The Riemann tensor for the EH instanton is self-dual, as the field strength tensor for the BPST instanton is. (ii) Like the BPST instanton, the EH instanton can be interpreted as a Euclidean tunneling trajectory interpolating between two topologically distinct vacua [15]. In the Yang–Mills case, different vacua are characterized by different Chern–Simons numbers. In the gravity case, there are two classical vacua with flat R^3 metric, but with different *orientation*. Following the EH instanton tunneling trajectory, flat R^3 space turns inside out and goes over to its mirror image.

Questions and Answers

Not everything is so rosy, however. Conformal gravity also has certain difficulties that we are in a position to discuss now.

First of all, when writing Eq. (10), we tacitly assumed (and this is true) that the one-loop counterterm has the same functional form as the tree action. However, the classical conformal symmetry of the Weyl action is broken by quantum effects. This means that we cannot guarantee that higher loop counterterms are all proportional to (7). The admixture of the structure R^2 cannot be ruled out. Thus, pure Weyl gravity is not renormalizable. Of course, one could consider the theory (5) with two charges. Its physics is roughly the same as for the conformal gravity, but it is much less beautiful and hence much more suspicious. The same concerns the $\mathcal{N} = 1$ supersymmetric version of Weyl theory. It is also asymptotically free, conformal symmetry is anomalous, and nonconformal counterterms are bound to appear at the two-loop level and higher.

Aesthetically more appealing are the models where conformal symmetry of the classical action is sustained at the quantum level. They are not only renormalizable, but simply finite: the β function vanishes identically and counterterms of dimension 4 do not appear whatsoever. The best known example of such a theory is $\mathcal{N} = 4$ supersymmetric Yang–Mills (SYM). Finite theories based on conformal gravity are also known. The minimal variant of $\mathcal{N} = 4$ conformal supergravity happens not to be finite, but the coupling constant ceases to run if an extra $\mathcal{N} = 4$ SYM multiplet is included with the gauge group $U(1) \times U(1) \times U(1) \times U(1)$ or $SU(2) \times U(1)$ [11].

If the β function vanishes, we do not have the mechanism of dimensional transmutation at our disposal and the question arises how the effective Einstein action involving a dimensional coupling is generated. The answer is rather transparent: conformal symmetry is not broken explicitly by quantum effects in this case, but it can be broken *spontaneously*. The point is that $\mathcal{N} = 4$ finite theories involve scalar Higgs fields. For certain nonzero values of the fields, the classical potential vanishes. Supersymmetry dictates that the potential is not generated at the quantum level either: classical flat directions remain flat in quantum theory. A set of all Higgs values where the potential vanishes, is called *vacuum valley* or *vacuum moduli space*. This is a situation of neutral equilibrium: no particular point on the vacuum moduli space is preferred, and we have a family of theories characterized by particular Higgs expectation values. This all is very well known for $\mathcal{N} = 4$ finite gauge theories, but it is also true for finite $\mathcal{N} = 4$ conformal supergravities.

Higgs expectation values bring about dimensional constants so that an effective low-energy theory is not conformal anymore. In the case of finite gauge theories, the effective theory is akin to the Standard Model, involving spontaneous breaking of gauge symmetry by the Higgs mechanism. The effective theory for the finite conformal supergravity involves Einstein's term and its superpartners.

Let us discuss another difficulty that conformal supergravity has. The Lagrangian (5) involves four derivatives of the metric. Field theories with higher derivatives are usually considered sick because they are intrinsically noncausal. The latter also applies to conformal gravity. To understand this, consider the theory involving on top of the higher derivative terms

also the Einstein term, $\mathcal{L} \sim m_{\rm P}^2 R + R^2$. The propagator of graviton has then the form[4)]

$$D(k^2) \propto \frac{1}{m_{\rm P}^2 k^2 - k^4} = \frac{1}{m_{\rm P}^2}\left(\frac{1}{k^2} - \frac{1}{k^2 - m_{\rm P}^2}\right). \quad (17)$$

In other words, on top of an ordinary massless graviton G, a massive particle G^* with *negative* residue at the pole appears. Production of particles with negative residues would violate unitarity.

However, it is known that unitarity is actually not violated here [16, 17]. What *is* violated is causality. The point is that, when loop corrections are taken into account, the massive pole is shifted from the real axis, and the "particle" G^* ceases to be an asymptotic state and cannot be produced in collision of usual massless gravitons. Indeed, nothing prevents the particle G^* from going into a set of massless gravitons, and this makes the polarization operator $\Pi(m_{\rm P}^2)$ corresponding to the propagator (17) complex. If G^* were a "normal" particle with positive metric, the resultant propagator

$$\frac{1}{k^2 - m_{\rm P}^2 - \Pi(m_{\rm P}^2)}$$

would involve a pole in the lower half-plane of k_0^2 ($\mathrm{Im}[\Pi(m_{\rm P}^2)] < 0$ in this normalization). When the residue is negative, the propagator

$$\frac{1}{-k^2 + m_{\rm P}^2 - \Pi(m_{\rm P}^2)}$$

has the pole in the upper half-plane of k_0^2 [$\Pi(m_{\rm P}^2)$ is determined by the same graphs as for a usual particle and has the same value]. This property prevents making a usual Wick rotation and is not consistent with causality.[5)]

Currently, it is not clear whether the causality breaking at the Planck scale persists in the finite superconformal theories discussed above. In [11], a careful optimism was expressed that maybe it does not. But even if it does, we do not see why it should be considered as a major problem. At a nonperturbative level, microcausality is broken in *any* gravity theories, with string theory not being an exception. In conformal supergravity models, it is probably also broken perturbatively.

So what?

[4)]We are not worried about numerical factors now.

[5)]In the papers [16], higher derivative theories were studied mainly in association with the Pauli–Villars regularization procedure. The conclusion was that the regularized Lagrangians lead to unitary amplitudes, but that causality is broken at the regulator scale.

6. SUPERGRAVITY AS A THEORY OF 3-BRANE: OGIEVETSKY–SOKATCHEV APPROACH

In the previous section, we argued that conformal supergravity (probably, a finite, anomaly-free version thereof) can be considered as a viable candidate for the fundamental gravity theory. It solves the problem of nonrenormalizability of standard gravity even better than string theory does (we say *better*, because perturbative calculations to any order in coupling constant present no essential technical difficulties there) and the difficulties it has are intrinsic for *any* gravity theory.

String theory has one attractive feature, however. It is formulated not in curved four-dimensional space, but in the flat multidimensional bulk. This gives a fundamental solution to the problem of time and brings forward hopes of constructing a self-consistent quantum theory.

We want to note here that similar hopes can actually be associated with *standard supergravity* if the latter is described in the superfield formalism due to Ogievetsky and Sokatchev [18].

The Ogievetsky–Sokatchev approach to supergravity has a lot of advantages compared to the standard Wess–Zumino approach. Unfortunately, the former is not so widely known, and we are in a position to explain briefly its basic features. In the Wess–Zumino approach, the basic superfield is E_M^A, a supersymmetric generalization of vierbein. This superfield has a lot of unphysical components; to get rid of them, one has to impose constraints of a rather complicated form.

The Ogievetsky–Sokatchev approach is based on a beautiful geometric construction. Consider a curved $(4+4)$-dimensional supermanifold (it has four bosonic coordinates x^m and four real or two complex fermionic coordinates θ_α) embedded into *flat* $(8+4)$-dimensional superspace involving four *complex* (which is equivalent to eight real) bosonic coordinates z^m and two complex fermionic coordinates. Such an embedding is characterized by the superfield $\mathcal{H}^m(x^n; \bar\theta^{\dot\alpha}, \theta_\alpha)$, where $\mathcal{H}^m$ coincides with the imaginary parts of flat coordinates z^m and x^m—with their real parts. The Lagrangian of the standard Einstein supergravity is none other than the supervolume of the associated hypersurface:

$$S_{\rm sugra} = m_{\rm P}^2 \int \mathrm{Ber}||E_M^A|| d^4x d^4\theta, \quad (18)$$

where E_M^A is the *induced* supervierbein on the hypersurface and "Ber" stands for the Berezinian (or superdeterminant). Now, E_M^A and $\mathrm{Ber}||E||$ can be expressed in terms of $\mathcal{H}^m(x^n; \bar\theta^{\dot\alpha}, \theta_\alpha)$ (in a not so

simple but explicit way). One can check that they obey the constraints that are imposed on E_M^A in the Wess–Zumino approach. On the other hand, no constraints on the *axial superfield* (we are using the Ogievetsky–Sokatchev terminology) $\mathcal{H}^m$ need to be imposed.

The Lagrangian (18) is invariant with respect to general reparametrizations of all bosonic and fermionic coordinates on the hypersurface. This group is too large, however, which is not convenient. In addition, such a generic reparametrization destroys the simple form

$$\mathrm{Im}(z^m) = \mathcal{H}^m\left(\mathrm{Re}(z^n); \bar\theta, \theta\right) \tag{19}$$

chosen by us to describe the hypersurface.

The form (19) is preserved by a subgroup of the general reparametrization group. To describe it, introduce left and right coordinates $x^m_{L,R} = x^m \pm i\mathcal{H}^m$ and require them to reduce to the familiar

$$x^m_{L,R} = x^m \pm i\bar\theta\sigma^m\theta \tag{20}$$

in the limit when the embedded hypersurface represents a hyperplane. Then, the transformations

$$\begin{aligned} x^m_L &\to f^m(x^n_L, \theta_\beta), \\ \theta_\alpha &\to \chi_\alpha(x^n_L, \theta_\beta) \end{aligned} \tag{21}$$

obviously preserve the form (19). To provide for the invariance of the action (18) or, which is the same, to provide for the fact that the transformations (21) represented a reparametrization of the coordinates on the hypersurface, it is sufficient to require that the super-Jacobian of the transformation (21) be equal to 1,

$$\begin{aligned} &\mathrm{Ber}\left|\left|\frac{\partial(x'_L, \theta')}{\partial(x_L, \theta)}\right|\right| \\ &= \det\left|\left|\frac{\partial x'^m_L}{\partial x^n_L} - \frac{\partial x'^m_L}{\partial\theta_\alpha}\frac{\partial\theta_\alpha}{\partial\theta'_\beta}\frac{\partial\theta'_\beta}{\partial x^n_L}\right|\right| \det{}^{-1}\left|\left|\frac{\partial\theta'_\alpha}{\partial\theta_\beta}\right|\right| = 1. \end{aligned} \tag{22}$$

The gauge symmetry (21) allows one to greatly reduce the number of components of $\mathcal{H}^m$. There are altogether 64 components. The transformations (21) involve 48 parameters, but the condition (22) fixes 8 of them leaving 40 free parameters. As a result, we obtain 24 (12 bosonic and 12 fermionic) gauge-invariant degrees of freedom. They exactly correspond to the counting in component approach [19]: The Lagrangian involves 38 components (16 for the vierbein e^m_a, 16 for the gravitino ψ^m_α, and 6 for the auxiliary fields S, P, A^m). There are 4 (general coordinate) plus 6 (local Lorentz) plus 4 (supersymmetry) = 14 gauge parameters. Now, $38 - 14 = 64 - (48 - 8) = 24$.

It is convenient to choose the *normal gauge* (analogous to the Wess–Zumino gauge used in the analysis of supersymmetric gauge theories), in which case

$$\mathcal{H}^m \sim e^m_a\bar\theta\sigma^a\theta + \text{other terms}. \tag{23}$$

One can then be directly convinced (though the calculation *is* tedious) that the bosonic part of the action (18) coincides (up to a total derivative!) with R. The other terms in the component Lagrangian are restored by supersymmetry.

Now, $\mathcal{N} = 1$ conformal supergravity can also be described in these terms: its Lagrangian can be expressed via the unconstrained axial superfield $\mathcal{H}^m$. This Lagrangian (see the papers [18] for explicit formulas) is invariant with respect to the general transformations (21) (not restricted by the requirement of unit super-Jacobian).

Note in passing that also the variant of supergravity with the cosmological term is nicely expressed in the Ogievetsky–Sokatchev formalism. It turns out that the corresponding action represents a *total derivative* and the problem is reduced to the choice of boundary conditions. Thus, the question why the cosmological term vanishes acquires the same status as the question why the θ term in QCD vanishes. No comprehensive answer to any of these questions is known, but we are sure at least that, if we start with a supersymmetric theory with vanishing cosmological term, the latter is not generated by quantum effects, by the same token as the θ term in QCD is not generated.

Our main point is that, once flat space appears in the formulation of the theory, a natural definition of time exists, which should allow one to present the equations of motion in the Cauchy form. The theory becomes quite similar to string theory, only it is in a sense much more complicated: the latter deals with embeddings of 2-surfaces into flat Minkowski bulk, while the former depends on embeddings of 4-surfaces (3-branes in modern terminology) there.

On the other hand, supergravity is still much *simpler* than the full string field theory. Indeed, in spite of the fact that the action (18) describes multidimensional geometry, it is *four-dimensional* in nature. The basic dynamical variables in such theory are embeddings themselves rather than frightening functionals in the loop space, which we would eventually have to learn to deal with if we stuck to the conventional string theory paradigm.

7. DISCUSSION

Before going further, let us reiterate briefly the main points of our reasoning so far (you may call it a *party line*, bearing in mind that the corresponding party is not numerous and in opposition).

(i) We do not know how to construct a consistent gravity theory strictly in a four-dimensional framework. The main problem here is the problem of time, which has not been fully solved even in classical general relativity and becomes a real mayhem when one attempts to quantize it.

(ii) Quantum version of Einstein's gravity has another problem: nonrenormalizability. It persists in supersymmetric generalizations.

(iii) The latter problem is cured in string theory, but a *simpler* and in many respects nicer medicine is provided by conformal gravity. The *effective* low-energy theory for conformal gravity is Einstein's theory (modulo the problem of the cosmological term, which is more tractable for supersymmetric versions of the theory, but is far from being fully resolved). In a nonsupersymmetric or $\mathcal{N} = 1, 2, 3$ supersymmetric versions of the theory involving a conformal anomaly, Einstein's constant is generated due to a dimensional transmutation mechanism. We like better $\mathcal{N} = 4$ finite superconformal theories, where Einstein's constant is generated due to spontaneous breaking of conformal symmetry when a particular point on flat Higgs moduli space is picked up.

(iv) With all probability, causality is broken in these theories at the perturbative level (though this was not explicitly demonstrated) due to the presence of higher derivatives in the Lagrangian and complexification of negative metric poles by the Lee and Wick mechanism. But *any* gravity theory is acausal in four dimensions.

(v) $\mathcal{N} = 1$ supergravity and conformal supergravity have a nice interpretation due to Ogievetsky and Sokatchev, where the classical field configuration can be thought of as an embedding of a 3-brane into eight-dimensional flat bulk space. This gives one a natural definition of time, and one can hope to construct a unitary quantum theory with a well-defined Hilbert space *in the bulk*. The reasons are the same as the reasons why we believe that string theory (we mean string theory in the second quantization framework, when it is a form of two-dimensional field theory) is unitary in the bulk.

As the reader has probably already guessed, we *believe*[6] that the future fundamental theory of gravity (and probably of Everything) is a variant of finite superconformal gravity theory. We also believe that this theory can be represented as a theory of 3-brane embedded into a higher dimensional flat space.

There are still several points that are not clear now. The last one is especially worrisome.

[6] As we live now in civilized times and the risk of being severely punished (being stoned, etc.) for a false prophecy is comparatively low, I am allowing myself to make one.

(i) We *believe* that Ogievetsky–Sokatchev supergravity is unitary and causal in the bulk, but do not know how to prove it. This is going to be a much more complicated problem than proving unitarity for string theory (such a *proof* is also absent at present).

(ii) The nice geometric interpretation discussed above has been found so far only for $\mathcal{N} = 1$ theories. Little is known in this respect about $\mathcal{N} = 4$ theory. An educated guess is that the bulk in this case is ten-dimensional rather than eight-dimensional. One can notice in this respect that, in the problem of embedding of a four-dimensional manifold into R^m, the dimensions 8 and 10 are distinguished. Namely, (i) one can always embed an n-dimensional manifold into R^{2n} without self-crossings, and (ii) one can always embed an n-dimensional manifold into R^{2n+2} without knots (so that all embeddings of a given manifold are topologically equivalent) [20].

(iii) The finite superconformal gravity theories discussed above do not have realistic matter content. They are based on the gauge group $SU(2) \times U(1)$ or $U(1)^4$, whereas we need the group $SU(3) \times SU(2) \times U(1)$ or larger, three fermion generations, etc. It is not clear, however, that realistic superconformal gravity theories will ever be found.

(iv) There is also a major philosophical problem. The physics of 20th century is based on positivistic philosophy. We want to formulate theory in terms of physical observables and dismiss as meaningless all attempts to talk about "real" electron trajectories, etc. A real physical observable is by definition something that can be measured by a real physical observer, who is four-dimensional, as we are. But if we treat the theory in a multidimensional bulk, the wave function of the Universe and (in the proposed approach) the 3-brane transition amplitudes can be measured only by a "divine" observer living in the bulk. This smells of mystics, but I do not know how to get rid of it here.

For any opponent, the negative program is usually much stronger than the positive one. That is why I want to finish with some comments on what, I think, the fundamental theory of everything is *not*.

I am personally rather skeptical towards the assertions that higher dimensions are *really* there. The point is that even ordinary field theory is ill-defined if the dimension of spacetime is five or more: the path integral simply does not have continuum limit there (at least, for $D \geq 5$, we are not aware of any example where such a limit exists). I cannot imagine that the string field theory path integral is defined any better. Thus, I do not believe in the ideas (rather popular now) of large extra dimensions, the brane new world, etc.

Fig. 2. M.C. Escher. Dragon.

It may be beneficial and even necessary to think of our physical space as being embedded into a multidimensional flat bulk, but the physical space itself should be four-dimensional. In other words, my attitude towards higher dimensions is close to the standpoint of the Catholic Church with respect to the heliocentric ideas of Kopernicus and Galileo. There were no problems as far as they were proposed as a convenient mathematical tool to facilitate calculation of physical observables like planet positions, etc. (for people of 16th century, the physical observer must, of course, dwell on Earth), but the suggestion that Earth *really* rotates around Sun was unacceptable.[7)]

[7)]My reasons are not religious, however, but simply a desire to be able to define the path integral.

Close to the end, but not in the very end, I want to present, on top of a historical philosophical analogy, an artistic one and simultaneously justify the queer title of this paper. "Dragon" is a gravure by Escher. It is reproduced in Fig. 2. As was emphasized in [21], this dragon seems to be very much three-dimensional; it kind of tries to escape the sheet of paper, where it is drawn. But the only "physical dragon" that is at our disposal is the gravure itself, which is two-dimensional. It tries to make us believe that its real dimensionality is more than two, but it is a *false* claim. Likewise, gravity may be conveniently formulated in higher dimensional terms, but our physical world has only four dimensions.

The last paragraph of the paper is reserved for a physical argument. The idea that an essentially four-

dimensional theory can be conveniently described with fictitious higher dimensional scaffolds is not new. This is exactly the content of Maldacena's conjecture on AdS/CFT correspondence: the correlators of four-dimensional SYM theory coincide with certain correlators in ten-dimensional supergravity defined on the boundary of some particular background [22]. Many other quantities in ten-dimensional theory can be defined and considered, but they are declared to be meaningless as far as SYM theory is concerned.

ACKNOWLEDGMENTS

I am indebted to Sergei Blinnikov, Ian Kogan, and Arkady Tseytlin for illuminating discussions.

REFERENCES

1. C. J. Isham, in *Proc. of GIFT International Seminar on Theoretical Physics, Salamanca, 1992*; gr-qc/9210011.
2. R. Arnowitt, S. Deser, and C. Misner, Phys. Rev. **117**, 1595 (1960).
3. R. Penrose, Riv. Nuovo Cimento **1**, 252 (1969).
4. T. Harada, Prog. Theor. Phys. **107**, 449 (2002).
5. K. Gödel, Rev. Mod. Phys. **21**, 447 (1949); C. W. Misner and A. H. Taub, Zh. Éksp. Teor. Fiz. **28**, 233 (1969) [Sov. Phys. JETP **28**, 122 (1969)]; M. Visser, *Lorentzian Wormholes: from Einstein to Hawking* (AIP, New York, 1995).
6. A. Carlini and I. D. Novikov, Int. J. Phys. D **5**, 445 (1996).
7. S. Hawking, Commun. Math. Phys. **87**, 395 (1982).
8. J. Wheeler, *Relativity, Groups, and Topology*, Ed. by C. DeWitt and B. DeWitt (Gordon and Breach, New York, 1964), p. 316; B. DeWitt, Phys. Rev. **160**, 1113 (1967).
9. E. D'Hoker and D. H. Phong, Phys. Lett. B **529**, 241 (2002); Nucl. Phys. B **636**, 3, 61 (2002); **639**, 129 (2002).
10. G. S. Danilov, hep-th/0112022.
11. E. S. Fradkin and A. A. Tseytlin, Phys. Rep. **119**, 233 (1985), and references therein.
12. A. D. Sakharov, Dokl. Akad. Nauk SSSR **12** (11), 70 (1968) [Sov. Phys. Dokl. **12**, 1040 (1968)].
13. A. V. Smilga, in *Proc. of the Int. Symp. on Group Theoretical Methods in Physics, Zvenigorod, 1982,* Vol. 2, p. 73.
14. T. Eguchi and A. J. Hanson, Ann. Phys. (N.Y.) **120**, 82 (1979).
15. A. V. Smilga, Nucl. Phys. B **234**, 402 (1984).
16. T. D. Lee and G. C. Wick, Nucl. Phys. B **9**, 209 (1969); Phys. Rev. D **2**, 1033 (1970).
17. I. Antoniadis and E. T. Tomboulis, Phys. Rev. D **33**, 2756 (1986).
18. V. I. Ogievetsky and E. S. Sokatchev, Yad. Fiz. **31**, 264 (1980) [Sov. J. Nucl. Phys. **31**, 140 (1980)]; Yad. Fiz. **31**, 821 (1980) [Sov. J. Nucl. Phys. **31**, 424 (1980)]; Sov. J. Nucl. Phys. **32**, 589 (1980); Sov. J. Nucl. Phys. **32**, 870 (1980).
19. P. van Nieuwenhuizen, Phys. Rep. **68**, 189 (1981), and references therein.
20. V. Guillemin and A. Pollack, *Differential Topology* (Prentice Hall, Englewood Cliffs (NJ), 1974).
21. D. R. Hofstadter, *Gödel, Escher, Bach: an Eternal Golden Braid* (Basic Books, 1979).
22. J. M. Maldacena, Adv. Theor. Math. Phys. **2**, 231 (1998); S. S. Gubser, I. R. Klebanov, and A. M. Polyakov, Phys. Lett. B **428**, 105 (1998).

Physics of Atomic Nuclei, Vol. 66, No. 11, 2003, pp. 2103–2111. Translated from Yadernaya Fizika, Vol. 66, No. 11, 2003, pp. 2152–2160.

FUTURE PUBLICATIONS

S-Wave of $\pi\pi$ Scattering from Data on the Reaction $\pi^- p \to \pi^0\pi^0 n$

N. N. Achasov and G. N. Shestakov

The results of recent experiments performed at KEK, Brookhaven National Laboratory, Institute for High-Energy Physics (Protvino), and CERN to study the reaction $\pi^- p \to \pi^0\pi^0 n$ are analyzed in detail. For S-wave $\pi\pi$ scattering in the channel of isospin $I = 0$, new data are obtained for the phase shift δ_0^0 and the inelasticity parameter η_0^0. Difficulties that arise in using, for the amplitudes of the S and D waves of the final $\pi^0\pi^0$ system, physical solutions selected on the basis of partial-wave analyses are discussed. It is noteworthy that other solutions are preferable in principle in the region of the invariant mass m of the $\pi^0\pi^0$ system above 1 GeV. With the aim of clarifying the situation and further studying the properties of the $f_0(980)$ resonance, it is proposed to perform, in the reaction $\pi^- p \to \pi^0\pi^0 n$, an especially careful examination of the region of m values in the vicinity of the $K\bar{K}$ threshold.

Phenomenological Analysis of Channels of the Production of Three or Four Alpha Particles in $^{16}O$$p$ Collisions at a Momentum of 3.25 GeV/c per Projectile Nucleon

É. Kh. Bazarov, V. V. Glagolev, K. G. Gulamov, V. V. Lugovoi, S. L. Lutpullaev, K. Olimov, A. A. Yuldashev, and B. S. Yuldashev

A phenomenological analysis of channels involving the production of three or four alpha particles in ^{16}Op collisions at a momentum of 3.25 GeV/c per projectile nucleon is performed for the first time under the conditions of 4π geometry. Azimuthal asymmetries and collinearity observed experimentally are described on the basis of a phenomenological model that assumes that the excitation of the target nucleus proceeds via a peripheral process, but that its decay is statistical. It is shown that the azimuthal asymmetries in question are due to the transverse motion of the fragmenting nucleus. It is found that the mean value of the transverse momentum of product alpha particles and the collinearity of their emission are independent of the transverse-momentum transfer to the target nucleus.

Production of Protons in $^{16}O$$p$ Collisions at a Momentum of 3.25 GeV/c per Projectile Nucleon

É. Kh. Bazarov, V. V. Glagolev, K. G. Gulamov, V. D. Lipin, S. L. Lutpullaev, K. Olimov, A. A. Yuldashev, B. S. Yuldashev, and Kh. Sh. Khamidov

The momentum features of protons originating as fragments from ^{16}Op collisions at a momentum of 3.25 GeV/c per projectile nucleon are analyzed for the first time under the conditions of 4π geometry. A universal regularity is observed in the production of protons traveling in the forward direction in the rest frame of the fragmenting nucleus: the mechanism of production of such protons (all of them, with the exception of evaporated ones) is independent of the primary energy or the type of the target nucleus. The shape of the momentum spectrum of protons appearing as fragments (especially slow ones) is shown to be strongly correlated with the degree of excitation of the fragmenting nucleus.

Estimating the Number of "Photon Plus Jet" Events to Determine the Gluon Distribution at the Tevatron in the RUN II Experiment

D. V. Bandurin and N. B. Skachkov

It is shown that, at an integrated luminosity of $L_{\rm int} = 3\ {\rm fb}^{-1}$, about one million events of the "prompt photon plus jet" type that are selected according to previously proposed criteria can be collected in the Run II experiment at the Tevatron. Such statistics would make it possible to advance into the kinematical region that was not explored in previous experiments aimed at measuring the proton structure functions and where

1063-7788/03/6611-2103$24.00

$2 \times 10^{-3} < x < 1.0$ at Q^2 values in the range $1.6 \times 10^3 \leq Q^2 \leq 2 \times 10^4$ $(\mathrm{GeV}/c)^2$, which, on average, is one order of magnitude higher than values reached in experiments conducted at the HERA collider.

Production of Triply Charmed Ω_{ccc} Baryons in e^+e^- Annihilation

S. P. Baranov and V. L. Slad

The total cross section and the differential cross sections for the production of triply charmed Ω_{ccc} baryons in e^+e^- annihilation are calculated at the Z-boson pole.

Production of Heavy Quarks on Protons within the Semihard QCD Approach

S. P. Baranov, N. P. Zotov, and A. V. Lipatov

The inclusive production of heavy quarks in $p\bar{p}$ interactions at the Tevatron and LHC energies is considered within the semihard QCD approach. The dependence of the total and differential cross sections for the production of b quarks and B mesons (as well as muons arising in the subsequent semileptonic decay $B \to \mu\nu_\mu X$) on various sets of unintegrated distributions of gluons is investigated. The results obtained by calculating azimuthal correlations between the transverse momenta of final-state particles are presented. The theoretical results of the present study are compared with the latest experimental data obtained by the D0 and CDF Collaborations at the Tevatron.

Production of a Pair of Charmed Mesons in Photon–Photon Interaction

A. V. Berezhnoy, V. V. Kiselev, and A. K. Likhoded

The exclusive production of a pair of charmed mesons in photon–photon interaction is calculated on the basis of the constituent model. The resulting predictions are compared with heavy-quark effective theory. It is shown that the light valence quark of the D meson plays a significant role not only in hadronization but also in the process leading to the production of a heavy c quark. Moreover, it is shown that, because of the strong interaction of a primary photon with the charge of a light quark, a similar situation persists even in the limit $m_Q \to \infty$, whence it follows that the application of heavy-quark effective theory to the case of photon–photon interaction is incorrect, since this theory disregards one of the dominant mechanisms of the production of heavy mesons.

Processes $e^+e^- \to c\bar{c}c\bar{c}$ and $e^+e^- \to J/\psi + gg$ at $\sqrt{s} = 10.59$ GeV

A. V. Berezhnoy and A. K. Likhoded

Data obtained in the BELLE experiment on the inclusive production of J/ψ particles in the processes $e^+e^- \to J/\psi + gg$ and $e^+e^- \to J/\psi + c\bar{c}$ are discussed. A comparison of these data with the predictions of perturbative QCD is performed either with the aid of information about the J/ψ wave function or without recourse to this information by using only the assumption of quark–hadron duality. In either case, there is pronounced disagreement between the results of the calculations and the data in question. The cross section for the process $e^+e^- \to J/\psi + gg$ is studied as a function of the effective gluon mass. Estimates are presented for the production of doubly charmed baryons Ξ_{cc}.

Elastic Scattering of Intermediate-Energy Protons by ^{9}Be Nuclei within the $2\alpha n$ Model

Yu. A. Berezhnoy and V. P. Mikhailyuk

A dispersive alpha-cluster model is developed for the case of the ^{9}Be nucleus. In the relevant calculations, two configurations are used for the ground-state density of this nucleus. The ^{9}Be nucleus is considered either as that which consists of a core (^{8}Be nucleus) and an additional cluster (neutron), which, with the highest probability, can execute vibrations about the center of mass of the core, or as that which consists of two alpha-particle clusters and a neutron that occur at the vertices of an equilateral triangle. On the basis of this approach and the theory of multiple diffractive scattering, polarization observables are calculated for elastic proton scattering by these nuclei. The observables of elastic p^9Be scattering that were calculated within this approach are in agreement with available experimental data.

T-Odd Correlation in $K^+ \to \pi l \nu \gamma$ Decays beyond the Standard Model

V. V. Braguta, A. A. Likhoded, and A. E. Chalov

The dependence of the T-odd correlation $\xi = \mathbf{q} \cdot [\mathbf{p}_\pi \times \mathbf{p}_l]/m_K^3$ in $K^+ \to \pi l \nu \gamma$, $l = e$, μ, decays on the parameters of the effective Lagrangian is considered. It is shown that the quantity under study is an effective one from the point of view of searches for new physics in the vector and the pseudovector sector of the Lagrangian being studied. No significant refinement of the currently existing constraints on the parameters of various extensions of the Standard Model can be achieved by studying the above T-odd correlation in the scalar and the pseudoscalar sector of this Lagrangian.

Measurement of Cross Sections for γ Transitions in Excited Nuclei Originating from the Interaction of 1.1-GeV Protons with Silicon Nuclei

A. A. Vasenko, N. D. Galanina, K. E. Gusev, U. S. Demidov, E. V. Demidova, I. V. Kirpichnikov, V. A. Kuznetsov, B. N. Pavlov, A. Yu. Sokolov, A. S. Starostin, and N. A. Khaldeeva

Cross sections are measured for processes in which the formation of excited nuclei in $^{28}\mathrm{Si}(p, xp, yn)A^*$ reactions is followed by a γ transition to a state at a lower excitation energy or to the ground state. The experiment was performed in an external proton beam from the accelerator installed at the Institute of Theoretical and Experimental Physics (ITEP, Moscow). A Ge(Li)–NaI(Tl) anticoincidence gamma spectrometer, which recorded prompt gamma radiation emitted by the excited final nucleus, was used to identify the reactions in question. The sensitivity of the experiment was 1.5 mb. The cross sections were obtained for 24 γ transitions in 17 product nuclei. The cross sections for disintegration reactions are estimated. A comparison with available experimental data and with the results of calculations by a semiempirical formula, as well as with the results of simulations of hadron interactions on the basis of the GEANT and INUCL codes, is presented.

Features of pC Interactions at a Momentum of 4.2 GeV/c versus the Degree of Centrality of a Collision between a Proton and a Carbon Nucleus: Kinematical Features of Secondaries

A. S. Galoyan, E. N. Kladnitskaya, O. V. Rogachevsky, R. Togoo, and V. V. Uzhinskii

The mean values of the momenta and emission angles of charged pions and protons in the laboratory frame are presented both for the total ensemble of interactions between 4.2-GeV/c protons and a carbon nucleus and for six groups of events characterized by different degrees of collision centrality. The distributions with respect to the total and the transverse momentum are presented for the particles being studied, along with the rapidity distributions. Our experimental data are compared with the predictions of the cascade–evaporation model and of two versions of the refined FRITIOF model. It is shown that, as the degree of collision centrality becomes higher, the mean momenta and rapidities of secondaries decrease, the transverse momenta remain virtually unchanged, and the mean angles of particle emission increase. This is consistent with particle cascading in nuclei. However, the mean transverse momentum $\langle p_t \rangle$ of participant protons that was obtained on the basis of the cascade–evaporation model decreases with increasing degree of collision centrality, in contrast to what is observed in our experiment. A satisfactory description of experimental data was obtained on the basis of the refined FRITIOF model taking into account Δ^+ and Δ^0 isobars. The stopping power of carbon nuclei for 4.2-GeV/c protons is also determined.

Transparency of Nuclei and Proton and Pion Ranges in Nuclear Matter at Intermediate Energies

I. V. Glavanakov

In the second resonance region of the photon energy, the differential yield of neutral and charged pions in the $(\gamma, \pi p)$ reactions on Li, C, and Al nuclei is measured as a function of the proton energy and the azimuthal angle of pion emission. These experimental data are analyzed on the basis of a model that includes single and double quasifree pion photoproduction. This makes it possible to obtain the energy dependences of the proton, neutral-pion, and charged-pion ranges and to estimate the transparency of nuclei.

Integration over Moduli Space in Superstring Theory

G. S. Danilov

A calculation of multiloop superstring amplitudes is considered, the equivalence of popular approaches to determining these amplitudes being discussed. A calculation of poorly defined integrals over singular configurations is clarified. Amplitudes obtained by a correct method do not involve divergences in any order of perturbation theory.

Properties of Products Originating from the Interaction of 35-MeV/nucleon ^{7}Li Ions with Pb Nuclei

N. A. Demekhina, G. S. Karapetyan, S. M. Lukyanov, Yu. É. Penionzhkevich, N. K. Skobelev, and A. B. Yakushev

The results are presented that were obtained by measuring and analyzing the yields and kinematical features of radioactive products of the reactions initiated in a lead target by lithium ions accelerated to an energy of 35 MeV/nucleon. The cross sections, charge and mass distributions, and kinematical and energy features of various reaction products associated with the fission and the evaporation channels of the decay of excited nuclei are determined. Quantities that are calculated in the present study include the momenta and kinetic energies of residual nuclei, as well as the momentum transfer and the excitation energy of intermediate nuclear systems formed upon complete and incomplete fusion. On the basis of an analysis of data obtained in our experiment, the total cross section for nuclear interaction and partial widths with respect to various channels of the decay of intermediate compound nuclei are determined in the energy range being investigated.

Excitation of the Discrete Levels of the ^{54}Fe and ^{56}Fe Nuclei in (e, e') Reactions

V. V. Denyak, V. M. Khvastunov, V. P. Likhachev, A. A. Nemashkalo, S. A. Pashchuk, and U. P. Schelin

The excitation of the discrete levels of the ^{54}Fe and ^{56}Fe nuclei in (e, e') reactions at an excitation energy of 8 MeV is investigated in the momentum-transfer range between 0.6 and 1.7 fm^{-1}. A nontraditional procedure of multipole analysis is employed in experimental-data processing. Information about the reduced probability and multipole orders is obtained for 12 low-lying states of the ^{54}Fe nucleus and for 10 states of the ^{56}Fe nucleus. Five levels in the ^{54}Fe nucleus and three levels in the ^{56}Fe nucleus are identified for the first time in (e, e') reactions. The latest compilation of data on discrete levels contains no information about two of them.

Phase Transitions between Axisymmetric and Nonaxial Nuclear Shapes

R. V. Jolos

Within the interacting-boson model, phase transitions between different nuclear shapes are considered in the space of three governing parameters. Depending on the values of these parameters, the equilibrium nuclear shape may be spherical, deformed axisymmetric, and deformed nonaxial. It is shown that the phase transition from an axisymmetric to a nonaxial deformation is a second-order phase transition. Within the Bohr–Mottelson model, an approximate solution is found that describes a nucleus in the vicinity of the critical point of the phase transition from a spherical shape to a nonaxial deformation. The results obtained for the energies and probabilities of $E2$ transitions are close to experimental data for ^{134}Ba.

Stability of the Vacuum in Nambu–Jona-Lasinio Models

I. T. Dyatlov

In Nambu–Jona-Lasinio models for a dynamical breakdown of chiral symmetry, nonperturbative divergences prevent a direct comparison of the vacuum energies of different solutions. In the presence of a few solutions to the equations for fermion masses, the choice of a stable vacuum can nevertheless be performed since, for unstable states, tachyons appear in the spectrum of composite scalar bosons of the model.

Isotopic Effect in the Widths of Giant Dipole Resonances of Light Nuclei

M. A. Elkin, B. S. Ishkhanov, I. M. Kapitonov, E. I. Lileeva, and E. V. Shirokov

An isotopic effect in the widths of giant dipole resonances is established on the basis of an analysis of the latest systematics of photoabsorption cross sections for nuclei containing 12 to 65 nucleons. This effect arises owing to isospin splitting of a giant resonance. It is enhanced by its configuration splitting.

Relativistic Description of $P\gamma^*\gamma$ Transition Form Factors within the Quasipotential Approach

A. A. Zarzhitsky and V. I. Savrin

The possibility of constructing a nonperturbative description of the $\pi^0\gamma^*\gamma$, $\eta\gamma^*\gamma$, and $\eta'\gamma^*\gamma$ transition form factors is investigated. The analysis is performed within the quasipotential approach in the lowest order in the electromagnetic coupling constant. This makes it possible to derive analytic expressions for the relevant transition form factors in terms of relativistic mason wave functions. A quantitative description of currently available experimental data can be obtained owing to a natural choice of the quasipotential wave function for pseudoscalar mesons. A comparison of wave-function parameters for the π^0, η, and η' mesons clearly demonstrates a relativistic character of the motion of quarks in light mesons.

Electroweak Radiative Effects in Polarized Møller Scattering

V. A. Zykunov

Bremsstrahlung-induced electroweak radiative corrections to observables of polarized Møller scattering are calculated. The covariant method is used to remove infrared divergences. Owing to this, the eventual result does not involve unphysical parameters. The electroweak corrections being considered reduce the polarization asymmetry in the region studied by the E-158 experiment at SLAC. For example, the asymmetry is shifted by approximately -11% at $E = 48$ GeV and $y = 0.5$.

Single-Particle Levels and Spin-Orbit Splittings in the Vicinity of the Doubly Magic Nucleus ^{48}Ca

V. I. Isakov

On the basis of a detailed analysis of available experimental data, the spectrum of single-particle states and the isotopic dependence of spin–orbit splitting are determined for nuclei in the vicinity of the neutron-rich nuclide ^{48}Ca. The spectrum of excited states of the isobaric nucleus ^{48}Sc is calculated.

Relativistic Analysis of Bremsstrahlung in the Process $pp \to pp\gamma$ with Allowance for Isobar Channels and Possibility of Choosing between Different Types of Nucleon–Nucleon Interaction

V. A. Knyr and N. A. Khokhlov

A relativistic quasipotential formalism for describing electromagnetic processes involving nucleons that takes into account an explicit coupling to the $N\Delta$ (1232 MeV) and NN^* (1440 MeV) channels is developed. On one hand, this formalism is a relativistic generalization of the Lomon–Ray approach to describing nucleon–nucleon scattering within a framework explicitly including isobar degrees of freedom; on the other hand, it relies on the formalism developed by Lev within relativistic quantum mechanics to construct the operator of the electromagnetic current of interacting particles. The formalism makes it possible to construct a consistent description of a two-nucleon system in the energy region extending up to 1 GeV. It is applied to describing the reaction $pp \to pp\gamma$ over a kinematical region in which corrections associated with a virtual delta isobar in the proton–proton system are of importance. The sensitivity of this reaction to the type of short-range component of the nucleon–nucleon potential and the possibility of choosing between the Moscow potential and meson-exchange potentials on the basis of experimental data are confirmed.

Yield of Neutrons upon the Irradiation of Thin Foils from TiD_2 with a Superstrong Laser Pulse

V. P. Krainov

The yield of neutrons from the thermonuclear-fusion reaction $D(d,n)^3He$ induced in a thin skin layer by the interaction of a high-intensity laser pulse of picosecond duration with thin foils made from TiD_2 is calculated. A multiple ionization of titanium atoms at the forward front of the laser pulse is considered. The heating of free electrons proceeds via inverse absorption induced by braking in elastic electron scattering on multiply charged titanium ions. The electron temperature is calculated. It proves to be about 10 keV at the laser-pulse intensity of 5×10^{18} W/cm^2 at the peak. The yield of neutrons is estimated at 10^4 per laser pulse. These results are in qualitative agreement with experimental data.

Leptonic Decays of the W Boson in an Intense Electromagnetic Field

A. V. Kurilin

The probability of W-boson decay into a lepton and neutrino in a strong electromagnetic field, $W^\pm \to \ell^\pm \nu_\ell$, is calculated. On the basis of the method for deriving exact solutions to relativistic wave equations for charged particles, an exact analytic expression is obtained for the partial decay width $\Gamma(\varkappa) = \Gamma(W^\pm \to \ell^\pm \nu_\ell)$ at an arbitrary value of the external-field-strength parameter $\varkappa = eM_W^{-3}\sqrt{-(F_{\mu\nu}q^\nu)^2}$. It is found that, in the region of comparatively weak fields ($\varkappa \ll 1$), corrections to the standard decay width of the W boson in a vacuum are about a few percent. As the external-field strength is increased, the partial width with respect to W-boson decay through the channel in question, $\Gamma(\varkappa)$, first decreases, the absolute minimum of $\Gamma_{\min} = 0.926\Gamma(0)$ being reached at $\varkappa = 0.6116$. A further increase in the external-field strength leads to a monotonic growth of the decay width of the W boson. In superstrong fields ($\varkappa \gg 1$), the probability of W-boson decay is greater than the corresponding probability of the decay $W^\pm \to \ell^\pm \nu_\ell$ in a vacuum by a factor of a few tens.

Neutron Emission from the Reaction $^{232}Th(n, xn'f)$

G. N. Lovchikova, A. M. Trufanov, M. I. Svirin, and V. A. Vinogradov

The energy distributions of neutrons accompanying the fission of ^{232}Th is measured by the time-of-flight technique at the bombarding-neutron energies of $E_n = 14.6$ and 17.7 MeV. The data obtained in this way are compared with the results of previous investigations. An excess of soft neutrons that was observed in the experimental spectra of neutrons from ^{238}U fission at $E_n = 13.2$, 14.7, 16.0, and 17.7 MeV in relation to the results of the calculations based on the model of two sources is also present in the spectra for ^{232}Th. The discrepancy between the results of the calculations and experimental data disappears as soon as one assumes the presence of a third source that is related to neutron emission from nonaccelerated fragments.

On the Pair Production of Vector Charmonia in Electron–Positron Annihilation into Two Photons at $\sqrt{s} = 10.6$ GeV

A. V. Luchinsky

The results recently obtained by the BELLE Collaboration from a measurement of the exclusive pair production of $c\bar{c}$ mesons in electron–positron annihilation deviate from theoretical predictions considerably. It was recently assumed that a significant part of this discrepancy may be attributed to the process $e^+e^- \to 2\gamma^* \to 2J/\psi$, and the cross section for this process was presented. It is shown that these results are erroneous and yield excessive cross-section values. Correct values are given for cross sections describing the pair production of various vector charmonia.

Potential of Present-Day Experiments Aimed at a Model-Independent Determination of Parameters Characterizing the Gamma Decay of Compound Heavy-Nucleus States

A. M. Sukhovoi and V. A. Khitrov

Experimental data on two-quantum cascades initiated by thermal-neutron capture in ^{184,186}W and ^{190,192}Os nuclei are analyzed from the point of view of prospects for improving reliability of a model-independent determination of the level density in a given interval of J^π and radiative strength functions for $E1$ and $M1$ transitions exciting these levels in the region $E_{\rm exc} \leq B_n$.

Properties of Multi-Skyrmions and Their Quantization in a Generalized Chiral Soliton Model

A. M. Shunderyuk

A semiclassical quantization of the Skyrme model featuring a sixth-order term in the derivatives of the chiral field in the Lagrangian is performed. The orbital, isotopic, interference, and flavor tensors of inertia are calculated. For this version of the model, numerical calculations are performed for the excitation energies of flavors in baryon systems.

A New Look at the KLOE Data on the Decay $\phi \to \eta\pi^0\gamma$

N. N. Achasov and A. V. Kiselev

The analysis of the recent high-statistical KLOE data on the $\phi \to \eta\pi^0\gamma$ decay is presented. This decay mainly goes through the $a_0\gamma$ intermediate state, which gives an opportunity to investigate properties of the α_0. It is shown that KLOE data prefer a higher a_0 mass and a considerably larger a_0 coupling to the $K\bar{K}$ than those obtained in the analysis of the KLOE group.

Near-Threshold Radiative 3π Production in e^+e^- Annihilation

A. I. Ahmedov, G. V. Fedotovich, E. A. Kuraev, and Z. K. Silagadze

We consider the $\pi^+\pi^-\pi_0\gamma$ final state in electron–positron annihilation at c.m. energies not far from the threshold. Both initial and final state radiations of the hard photon are considered but without interference between them. The amplitude for the final-state radiation is obtained by using the effective Wess–Zumino–Witten Lagrangian for pion–photon interactions valid for low energies. In real experiments, energies are never so small that ρ and ω mesons have a negligible effect. So, a phenomenological Breit–Wigner factor is introduced in the final-state radiation amplitude to account for the vector meson influence. Using radiative 3π production amplitudes, a Monte Carlo event generator was developed which could be useful in experimental studies.

Description of Composite Systems in the Spectral Integration Technique: The Gauge Invariance and Analyticity Constraints for the Radiative Decay Amplitudes

V. V. Anisovich and M. A. Matveev

The constraints following from gauge invariance and analyticity are considered for the amplitudes of radiative transitions of composite systems when composite systems are treated in terms of spectral integrals. We discuss gauge-invariant amplitudes for the transitions $S \to \gamma S$ and $V \to \gamma S$ with scalar S and vector V mesons being two-particle composite systems of scalar (or pseudoscalar) constituents, and we demonstrate the mechanism of cancellation of false kinematical singularities. Furthermore, we explain how to generalize the our consideration to quark–antiquark systems, in particular, to the reaction $\phi(1020) \to \gamma f_0(980)$. Here, we also consider in more detail the quark-model nonrelativistic approach for this reaction.

Lepton-Pair Production in Relativistic-Ion Collisions and Its Correspondence with the Crossing Process

E. Bartoš, S. R. Gevorkyan, and E. A. Kuraev

Using the Sudakov technique, we sum the perturbation series for the $3 \to 3$ process and obtain a compact analytic expression for the amplitude of this process, this expression taking into account all possible Coulomb interactions between colliding particles. Comparing it with the amplitude of lepton-pair production in heavy-ion collisions—i.e., in the process $2 \to 4$—we show that the amplitudes obtained in the high-energy limit lose the crossing-symmetry property (which holds only at the Born level).

On Rescattering Effects in the Reaction $\pi^- d \to \pi^- d$

V. V. Baru, A. E. Kudryavtsev, and V. E. Tarasov

Rescattering corrections to the impulse approximation for the processes $\pi^- d \to \pi^- d$ and $\gamma d \to \pi^0 d$ are discussed. It is shown that the rescattering effects give a nonnegligible contribution to the real part of these amplitudes. At the same time, the contributions from the imaginary parts of impulse and rescattering corrections drastically cancel each other. This cancellation means that the processes $\pi^- d \to \pi^0 nn$ and $\gamma d \to \pi^+ nn/\pi^- pp$ are strongly suppressed near the threshold as required by the Pauli principle.

Study of Collective Flow Effects in CC Collisions at a Momentum of 4.2 GeV/c per Nucleon

L. V. Chkhaidze, T. D. Djobava, L. L. Kharkhelauri, E. N. Kladnitskaya, and A. A. Kuznetsov

The directed (in-plane) flows of protons, pions, and projectile light fragments (d, t, ^{3}He, ^{4}He) have been observed by investigating the dependence of the mean transverse momentum in the reaction plane $\langle p_x \rangle$ on the rapidity y in the c.m. The comparison of our in-plane flow results of protons with flow data for various projectile/target configurations was made using the scaled flow $F_s = F/(A_p^{1/3} + A_t^{1/3})$. F_s demonstrates a common scaling behavior for flow values from different systems. From azimuthal distributions of protons and π^- mesons the out-of-plane (squeeze-out) flow effects have been observed and the parameter a_2 (the measure of the anisotropic emission strength) have been extracted. The quark–gluon string model reproduces quite well the experimental results.

Signals of the Abelian Z' Boson within the Analysis of the LEP2 Data

V. I. Demchik, A. V. Gulov, V. V. Skalozub, and A. Yu. Tishchenko

The preliminary LEP2 data on the $e^+e^- \to l^+l^-$ scattering are analyzed to establish a model-independent search for the signals of virtual states of the Abelian Z' boson. The recently introduced observables make it possible to pick up uniquely the Abelian Z' signals in these processes. The mean values of the observables are in accordance with the Z' existence. However, the accuracy of the experimental data is insufficient for detecting the signal at higher than the 1σ confidence level. The results of other model-independent fits and further prospects are discussed.

$SU(2) \times SU(2)$ Chiral Quark Model with Nonlocal Interaction

A. E. Dorokhov, A. E. Radzhabov, and M. K. Volkov

Starting with the model with the chiral invariant $SU(2) \times SU(2)$ four-quark interaction with a nonlocal kernel, we describe masses and interactions of light mesons. The nonlocal kernel is chosen in the form that ensures the absence of ultraviolet divergences in the Feynman diagrams and poles in the quark propagator. Within this model we demonstrate that in the chiral limit the pion mass equals zero and the Goldberger–Treiman relation is fulfilled. The sigma-meson mass and the widths of strong decays $\sigma \to \pi\pi$, $\rho \to \pi\pi$ are estimated.

On the Determination of Quark Masses from the Dalitz Plot of the Decay $\eta \to \pi^+\pi^-\pi^0$

B. V. Martemyanov and V. S. Sopov

The experimental Dalitz-plot distribution of $\eta \to \pi^+\pi^-\pi^0$ decay is fitted using the theoretical one obtained in Chiral Perturbation Theory with unitarity corrections taken into account. The fit shows that the difference of light quark masses is larger than that expected from electromagnetic mass differences of neutral and charged kaons.

Radiative Corrections to QCD Amplitudes in Quasi-Multi-Regge Kinematics

V. S. Fadin, M. G. Kozlov, and A. V. Reznichenko

Radiative corrections to QCD amplitudes in the quasi-multi-Regge kinematics are interesting, in particular, since the Reggeized form of these amplitudes is used in the derivation of the NLO BFKL. This form is a hypothesis which must at least be carefully checked, if not proved. We calculate the radiative corrections in the one-loop approximation using the s-channel unitarity. Compatibility of the Reggeized form of the amplitudes with the s-channel unitarity requires fulfillment of the set of nonlinear equations for the Reggeon vertices. We show that these equations are satisfied.